NASA TECHNICAL TRANSLATION

NASA TT F-15,010

ON THE PITCH DAMPING MOMENT IN HOVERING OF A RIGID HELICOPTER ROTOR

K. Takasawa

Translation of "Rijiddo herikoputa rota no hobaringu no okeru tateyure gensui momento ni tsuite," Koku Uchu Gijutsu Kenkyusho Hokoku, NAL TR-256, November 1971, 80 pp.

NATIONAL AERONAUTICS AND SPACE ADMINISTRATION
WASHINGTON, D.C. 20546 SEPTEMBER 1973

STANDARD TITLE PAGE

1. Report No. NASA TT F-15,010	2. Government Accession No.	3. Recipient's Catalog No.
4. Title and Subtitle: ON THE PITCH DAMPING MOMENT IN HOVERING OF A RIGID HELICOPTER ROTOR		5. Report Date: September 1973 6. Performing Organization Code
7. Author(s): K. Takasawa		8. Performing Organization Report No. 10. Work Unit No.
9. Performing Organization Name and Address: Leo Kanner Associates, P.O. Box 5187, Redwood City, California 94063		11. Contract or Grant No. NASw-2481 13. Type of Report and Period Covered: Translation
12. Sponsoring Agency Name and Address: National Aeronautics and Space Administration, Washington, D.C. 20546		14. Sponsoring Agency Code

15. Supplementary Notes

Translation of "Rijiddo herikoputa rota no hobaringu ni okeru tateyure gensui momento ni tsuite," Koku Uchu Gijutsu Kenkyusho Hokoku, NAL TR-256, November, 1971, 80 pp.

16. Abstract

The aerodynamic damping moment in pitch was measured with a hovering helicopter rotor. Three kinds of model blades with different rigidity were tried. A flow visualization study was performed for the purpose of determining the relative position between the blade and the vortices in steady hovering state. The perfectly rigid rotor was determined. Aerodynamic damping moment in pitch was analyzed. A quasi-steady theory is devised. A simple formula for calculating the pitch damping derivative of a helicopter rotor with spring constrained flapping hinge is proposed. The validity of the formula is ascertained by comparison with experimental results.

17. Key Words (Selected by Author(s))	18. Distribution Statement: Unclassified - Unlimited		
19. Security Classif. (of this report): Unclassified	20. Security Classif. (of this page): Unclassified	21. No. of Pages: 140	22. Price

TABLE OF CONTENTS

ON THE PITCH DAMPING MOMENT IN HOVERING OF A RIGID HELICOPTER ROTOR

Kingo Takasawa
Flight Experimentation Section

Coordinates

/1*

(i) $X_iY_iZ_i$ Coordinates

Right-hand rectangular coordinate axes in which the origin is taken at the center of the rotor. They are fixed in space. The X_i axis faces upward, and the Z_i axis faces downward. The unit axial vectors are I, J, K.

(ii) XYZ Coordinates

Right-hand rectangular coordinate axes in which the origin is taken at the center of the rotor. They are fixed to the rotor. Pitching motion with an angular velocity $\dot{\theta}j$ is performed around the Y axis. They coincide with coordinates $X_iY_iZ_i$ at time t = 0. The unit vectors in the axial direction are i, j, k.

(iii) x'y'z' Coordinates

Right-hand rectangular coordinate axes in which the origin is taken at the center of the rotor. They are fixed to the rotor blade. The y' axis faces outward in the radial direction, and the z' axis faces upward. The unit vectors in the axial direction are i^*, j^*, k^*.

(iv) τrσ Coordinates

They are the curve coordinates used in Ichikawa's monographs [1, 2, 3]. The relationship in Eq. (4.1) applies between them /2
and the x'y'z' coordinates.

The XYZ coordinates, the x'y'z' coordinates, and the τrσ coordinates are depicted graphically in Fig. 66. The $X_iY_iZ_i$ coordinates, the XYZ coordinates, and the x'y'z' coordinates are depicted graphically in Fig. 4.

Symbols

A_1 Coefficient of blade vibration equation. Refer to Eq. (1.17).

---

*Numbers in the margin indicate pagination in the foreign text.

A_2 Coefficient of blade vibration equation. Refer to Eq. (1.18).

A_3 Coefficient of blade vibration equation. Refer to Eq. (1.21).

a Acceleration vector

a Two-dimensional lift curve slope

b' Half chord length

b_o' : y' = Half chord length at position of $(R_2' + R_1')/2$ (Fig. 59).

C(k) Theodorsen's function

C'(k,m,h) Lift deficiency function derived by Loewy

$$C_{lj}: \begin{cases} 1/2 & \text{for } l=0 \\ \cos l\theta_j & \text{for } l=1, 2, 3, \cdots J \end{cases}$$

c' Chord length

D Influence function in seeking the induction velocity. Refer to Eq. (4.12)

D_1 Coefficient of blade vibration equation. Refer to Eq. (1.19).

D_2 Coefficient of blade vibration equation. Refer to Eq. (1.20).

EI Flexural rigidity of blade

e Bottom of natural logarithm

F(k) Real part of C(k)

F'(k,m,h) Real part of C'(k,m,h)

F_A Vector of air force operating on unit wing span of blade

F_A Absolute value of F_A

F_M Vector of mass force operating on unit wing span of blade

$$FW: FW_{pq} = \int_0^\pi \cos p\theta \cos q\theta \, d\theta$$

$$FX: FX_{pq} = \int_0^\pi \cos p\theta \cos q\theta \frac{\cos\phi - \cos\theta}{|\cos\phi - \cos\theta|} d\theta$$

$$FY: FY_{pq} = \int_0^\pi \cos p\theta \cos q\theta \frac{\cos\phi - \cos\theta}{|\cos\phi - \cos\theta|} \times \log|\cos\phi - \cos\theta| \, d\theta$$

$$FZ: FZ_{pq} = \int_0^\pi \cos p\theta \cos q\theta \frac{1}{\cos\phi - \cos\theta} d\theta$$

f General coordinate expressing flexibility of blade

$_0f$ Steady component of f

f_{S+} $\sin(\Omega+p)t$ component of f

f_{S-} $\sin(\Omega-p)t$ component of f

f_{C+} $\cos(\Omega+p)t$ component of f

f_{C-} $\cos(\Omega-p)t$ component of f

G Influence function in seeking the induction velocity. Refer to Eq. (4.12).

$G(k)$ Imaginary part of $C(k)$

$G'(k,m,h)$ Imaginary part of $C'(k,m,h)$

$H_{(P')}$ $H_{(p')} = \sqrt{r'^2 + h^2}/2$

$H_\nu^{(2)}$ Second type Hankel function

h' Distance between center of gravity of movable part of experimental apparatus and space between pitching axes, spaces of vortex sheets in Loewy's theory

h Parameter derived from Ichikawa's theory, $h \equiv W/\Omega$

I Inertia efficiency around pitching axis of movable part of experimental apparatus

I_ν First type transformed Bessel function

I_1 Contribution of vortex with replaced wing surface appearing in lift surface equation

I_2 Contribution of vortex with replaced trailing vortex sheet appearing in lift surface equation

I_3 Contribution of vortex with replaced shed vortex sheet appearing in lift surface equation

$I_3^{(2)}$ Contribution to lift surface equation when the shed vortex pattern at the point where the downwash is calculated is regarded as extending to an infinite distance on both sides in the wing span direction

I Unit vector in the X_1 coordinate axial direction

ΔI_3 $\Delta I_3 = I_3 - I_3^{(2)}$

i Imaginary unit

i Unit vector in X axial direction

i_I Unit vector in x axial direction in xyz coordinate axis of reference [1], $i_I = i$

i^* Unit vector in x' axial direction

J_o First type Bessel function

J_1 Second type Bessel function

J Unit vector in Y_1 axial direction

j Unit vector in Y axial direction

j_I Unit vector in y axial direction in xyz coordinate axis of reference [1], $j_I = -j$

j^* Unit vector in y' axial direction

K_ν Second type transformed Bessel function

K_E Coefficient for estimating the pitch damping of an entirely rigid blade, excluding the pitch damping caused by the elasticity of the blade from the pitch damping obtained experimentally

K Unit vector in the Z_1 axial direction

k Unit vector in the Z axial direction

k_I Unit vector in the z axial direction in xyz coordinate axis of reference [1], $k_I = -k$

k^* Unit vector in the z' axial direction

k Dimensionless vibration frequency, refer to Eq. (3.25) /3

k_0 Dimensionless vibration frequency, refer to Eq. (3.25)

$\bar{L}$ Amplitude of unsteady lift operating on unit wing span

L_ν Struve function, refer to Eq. B5

m p/Ω

M_H Moment generated around the hub of the reference blade

M_Y Moment operating around the Y axis

$\partial M/\partial\dot{\theta}$ Pitch damping derivative

$(\partial M/\partial\dot{\theta})_R$ Derivative of the pitch damping generated directly because of the pitching of the rotor. Can also be called the pitch damping considered when one has assumed an entirely rigid rotor blade.

$(\partial M/\partial\dot{\theta})_E$ Coefficient of pitch damping generated through the elastic deformation occurring in the blade when the rotor undergoes pitch damping

$$N_A: N_A \equiv q\int_0^\infty \frac{\lambda_1 e^{-i\lambda_1}}{[\lambda_1^2+q^2]^{3/2}}\,d\lambda_1$$

$$N_B: N_B(q) \equiv q\int_0^\infty \frac{e^{-i\lambda_1}}{[\lambda_1^2+q^2]^{3/2}}\,d\lambda_1$$

$$N_C: N_C(\tau) \equiv \int_0^\infty \left[\frac{\tau}{\sqrt{\tau^2+\lambda_2^2}} - \frac{|\tau|}{\tau}\right]\frac{e^{-i\lambda_2}}{\lambda_2}\,d\lambda_2$$

ΔN_A Nonsingular portion of N_A: $\Delta N_A \equiv N_A(q) - \frac{q}{|q|}$

ΔN_B Nonsingular portion of N_B: $\Delta N_B = N_B(q) - \frac{1}{q} - i\frac{q}{|q|}$

ΔN_C Nonsingular portion of N_C: $\Delta N_C = N_C - \frac{\tau}{|\tau|}\log|\tau| - \frac{\tau}{|\tau|}\left(\gamma + \log 2 + \frac{\pi}{2}i\right)$

n Number of rotor cycles after the generation of a given vortex until the present time

P Point where the induction velocity is sought P(x',y',z'), P(τ,r,σ)

P' Point where there is a vortex P(ξ',η',ζ'), P(τ',r',σ')

p Pitching vibration frequency p = 2π/T

p Pressure*

p p/Ω

Δp Pressure difference between upper and lower wing surfaces

Q Number of blades

Q_f General force

q Blade numbers. Assigned in ascending order (0, 1, 2, ...) in the same direction as the direction of the rotor revolution.

$$q: q \equiv \frac{\omega(y'-\eta')}{V(\eta')}$$

R Distance between point P and point P'

R_1' Inside radius of wing area making up blade, $R_1 = R_1'/b'$

R_2' Outside radius of wing area making up blade, $R_2 = R_2'/b'$

r Position vector

r_τ Vector in the tangential direction of the τ coordinate curve of the τrσ coordinate; refer to Eqs. (4.3) and (4.4).

*[Note: Original does not differentiate between symbols for pitching vibration frequency and pressure.]

r	r coordinate of point P
r'	r coordinate of point P'
S'	Blade length, $S' = R_2'$
S_R'	Length from hub to inside of wing area, $S_R' = R_1'$
s'	Length from hub along central line of blade, $s = s'/R_2'$
T	Pitching cycle
T	Kinetic energy*
t	Present time
t'	Time at which a certain vortex occurred
Δt	Time after the vortex $\gamma_{ng}(\xi',t)$ occurred until the present time
U	Strain energy
$\delta u'$	x' direction components of virtual displacement
V	Main stream velocity, $V = y'\Omega$
v_X	Velocity component in X direction at a point on the blade
v_Y	Velocity component in Y direction at a point on the blade
v_Z	Velocity component in Z direction at a point on the blade
v_i	Steady induction velocity on rotor surface
v_a	Unsteady components in the induction velocity
$\bar{v}_a$	Amplitude of v_a
$\bar{v}_{as}$	Steady components in the induction velocity
$\delta v'$	y' direction components of virtual displacement
W	Weight of movable parts of experimental apparatus
	Rotor ascending velocity
W	Function expressing contribution of the vortex in the wake*
δW	Virtual work
$\delta w'$	z' direction components of virtual displacement
x'	x' coordinates at point where induction velocity is sought

$$x: x \equiv \frac{x' - (x_t' + x_t')/2}{b'}$$

*[Note: Original does not differentiate between symbols for pitching cycle and kinetic energy; likewise, symbols W.]

x_1' x' coordinates at front edge of blade

x_t' x' coordinates at rear edge of blade

$$x_m' : x_m = \frac{x_t' + x_t'}{2b'}$$

y' y' coordinates at point where induction velocity is sought

y_Λ' y' coordinates at place where circulation distribution along the blade radius attains the maximum /4

z' Blade flexibility

z_a' z' coordinates at point on blade camber line

$z_q'(t)$ Z_I coordinates of q blade at present time

$z_q^{*\prime}(t)$ Z_i coordinates of q*-th blade at point in time when a vortex occurred immediately below q blade at the present time

Γ_α' Bound vortex of standard blade

$\overline{\Gamma}_\alpha'$ Amplitude of Γ_α'

$\overline{\Gamma}$ $\overline{\Gamma} \equiv \overline{\Gamma}_\alpha' e^{ik}/b$ (Chapter 2)

Γ_q' Bound vortex of q-th blade

Γ' Bound vortex of blade

Γ_0' Bound vortex of standard blade

$$\Gamma : \Gamma \equiv \frac{\Gamma_{a'}}{b_0'} e^{i\frac{\omega x_t'}{V(\gamma')}} \quad \text{(Chapter 3)}$$

$$\Gamma : \Gamma_{a'}/b_0'$$

γ Lock number (Chapter 1)

γ_α Vortex surface expressing standard blade

$\tilde{\gamma}_\alpha$ Amplitude of γ_α

γ_{00} Shed vortex following immediately after standard blade

γ_{0q} Shed vortex following immediately after q-th blade

γ_{nq} Shed vortex occurring from the q-th blade before n rotations

γ Euler's constant (Chapter 3)

γ_α Components in the vertical direction to the main stream of the vortex expressing the wing surface (Chapter 3

γ_W Components in the vertical direction to the main stream of the vortex in the wake

γ Surface velocity of the vortex sheet

γ_{B0} γ vortex replacing the standard blade

γ Components in the r_2 direction of the vortex; refer to Eq. (4.5)

γ^N Components in the j^* direction of γ

Δ'_{qj} Intensity of vortex occurring from between the j-th dividing point on the q-th blade and the j+1-th dividing point

$$\Delta_{qj}: \Delta_{qj} \equiv 2\Delta_{qj}/(x_{i'} - x_{i'})$$

Δ'_{1j} Intensity of vortex in 1-th layer immediately below the q-th blade. j indicates that it is the j-th vortex filament from the inside.

δ r_τ direction components of the vortex, refer to Eq. (4.5).

δ_α Mainstream direction components of the vortex expressing the wing surface

δ^N i^* direction components of γ

δ_{B0} δ replacing the standard blade

δ_W Mainstream direction components of the vortex in the wake

ζ' z' coordinates of the vortex

ζ'_{qj} Z_i coordinates of the vortex filament replacing the vortex occurring from between the j-th dividing point on the q-th blade and the j+1-th dividing point

ζ'_{1j} Z_i coordinates of vortex in the 1-th layer immediately below the q-th blade. j indicates that it is the j-th vortex filament from the inside

η' y' coordinates of the vortex

η'_{Qj} y' coordinates of the dividing point of the blade

η'_{qj} y' coordinates of the vortex filament occurring from between the j-th dividing point on the q-th blade and the j+1-th dividing point

η'_{1j} y' coordinates of the vortex in the 1-th layer immediately below the q-th blade. j indicates that it is the j-th vortex filament from the inside.

θ Pitching angle, i.e., angle of inclination of rotor surface

θ Coordinates with changed η

$$\eta \equiv \frac{R_2+R_1}{2} - \frac{R_2-R_1}{2}\cos\theta$$

$\overline{\theta}$ Pitching amplitude

θ_j Chebyshev's dividing point

$$\theta_j \equiv \frac{2j-1}{2(J+1)}\pi \qquad (j=1,2,3,\cdots J+1)$$

θ_j θ coordinates corresponding to η_{0j}

θ_c Corrective pitch angle

θ_Λ θ coordinates corresponding to y_Λ'

θ_X Effective angle of incidence

Λ_1 Refer to Eq. (2.25)

Λ_2 Refer to Eq. (3.41)

λ Dummy parameter

$$\lambda_1 : \lambda_1 \equiv \frac{\omega\lambda'}{V(\gamma')}$$

$$\lambda_2 : \lambda_2 \equiv \frac{\omega\lambda'}{V(\gamma')}$$

λ^* Dummy parameter

λ' $\lambda' = \xi' - x'$

$\mu(s)$ Mode function expressing blade flexibility

ν Mass per unit length of blade

ξ' x' coordinates of vortex

π Pi, ratio of the circumference of a circle to its diameter

ρ Air density

σ Solidity ratio ($Qc'/\pi R_2'$)

σ σ coordinates at point P

σ' σ coordinates at point P'

$$\tau: \tau \equiv \frac{\omega(y'-\eta')}{V(y')}$$

τ τ coordinates at point P

τ' τ coordinates at point P'

τ^* $\tau^* \equiv \tau - 4\pi n - 2\pi q/Q$

ϕ Disturbance potential

ψ Coodinate with changed y /5

$$y = \frac{R_2+R_1}{2} - \frac{R_2-R_1}{2}\cos\phi$$

ϕ_i Multhopp's dividing point

$$\phi_i = \frac{i\pi}{N+1} \qquad (i=1,2,\cdots N)$$

ψ Azimuth angle of blade

ψ_q Azimuth angle of q-th blade ($\psi_q = \psi_0 + 2\pi q/Q$)

$\overline{\psi}_q$ Phase difference between bound vortex of standard blade and bound vortex of q-th blade

ω Vibration frequency of blade

ω_B Primary flexural characteristic frequency of blade which is not rotating

Ω Rotary angle velocity of rotor

Superscripts

' Used in cases when a quantity related to the length has dimensions

• Time derivative

- Indicates amplitude

Subscripts

U Quantity on upper surface of wing

L Quantity on lower surface of wing

R Indicates real part

\+ Quantity related to frequency components of $\Omega + p$

\- Quantity related to frequency components of $\Omega - p$

Introduction

Those types of helicopter rotors which do not have flapping hinges are called non-articulated rotors or rigid rotors. Many years ago, rotors of this type were used in lightweight helicopters such as single-seat flying platforms. In recent years, thanks to the progress made recently in blade construction and materials, rigid rotors have been adopted in high-grade four or five seat helicopters such as the XH-51, AH-56, or BO-105.

In rotors of this type, the control moment produced by the air force operating on the blades is transmitted directly to the airframe. Consequently, it is possible to produce a powerful control moment with an extremely small time lag as compared with the conventional helicopter rotors of the past. Besides, by selecting the flapwise flexural characteristic frequency of the blades in a suitable manner, one can obtain a pitch damping and roll damping greater than in the conventional rotors of the past [4]. Another advantage in the way of increasing the speed is the fact that the rotor hub can be formed with a smart appearance, since there are no flapping hinges. Because of these considerations, rigid rotors are regarded as promising both from the standpoint of the piloting safety and from the standpoint of increasing the speed.

However, at the present time, methods of calculating the pitch and roll damping have not yet been established. There are studies by Payne [5], Beppu [6], Townsent [7], and Naito concerning the pitch and damping of rigid rotors in the hovering state.

Payne demonstrates that there is no difference between cases when the flapping hinge is constrained by springs and cases when the flapping hinge is mounted on the hub with an offset. He proves theoretically that the pitch damping changes when the spring strength or the size of the offset changes.

Beppu demonstrated, with respect to a rotor with a flapping hinge with hinge offset constrained by springs, that pitch damping occurs because of three reasons. First, it occurs on account of delay of the tip pass plane. Second, it occurs on account of the hinge offset; and third, during blade flapping, it is transmitted to the airframe through the hinge springs. The first two causes are well known in the conventional articulated

rotors of the past, but the third one is characteristic of rotors in which the flapping hinge is constrained by means of springs. In rotors of this type, the damping caused by the hinge offset will decrease as the strength of the spring is increased. However, it was demonstrated theoretically that the pitch damping transmitted through the springs will first of all increase as the strength of the springs is increased, but that it will decrease after the maximum value has been reached. As a result, in rotors having flapping hinges with hinge offsets which are constrained by springs, on the whole the pitch damping will increase as the strength of the springs is increased, and it will then decrease after the maximum value has been reached. This has also been confirmed by large-scale experiments. Examples of the theoretical calculations by Beppu and examples of his experimental values are given in Fig. 1. The moment produced by the spring and the moment produced by the air force are plotted on the abscissa. On the ordinate is plotted the pitch damping divided by the product of the inertia efficiency around the blade hinge and the rotary angle velocity of the rotor. When there is a weak spring strength, there is good agreement between the experimental and theoretical values, but the divergence between them increases as the spring strength is increased. Beppu mentions, as the reason for this, the fact that the air force can not be calculated accurately.

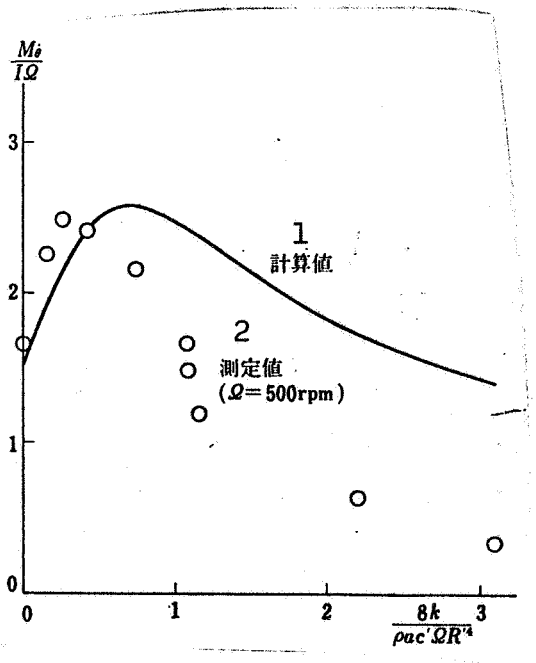

Fig. 1. Comparison of experimental and calculated values of pitch damping [6].

Key: 1. Calculated values
2. Measured values

Townsent, dealing with rotors in which the blades are mounted directly on the hub, assumes that bending and twisting deformations do not occur in the blade. Estimating the air force simply, he obtained a formula for seeking the pitch damping.

/6

$$\frac{\partial M}{\partial \theta} = -\frac{Q}{16}\rho ac' R_3'^4 \Omega \qquad \text{(i)}$$

Here, a is the lift inclination assumed for two-dimensional steady wings. In this monograph we adopt the following equation as a basis for organizing various pitch dampings obtained either experimentally or analytically. In this equation, the theoretical value 2π is used for a.

$$\frac{\partial M}{\partial \theta} = -\frac{Q}{16}\rho(2\pi)c'R_2^4\Omega \qquad \text{(ii)}$$

Naito conducted experiments concerning rotors with the blades mounted directly on the hub. Figure 2 is an example of the results. In the figure, ω_B is the primary flexural characteristic frequency of the blade at the stationary state. This is a parameter representing the blade's rigidity. The solid line indicates the calculated values obtained by using Eq. (2). The experimental apparatus is shown in Fig. 3. Naito derives the following two conclusions from the results of these experiments.

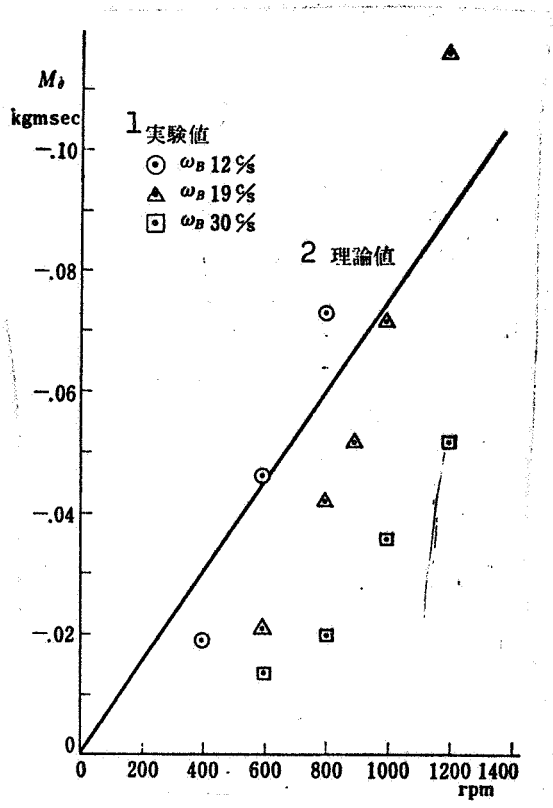

Fig. 2. Comparison of experimental and theoretical values for pitch damping of rotors with two blades.

Key: 1. Experimental values
2. Theoretical values

(i) When the rotor revolution speed is smaller than the primary flexural characteristic frequency of the blades, the value of the pitch damping is about one third of that indicated in Eq. (2). /7

(ii) The pitch damping will increase rapidly when the rotor revolution speed is increased. However, it is believed that this is because periodical elastic deformations occur in the blades on account of the Coriolis force, so that there are fluctuations of the effective angle of incidence of the blade section.

Beppu's experiments when the springs were strong, as well as Naito's experiments, reveal that the experimental values of the pitch damping are much smaller than the theoretical values.

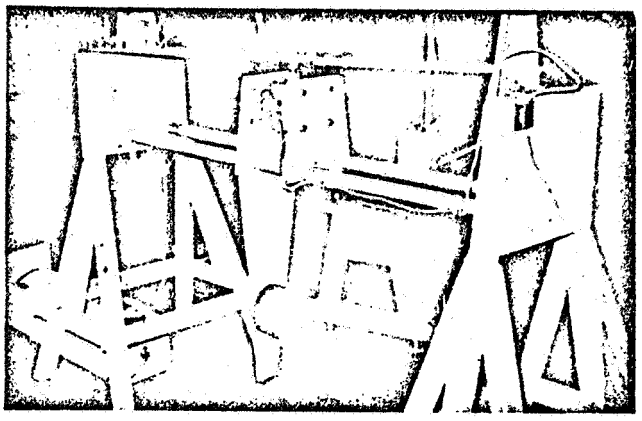

Fig. 3. Pitch damping experimental apparatus (1) (provided by Mr. Naito).

The four studies described above have made it clear approximately what values are assumed by the pitch damping of a rigid rotor, and how these values change together with fluctuations of the spring strength and the blade rigidity. However, nothing at all has been said to explain the reason why calculated values are much smaller than the measured values in cases when the spring strength is great enough or when the primary flexural characteristic frequency of the blades is great enough in comparison with the revolution speed of the rotor. In connection with the problem of pitch damping, this question is a question pertaining to the mechanism by which air forces are produced. If it were possible to elucidate the mechanism of production of air forces, one could explain the reason for the small pitch damping values, and one could obtain an adequate understanding concerning pitch damping of rigid rotors. This research attempts to elucidate the mechanism by which are produced the air forces which govern pitch damping. Using the pitch damping calculation method obtained as a result, it attempts to calculate the pitch damping, and it also attempts to prove, by comparison with experiments, that this calculating method is a valid one.

In order to elucidate the fundamental properties of the phenomena, pitch damping at the state of hovering will be discussed with reference to a rotor in which it is possible to perform pitching alone. The model is as shown in Fig. 4; pitching motion can be performed around the Y_i axis. This model is nearly the same as that used in the experiments of Beppu and Naito. The rotor's center of rotation is exactly on the pitching axis. Therefore, pure pitching, containing no translation, is produced. Since the blade, naturally, does not perform flapping, there is not produced in this case any of the pitch damping which is caused by retardation of the tip pass plane, which plays such an important role in pitch damping of articulated rotors.

This research consists of both experiments and analysis. The experiments are described in Chapter 1. The experiments were carried out with the apparatus shown in Figs. 3 and 5. The rotor surface shakes like a pendulum with a small amplitude around the pitching axis. The vibration amplitude of the rotor surface decreases gradually on account of the pitch damping moment.

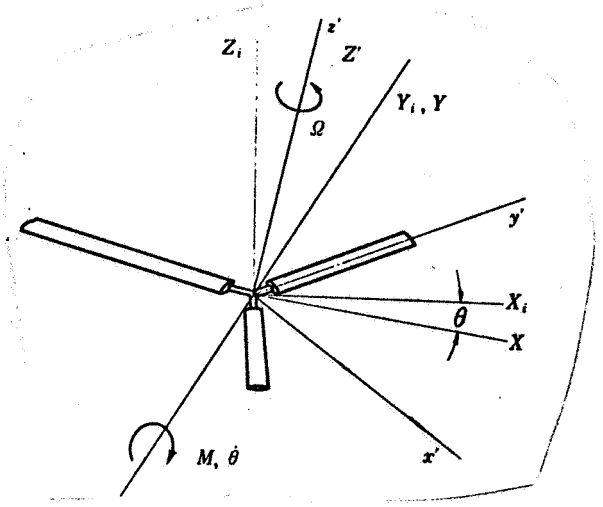

Fig. 4. Rigid rotor in which pitching is performed around the Y axis.

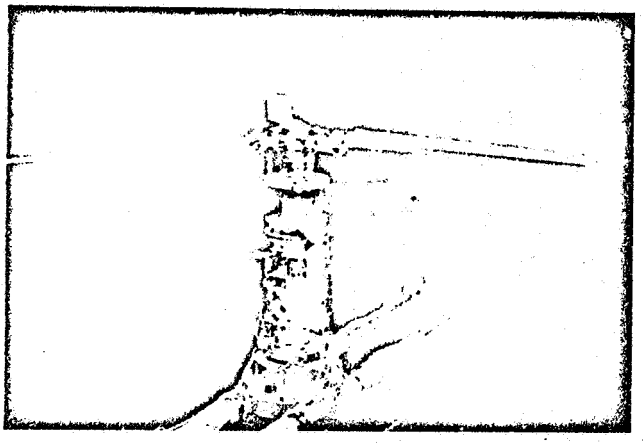

Fig. 5. Pitch damping experimental apparatus.

The pitch damping $\partial M/\partial\dot{\theta}$ can be sought from this amplitude damping. It is believed that the measured $\partial M/\partial\dot{\theta}$ is the sum of $(\partial M/\partial\dot{\theta})_R$, the portion produced by pitching of the rotor surface, and $(\partial M/\partial\dot{\theta})_E$, the portion generated during pitching through the bending deformation occurring in the blades. The former, $(\partial M/\partial\dot{\theta})_R$, increases exactly in proportion to the revolution speed of the rotor, but the latter, $(\partial M/\partial\dot{\theta})_E$, increases even more rapidly than the increase in the revolution speed of the rotor. It is this which is the cause of the rapid increase in the pitch damping, which has already been seen in Fig. 2.

In Chapter 1, Section 3, the strip theory making use of two-dimensional quasi-steady air forces is used to perform analyses in which the bending deformation effects of the blades are treated aeroelastically. It is shown that the measured value of $\partial M/\partial\dot{\theta}$ can be separated into $(\partial M/\partial\theta)_R$ and $(\partial M/\partial\dot{\theta})_E$.

In Chapter 1, Section 4, the appearance of the vortex in the rotor wake was observed, and smoke experiments were performed in order to obtain data about the vortex positions which would serve as the foundation for subsequent analysis.

In Chapters 2 and 3, the pitch damping is calculated using two existing vibrating wing theories concerning helicopter rotors. By comparing the results with the experimental results described in Chapter 1, one can estimate the characteristics of the air forces governing pitch damping.

In Chapter 4 is derived a lifting line equation suitable for analyzing pitch damping. This takes its departure from the /8

lift surface integral equation in [1] concerning steady rotation wings. The equation is derived when it is assumed that there is a small inflow and that the influence of distant vortices is negligible.

Next, this calculating method was applied, and the pitch damping was calculated for a model in which the fluctuations in the distance between the blade and the wake vortex were taken into consideration. The results agreed with the experimental values better than the calculated values obtained by using other theories.

In Chapter 4 is proposed a formula for calculating simply $M_{\dot{\theta}}$, the derivative of pitch damping which occurs when a rigid rotor performs pitching at a definite angular velocity. It was proved, by a comparison with the experimental values in [6], that the results obtained by using this formula are quite good.

CHAPTER 1. EXPERIMENTAL RESEARCH IN PITCH DAMPING

The pitch damping of a rigid rotor in a state of hovering was sought experimentally. The appearance of the vortex in the rotor wake was investigated by means of smoke experiments.

There are two types of experimental devices for measuring pitch damping. Photographs of both types are shown in Figs. 3 and 5. The salient features of both of them are as shown in Fig. 6. The rotor and its supporting frame are supported by bearings at both ends. The bearing shafts are horizontal, and the rotor hub is located on this axis. The rotor shakes like a pendulum inside a vertical plane, centering around the axis. The experiments were performed in a room with a high enough ceiling, and the angle of incidence and the direction of rotation were set so that the rotor wake would blow up toward the ceiling. Therefore, it is not necessary to consider the influence of the ground effect. Naturally, the surroundings may be considered to be windless, and the rotor current will not be disturbed by external currents.

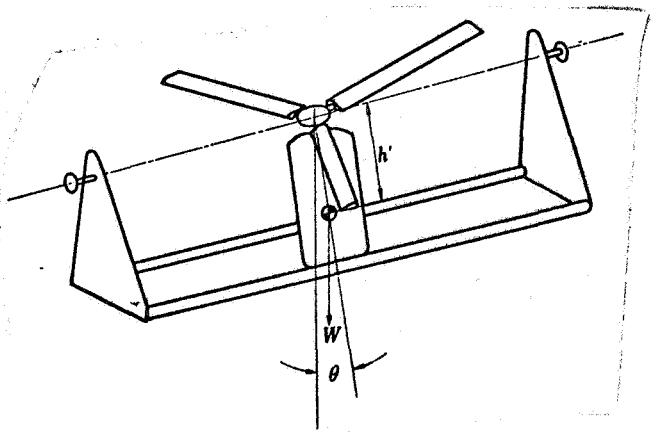

Fig. 6. Diagram of the experimental apparatus.

After setting the pitch angle of the blades and rotating the rotor at a definite speed, if one inclines the supporting frame

and then releases the hand, the pitching amplitude will be damped gradually. The pitch damping is sought from this amplitude damping. The experiments were performed with rotors having two blades and rotors having three blades.

1.1. Experiments with Rotors Having Two Blades

/9

Experimental Apparatus

A photograph of the equipment is shown in Fig. 3. Figures 7 and 8 are explanatory diagrams of the equipment and of the measuring instruments. The dimensions and other data about the equipment are shown in Table 1.

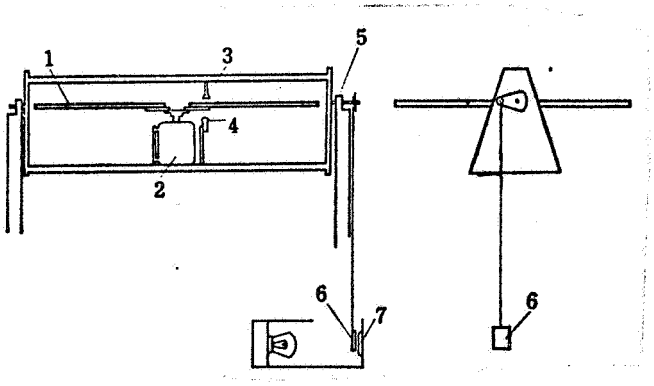

Fig. 7. Pitch damping experimental apparatus, rotor with two blades.

1. Blade
2. Motor
3. CdS
4. Miniature light bulb
5. Bearing
6. Shutter
7. CdS

Since the purpose of the experiments is to measure the pitch damping which occurs on account of the portion inhibiting the pitching, among the moments which are produced around the pitching axis by the air forces which are produced accompanying the rotation of the rotor, it is necessary to exert the utmost effort to avoid pitch damping caused by mechanical friction. Therefore, the following method was used to measure the rotor revolution speed and the pitching angle. Please refer to Fig. 7. The rotor blade (1) which is turned by the motor (2) is supported, along with the supporting frame, by bearings (5) and performs pitching. The light from the miniature light bulb (4) shines on the CdS element (3). Whenever the blade passes through this space, the light is interrupted, and the electrical resistance of the CdS element increases. /10 The current passing through the circuit in Fig. 8 into the vidicorder displays pulse-like reductions each time the blades pass through, and pulses indicating the passages of the blades are plotted on the recording chart. The revolution speed of the rotor can be discovered by reading these pulses and the time marks. The pitching angle was measured in the following manner. A douser which is eccentric from the pitching axis was lowered down and was arranged so that it would move vertically along with the pitching motion.

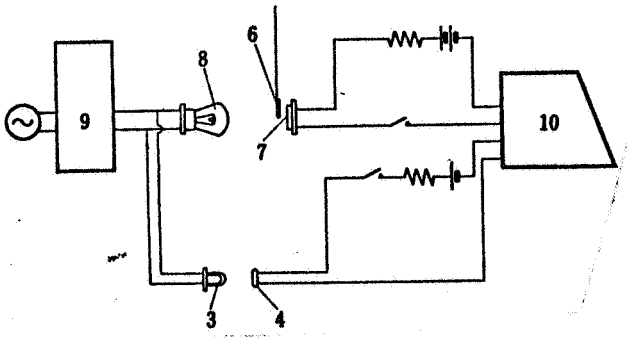

Fig. 8. Device for measuring the rotor revolution speed and pitching angle.

3. Miniature light bulb
4. CdS
6. Shutter
7. CdS
8. Light bulb
9. D.C. power source

The light quantities entering the CdS element (7) would fluctuate as the douser moved up and down, varying the input current for the vidicorder. On the recording chart is plotted the damping vibration curve corresponding to the time changes in the pitching angle. It was confirmed by static calibration that there is a linear relationship between the pitching angle and the movement of the bright spot on the recording chart. Since the time lag of the measuring system is quite small in comparison with the pitching period of 1 second, it is believed that the record indicates correctly the temporal changes in the pitching even in dynamic measurements. The light bulb (8) is turned on by means of D.C. in order to prevent the 100 c/s noise from entering the record.

TABLE 1. SPECIFICATIONS OF PITCH DAMPING EXPERIMENTAL APPARATUS A (TWO BLADES).

Rotor diameter	1100 mm
Inertia efficiency around the pitching axis	0.105 kg/m/s^2
Weight of the portion performing shaking motion	22.2 kg
Position of center of gravity (under the pitching axis)	0.18 m
Pitching period	1.02 sec
Specifications of Mounted Blade A	
Profile	NACA 0012
Radius	550 mm
Chord length	80 mm
Lock number	4.436
Flexural primary characteristic frequency	1170 rpm
Material	Japanese cypress

Measuring Methods

Before making the general measurements, the flexural primary characteristic frequency of the blades, the pitching period, and the inertia efficiency around the pitching axis are measured. The flexural primary characteristic frequency of the blades was measured by means of a Tamaru type vibration tester [29]. When the righting moment occurring when the pitching axis has been inclined and the pitching period are measured, the inertia efficiency around the pitching axis can be sought with Eq. (1.1).

$$I=\frac{WhT^2}{4\pi^2} \tag{1.1}$$

Setting the pitching angles of the blades at 0, 3, 6, 9, and 12°, we took a time record of the rotor revolution speeds and the pitching angles several times each, with the rotor revolution speeds set at 300, 400, 500, and 600 rpm for each angle of incidence. According to the time records which were obtained, the pitching can be regarded as damping vibration of a secondary system. Thus, the pitching was sought by means of Eq. (1.2).

$$\frac{\partial M}{\partial \theta}=\frac{2I\ln(\theta_2/\theta_1)}{t_2-t_1} \tag{1.2}$$

Even when the rotor is not turning, a damping coefficient of -0.002 kg/m/s is obtained for the value of $\partial M/\partial\theta$ on account of the bearing friction. Therefore, this was subtracted from the values obtained by means of Eq. (1.2), and the result was used as the measured value of the pitch damping. Vertical loads in the opposite direction are produced in both bearings by the gyro moment which occurs when pitching motion is performed by the parts in which the blades and motor are rotating. There is concern that the measured values of the pitch damping might change because of this. However, when this was investigated, it was learned in the final analysis that it is negligible. This was checked in the following manner. First, the pitch damping was compared when the motor was rotated with the blades removed and when the motor was not rotated, and it was ascertained that there were no differences. That is, it was learned that the vertical loads applied on the bearings by the gyro moment produced because of the rotation of the motor do not exert any influence on the pitch damping. Next, the load applied on the bearings by the gyro moment which occurs when the blades are rotating was calculated. It was found to be 0.21 kg even at a revolution speed of 400 rpm and an amplitude of 5.7°. It was learned that this is negligible, since it amounts to approximately 1% of the load of the motor and the supporting frame.

Measurement Results

The measured values are shown in Fig. 9. The blades are made of Japanese cypress, and twisting occurs during their rotation. It is believed that there are divergences between the set values of the pitch angles and the actual pitch angles. As is clear from the figure, it was observed that the pitch damping increases more rapidly than the rotor revolution speed increases. The solid line in the figure is the calculated values obtained with Eq. (2); the values are some two to three times greater than the measured values. When the pitch angle is 0°, the relationship between $\partial M/\partial\dot{\theta}$ and the rotor revolution speed is different from that which applies when there are other pitch angles. It is believed that this is because the state of the air currents around the rotor is entirely different, as is clear from the photograph in Fig. 51. /11

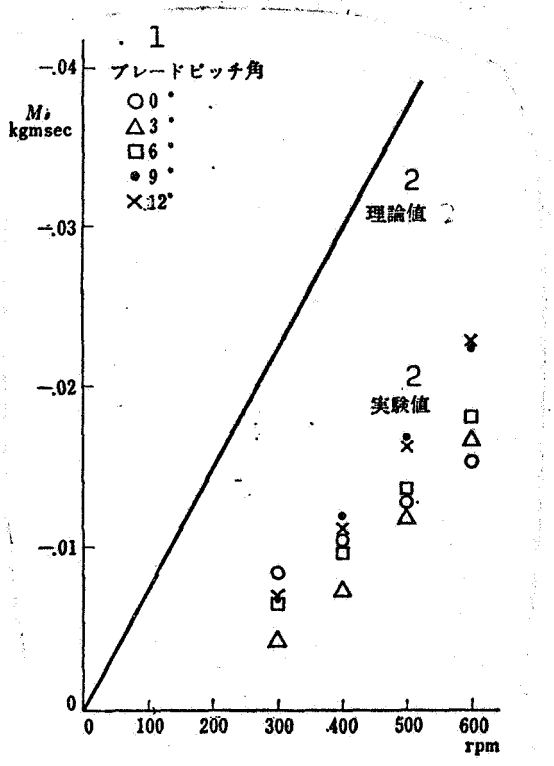

Fig. 9. Comparison of the experimental and theoretical values of pitch damping for a rotor with two blades. $R_2' = 0.55$ m; $b' = 0.040$ m; $p = 1.02$ c/s.

Key: 1. Blade pitch angle
2. Theoretical value

1.2. Experiments with Three-Bladed Rotors

The experiments with three-bladed rotors were performed by the same methods and for the same purposes as those with two-bladed rotors. A brief diagram of the equipment is shown in Fig. 10. The measurements are shown in Table 2.

Experimental Apparatus

The blades, which are made of aluminum, have a small wing chord and a great twisting rigidity. Thus, there is no need for concern about the possible occurrence of twisting deformations during rotation. The blade pitch angle can be selected at will within a range of ±16°. The following arrangement is used to measure the revolution speeds of the rotor. As is shown in Fig. 11,

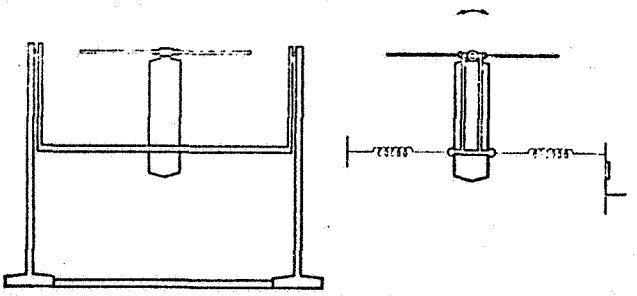

Fig. 10. Pitch camping experimental apparatus, rotor with three blades.

the light from the spotlight (1) going into the photocell (2) is interrupted every time the blades pass by, causing pulse-like variations in the photocell output. The photocell output is amplified and then introduced into the frequency counter (6). The rotor revolution speed is indicated digitally here every 10 seconds. A damping meter [8, 9] (6) was used to seek the

TABLE 2. SPECIFICATIONS FOR PITCH DAMPING EXPERIMENTAL APPARATUS B (THREE BLADES).

Rotor diameter	1800 mm
Inertia efficiency around pitching axis	0.92 kg/m/sec^2
Pitching period	1.323 sec

pitch damping from the time fluctuations of the pitching angle. The pitching angle was detected by means of a spring and straight gauge device such as that shown in Fig. 12. Whenever the rotor is inclined, the spring (1) contracts, and the leaf spring (2) deflects. There are fluctuations in the resistance of the strain gauge (3) which is attached to the leaf spring. The input current of the strain meter (4) changes in accordance with the resistance fluctuations. After the A.C. components have been amplified, the noise is removed by the low pass filter (5), and the current enters the damping meter (6). When a signal current with harmonic vibrations which are damped in the manner shown in Eq. (1.3) are applied to the damping meter, it is possible to take readings of the values of α and ω from the numerical values indicated digitally.

$$V(t) = V_0 e^{-\alpha t} \cos \omega t \qquad (1.3)$$

In pitch damping experiments, the input voltage of the damping meter is quite close to that given in the above equation. Therefore, the pitch damping was sought from the numerical values indicated by the damping meter. /12

The experiments were performed for three sets of blades with different Lock numbers and different rigidity. The characteristics of each of the blades are shown in Table 3, and

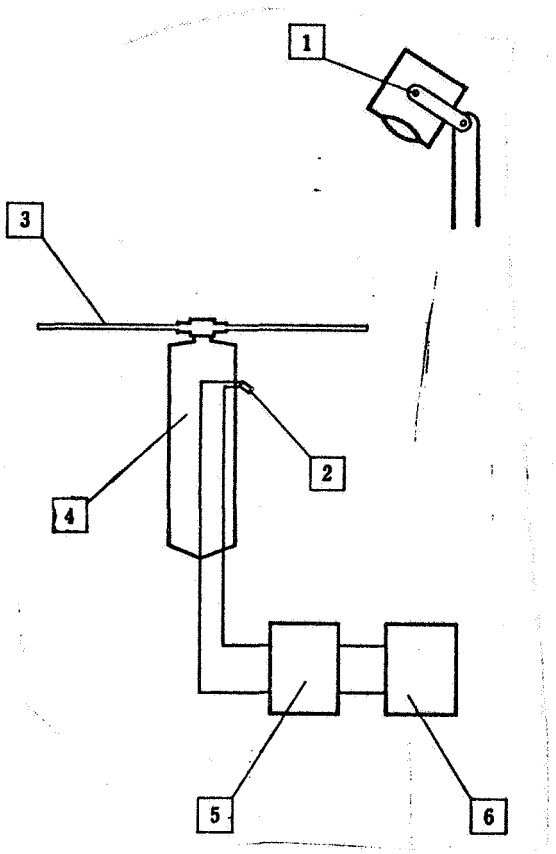

Fig. 11. Device for measuring rotor revolution speed.

1. Spotlight
2. Motor
3. Blade
4. Motor
5. Amp and filter
6. Frequency counter

a diagram is shown in Fig. 13. The B blade was a hollowed-out plate, and the C and D blades were made of a framework formed by hollowing out a plate, to which aluminum plates with a thickness of 0.5 mm were bonded. Both B and C plates have the same NACA 0012 wing section, but D is NACA 0018. Since the construction of C was different, its primary flexural characteristic frequency was 24% greater than that of B. In D, there was an increase of the wing thickness, so that the primary flexural characteristic frequency has increased by 64% over that of B.

The damping of the amplitude caused by bearing friction was corrected in the same way as in the case of the two-bladed rotors.

The influence of the vertical loads applied on the bearings by the gyro moment occurring when the rotary parts perform pitching movement is negligible. The specifications of the experimental apparatus are shown in Table 2.

Measuring Methods

The pitch angles were set at 4, 6, 8, and 10° for each of the three sets of blades mentioned above. At each pitch angle, the rotor revolution speeds were varied within the range of 250 rpm to 450 rpm, and the pitch damping was measured. Since the rotor revolution speed and the pitch damping can be indicated digitally, as was mentioned previously, it was therefore possible to obtain quite a large amount of experimental values. The primary flexural characteristic frequency of the blade was measured with a strain gauge.

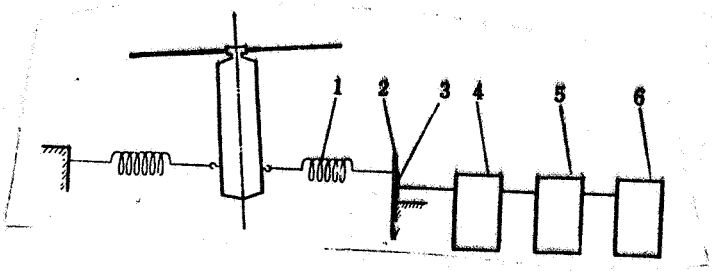

Fig. 12. Device for measuring the pitching angle.

1. Spring
2. Leaf spring
3. Strain gauge
4. Strain meter
5. Amp and filter
6. Damping meter

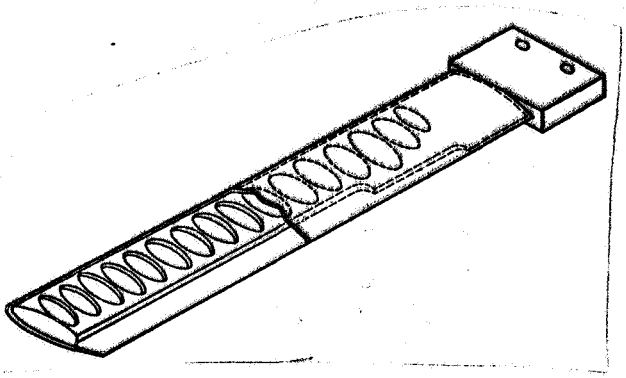

Fig. 13. Diagram of construction of C and D blades.

Measurement Results

The measurement results are shown graphically in Figs. 14-25, with the rotor revolution speed plotted on the abscissa and the pitch damping $\partial M/\partial\theta$ plotted on the ordinate.

The following conclusions can be reached from a survey of the experimental values. /16

1) The pitch damping increases abruptly, rather than increasing in linear proportion to the rotor revolution speed.

2) When there are the same pitch angles and the same rotor revolution speeds, the B blade has the greatest pitch damping. It is followed by the C blade and the D blade in descending order.

TABLE 3. CHARACTERISTICS OF B, C, AND D BLADES

	B	C	D
Wing type	NACA 0012	NACA 0012	NACA 0018
R_T	800 mm	800 mm	800 mm
c'	48 mm	48 mm	48 mm
f	1.632	2.454	1.836
ω_s	464 rpm	577 rpm	755 rpm

3) There are cases when the points are quite dispersed in the experimental results and also cases when they are hardly dispersed at all.

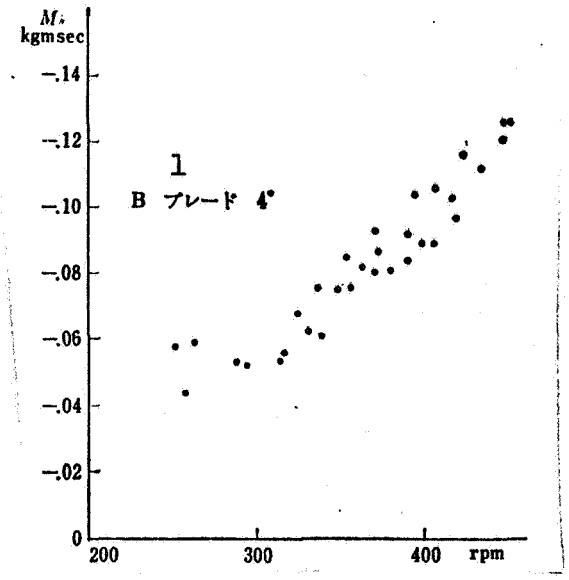

Fig. 14. Measurement results for pitch damping of three-bladed rotors. $R_2' = 0.800$ m; $b' = 0.024$ m; $p = 0.756$ c/s.

Key: 1. B blade 4°

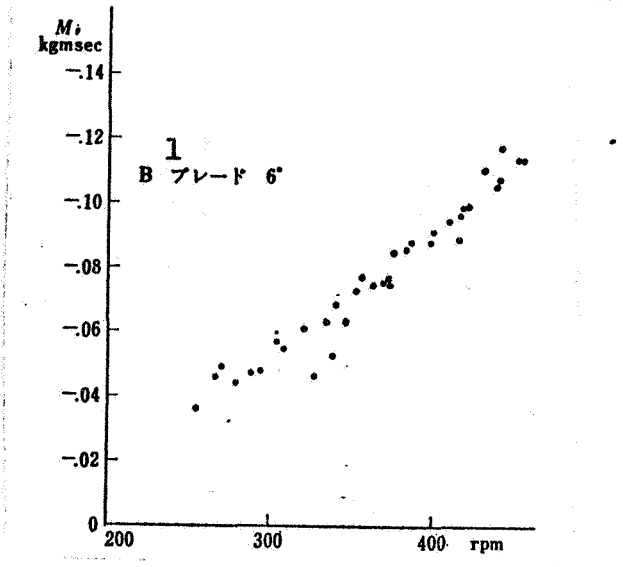

Fig. 15. Measurement results for pitch damping of three-bladed rotors. $R_2' = 0.800$ m; $b' = 0.024$ m; $p = 0.756$ c/s.

Key: 1. B blade 6°

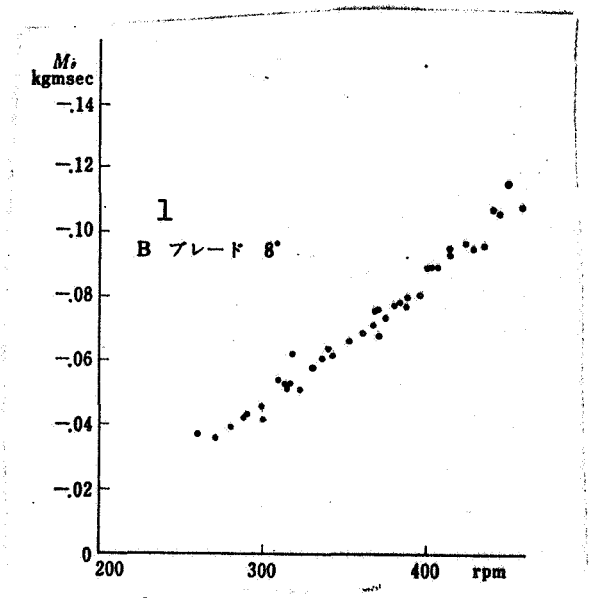

Fig. 16. Measurement results for pitch damping of three-bladed rotors. $R_2' = 0.899$ m; $b' = 0.024$ m; $p = 0.756$ c/s.

Key: 1. B blade 8°

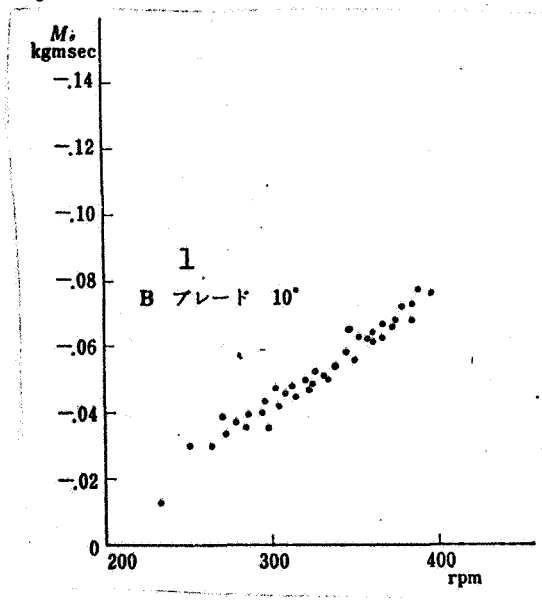

Fig. 17. Measurement results for pitch damping of three-bladed rotors. $R_2' = 0.800$ m; $b' = 0.024$ m; $p = 0.756$ c/s.

Key: 1. B blade 10°

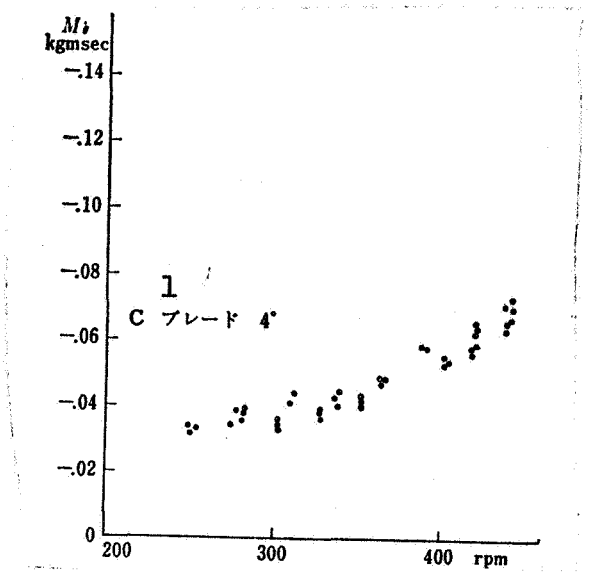

Fig. 18. Measurement results for pitch damping of three-bladed rotors. $R_2' = 0.800$ m; $b' = 0.024$ m; $p = 0.756$ c/s.

Key: 1. C blade 4°

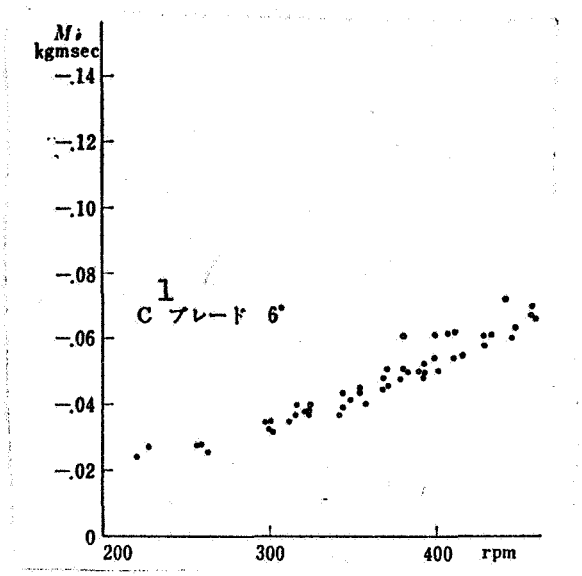

Fig. 19. Measurement results for pitch damping of three-bladed rotors. $R_2' = 0.800$ m; $b' = 0.024$ m; $p = 0.756$ c/s.

Key: 1. C blade 6°

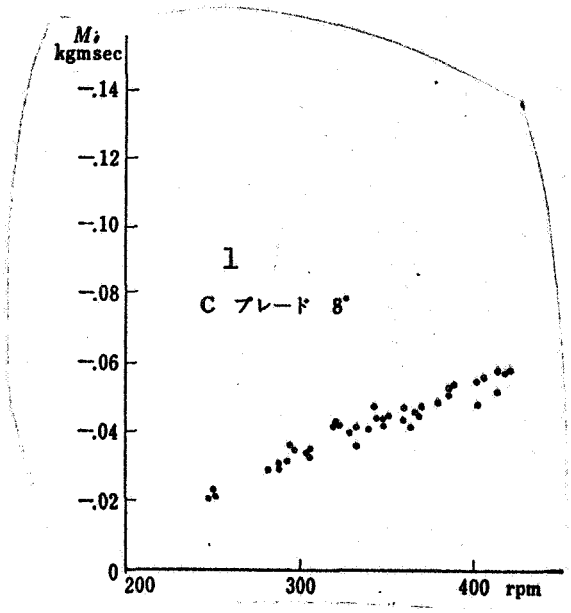

Fig. 20. Measurement results for pitch damping of three-bladed rotors. $R_2' = 0.800$ m; $b' = 0.024$ m; $p = 0.756$ c/s.

Key: 1. C blade 8°

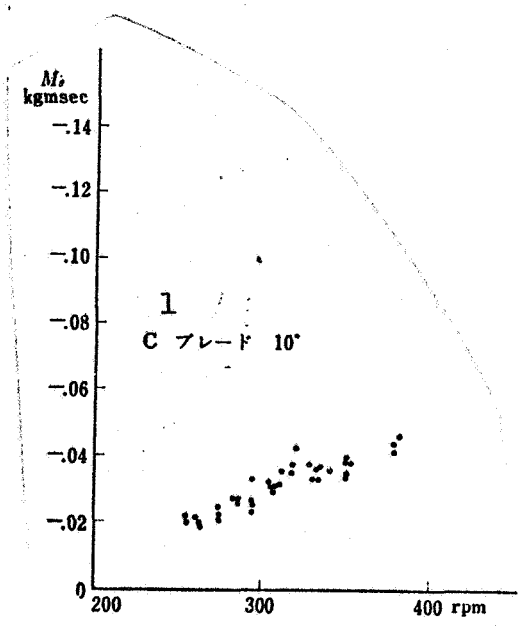

Fig. 21. Measurement results for pitch damping of three-bladed rotors. $R_2' = 0.800$ m; $b' = 0.024$ m; $p = 0.756$ c/s.

Key: 1. C blade 10°

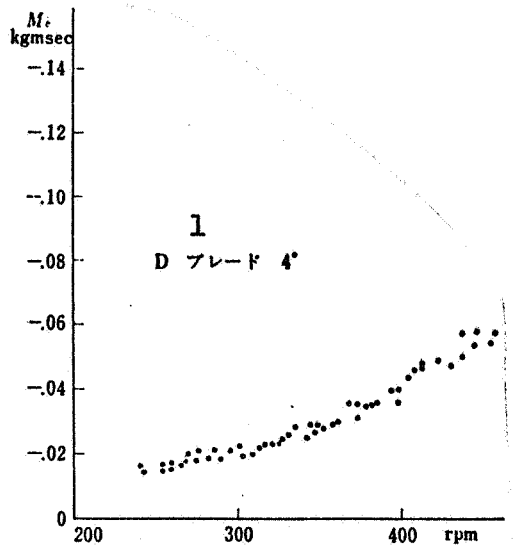

Fig. 22. Measurement results for pitch damping of three-bladed rotors. $R_2' = 0.800$ m; $b' = 0.024$ m; $p = 0.756$ c/s.

Key: 1. D blade 4°

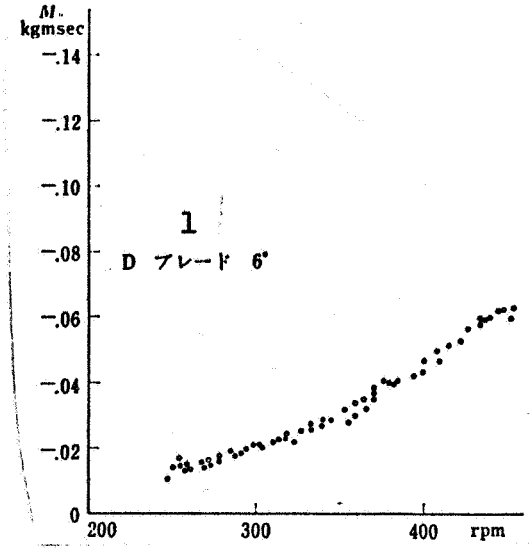

Fig. 23. Measurement results for pitch damping of three-bladed rotors. $R_2' = 0.800$ m; $b' = 0.024$ m; $p = 0.756$ c/s.

Key: 1. D blade 6°

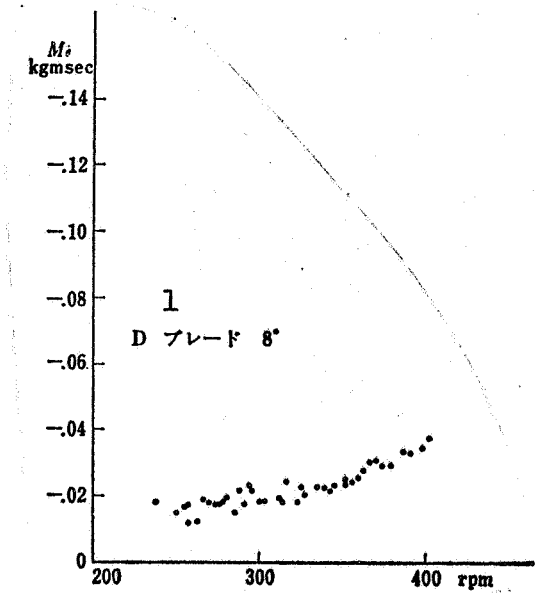

Fig. 24. Measurement results for pitch damping of three-bladed rotors. $R_2' = 0.800$ m; $b' = 0.024$ m; $p = 0.756$ c/s.

Key: 1. D blade 8°

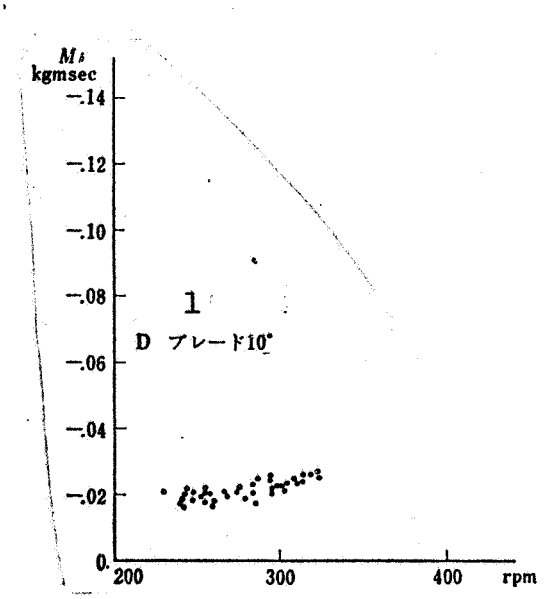

Fig. 25. Measurement results for pitch damping of three-bladed rotors. $R_2' = 0.800$ m; $b' = 0.024$ m; $p = 0.756$ c/s.

Key: 1. D blade 10°

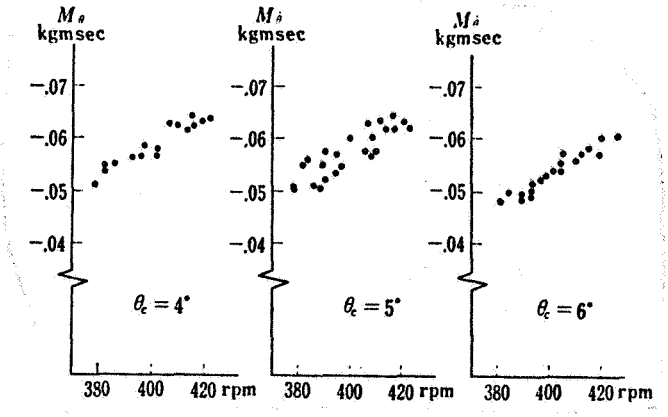

Fig. 26a. Pitch damping of C blades at rotor revolution speeds in the vicinity of 400 rpm. $R_2' = 0.800$ m; $b' = 0.024$ m; $p = 0.756$ c/s.

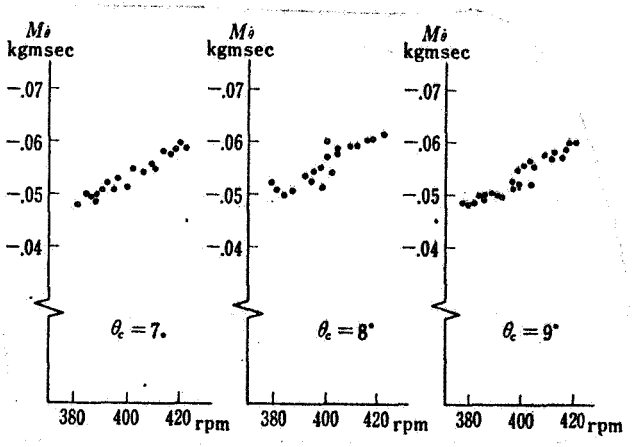

Fig. 26b. Pitch damping of C blades at rotor revolution speeds in the vicinity of 400 rpm. $R_2' = 0.800$ m; $b' = 0.024$ m; $p = 0.756$ c/s.

4) In the B and C blades, the pitch damping decreases considerably when there is a pitch angle of 10°. In the D blade, it decreases when there is a pitch angle of 8°.

5) In the D blade, the increase of the pitch damping together with the increase of the rotor revolution speed is much more pronounced than in the other types of blades.

In addition to the series of measurements already mentioned, the fluctuations of the pitch damping were investigated for the C blade by varying the pitch angle from 4° to 9° with a revolution speed in the vicinity of 400 rpm. The results are shown in Fig. 26.

In all of the experimental values, the pitch damping was much smaller than the value indicated by Eq. (2). This was true in the same way as in the results for two-bladed rotors.

1.3. Aeroelastic Analysis of Pitch Damping

As was mentioned above, even when the other conditions are exactly the same, there will be quite far-reaching changes in the pitch damping when the flexural rigidity of the blades changes. Thus, it is desired to make clear the relationship between the flexural rigidity of the blades and the pitch damping.

According to the studies of Naito, it has been found that when rotor blades having the same geometric shape are rotated at the /17
same pitch angle and the same revolution speed, the pitch damping will be greater the greater is the primary flexural characteristic frequency of the blades. Furthermore, the pitch damping does not increase in linear proportion to the rotor revolution speed, but the rate of increase of the pitch damping will be greater the higher is the revolution speed.

According to the studies of Townsent, in blades in which bending and twisting deformations do not occur at all, the pitch damping is linearly proportional to the rotor revolution speed, as in Eq. (1).

When we consider these two facts in conjunction with each other, it would appear that the pitch damping in actual blades can be divided up into a portion which is in linear proportion to the revolution speed and a portion which varies nonlinearly with respect to the revolution speed. As Townsent assumed, the former is pitch damping which occurs in rotor blades where elastic deformations do not occur. It is generated directly by the rotor surface's pitching motion. On the other hand, in the latter case, elastic deformations occur in the blades together with the pitching motion of the rotor, and the pitch damping is generated through these deformations. The latter is powerfully influenced by the primary flexural characteristic frequency of the blade.

Let us suppose, for the sake of argument, that the pitch damping of rotors can be divided up systematically into these two clear-cut divisions. If this were possible, the former, $M_{\dot{\theta}_R}$, that is, the pitch damping generated directly by the pitching motion of the rotor surface, would be linearly proportional to the rotor revolution speed. All blades ought to have the identical value as long as the rotor revolution speed, the pitch angle, and the geometric conditions were the same. Let us consider the method of abstracting these portions which are unrelated to blade deformation from the pitch damping experimental data and of comparing the values with Townsent's calculated values.

It was assumed that the air forces operating on the rotor blades can be calculated simply by means of quasi-steady two-dimensional theory. This problem was analyzed by the Rayleigh-Ritz method, taking into consideration the fact that bending elastic deformations occur in the blades. We will consider cases in which the rotating angular velocity of the rotor has a constant value Ω and the rotor surface performs a sinusoidal pitching motion expressed by $\theta = \bar{\theta} \sin pt$. We sought the bending elastic deformations of the blades which occur together with pitching. Next, we calculated the pitch damping from the temporal variations in the moment generated around the pitching axis. It is assumed that the air forces operate on the central line of the blade and that the mass is also concentrated on the central line. It is assumed that the blades only undergo bending deformations

but do not become elongated. A simple bending motion was assumed.

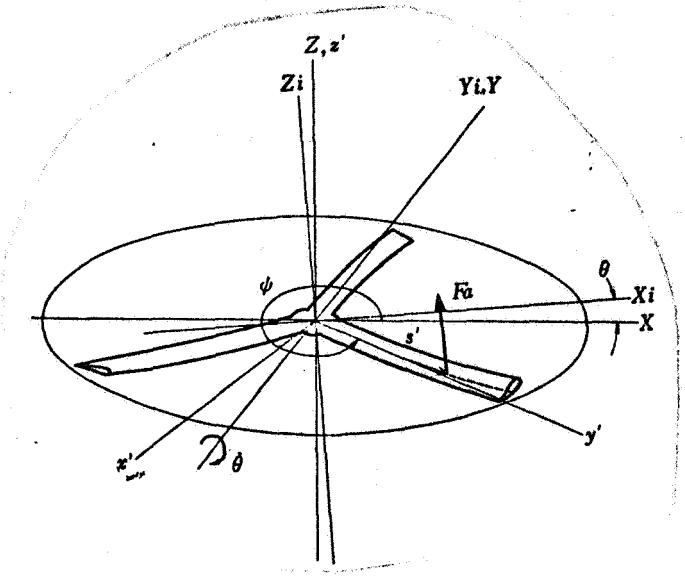

Fig. 27. Bending deformations of blades which occur together with pitching.

In Fig. 27, the XYZ coordinate system and the x'y'z' coodinate system used during analysis are shown in contrast with the $X_iY_iZ_i$ coordinate system fixed in space. The XYZ system is a dynamic coordinate system with a pitching angular velocity $\dot{\theta}_j$. The x'y'z' coordinate system is a dynamic coordinate system rotating around the pitching axis and the shaft axis. Its angular velocity is

$$\dot{\theta}j+\Omega k=-\dot{\theta}\cos\psi_q i_q^*+\dot{\theta}\sin\psi_q j_q^*+\Omega k_q^* \quad (1.4)$$

The position vector r at a point on the blade can be written as follows:

$$r=y'_q j_q^*+z_q' k_q^* \quad (1.5)$$

The velocity vector v at the same point can be written as follows:

/1

$$\begin{aligned} v=&(z'_q\dot{\theta}\sin\psi_q-y_q'\Omega)i_q^*\\ &+(\dot{y}_q'+z_q'\dot{\theta}\cos\psi_q)j_q^*\\ &+(\dot{z}_q'-y_q'\dot{\theta}\cos\psi_q)k_q^* \end{aligned} \quad (1.6)$$

The length along the blade measured from the hub center toward the tip is s'. When there are Q blades, from blade 0 to blade Q-1, the kinetic energy of the blade is:

$$T=\sum_{q=0}^{Q-1}\frac{1}{2}\int_0^{s'}\nu|v_q|^2ds' \quad (1.7)$$

When the blades undergo bending deformation, the strain energy stored up inside the blades will be:

$$U=\sum_{q=0}^{Q-1}\frac{1}{2}\int_0^{S'}EI\left(\frac{\partial^2 z'_q}{\partial s'^2}\right)^2 ds' \tag{1.8}$$

Next, let us consider the air forces operating on the blades. It is assumed that the air forces operate vertically on the center line of the blades and that they are within a plane including the z' axis. This signifies that we are ignoring the drag operating on the blades, but this is because the contribution of the drag to the pitch damping is a secondary microquantity. The magnitude of the air forces operating on the portion of the blade with length ds' is:

$$F_{Aq}ds'=\rho ab' y_q'^2\Omega^2\left(\theta_0-\frac{\dot{z}_q'-y_q'\dot{\theta}\cos\phi_q+v_i}{y'\Omega}\right)ds' \tag{1.9}$$

The directional cosine vector with respect to the x'y'z' coordinate system of the air force vector is:

$$-\partial z_q'/\partial s' j_q^*+\partial y_q'/\partial s' k_q^*$$

and the air force vector is:

$$F_{Aq}ds'=\left(-F_{Aq}\frac{\partial z_q'}{\partial s'}j_q^*+F_{Aq}\frac{\partial y_q'}{\partial s'}k_q^*\right) \tag{1.10}$$

The bending mode function of the blade is expressed as $\mu(s)$. The deformation of the blade at this time can be written as follows, using the general coordinate f:

$$z_q'=S'\mu(s)f_q \tag{1.11-1}$$

$$y_q'=S'\int_0^s\sqrt{1-(d\mu/ds)^2 f_q^2}\,ds \tag{1.11-2}$$

$\mu(s)$ is selected so that $\mu(s) = 1$ when $s = 1$. $S'f_q$ is the amount of deflection at the blade tip.

We are here considering a case in which the rolling motion of the rotor blade system is constrained and the rotating angular velocity Ω of the rotor is constant. Thus, we will describe the movement in which the general coordinates are considered to be the f_q, which are Q in number, representing the deformation of the blades and the θ, which represents the pitching. The virtual displacement δu_q which occurs at one point $(0, y_q', z_q')$ on the blade when virtual displacements δf_q and $\delta\theta$ have occurred in the general coordinates is:

$$\begin{aligned}\delta u_q &= r(f_q+\delta f_q, \theta+\delta\theta) - r(f_q, \theta) \\ &= \frac{\partial y_q'}{\partial f_q}\delta f_q j_q^* + \frac{\partial z'_q}{\partial f_q}\delta f_q k_q^* \\ &\quad + (\delta\theta j)\times(y_q' j_q^* + z'_q k_q^*)\end{aligned}$$

As for the external forces operating on the blades, we consider the air force as well as the moment M_Y which is imposed from outside in order to continue the pitching. The virtual work is:

$$\delta w = \sum_{q=0}^{Q-1}\int_{S_R'}^{S'} F_A \cdot \delta u_q ds' + [M_Y j]\cdot[\delta\theta j]$$

If we take the variations concerning δf and $\delta\theta$, the general forces will be:

$$Qf_q = -F_{Aq}\frac{\partial z_q'}{\partial s'}\frac{\partial y'}{\partial f_q} + F_{Aq}\frac{\partial y_q'}{\partial s'}\frac{\partial z_q'}{\partial f_q} \tag{1.12-1}$$

$$\begin{aligned}Q_\theta = &-\sum_{q=0}^{Q-1} F_{Aq}\frac{\partial z_q'}{\partial s'} z_q' \cos\phi_q \\ &-\sum_{q=0}^{Q-1} F_{Aq}\frac{\partial y_q'}{\partial s'} y'_q \cos\phi_q + M_Y\end{aligned} \tag{1.12-2}$$

The Lagrange kinetic equations are:

$$\frac{d}{dt}\left(\frac{\partial T}{\partial \dot{f}_q}\right) - \frac{\partial T}{\partial f_q} + \frac{\partial U}{\partial f_q} = Q_{fq} \tag{1.13-1}$$

$$\frac{d}{dt}\left(\frac{\partial T}{\partial \dot{\theta}}\right) - \frac{\partial T}{\partial \theta} + \frac{\partial U}{\partial \theta} = Q_\theta \tag{1.13-2}$$

When f_q, $\dot{f}_q$, and $\dot{\theta}$ are minute, these equations can be written approximately in the following manner:

$$\begin{aligned}
&\int_0^1 \nu\mu_{(s)}^2 ds\ddot{f}_q+\rho aS'^2\Omega\int_{s_R}^1 \frac{b'}{S'} s\mu^2(s)ds\dot{f}_q \\
&\quad+\left\{\Omega^2\int_0^1 \nu s\int_0^s\left(\frac{d\mu}{ds}\right)^2 dsds\right. \\
&\quad\left.+\frac{1}{S'^4}\int_0^1 EI\left(\frac{d^2\mu}{ds^2}\right)^2 ds\right\}f_q \\
&=\int_0^1 \nu s\mu_{(s)}ds\cos\psi_q\ddot{\theta}-2\int_0^1 \nu s\mu_{(s)}ds\sin\psi_q\Omega\dot{\theta} \\
&\quad+\rho aS'^2\int_{s_R}^1 \frac{b'}{S'} s^2\mu_{(s)}ds\cos\psi_q\Omega\dot{\theta} \\
&\quad+\rho aS'^2\int_{s_R}^1 \frac{b'}{S'}\left\{s^3\Omega^2\theta_c-s\Omega\frac{v_i}{S'}\right\}\mu_{(s)}ds
\end{aligned} \tag{1.14-1}$$

$$\begin{aligned}
&\sum_{q=0}^{Q-1}\int_{s_R'}^{S'} F_{Aq}s'\cos\psi_q ds'+\sum_{q=0}^{Q-1}\int_0^{S'}(-\nu s'z_q'\Omega^2\cos\psi_q \\
&\quad-\nu\ddot{z}_q's'\cos\psi_q+\nu s'^2\ddot{\theta}\cos^2\psi_q \\
&\quad-2\nu s'^2\Omega\dot{\theta}\sin\psi_q\cos\psi_q)ds'=M_Y
\end{aligned} \tag{1.14-2}$$

Thus, we have obtained the kinetic equation for flapping in cases when a pitching moment M_Y is given from outside to rotor blades with constrained rolling motion under conditions of a uniform rotor rotating angular velocity and they continue sinusoidal pitching $\theta = \bar{\theta}\sin pt$. We have also obtained the formula to obtain the necessary pitching moment M_Y. A_1, A_2, D_1, D_2, and A_3 are defined as follows. /19

$$\begin{aligned}
A_1&\equiv\rho aS'^2\int_{s_R}^1 \frac{b'}{S'} s\mu_{(s)}^2 ds\Big/\int_0^1 \nu\mu_{(s)}^2 ds \\
A_2&\equiv\rho aS'^2\int_{s_R}^1 \frac{b'}{S'} s^2\mu_{(s)}ds\Big/\int_0^1 \nu\mu_{(s)}^2 ds \\
D_1&\equiv\int_0^1 \nu s\mu_{(s)}ds\Big/\int_0^1 \nu\mu_{(s)}^2 ds \\
D_2&\equiv\int_0^1 \nu s\int_0^s\left(\frac{d\mu}{ds}\right)^2 dsds\Big/\int_0^1 \nu\mu_{(s)}^2 ds \\
A_3&\equiv\rho aS'^2\int_{s_R}^1 \frac{b'}{S'}\left\{s^3\Omega^2\theta_c-s^2\Omega\frac{v_i}{S'}\right\}\mu_{(s)}ds\Big/\int_0^1 \nu\mu_{(s)}^2 ds
\end{aligned}$$

If the downwash on the rotor surface v_i has a uniform value even when the rotor is performing pitching motion, the last term on the right side of Eq. (14-1) will be uniform and will determine the coning of the blades.

In actual blades, it is extremely difficult to seek with accuracy the EI distribution and the bending mode and to calculate

$$\int_0^1 EI\left(\frac{d^2\mu}{ds^2}\right)^2 ds \Big/ S^4$$

Therefore, the following method is used. In stationary blades, in accordance with (1.14-1), the bending vibration equation of the blades can be written as follows:

$$\int_0^1 \nu\mu_{(s)}^2 ds\ddot{f} + \frac{1}{S^4}\int_0^1 EI\left(\frac{d^2\mu}{ds^2}\right)^2 dsf = 0 \tag{1.15}$$

The primary flexural characteristic frequency of the stationary blades can be measured easily. If this is written as ω_B,

$$\omega_B^2 = \frac{1}{S^4}\int_0^1 EI\left(\frac{d^2\mu}{ds^2}\right)^2 ds \Big/ \int_0^1 \nu\mu_{(s)}^2 ds \tag{1.16}$$

If we use ω_B and the previously defined A_1, A_2, D_1, D_2, and A_2, Eq. (1.14-1) can be written as follows:

$$\ddot{f}_q + A_1\Omega\dot{f}_q + \left(D_2 + \frac{\omega_B^2}{\Omega^2}\right)\Omega^2 f_q = D_1\cos\phi_q\ddot{\theta} - 2D_1\sin\phi_q\Omega\dot{\theta} + A_2\cos\phi_q\Omega\dot{\theta} + A_3 \tag{1.17}$$

In the question of pitch damping, the acceleration frequency is approximately Ω, and $\sqrt{D_2 + (\omega_B^2/\Omega^2)}\,\Omega$ is greater than Ω. In cases when $\theta = \bar{\theta}\sin pt$, the particular solution of Eq. (1.17) is:

$$f_q = {}_0f + f_{S+}\sin(\phi_q + pt) + f_{C+}\cos(\phi_q + pt) + f_{S-}\sin(\phi_q - pt) + f_{C-}\cos(\phi_q - pt) \tag{1.18}$$

Here we use $p \equiv p/\Omega$ and write f_{S+}, f_{C+}, f_{S-}, f_{C-}, and ${}_0f$.

$$f_{S+}=\frac{-D_1 p\,(1+p/2)\{D_2+\omega_B^2/\Omega^2-(1+p)^2\}+\frac{1}{2}A_1A_2p(1+p)}{\{D_2+\omega_B^2/\Omega^2-(1+p)^2\}^2+A_1^2(1+p)^2}\bar{\theta} \tag{1.19-1}$$

$$f_{C+}=\frac{A_1D_1p(1+p/2)(1+p)+\frac{1}{2}A_1p\{D_2+\omega_B^2/\Omega^2-(1+p)^2\}}{\{D_2+\omega_B^2/\Omega^2-(1+p)^2\}^2+A_1^2(1+p)^2}\bar{\theta} \tag{1.19-2}$$

$$f_{S-}=\frac{-D_1 p\,(1-p/2)\{D_2+\omega_B^2/\Omega^2-(1-p)^2\}+\frac{1}{2}A_1A_2p(1-p)}{\{D_2+\omega_B^2/\Omega^2-(1-p)^2\}^2+A_1^2(1-p)^2}\bar{\theta} \tag{1.19-3}$$

$$f_{C-}=\frac{A_1D_1p(1-p/2)(1-p)+\frac{1}{2}A_1p\{D_2+\omega_B^2/\Omega^2-(1-p)^2\}}{\{D_2+\omega_B^2/\Omega^2-(1-p)^2\}^2+A_1^2(1-p)^2}\bar{\theta} \tag{1.19-4}$$

$${}_0f=\frac{A_3}{(D_2+\omega_B^2/\Omega^2)\Omega^2} \tag{1.19-5}$$

${}_0f$ is coning.

If f_q is found, z_q', $\dot{z}_q'$, $\tilde{z}_q'$, y_q' can be sought. Assuming in (1.14-2) that $\theta = \bar{\theta}\sin pt$, if we express z_q', z_q', $\tilde{z}_q'$, y_q' using f_q, it is possible to seek M_y. Using the method shown in Appendix A, we can express the pitch damping derivative as follows:

$$M_\dot{\theta}\equiv-\int_0^{2\pi/p}M_Y\theta dt/\pi\bar{\theta}^2p \tag{1.20}$$

If we use Eq. (1.14-2),

$$\begin{aligned}M_\dot{\theta}=&-\int_0^{2\pi/p}\sum_{q=0}^{Q-1}\int_{S_R'}^{S'}F_{Aq}s'\theta\cos\psi_q ds'/\pi\bar{\theta}^2p\\&-\int_0^{2\pi/p}\sum_{q=0}^{Q-1}\int_0^{S'}(-\nu s'z_q'\Omega^2\cos\psi_q-\nu\ddot{z}_q's'\cos\psi_q\\&+\nu s'^2\ddot{\theta}\cos^2\psi_q-2\nu s'^2\Omega\dot{\theta}\sin\psi_q\cos\psi_q)\\&\times ds'\dot{\theta}dt/\pi\bar{\theta}^2p\end{aligned} \tag{1.21}$$

The first term on the right side is the contribution of the moment made up by the air forces operating on the blade, and the second term on the right side is the contribution of the moment made up by the inertial force operating on the blade.

When calculations are carried out,

$$M_\phi = -\frac{Q}{2}\rho a S'^5\Omega\int_{s_R}^1 s^3\frac{b'}{S'}ds + \frac{Q}{2}\rho a S'^5\Omega \times \frac{f_{S+}(1+p)+f_{S-}(1-p)}{\bar{\theta}p}\int_{s_R}^1 s^2\mu\frac{b'}{S'}ds - \frac{Q}{2}S'^3\Omega\frac{f_{C+}(2p+p^2)+f_{C-}(-2p+p^2)}{\bar{\theta}p} \times\int_0^1 \nu\mu s ds \qquad (1.22)$$

/20

The sum of the first and second terms on the right side of Eq. (1.22) is the same as the first term on the right side of Eq. (1.21). The third term on the right side of Eq. (1.22) is the same as the second term on the right side of Eq. (1.21). At first glance, the third term on the right side of Eq. (1.22) gives the impression that damping occurs even in cases when air forces are not operating on the rotor blades. However, actually, when a is 0, A_1 and A_2 will be 0; and, as is seen in Eqs. (1.19-2) and (1.19-4), f_{C+} and f_{C-} will be 0. Consequently, the third term on the right side of Eq. (1.22) will be 0. In equations expressing damping in systems with a great degree of freedom, inertia terms are frequently seen to appear. The vibration damper [31] is a simple example of this. The significance of this term has been discussed in Appendix C.

The pitch damping sought in the experiments described in sections 1 and 2 corresponds to the entire right side of Eq. (1.22). When bending elastic deformation does not occur in the blades, the second and third terms on the right side of Eq. (1.22) will be 0, and the only pitch damping coefficient will be the first term on the right side. This is the pitch damping $M_{\dot{\theta}R}$ which is generated directly by the pitching on the rotor surface, which was already described.

Here, let us define K_E in the following manner:

$$K_E = \frac{M_\phi}{M_{\phi R}} = \frac{\left[-\frac{Q}{2}\rho a S'^5\Omega\int_{s_R}^1 s^3\frac{b'}{S'}ds + \frac{Q}{2}\rho a S'^5\Omega\frac{f_{S+}(1+p)+f_{S-}(1-p)}{\bar{\theta}p}\int_{s_R}^1 s^2\mu\frac{b'}{S'}ds - \frac{Q}{2}S'^3\Omega\frac{f_{C+}(2p+p^2)+f_{C-}(-2p+p^2)}{\bar{\theta}p}\int_0^1\nu\mu s ds\right]}{-\frac{Q}{2}\rho a S'^5\Omega\int_{s_R}^1 s^3\frac{b'}{S'}ds} \qquad (1.23)$$

As $\mu_{(s)}$ here let us use

$$\mu_{(s)} = 2s^2 - \frac{4}{3}s^3 + \frac{1}{3}s^4 \qquad (1.24)$$

which satisfies the mechanical and geometrical conditions on both ends of the blade and which is also the simplest form. If we suppose that the chord length of the blade and the mass distribution are uniform, A_1, A_2, D_1, and D_2 will be:

$$A_1=\frac{73}{91}\frac{\rho ab'S'}{\nu}$$

$$A_2=\frac{639}{728}\frac{\rho ab'S'}{\nu}$$

$$D_1=\frac{9}{8}$$

$$D_2=\frac{61}{52}$$

K_E is a function when the Lock number is $\gamma = 6\rho ab'S'/\nu$, ω_B/Ω, p/Ω. It can be calculated in the manner demonstrated in Figs. 28 to 31.

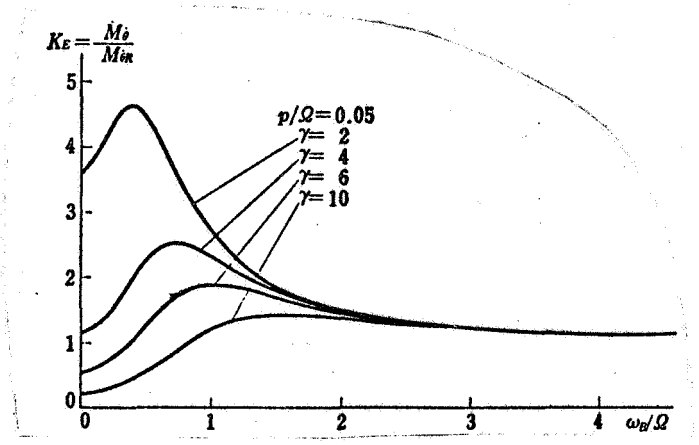

Fig. 28. Effects of blade rigidity on pitch damping.

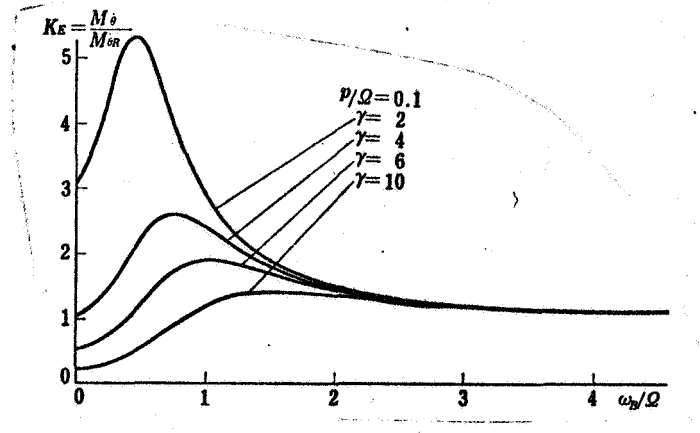

Fig. 29. Effects of blade rigidity on pitch damping.

When the measured values shown in Figs. 16 to 27 are divided by the corresponding K_E, we will obtain the pitch damping coefficients of imaginary blades in which no bending deformations at all will occur. The measured values of the pitch damping coefficients were divided by K_E and were then rendered nondimensional by using Eq. (2). The results are shown in Figs. 32 to 43. It is clear from these figures that in most cases the nondimensionalized pitch damping derivatives will have a more or less uniform value even when the rotor revolution speed changes. It is believed, on this account, that the pitch damping can be separated into two portions: $M_{\dot\theta_E}$, the portion which is generated through elastic deformation of the blades; and $M_{\dot\theta_R}$, the portion which is generated directly by pitching of the rotor surface. Not all of the values given in Figs. 32 to 43 are the same for all the blades.

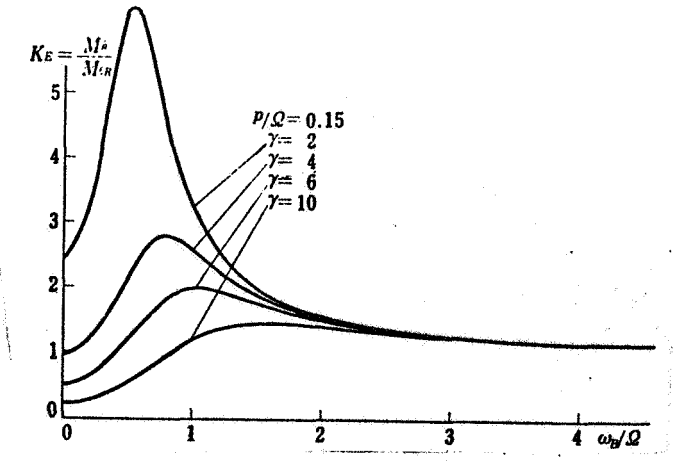

Fig. 30. Effects of blade rigidity on pitch damping.

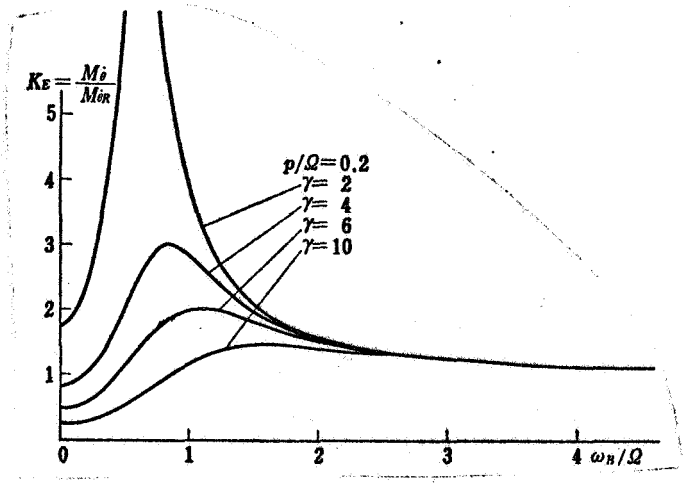

Fig. 31. Effects of blade rigidity on pitch damping.

The reason for this is attributable, not only to the measurement errors accompanying the experiments, but also to the fact that the air forces and the bending mode were supposed in simple form when K_E was sought.

It is clear from Figs. 32 to 43 that the pitch damping which is generated directly by pitching of the rotor surface is about one-fourth of the value calculated using Eq. (2). In Eq. (2), the pitch damping is calculated by means of strip theory, using the air forces sought by two-dimensional quasi-steady theory. Therefore, it was found that in problems where one is seeking the pitch damping, it is not appropriate to use such a simple method to seek the air forces. The fact that the air forces governing the pitch damping are about one-fourth of the air forces calculated by two-dimensional quasi-steady

Caption to Figs. 32-43. Comparison of measured values of non-dimensionalized pitch damping from which the effect of the blade bending deformation has been eliminated with various theoretical values.

A. Two-dimensional quasi-steady theory. B. Two dimensional unsteady theory. C. Two-dimensional unsteady theory including the wake vortex. D. Three-dimensional quasi-steady theory. E. Three-dimensional unsteady theory. F. Three-dimensional quasi-steady theory including the effects of the wake vortex. G. Three-dimensional quasi-steady theory including the wake vortex and also the fluctuations of the blade distance.

General Key:

1. Experimental values
2 B (C) blade, ...°

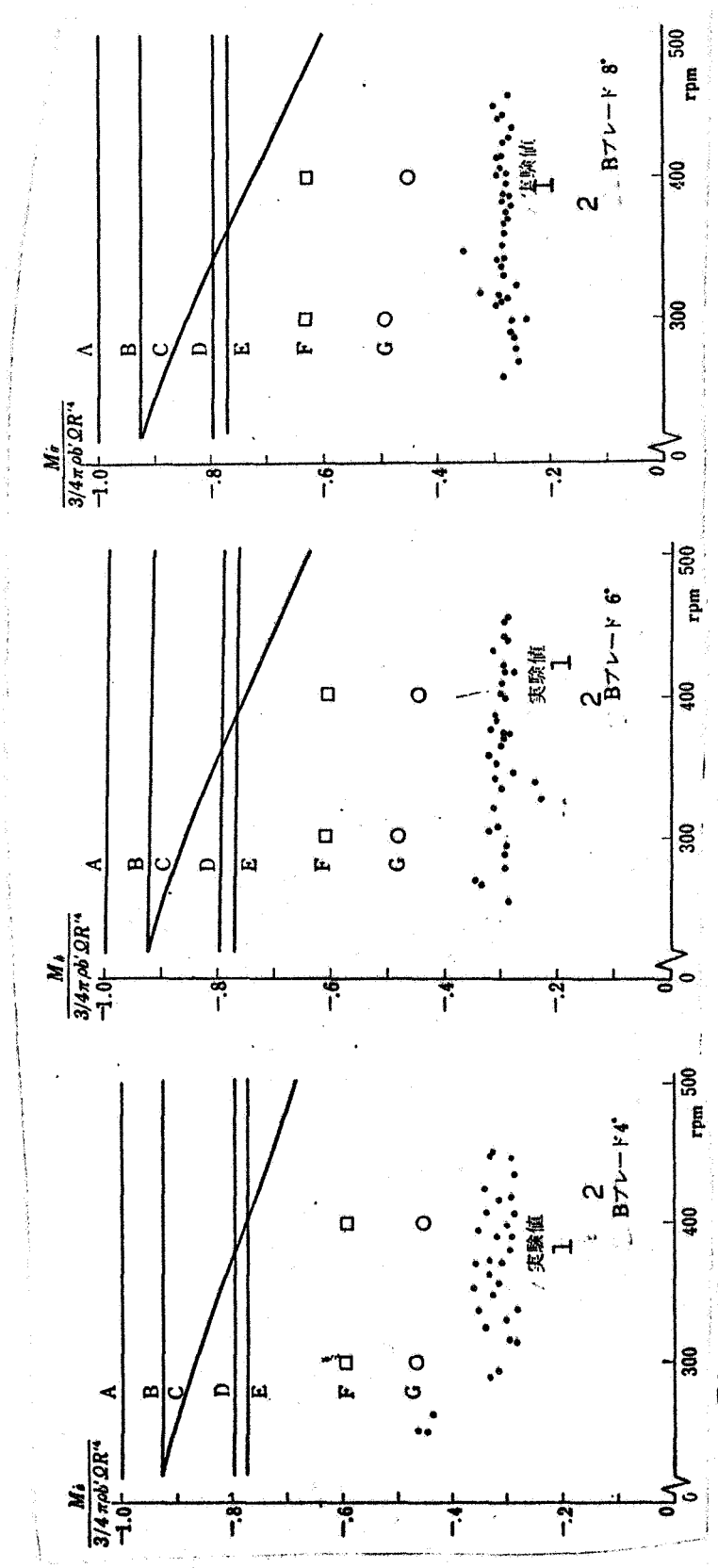

Fig. 32.

Fig. 33.

Fig. 34.

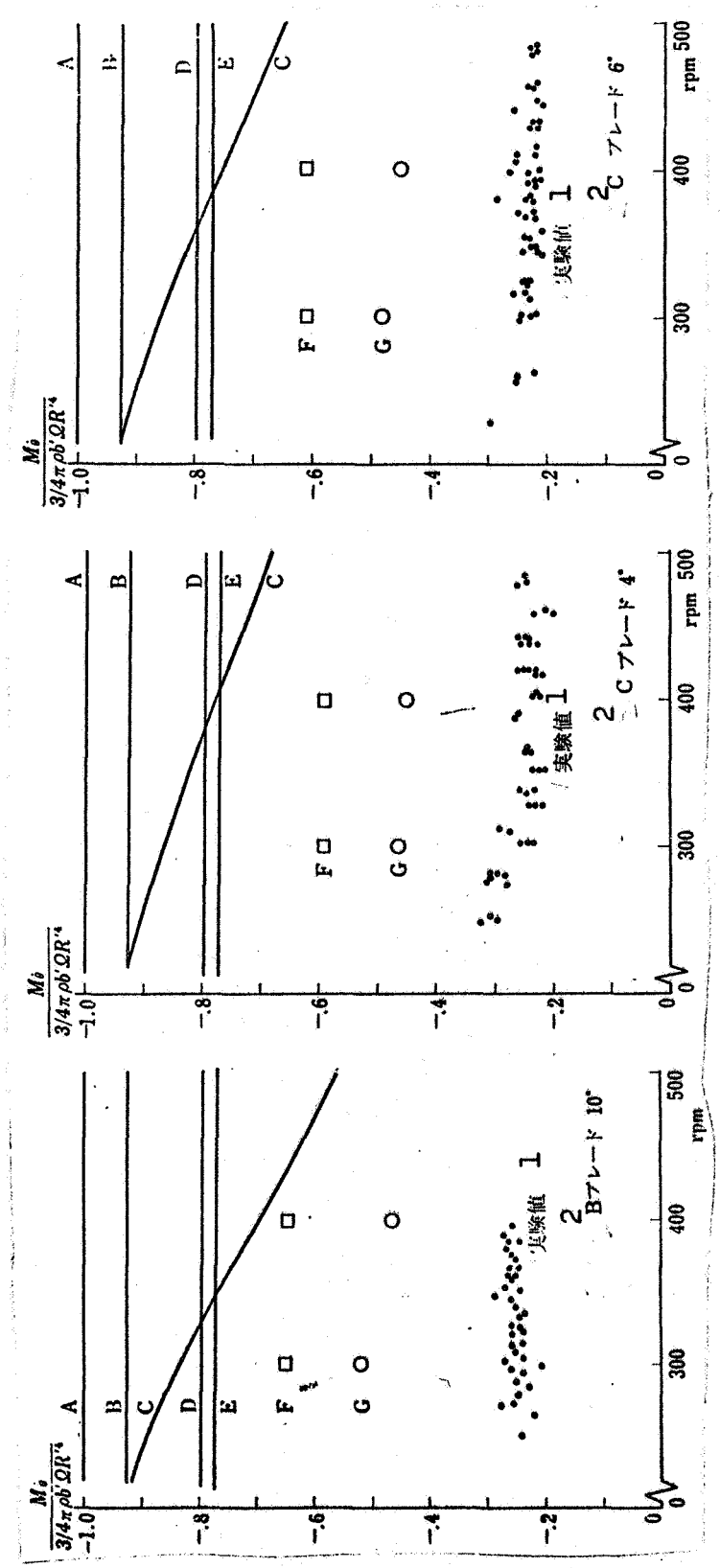

Fig. 35.

Fig. 36.

Fig. 37.

Fig. 38.

Fig. 39.

Fig. 40.

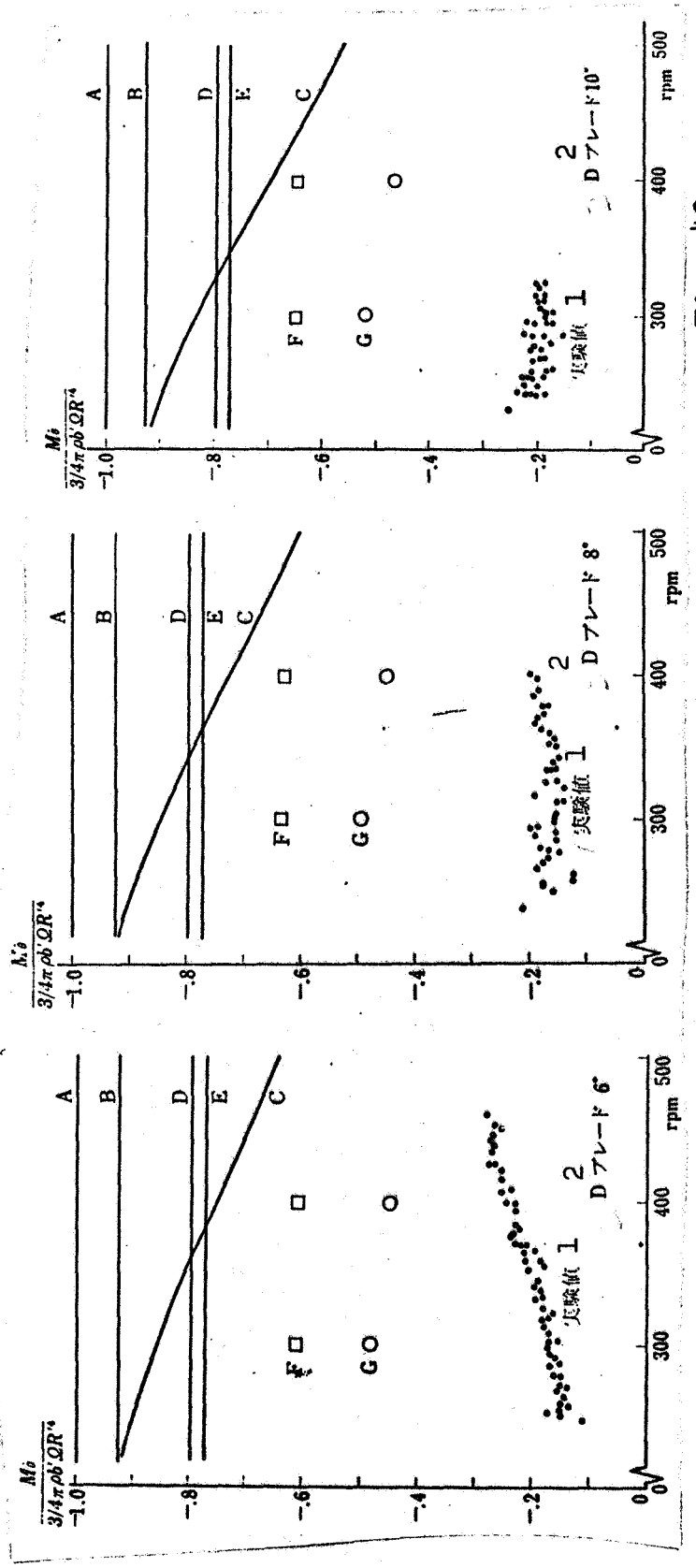

Fig. 41.

Fig. 42.

Fig. 43.

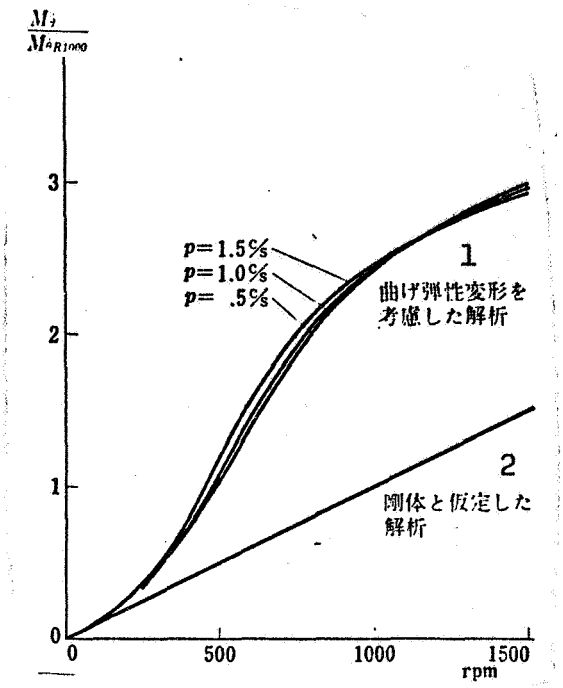

Fig. 44. Changes in the pitch damping accompanying increases of the rotor revolution speed in a certain rotor blade.

Key: 1. Analysis taking into consideration the bending elastic deformation
2. Analysis assuming a rigid body

theory indicates that a unique air force generation mechanism is present there. In Chapter 2 and beyond, the air forces governing the pitch damping are sought, assuming that bending deformations do not occur in the blades, and the results are compared with the experimental values shown in Figs. 32 to 43.

It has been established clearly that the pitch damping undergoes changes on account of elastic deformations of the blades. Let us now show, with reference to a concrete example of rotor blades, the manner in which the pitch damping caused by elastic deformation increases. Figure 44 shows the manner in which the pitch damping changes when the rotor rotating angular speed Ω is varied in cases when the primary flexural natural frequency ω_B of the blades is 1000 rpm and γ is 2. In cases when elastic deformations of the blades do not occur, the pitch damping will be linearly proportional to the revolution speed. On the other hand, when there are elastic deformations, there is added a pitch damping increment which is nonlinear with respect to the revolution speed.

When it is assumed that there are elastic deformations of the blades, the pitch damping is a function not only of Ω, but also of p/Ω, ω_B/Ω, γ. In Figs. 28 to 31, the manner in which the values of $M_\theta/M_{\dot\theta_R}$ undergo changes together with fluctuations of ω_B/Ω and γ in cases when the p/Ω is 0.05, 0.1, 0.15, and 0.2. It is clear that in all cases $M_\theta/M_{\dot\theta_R}$ increases suddenly when ω_B/Ω is in the vicinity of 1. Naturally, in the analysis performed in this section, it was assumed that the bending mode is as shown in Eq. (1.24), and it would have no meaning at all in the sections where ω_B/Ω is close to 0. It is clear that in cases when γ is great and the air forces make a greater contribution than the Coriolis forces operating on the blades, there will not be any greater increase in the pitch damping caused by elastic

deformation. In Figs. 45 to 48 is shown the manner in which parameters f_{S-}, f_{S+}, f_{C-}, and f_{C+}, which represent the elastic deformation of the blades, fluctuate in accordance with ω_B/Ω and γ. One can discern how the elastic deformation increases as the ω_B/Ω approaches 1 from a larger value. In Fig. 49 is shown the manner in which the bending deformation of the three blades fluctuates together with the passage of time in cases when Ω = 600 rpm, p = 2c/s, ω_B = 600 rpm, and γ = 4.

1.4. Smoke Experiments with Rotor

Vortices are constantly being produced by airplane propellers and helicopter rotors, and it is believed that the vortices are present in a spiral shape in the wake. In actual fact, when a flying boat takes off from the water, the water spray collects around the vortex produced from the tip parts of the propellers, and the sprial shapes are visible. On days when there is a high humidity, the steam in the so-called tip vortex produced from the tip parts of the blades of helicopters will condense, and it will sometimes be possible to observe a spiral shaped vortex [10].

Gray [11] photographed the tip vortices of helicopter rotors by putting cotton immersed in titanium tetrachloride into the blades in order to produce smoke.

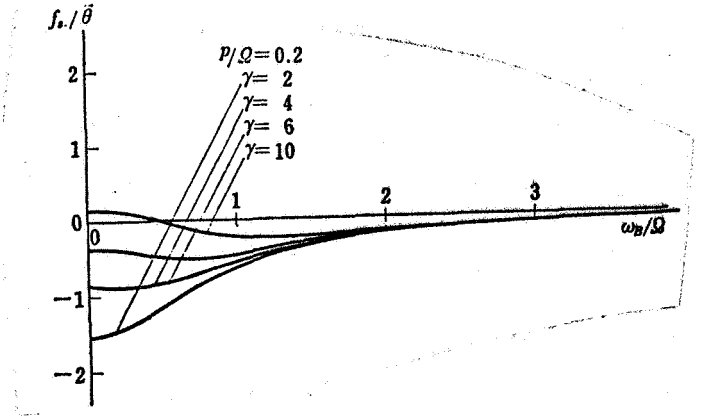

Fig. 45. The sin (Ω - p)t components in bending deformation of blades.

Simons, Pacifico and Jones [12] photographed the tip vortices by spraying a fine kerosene mist onto the rotor. /28

Jenny, Olson and Landgrebe [10] have used ammonium sulfide to photograph, not only the tip vortices, but also the vortex layers on the inside.

It is known from these studies that the vortices generated from the parts near the blade tips are caught up swiftly and from the tip vortex. However, it is not clear what happens in the wake to the vortices which emerge from farther inside. The relative positions of the blades and the vortices have been discussed in cases when the set pitch angle of the blade section and the revolution speeds have been changed, but it

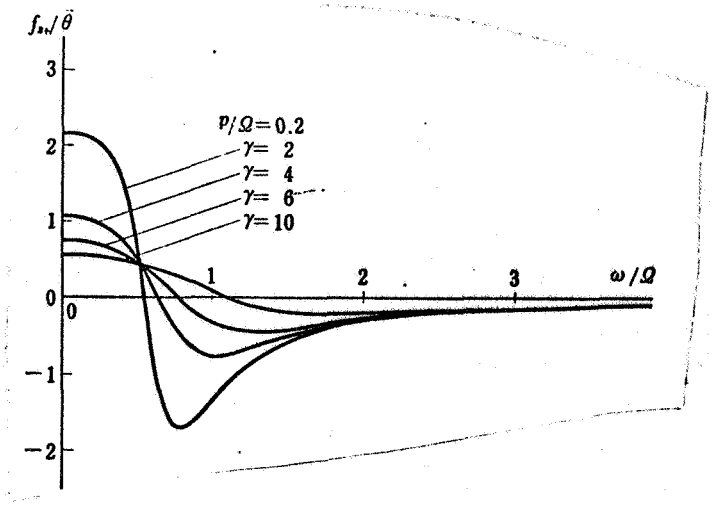

Fig. 46. The sin $(\Omega + p)t$ components in bending deformation of blades.

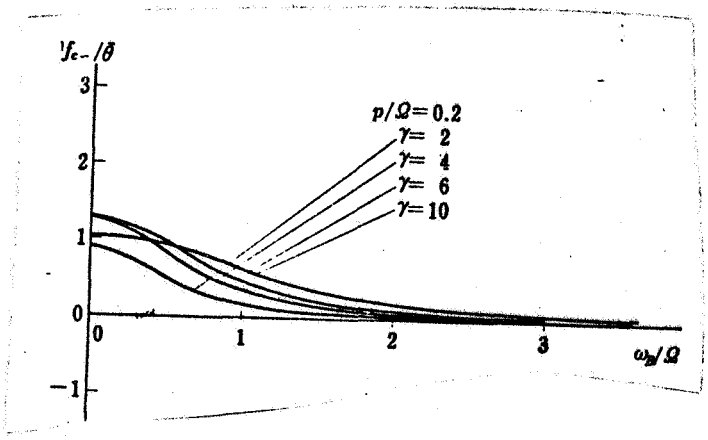

Fig. 47. The $\cos(\Omega - p)t$ components in bending deformation of blades.

has not yet been made clear how they change in accordance with the blade dimensions and the amount of wash-out.

Thus, smoke experiments were carried out concerning three-bladed rotors. The arrangement of the experimental apparatus is shown in Fig. 50. The revolution speed of the rotor was set by means of a frequency counter. The stroboscope was adjusted at the point where the value of the rotor revolution speed reached the prescribed value. Then the spotlight was extinguished, smoke was produced, and the photographs were taken. The smoke was produced by spraying air into liquid titanium tetrachloride, introducing it into a nozzle, and spraying it out slowly from the rotor upstream. When this is done, minute crystals of titanium tetrachloride are produced by the steam in the air. A vinyl pipe with many small holes with a diameter of 4 mm /29 was used so that powder crystals would not adhere to the nozzle.

The rotor revolution speeds were 300 rpm and 400 rpm, and tests were made with blade pitch angles of 0°, 4°, 8°, 12°, and 16°. Photographs of typical vortices are shown in Fig. 51. The vortex positions measured from the photographs are shown in Fig. 52. Fig. 52a shows the positions of the tip vortices. They are divided into three groups: the first layer, second layer, and third layer, beginning from the upper right. Fig. 52b indicates the position of the vortex in the axial direction at a position of a radius 2/3·R of the vortex on the inside. Like the tip vortex, this is also divided up into three groups.

Models of the vortex in the rotor wake in the state of hovering can be produced in the basis of the measured vortex positions. Such models are shown in Fig. 53.

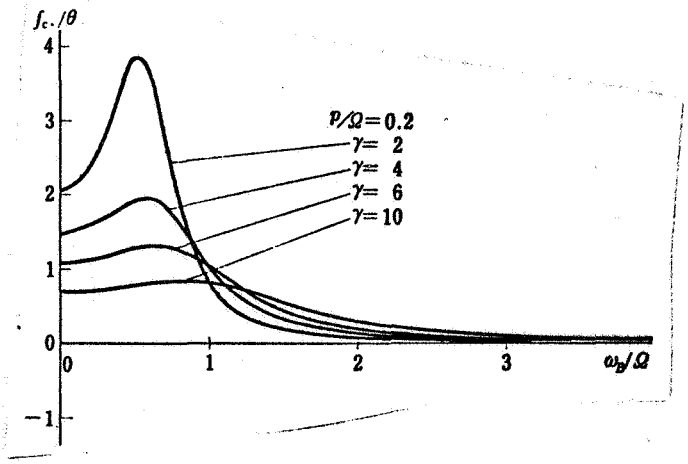

Fig. 48. The cos (Ω - p)t components in bending deformation of blades.

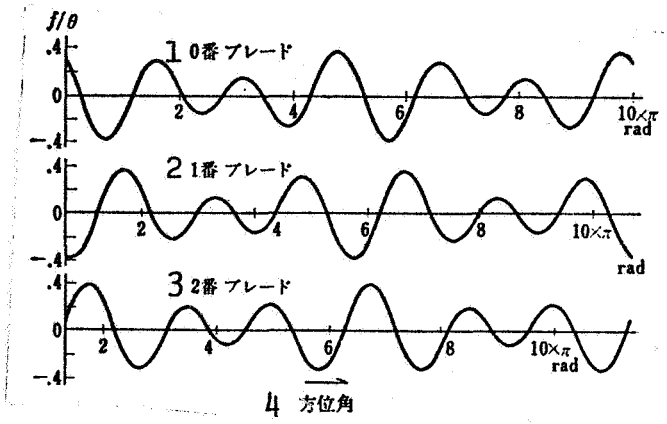

Fig. 49. Temporal changes in bending deformation of blades, Ω = 600 rpm, p = 2c/s, ω_B = 600 rpm, Lock number 4.

Key: 1. 0 blade
2. 1 blade
3. 2 blade
4. Azimuth angle

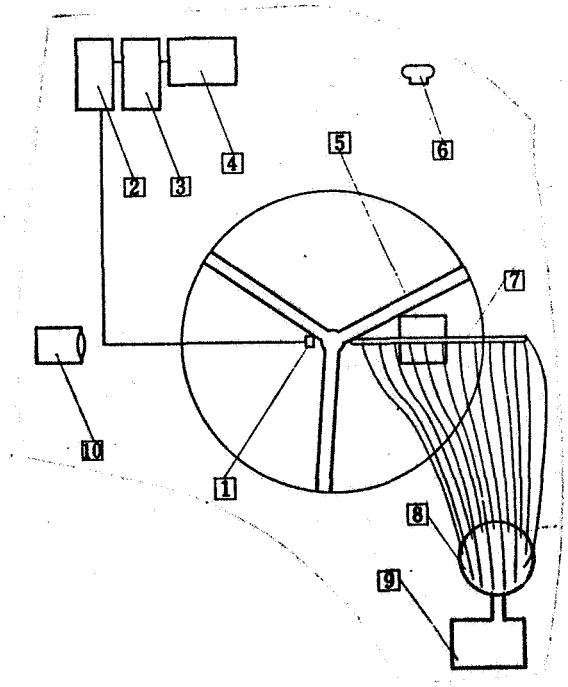

Fig. 50a. Layout of smoke experiment apparatus.

Fig. 50a Key:
1. Photocell
2. Amp
3. Filter
4. Frequency counter
5. Stroboscope
6. Camera
7. Fuming nozzle
8. Container for fuming agent
9. Blower
10. Spotlight

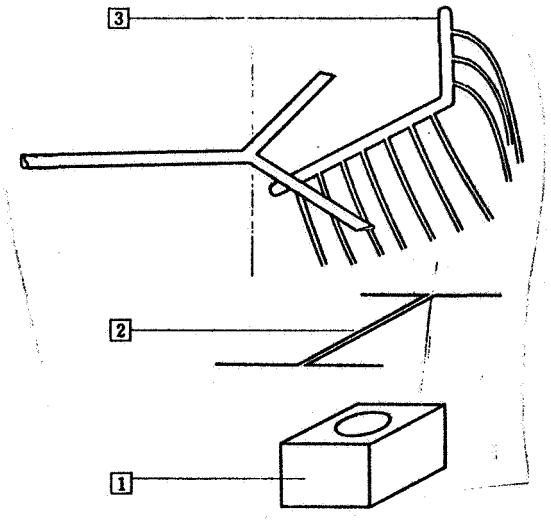

Fig. 50b. Diagram of the method of illumination and the fuming nozzle.

Key: 1. Stroboscope
2. Slit
3. Fuming nozzle

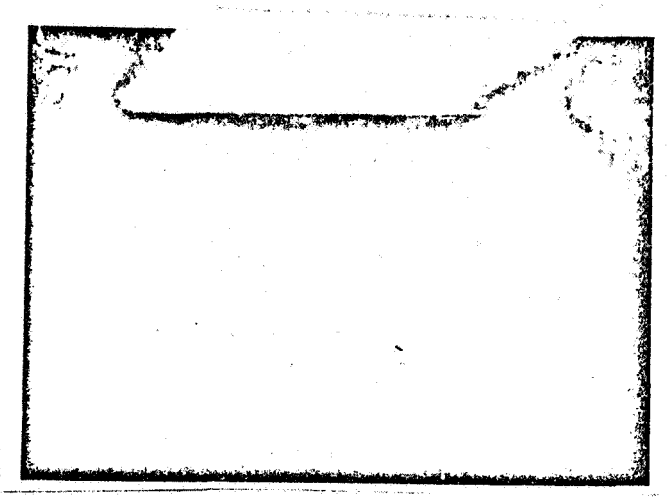

Fig. 51a. Blade wake (400 rpm, 0°)

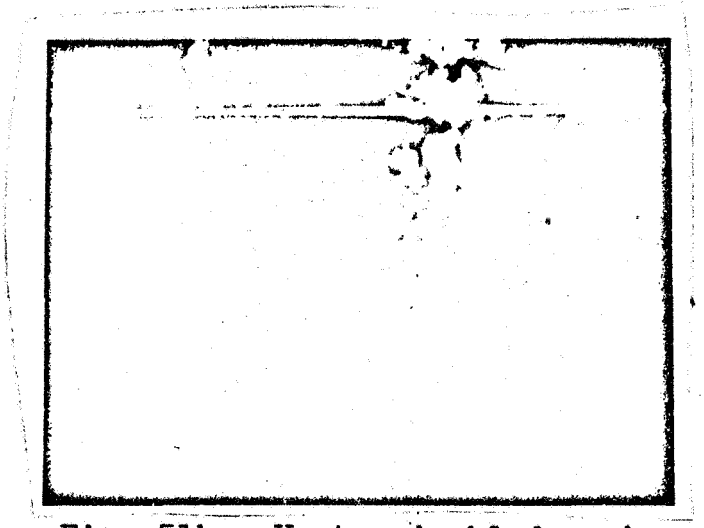

Fig. 51b. Vortex in blade wake (300 rpm, 4°)

/30

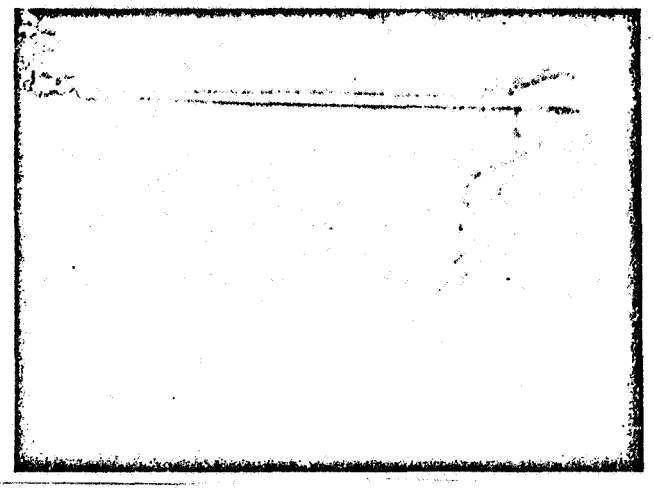

Fig. 51c. Vortex in blade wake (300 rpm, 8°)

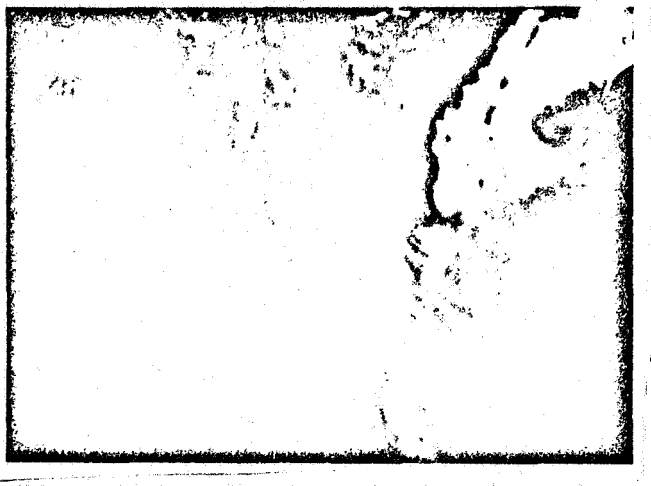

Fig. 51d. Vortex in blade wake (300 rpm, 12°)

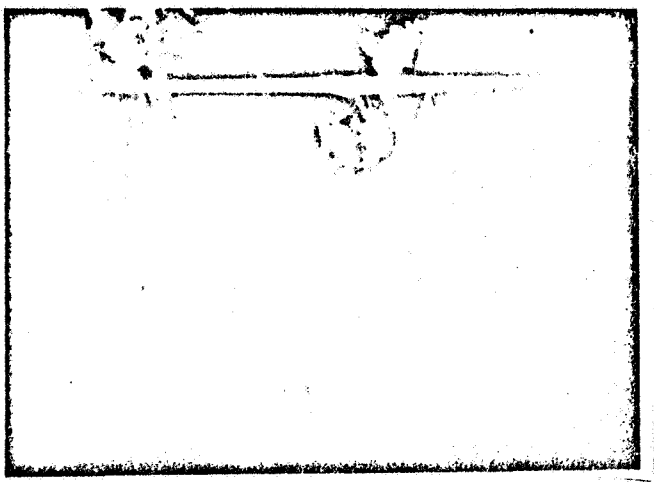

Fig. 51e. Vortex in blade wake (300 rpm, 16°)

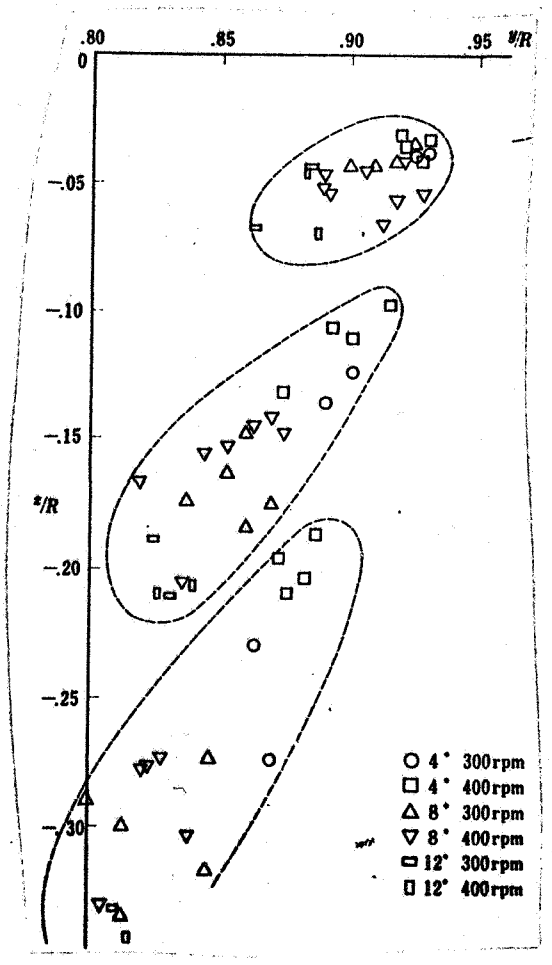

Fig. 52a. Tip vortex positions at state of hovering

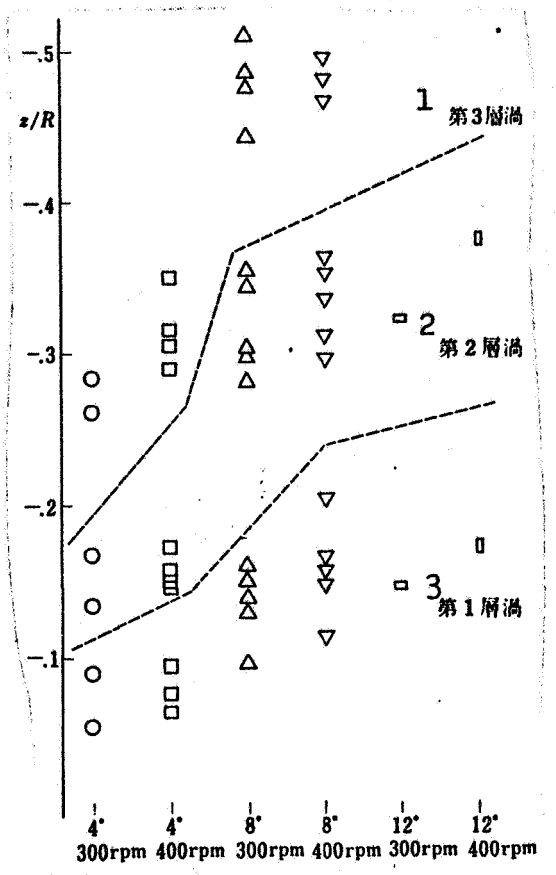

Fig. 52b. Axial positions of inside vortex layers at $y' = 2/3 \cdot R_2'$ at state of hovering

Key: 1. Third layer vortex
2. Second layer vortex
3. First layer vortex

TABLE 4. VENA CONTRACTA RATIO OF INSIDE VORTEX

		300 rpm		400 rpm	
		radial direction	axial direction	radial direction	axial direction
4°	第1層	0.943	0.111	0.950	0.107
	第2層	0.908	0.240	0.912	0.228
	第3層	0.899	0.368	0.913	0.433
6°	第1層	0.935	0.136	0.934	0.147
	第2層	0.899	0.296	0.896	0.316
	第3層	0.874	0.492	0.869	0.524
8°	第1層	0.928	0.160	0.918	0.189
	第2層	0.890	0.352	0.880	0.406
	第3層	0.848	0.617	0.825	0.618
10°	第1層	0.921	0.185	0.902	0.229
	第2層	0.882	0.406	0.865	0.495
	第3層	0.822	0.739	0.783	0.711

TABLE 5. POSITION OF TIP VORTEX

		300 rpm		400 rpm	
		radial direction	axial direction	radial direction	axial direction
4°	第1層	0.929	0.037	0.928	0.040
	第2層	0.892	0.131	0.896	0.114
	第3層	0.861	0.254	0.871	0.205
6°	第1層	0.916	0.040	0.916	0.045
	第2層	0.874	0.149	0.877	0.135
	第3層	0.847	0.276	0.853	0.241
8°	第1層	0.903	0.045	0.907	0.052
	第2層	0.858	0.167	0.864	0.160
	第3層	0.833	0.296	0.837	0.278
10°	第1層	0.889	0.050	0.897	0.057
	第2層	0.840	0.185	0.848	0.180
	第3層	0.818	0.317	0.823	0.315

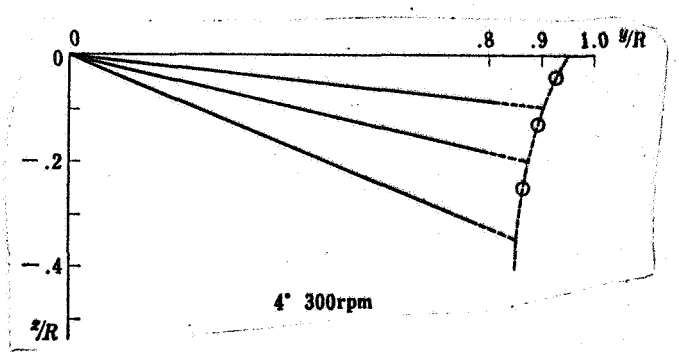

Fig. 53a. Model of rotor wake vortex obtained from smoke experiments

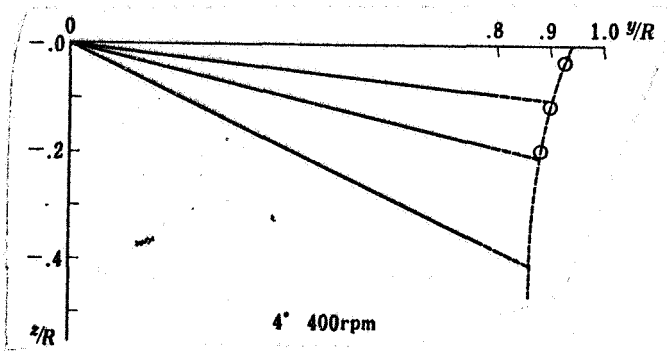

Fig. 53b. Model of rotor wake vortex obtained from smoke experiments

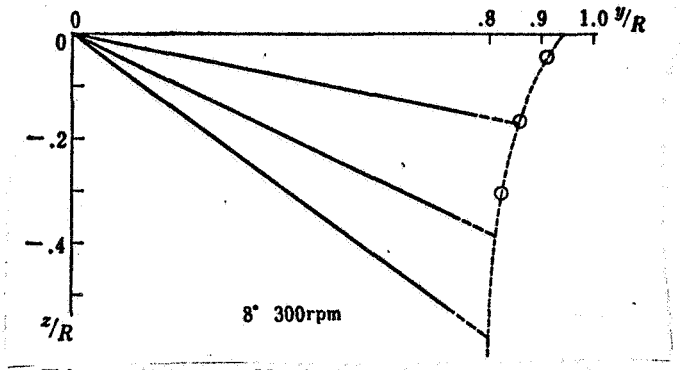

Fig. 53c. Model of rotor wake vortex obtained from smoke experiments

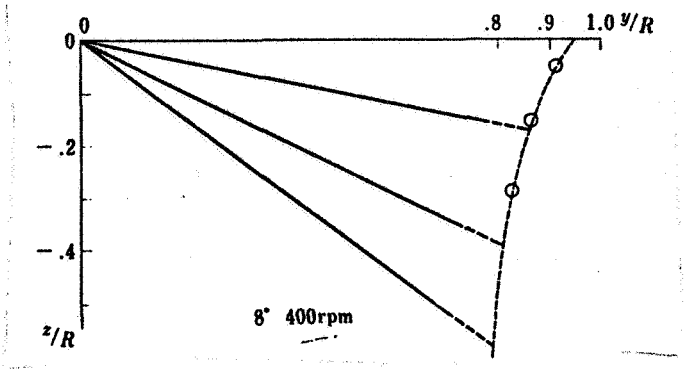

Fig. 53d. Model of rotor wake vortex obtained from smoke experiments

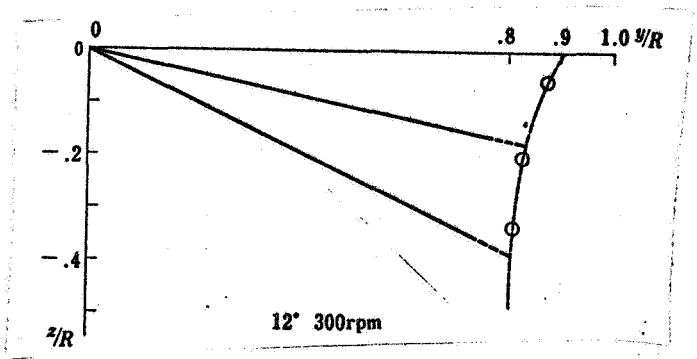

Fig. 53e. Model of rotor wake vortex obtained from smoke experiments

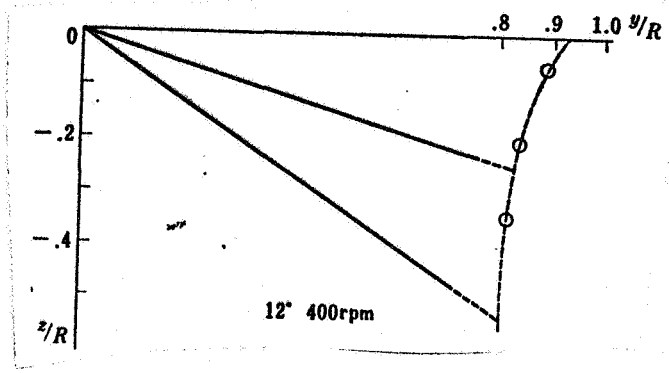

Fig. 53f. Model of rotor wake vortex obtained from smoke experiments

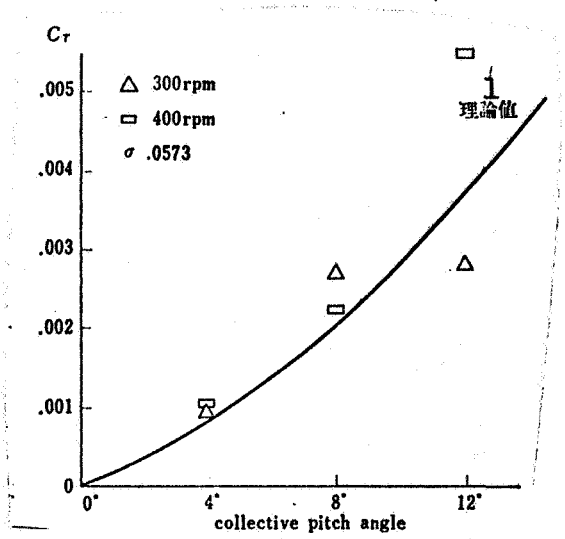

Fig. 53g. Comparison of thrust coefficient calculated with the flow velocity obtained from smoke experiments and the theoretical values

Key: 1. Theoretical value

The thrust coefficients were calculated using the flow velocity obtained from the models and the wake sectional area, and these were compared with the theoretical values for hovering rotors [13]. The results are shown in Fig. 53g. There is fairly good agreement at pitch angles of 4° and 8°. There is much divergence at a pitch angle of 12°. /34

CHAPTER 2. ANALYSIS OF PITCH DAMPING APPLYING LOEWY'S THEORY [14]

As was mentioned in Chapter 1, Section 3, the air forces which cause pitch damping in a rigid rotor are much smaller than those which would be anticipated from steady two-dimensional wing theory. As for the reason for this, the following may first be mentioned. Since the angle of incidence of the blade section fluctuates on account of pitching of the rotor, the so-called unsteady effect results in fluctuations in the phase of the air forces, probably leading to a reduction in the damping. In the case of a rotor, in the wake region near the rotor surface there are present large amounts of shed vortices which have been left by the preceding blade of previously by the blade under consideration itself. Therefore, it is possible that there may be produced on the rotor blade an induction velocity which is far greater than that which occurs in the case of a wing advancing straight forward. It is believed for this reason that the amplitude and phase of the air forces operating on a vibrating rotor will fluctuate over a broader range than in the case of a wing advancing straight forward. This phenomenon was theorized by Loewy with reference to rotors in vertical flight. In this theory, the amplitude and phase of the air forces are sought as functions of the non-dimensional frequency k, the ratio m between the blade frequency and rotor revolution speed, and the interval h between the vortex layers. As a result, when m is close to 1 and k is small, the real part of the list deficiency function -- that is, the portion of the air forces having the same phase as the fluctuations of the angle of incidence -- will be extremely small, and there will be a decrease in the air forces inhibiting the blade vibrations.

This theory was also compared with the experiments performed by Daughaday et al. [15] and by Brooks and Silviera [16]. As a result, it was learned that the phenomenon pointed out by Loewy does really occur, and that even quantitatively rather good results can be obtained.

Timman and Van De Vooren [17] have also devised a vibrating wind theory in which the vortex left by the preceding blade is taken into consideration. They have used this theory in analyzing blade flutter in helicopters.

In this chapter let us apply Loewy's theory to an analysis of pitch damping. In problems of analysis of the pitch damping of rigid rotors, blade vibrations of the same frequency as the revolution speed are subjected to amplitude modulation by vibrations of pitching on the rotor surface with a lower frequency. Therefore, the ratio between the blade frequency and the rotor revolution speed comes close to 1. Naturally, there is a small interval between the vortex layers. For this reason, it is expected that quite small values would be obtained if the pitch damping were calculated applying Loewy's theory.

2.1. Introduction to Loewy's Theory

Before applying it, let us introduce Loewy's theory. This theory attempts to derive, concerning rotors, the same sort of two-dimensional vibrating wing theory as in Theodorsen's theory [18]. In a wing advancing straight forward, it is held that the vortices generated from a vibrating wing are left in the wing's wake, where they line up more or less in a straight line. On the other hand, in a rotor, the vortices generated from the vibrating wing are piled up in overlapping fashion in the vicinity of the wing, producing a strong induction velocity on the wing surface. The characteristic feature of Loewy's theory is in the manner with which these wake vortices are treated.

The blades are treated as vibrating foil, and a shed vortex is produced from the rear edge every time there is a fluctuation in the bound vortex. When the blade wing chord, the revolution speed, and the effective angle of incidence undergo vibrational changes, it is assumed that the amplitude changes in an extremely leisurely manner in the radial direction. For this reason, the events occurring at definite positions on the blades on both sides of the radial direction are regarded as being identical from the aerodynamic point of view.

Let us consider a cylindrical surface at a vertical angle to a blade which encompasses a definite number of vortex streets. The cylindrical surface expands at a definite azimuth angle in a

radial position on both sides of a specific blade. This is shown in outline in the diagram in Fig. 54. When there is little inflow, there will be a small angle between the vortex streets and the blade rotating surface. The intervals between the vortex streets will be determined by the downwash at each place and by the ascent speed of the rotor. Ordinarily, the intervals are not equal, but in Loewy's theory it is assumed that they have equal intervals. Among /35
the vortices in the circumference of the blades, only those which are near the blades are believed to make a major contribution to the unsteady induction velocity on the blades. Thus, the azimuth angle on both sides of the blade may be small, and the number of vortex streets may also be small. On this account it is believed that the distant vortices have a small contribution and that it is not absolutely essential to treat the position and magnitude of the distant vortices with great precision. Thus, the cylindrical surface mentioned above can be replaced by a plane expanding to infinity on both sides and below.

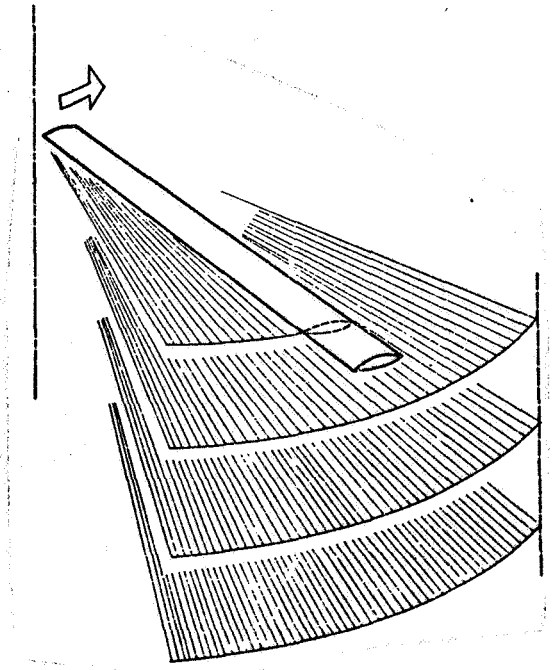

Fig. 54. Shed vortex sheet in rotor wake in state of hovering

Since each vortex street was generated before rotation from the q-th blade, it is defined as γ_{nq}. At the same time, γ_{nq} also expresses the circulation per unit length. The lowest among the vortex streets depicted in Fig. 55 is $\gamma_{1,1}$ when the rotor consists of two blades, or $\gamma_{1,0}$ when the rotor consists of three blades. In general terms, a model such as that shown in Fig. 56 is obtained.

On account of the viscosity, a vortex will be damped with the passage of time. However, we will ignore the damping of the vortex because the time required to damp a vortex to a pronounced degree is greater than the period of rotation of the rotor.

If it is assumed that the wing has a small thickness, a small maximum camber, and a small angle of incidence, and also that the wing displacement in the rotor axis direction is also small, then in accordance with foil theory it is possible to describe the boundary conditions on the plane where $Z_1 = 0$, and the problem can be linearized.

(2.1)

Here, v_a is the unsteady component of the induction velocity, and v_{as} is the steady component.

The standard blade is replaced by a disturbed vortex in which the strength per unit length is γ_a. The unsteady induction velocity induced on the standard blade is determined by the distributed vortex representing the wing surface and the shed vortex. Let us discuss the relationships between the induction velocity, the shed vortex, and the bound vortex with partial reference to cases when the blade performs sinusoidal motion.

The unsteady induction velocity is induced by the distributed vortex representing the wing surface and by the shed vortex. However, if we consider a model such as that in Fig. 56, an expression such as Eq. (2.2) can be written in accordance with the Biot-Savart law.

$$\begin{aligned} v_a(x',t)=\frac{-1}{2\pi}\Bigg\{&\int_{-b'}^{b'}\frac{\gamma_a(\xi',t)}{x'-\xi'}d\xi' \\ &+\int_{b'}^{\infty}\frac{\gamma_{00}(\xi',t)}{x'-\xi'}d\xi' \\ &+\sum_{q=1}^{Q-1}\sum_{n=0}^{\infty}\int_{-\infty}^{\infty}\frac{\gamma_{nq}(x'-\xi')}{(x'-\xi')^2+(nQ+q)^2(h')^2}d\xi' \\ &+\sum_{n=1}^{\infty}\int_{-\infty}^{\infty}\frac{\gamma_{n0}(x'-\xi')}{(x'-\xi')^2+(nQ)^2(h')^2}d\xi'\Bigg\} \end{aligned} \tag{2.2}$$

Next let us discuss the relationships between γ_a, γ_{00}, γ_{n0}, and γ_{nq} which appear in the above equation. The unsteady bound vortex of the q-th blade is defined as Γ_q'. If it is assumed that the vibration amplitudes of the bound vortices are the same for all the blades and that only their phases are different, the following can be written. The unsteady component of the bound vortices for the standard blade in particular is written Γ_a'. $\bar{v}_a$ and $\bar{\gamma}_a$ are complex quantities.

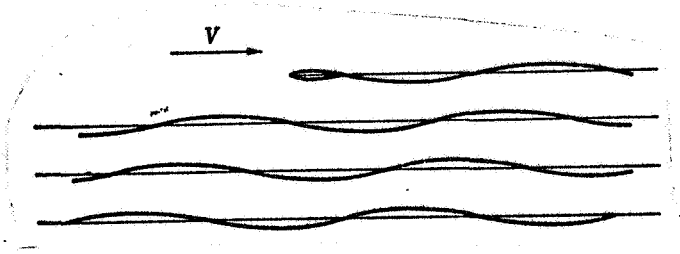

Fig. 55. Two-dimensional model of rotor blade and returning wake

$$\left.\begin{aligned} &\Gamma_a'=\int_{-b'}^{b'}\gamma_a d\xi' \\ &v_a=\bar{v}_a e^{i\omega t} \qquad \gamma_a=\bar{\gamma}_a e^{i\omega t} \\ &\Gamma_a'=\bar{\Gamma}_a e^{i\omega t} \qquad \Gamma_q'=\bar{\Gamma}_a' e^{i(\omega t+\hat{\varphi}_q)} \end{aligned}\right\} \tag{2.3}$$

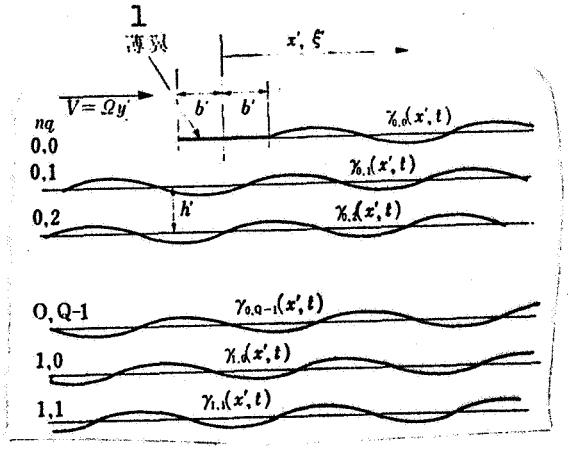

Fig. 56. Model and symbols for rotors with Q blades

Key: 1. Foil

A shed vortex is generated from the rear edge of the blades every time there are fluctuations of the bound vortices of the blades, and there is the following relationship in the vicinity of the rear edge of the standard blade. /36

$$\gamma_{00}(b', t)d\xi' = -\frac{d\Gamma_a'}{dt}dt = -i\omega\bar{\Gamma}_a' e^{i\omega t}dt \quad (2.4)$$

The following applies generally in the vicinity of the rear edge of the q-th blade:

$$\gamma_{0q}\left(b' - \frac{2\pi y' q}{Q}, t\right)d\xi' = -\frac{d\Gamma_q'}{dt}dt = -i\omega\bar{\Gamma}_a' e^{i(\omega t + \bar{\varphi}_q)}dt \quad (2.5)$$

Shed vortex $\gamma_{nq}(\xi', t)$ in which the x' coordinate is ξ' at the present time is a vortex which was generated from the q-th blade a certain time Δt previously.

$$\gamma_{nq}(\xi', t)d\xi' = -\frac{d\Gamma_q'}{dt}dt_{t=t-\Delta t} = -i\omega\bar{\Gamma}_a' e^{i(\omega t + \bar{\varphi}_q - \omega\Delta t)} \quad (2.6)$$

Referring to Fig. 60, we find that Δt is as follows.

$$\Delta t = \frac{2\pi}{\Omega}\frac{q}{Q} + \frac{\xi' - b'}{\Omega y'} + \frac{2\pi}{\Omega}n \quad (2.7)$$

Since $d\xi'/dt = \Omega y'$, generally $\gamma_{nq}(\xi', t)$ will be:

$$= -\frac{i\omega\Gamma_a'}{\Omega y'} e^{i\left(\omega t + \bar{\varphi}_q - \omega\frac{2\pi}{\Omega}\frac{q}{Q} - \omega\frac{\xi' - b'}{\Omega y'} - \omega\frac{2\pi}{\Omega}n\right)} \quad (2.8)$$

Let us rewrite Eq. (2.2), substituting $\gamma_{nq}(\xi', t)$. If we consider Eq. (2.3) at the same time, it is not necessary to consider the term $e^{i\omega t}$. If we introduce a dimensionless frequency $k = \omega b'/\Omega y'$ and non-dimensionalize the length by the half chord length, it will be possible to write Eq. (2.2) in the following manner, However, $\bar{\Gamma}$ is $\bar{\Gamma} \equiv \bar{\Gamma}_a' e^{ik/b'}$.

$$v_a(x)=-\frac{1}{2\pi}\int_{-1}^{1}\frac{\bar{\gamma}_a(\xi)}{x-\xi}d\xi+\frac{ik\bar{\Gamma}}{2\pi}\int_{1}^{\infty}\frac{1}{x-\xi}e^{-ik\xi}d\xi+\frac{ik\bar{\Gamma}}{2\pi}\left[\sum_{q=1}^{Q-1}\sum_{n=0}^{\infty}\int_{-\infty}^{\infty}e^{i\left(\bar{\varphi}_q-\alpha\frac{2\pi}{D}\frac{q}{Q}-\alpha\frac{2\pi}{D}n-k\xi\right)}\right.$$
$$\left.\times\frac{x-\xi}{(x-\xi)^2+(nQ+q)^2h^2}d\xi+\sum_{n=1}^{\infty}\int_{-\infty}^{\infty}e^{i\left(-\alpha\frac{2\pi}{D}n-k\xi\right)}\frac{x-\xi}{(x-\xi)^2+n^2Q^2h^2}d\xi\right] \tag{2.9}$$

Performing complex integration, we obtain:

$$\int_{-\infty}^{\infty}\frac{e^{-ik\xi}(x-\xi)}{(x-\xi)^2+A^2}d\xi=i\pi e^{-k(ix+A)} \tag{2.10}$$

Thus, Eq. (2.9) becomes:

$$v_a(x)=-\frac{1}{2\pi}\int_{-1}^{1}\frac{\bar{\gamma}_a(\xi)}{x-\xi}d\xi+\frac{ik\bar{\Gamma}}{2\pi}\int_{1}^{\infty}\frac{e^{-ik\xi}}{x-\xi}d\xi-\frac{k\bar{\Gamma}W}{2}e^{-ikx} \tag{2.11}$$

Here,

$$W=\sum_{q=1}^{Q-1}\sum_{n=0}^{\infty}e^{i\left\{\bar{\varphi}_q-\alpha\frac{2\pi}{D}\frac{q}{Q}-\alpha\frac{2\pi}{D}n-kh(nQ+q)\right\}}+\sum_{n=1}^{\infty}e^{i\left(-\alpha\frac{2\pi}{D}n-kh\,nQ\right)} \tag{2.12}$$

Söngen [31] demonstrates that, if $f_{(1)}$ is finite, the solution of the integral equation (2.13) can be written as in (2.14).

$$g_{(x)}=\frac{1}{2\pi}\int_{-1}^{1}\frac{f_{(\xi)}}{x-\xi}d\xi \tag{2.13}$$

$$f_{(x)}=-\frac{2}{\pi}\sqrt{\frac{1-x}{1+x}}\int_{-1}^{1}\sqrt{\frac{1+\xi}{1-\xi}}\frac{g_{(\xi)}}{x-\xi}d\xi \tag{2.14}$$

In our problem, according to Kutta's conditions, $\bar{\gamma}_{a(1)}=0$. Therefore, Eq. (2.11) will be written as follows:

$$\bar{\gamma}_a(x)=\frac{-2}{\pi}\sqrt{\frac{1-x}{1+x}}\left[\int_{-1}^{1}-\sqrt{\frac{1+\xi}{1-\xi}}\frac{v_a(\xi)}{x-\xi}d\xi+\frac{ik\bar{\Gamma}}{2\pi}\int_{-1}^{1}\sqrt{\frac{1+\xi}{1-\xi}}\frac{1}{x-\xi}\int_{-1}^{\infty}\frac{e^{-ik\lambda}}{\xi-\lambda}d\lambda\right.$$
$$\left.-\frac{k\bar{\Gamma}W}{2}\int_{-1}^{1}\sqrt{\frac{1+\xi}{1-\xi}}\frac{1}{x-\xi}e^{-ik\xi}d\xi\right] \tag{2.15}$$

Since there is the following relationship between $\bar{\Gamma}$ and $\bar{\gamma}_a$, /37 we will obtain $\bar{\Gamma}$ if we eliminate $\bar{\gamma}_a$.

$$\bar{\Gamma}=e^{ik}\int_{-1}^{1}\bar{\gamma}_a(x)\,dx \tag{2.16}$$

$$\bar{\Gamma}=\frac{2\int_{-1}^{1}\sqrt{\frac{1+\xi}{1-\xi}}v_a(\xi)d\xi}{i\pi k\left\{\frac{1}{2}[H_1^{(2)}(k)+iH_0^{(2)}(k)]+[J_1(k)+iJ_0(k)]W\right\}} \tag{2.17}$$

W represents the contribution of the returning vortex. If W = 0, it is quite natural that Eq. (2.17) will agree with Theodorsen's theoretical equation. Needless to say, if we approach closer to $k \to 0$, the denominator will be -1, and the equation will agree with the equation of the two-dimensional steady wing theory.

Next, let us seek the air forces operating on the wing. The linearized Bernoulli's equation with respect to an unsteady current will be:

$$\frac{\partial \phi}{\partial t} + \frac{V}{b}\frac{\partial \phi}{\partial x} + \frac{p}{\rho} = f(t) \tag{2.18}$$

The relationship between the velocity difference between the upper and lower surfaces of the wing and the distributed vortex will be:

$$\frac{\partial \phi_U}{\partial x} - \frac{\partial \phi_L}{\partial x} = b'\gamma \tag{2.19}$$

If we integrate from the front edge of the wing up to the point under consideration, we obtain:

$$\phi_U - \phi_L = b'\int_{-1}^{x} \gamma_a(\xi, t)\, d\xi \tag{2.20}$$

If we compile Bernoulli's equations along two routes passing through the upper and lower surfaces of the wing, take the difference, and eliminate ϕ_U and ϕ_L by using Eqs. (2.19) and (2.20), we obtain:

$$p_U - p_L = \Delta p = -\rho\left[V\gamma_a(x,t) + b'\frac{\partial}{\partial t}\int_{-1}^{x}\gamma_a(\xi,t)\,d\xi\right] \tag{2.21}$$

When there is sinusoidal movement, Δp can be written as $\Delta p = \Delta \bar{p} e^{i\omega t}$. Therefore,

$$\frac{\Delta \bar{p}(x^*)}{\rho \Omega y'} = -\bar{\gamma}_a(x^*) - ik\int_{-1}^{x^*}\bar{\gamma}_a(\xi^*)\,d\xi^* \tag{2.22}$$

When the calculations are carried out, we obtain the following results.

$$\begin{aligned}\frac{\Delta \bar{p}(x^*)}{\rho \Omega y'} = {} & \frac{-2}{\pi}[1 - C'(k,m,h)] \\ & \times \sqrt{\frac{1-x^*}{1+x^*}}\int_{-1}^{1}\sqrt{\frac{1+\xi}{1-\xi}}\, v_a(\xi)\,d\xi \\ & + \frac{-2}{\pi}\int_{-1}^{1}\left[\sqrt{\frac{1-x^*}{1+x^*}}\sqrt{\frac{1+\xi}{1-\xi}}\,\frac{1}{x^*-\xi}\right. \\ & \left. - ikA_1(x^*,\xi)\right] v_a(\xi)\,d\xi\end{aligned} \tag{2.23}$$

Here,

$$C'(k,m,h) \equiv F'(k,m,h) + iG'(k,m,h) = \frac{H_1^{(2)}(k) + 2J_1(k)W}{H_1^{(2)}(k) + iH_0^{(2)}(k) + 2[J_1(k) + iJ_0(k)]W} \tag{2.24}$$

$$\Lambda_1(x^*, \xi) = \frac{1}{2}\log\left|\frac{1 - x^*\xi + \sqrt{1-\xi^2}\sqrt{1-x^{*2}}}{1 - x^*\xi - \sqrt{1-\xi^2}\sqrt{1-x^{*2}}}\right| \tag{2.25}$$

C'(k,m,h) corresponds to Theodorsen's function C(k) in the case of a vibrating wing which advances straight forward. At the ultimate limit where h has been enlarged infinitely, W will approach 0. Therefore, C'(k,m,h) will approach C(k).

2.2. Analysis of Pitch Damping

Let us apply Loewy's theory to an analysis of the pitch damping. We sought the air force moment generated around the pitching axis when the rotor surface is performing sinusoidal pitching as expressed by $\theta = \bar{\theta} \sin pt$, in the same way as in Chapter 1, Section 3, and calculated the pitch damping from the time changes in the moment. It is assumed that the blades have an extremely great rigidity and that elastic deformation does not occur. When the blade does not undergo deformation, it is clear from Eq. (1.5) that the components of the blade velocity which are inside the rotating surface are $y'\Omega$, and the components which are vertical to the rotating surface are $-y'\dot{\theta}\cos\psi$. Among the air forces operating on the blades, the steady components are unrelated to the moment around the Y axis, as has already been stated in Eq. (1.28). Thus, we will write only the unsteady portions among the boundary conditions in Eq. (2.1)

$$-y'\bar{\theta}p\cos pt\cos\Omega t = -\frac{1}{2}y'\bar{\theta}p[\cos(\Omega+p)t + \cos(\Omega-p)t] = v_a \tag{2.26}$$

In Loewy's theory, the wings perform sinusoidal motion with a frequency of ω, but in problems of pitch damping the wings perform a motion synthesizing two sinusoidal motions which have different frequencies. However, since both the equation defining the mutual relationships between the vortices and the equation for seeking the induction velocity are linear, separate sets of relative equations are obtained for the $(\Omega + p)$ and the $(\Omega - p)$ frequency components.

The equation for the relationship between the induction velocity and the vortices is as follows, with reference to Eqs. (2.11) and (2.12):

$$-\frac{1}{2}yb'\bar{\theta}p=\frac{-1}{2\pi}\int_{-1}^{1}\frac{\bar{\gamma}_{a\pm}(\xi)}{x-\xi}d\xi + \frac{ik\bar{\Gamma}_{\pm}}{2\pi}\int_{1}^{\infty}\frac{e^{-ik_{\pm}t}}{x-\xi}d\xi-\frac{k_{\pm}\bar{\Gamma}_{\pm}W_{\pm}}{2}e^{-ik_{\pm}x} \tag{2.27}$$

Here, /38

$$W_{\pm}=\sum_{q=1}^{Q-1}\sum_{n=0}^{\infty}e^{i\left(\bar{\psi}_q-[\Omega\pm p]\frac{2\pi}{\Omega}\frac{q}{Q}-[\Omega\pm p]\frac{2\pi}{\Omega}n-k_{\pm}[nQ+q]h\right)}+\sum_{n=1}^{\infty}e^{i\left(-[\Omega\pm p]\frac{2\pi}{\Omega}n-k_{\pm}nQh\right)} \tag{2.28}$$

The intervals between the vortices h' are determined in the following manner [13].

$$h'=\frac{\pi b'}{2}\left(-1+\sqrt{1+\frac{8y'\theta_e}{Qb'}}\right) \tag{2.29}$$

The following considerations are entertained concerning the phase difference ψ_q between the standard blade and the q-th blade. Loewy's theory is a foil theory and always describes the boundary conditions on the plane where $Z_1 = 0$. It also assumes that the intervals between the blade and the vortex and those between vortices are always a constant value h'. Consequently, when this theory is applied to pitch damping analysis, it is a precondition that the relative positions between the blade and the vortex remain unchanged. Under these preconditions, the phase differences of the bound vortices will be equal to the phase differences between the velocity components which are vertical to the blade rotating surface. Thus, it is assumed that:

$$\bar{\psi}_q=2\pi q/Q \tag{2.30}$$

$$\therefore\ W_{\pm}=\sum_{j=1}^{\infty}e^{i\left(\mp\frac{2\pi p}{\Omega Q}-k_{\pm}h\right)j}=\frac{e^{i\left(\mp\frac{2\pi p}{\Omega Q}-k_{\pm}h\right)}}{1-e^{i\left(\mp\frac{2\pi p}{\Omega Q}-k_{\pm}h\right)}} \tag{2.31}$$

With reference to Eq. (2.17), the $\bar{\Gamma}_{\pm}$ determining the bound vortices can each be written in the following manner.

$$\Gamma_{\pm}=\frac{-\pi yb'\bar{\theta}p}{ik_{\pm}\left\{\frac{1}{2}[H_1^{(2)}(k_{\pm})+iH_0^{(2)}(k_{\pm})]+[J_1(k_{\pm})+iJ_0(k_{\pm})]W_{\pm}\right\}} \tag{2.32}$$

With reference to Eq. (2.23), $\Delta\bar{p}_+$ and $\Delta\bar{p}_-$ can each be written in the following manner.

$$\frac{\Delta\bar{p}_\pm(x^*)}{\rho\Omega y'}=\frac{-2}{\pi}[1-C'(k_\pm, m_\pm, h)]\sqrt{\frac{1-x^*}{1+x^*}}\int_{-1}^{1}\sqrt{\frac{1+\xi}{1-\xi}}\left(-\frac{1}{2}yb'\bar{\theta}p\right)$$
$$+\frac{-2}{\pi}\int_{-1}^{1}\left[\sqrt{\frac{1-x^*}{1+x^*}}\sqrt{\frac{1+\xi}{1-\xi}}\frac{1}{x^*-\xi}-ik_\pm A_1(x^*,\xi)\right]d\xi\left(-\frac{1}{2}yb'\bar{\theta}p\right)$$

If we carry out integration for ξ, we obtain:

$$\frac{\Delta\bar{p}_\pm(x^*)}{\rho\Omega y'}=-C'(k_\pm, m_\pm, h)\sqrt{\frac{1-x^*}{1+x^*}}yb'\bar{\theta}p-ik_\pm\sqrt{1-x^{*2}}yb'\bar{\theta}p \tag{2.33}$$

The amplitude of the unsteady components of the lift which operate on the portions with a width of dy' at a place y' away from the rotor hub is:

$$L_\pm dy'=b'^2\int_{-1}^{1}-\Delta p_\pm(x^*)\,dx^*dy$$
$$=\pi\rho\Omega\bar{\theta}pb'^4y^2\left\{C'(k_\pm, m_\pm, h)+\frac{ik_\pm}{2}\right\}dy \tag{2.34}$$

Since the phase is $2\pi q/Q$ ahead of the standard blade, the unsteady component of the lift operating on the q-th blade is:

$$L_{\pm q}dy'$$
$$=\pi\rho\Omega\bar{\theta}pb'^4y^2\left\{C'(k_\pm, m_\pm, h)+\frac{ik_\pm}{2}\right\}dye^{i2\pi q/Q}$$

The moment produced around the Y axis by the unsteady components of the lift operating on the blades is:

$$M_Y=-\sum_{q=0}^{Q-1}\int_{R_1}^{R_2}b'^2\bar{L}_{+q}ydy\cos\left(\Omega t+\frac{2\pi q}{Q}\right)e^{i(\Omega+p)t}$$
$$-\sum_{q=0}^{Q-1}\int_{R_1}^{R_2}b'^2\bar{L}_{-q}ydy\cos\left(\Omega t+\frac{2\pi q}{Q}\right)e^{i(\Omega-p)t} \tag{2.35}$$

In a rotor which is performing pitching and in which the inclination of the rotor surface is expressed by $\theta = \bar{\theta}\sin pt$, if the time changes in the moment around the pitching axis is known, it is possible to calculate the pitch damping by the method in Appendix A.

$$\frac{\partial M}{\partial\bar{\theta}}=\frac{1}{\pi\bar{\theta}}\int_0^{2\pi/p}M_Y\cos ptdt \tag{2.36}$$

Concretely speaking, when we write Eq. (2.31),

$$\frac{\partial M}{\partial \theta} = -\frac{\pi Q \rho \Omega b^5 R_2^4}{4} \int_{R_1}^{R_2} \frac{4}{R_2^4} \times \frac{F'(k_+, m_+, h) + F'(k_-, m_-, h)}{2} y^3 dy$$

When numerical integration is performed by Chebyshev's integration formula [3],

$$\frac{\partial M}{\partial \theta} = -\frac{\pi Q \rho \Omega b^5 R_2^4}{4} \frac{\pi}{J} \sum_{j=1}^{J} \varphi(\theta_j) \tag{2.37}$$

Here,

$$\varphi(\theta_j) = 4\left(\frac{R_2 - R_1}{2R_2}\right)^4 \frac{F'(k_{+j}, m_+, h_j) + F(k_{-j}, m_-, h_j)}{2} \times \left(\frac{R_2 + R_1}{R_2 - R_1} - \cos\theta_j\right)^3 \sin\theta_j$$

$$\theta_j = \frac{2j-1}{2(J+1)}\pi$$

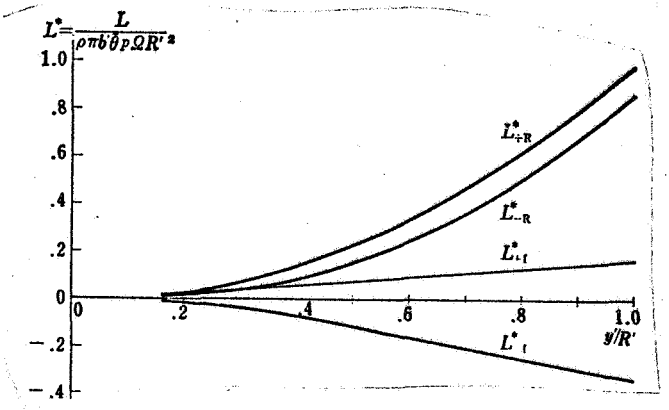

Fig. 57. Lift distribution calculated using Loewy's theory.
p = 0.756 c/s, Ω = 300 rpm, θ_c = 4°

In Fig. 57 is shown the lift distribution of the blade in the radial direction, when the rotor revolution speed is 300 rpm and the pitching frequency is 0.756 c/s. In Fig. 58 are shown the results of calculations of the pitch damping for various angles of incidence when the pitching frequency was 0.756 c/s. In particular, at the extreme limit where W approaches 0, there is good agreement with Theodorsen's theory, and the data are shown in the figure for the sake of comparison. /39

In Figs. 32 to 43 are given comparisons of the values estimated from the experimental values when it was assumed that elastic deformation of the blades does not occur and the pitch damping values calculated by means of Loewy's theory.

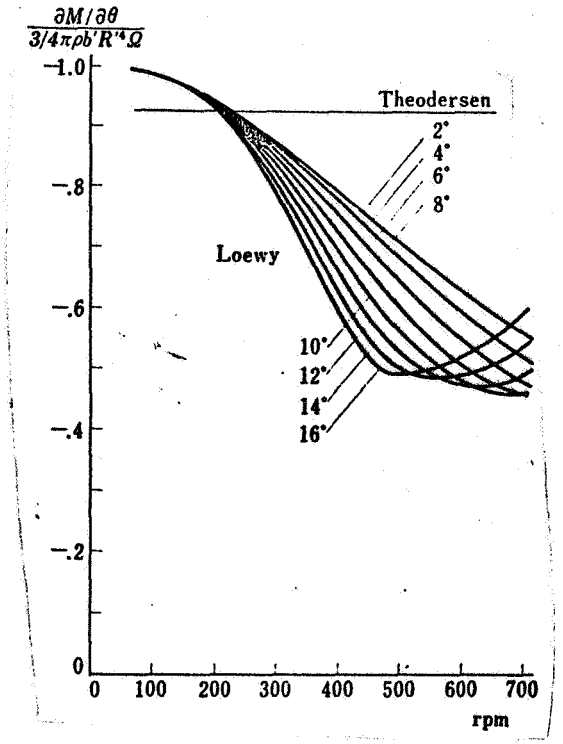

Fig. 58. Pitch damping calculated by using Theodorsen's theory and Loewy's theory

The calculated values are much larger than the measured values, but they are smaller than the values from Townsent's theory [7] or from Theodorsen's theory [18].

As the rotor revolution speed increases, the calculated values approach closer and closer to the experimental values. This is because the ratio m between the frequency of the blades and the rotor revolution speed approaches 1.

The non-dimensionalized measured values will not change even when the rotor revolution speed is varied, but the calculated values will decrease as the rotor revolution speed is increased.

Within the range of the calculations performed, there are not very many differences in the calculated values even if the pitch angles of the blades are changed.

It is clear from the results given above that the pitch damping cannot be explained adequately in terms of Loewy's theory. However, it was confirmed that it is possible that the vortex in the wake may possibly reduce the pitch damping to a considerable degree. A pronounced reduction in the air forces cannot be calculated, unlike the case when analyzing the blade flutter [15, 16], because m does not approach close enough to 1.

CHAPTER 3. ANALYSIS OF PITCH DAMPING APPLYING THE THEORY OF ASHLEY ET AL.

In Fig. 61 is plotted the lift distribution of the blades in the radial direction as calculated according to Loewy's theory. Since Loewy's theory is a two-dimensional theory, the air forces will not become 0 at the blade tips. However, in problems of pitch damping, the moment produced by the air forces is quite important, and it is necessary to be able to seek accurately the air forces in the vicinity of the wing tip. For this reason, there arises the necessity of using vibrating wing theory with a finite wing span in the calculations. /40

Ashley et al. have compiled a theory for calculating the air forces operating in cases when the rotor blades of helicopters are vibrating. This theory is an expansion of Reissner's theory about vibrating wings with a finite wing span [20].

Ashley et al. have also compiled a theory for calculating the air forces in cases when the blades are not vibrating, taking into consideration the fact that the wing span is finite.

In this chapter let us first introduce the paper of Ashley et al. Next let us calculate the pitch damping by means of wing theory taking into consideration the unsteady and quasi-steady finite wing span. It will be clarified as a result the degree of influence exerted on the pitch damping by (1) the effect of the finite wing span, the (2) the differences between the unsteady treatment and the quasi-steady treatment.

3.1. Introduction of the Theory of Ashley et al. [19]

This theory aims at expanding the "theory of vibrating wings with finite wing span" derived by Reissner [20] so that it can be applied to cases when the values of the main stream fluctuate in the wing span direction, and at applying this to helicopter rotors.

Let us focus attention on one of the rotor blades. There is always a vortex emerging from the rear edge of this blade in the wake. The vortex expands behind the blade, forming a plane. The vortex plane induces downwash on the blade. If we assume that the vortex close to the blade makes the chief contribution to the unsteady components of the downwash on the blade, it will be sufficient to focus attention only on the vortex within a very limited azimuth angle behind the blade. It is supposed that the vortex layer is inside the rotor rotating plane. Furthermore, since the blades are rotating, the vortex plane assumes an arc shape. However, within the range of the small azimuth angles, it may be regarded as having a linear shape vertical to the blade. If we assume that it is not necessarily essential to treat the position and magnitude of the distance vortices with great precision, the vortex plane will begin from the rear edge of the blade, as shown in Fig. 59, and will assume a band shape expanding towards the rear into a semi-infinite distance. In cases when there is a small inflow on the rotor surface, the vortex plane left by the preceding blade will be present, as was already mentioned before in the section devoted to Loewy's theory in Chapter 2. However, Ashley et al. proceed with their discussion without taking this returning vortex into consideration.

When one is dealing with vibrating wings with a small wing thickness, a small maximum camber, a small angle of incidence, and

and a small maximum wing displacement in the Z_1 direction, the problem can be linearized if the boundary conditions are described by the so-called foil theory in terms of the projection of the wing onto the $Z_1 = 0$ plane. The boundary conditions are as follows.

$$\frac{\partial z_a'}{\partial t} + V_{(y')}\frac{\partial z_a'}{\partial x'} = v_a + v_{as} \tag{3.1}$$

Here, v_a represents the unsteady components of the induction velocity, and v_{as} represents the steady components. In pitch damping problems there is no need to consider the steady components.

In cases when the blades are undergoing sinusoidal vibrations, v_a can be posited as $v_a(x',y',t) = \bar{v}_a(x',y')e^{i\omega t}$. The intensity of the unsteady components of the vortices in the wing chord and the wing span directions is represented as γ and δ, as is shown in Fig. 59. Subscript a is added to the values on the wing surface, and subscript w is added to the values in the wake.

$$\begin{aligned}
\gamma_a(\xi',\eta',t) &= \bar{\gamma}_a(\xi',\eta')e^{i\omega t}\\
\delta_a(\xi',\eta',t) &= \bar{\delta}_a(\xi',\eta')e^{i\omega t}\\
\gamma_W(\xi',\eta',t) &= \bar{\gamma}_W(\xi',\eta')e^{i\omega t}\\
\delta_W(\xi',\eta',t) &= \bar{\delta}_W(\xi',\eta')e^{i\omega t}
\end{aligned}$$

The bound vortices will be $\Gamma_a'(\eta',t) = \bar{\Gamma}_a'(\eta')e^{i\omega t}$, and the following relationship will apply between $\bar{\delta}_a(\xi',\eta')$ and $\bar{\Gamma}_a'(\eta')$.

$$\bar{\Gamma}_a'(\eta') = \int_{x_t'}^{x_t'} \bar{\gamma}_a(\xi',\eta')\,d\xi' \tag{3.2}$$

In potential flow, the velocity induced by the vortex can be sought by means of the Biot-Savart law.

$$\begin{aligned}
v_a(x',y') = &\frac{-1}{4\pi}\iint_{R_a}\frac{\bar{\gamma}_a(\xi',\eta')[x'-\xi'] + \bar{\delta}_a(\xi',\eta')[y'-\eta']}{[(x'-\xi')^2+(y'-\eta')^2]^{3/2}}\,d\xi'd\eta'\\
&-\frac{1}{4\pi}\iint_{R_W}\frac{\bar{\gamma}_W(\xi',\eta')[x'-\xi'] + \bar{\delta}_W(\xi',\eta')[y'-\eta']}{[(x'-\xi')^2+(y'-\eta')^2]^{3/2}}\,d\xi'd\eta'
\end{aligned} \tag{3.3}$$

/41

The following relationship applies between the shed vortex in the wake and the bound vortex.

$$\gamma_W(x_t',\eta)\,d\xi' = -\frac{d\Gamma_a'(\eta')}{dt}\,dt \tag{3.4}$$

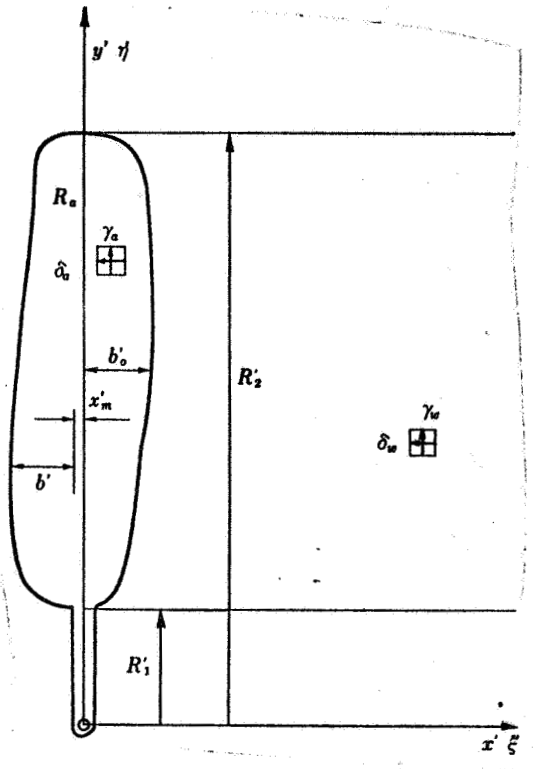

Fig. 59. Model and symbols for wing located in a current in which the main stream velocity fluctuates in the wing span direction

If we assume a sinusoidal motion,

$$\bar{\gamma}_W(\xi',\eta') = -\frac{i\omega}{V(\eta')}\Gamma_a'(\eta')e^{-i\omega\frac{\xi'-x_t'}{V(\eta')}} \tag{3.5}$$

Since $\partial\gamma/\partial\eta' = \partial\delta/\partial\xi'$, and also since γ is not present in front of the front edge of the wing,

$$\bar{\delta}_a(\xi',\eta') = \frac{\partial}{\partial\eta'}\int_{x_t'}^{\xi'}\bar{\gamma}_a(\lambda^*,\eta')\,d\lambda^* \tag{3.6}$$

$$\begin{aligned}\bar{\delta}_W(\xi',\eta') &= \frac{\partial}{\partial\eta'}\int_{x_t'}^{x_t'}\bar{\gamma}_a(\lambda^*,\eta')\,d\lambda^* + \frac{\partial}{\partial\eta'}\int_{x_t'}^{\xi'}\bar{\gamma}_W(\lambda^*,\eta')\,d\lambda^* \\ &= \frac{\partial\Gamma_a'}{\partial\eta'} + \frac{\partial}{\partial\eta'}\int_{x_t'}^{\xi'}\left(-\frac{i\omega}{V(\eta')}\right)\Gamma_a'(\eta')e^{-i\omega\frac{\lambda^*-x_t'}{V(\eta')}}\,d\lambda^*\end{aligned} \tag{3.7}$$

Let us further posit that $\bar{\Gamma}(\eta) \equiv \bar{\Gamma}_a(\eta')/b_0' \cdot e^{\frac{i\omega x t'}{V(\eta')}}$.

$$\bar{\gamma}_W(\xi',\eta') = -\frac{i\omega b_0'}{V(\eta')}e^{-i\omega\frac{\xi'}{V(\eta')}} \tag{3.8}$$

$$\begin{aligned}\bar{\delta}_W(\xi',\eta') &= \frac{\partial}{\partial\eta'}b_0'\Gamma(\eta')e^{-i\omega\frac{x_t'}{V(\eta')}} + \frac{\partial}{\partial\eta'}\int_{x_t'}^{\xi'}\left(-\frac{i\omega b_0'}{V(\eta')}\Gamma(\eta')e^{-i\omega\frac{\lambda^*}{V(\eta')}}\,d\lambda^*\right. \\ &= b_0'\frac{d}{d\eta'}\left[\Gamma(\eta')e^{-i\omega\frac{\xi'}{V(\eta')}}\right]\end{aligned} \tag{3.9}$$

If we substitute Eqs. (3.8) and 3.9) in Eq. (3.3),

$$\begin{aligned}v_a(x',y') = &-\frac{1}{4\pi}\iint_{R_a}\frac{\bar{\gamma}_a(\xi',\eta')[x'-\xi'] + \bar{\delta}_a(\xi',\eta')[y'-\eta']}{[(x'-\xi')^2+(y'-\eta')^2]^{3/2}}\,d\xi'd\eta' \\ &-\frac{1}{4\pi}\iint_{R_W}\frac{-\frac{i\omega b_0'}{V(\eta')}\Gamma(\eta')e^{-i\omega\frac{\xi'}{V(\eta')}}[x'-\xi'] + b_0'\frac{\partial}{\partial\eta'}\left[\Gamma(\eta')e^{-i\omega\frac{\xi'}{V(\eta')}}\right][y'-\eta']}{[(x'-\xi')^2+(y'-\eta')^2]^{3/2}}\,d\xi'd\eta'\end{aligned} \tag{3.10}$$

The terms on the right side of Eq. (3.10) are expressed as I_1, I_2, and I_3.

$$I_1 \equiv -\frac{1}{4\pi}\iint_{R_a}\frac{\bar{\gamma}_a(\xi',\eta')[x'-\xi']+\bar{\delta}_a(\xi',\eta')[y'-\eta']}{[(x'-\xi')^2+(y'-\eta')^2]^{3/2}}d\xi'd\eta'$$

$$I_2 \equiv \iint_{R_W}\frac{\frac{\partial}{\partial\eta'}\left[\Gamma(\eta')e^{-i\frac{\omega\xi'}{V(\eta')}}\right][y'-\eta']}{[(x'-\xi')^2(y'-\eta')^2]^{3/2}}d\xi'd\eta'$$

$$I_3 \equiv \iint_{R_W}\frac{\Gamma(\eta')/V(\eta')\cdot e^{-i\frac{\omega\xi'}{V(\eta')}}[x'-\xi']}{[(x'-\xi')^2+(y'-\eta')^2]^{3/2}}d\xi'd\eta'$$

If we write Eq. (3.10) using I_1, I_2, and I_3, we obtain:

$$v_a(x',y') = I_1 - \frac{b_0'}{4\pi}[I_2 - i\omega I_3] \tag{3.11}$$

I_1 expresses the contribution of the vortex with the replaced wing surface. I_2 expresses the trailing vortex in the wake, and I_3 the shed vortex in the wake.

A few modifications must be made in the physical model in order to make Eq. (3.10) more suitable for mathematical operations. Two of them are exactly the same as those carried out in Reissner's theory, and the other one is peculiar for cases when the velocity of the main stream changes in the wing span direction.

(a) As far as the effects of the vorteces with the replaced wing surface $\bar{\gamma}_a(\xi', \eta')$ and $\bar{\delta}_a(\xi', \eta')$ upon the induction velocity $\bar{v}_a(\xi', \eta)$ are concerned, the vortices with the replaced wing surface are handled as if the wing were a two-dimensional wing having everywhere the same load distribution as the aerodynamic load distribution in the wing chord direction at the y' position.

/42

$$\bar{\delta}_a(\xi',\eta') \cong 0$$

$$\bar{\delta}_a(\xi',\eta') \cong \bar{\gamma}_a(\xi',y')$$

$$I_1 \cong \frac{-1}{2\pi}\int_{x_l'}^{x_t'}\frac{\bar{\gamma}_a(\xi',y')}{x'-\xi'}d\xi' \tag{3.12}$$

In helicopter blades, the wing span is great enough in comparison with the wing chord, and events on the wing surfaces do not differ very rapidly on both sides of the point where the induction velocity is to be calculated, with the exception of the vicinity of the wing tips. Therefore, it is believed that a simplification like that in Eq. (3.12) is not altogether impossible.

(b) The pattern of the trailing vortex in the wake is expanded from the rear edge further into the wing surface, as far as the line in the wing span direction passing through the points (x', y') where the induction velocity is to be sought. That is,

in I_2

in I_2, the integration zone with respect to ξ' is changed from $x_t' \to \infty$ to $x' \to \infty$.

$$I_2 \cong \int_{R_1'}^{R_2'} \int_{x'}^{\infty} \frac{\frac{\partial}{\partial \eta'}\left[\Gamma(\eta') e^{-i\frac{\omega \xi'}{V(\eta')}}\right][y'-\eta']}{[(x'-\xi')^2+(y'-\eta')^2]^{3/2}} d\xi' d\eta'$$

$$= \int_{R_1'}^{R_2'} \frac{d\Gamma(\eta')}{d\eta'} e^{-i\frac{\omega x'}{V(\eta')}} \left\{ \int_0^{\infty} \frac{e^{-i\frac{\omega \lambda'}{V(\eta')}}[y'-\eta']}{[\lambda'^2+(y'-\eta')^2]^{3/2}} d\lambda' \right\} d\eta'$$

$$-i\omega \int_{R_1'}^{R_2'} \Gamma(\eta') \frac{d}{d\eta'}\left[\frac{1}{V(\eta')}\right] e^{-i\frac{\omega x'}{V(\eta')}} \left\{ \int_0^{\infty} \frac{[\lambda'+x'][y'-\eta'] e^{-i\frac{\omega \lambda'}{V(\eta')}}}{[\lambda'^2+(y'-\eta')^2]^{3/2}} d\lambda' \right\} d\eta' \tag{3.13}$$

(c) The portion corresponding to the difference between the pattern of the shed vortex in the wake and the position in the wing span direction where the induction velocity is to be sought, that is, the shed vortex at y', is expanded as far as the line in the wing span direction passing through points (x', y'). Furthermore, in this portion, the wave length factor $e^{-i\frac{\omega \xi'}{V(\eta')}}$ is replaced by the wave length factor at the y' position, $e^{-i\frac{\omega \xi'}{V(y')}}$.

In cases when $I_3 = I_3^{(2)} + \Delta I_3$, it is assumed that $I_3^{(2)}$ is the pattern of the shed vortex at y'. With respect to ΔI_3, the integration zone changes from $x_t' \to \infty$ to $x' \to \infty$, and $e^{-i\frac{\omega \xi'}{V(\eta')}}$ changes to $e^{-i\frac{\omega \xi'}{V(y')}}$. The change in the wave length factor is peculiar to the theory of Ashley et al., in which the main stream value changes in the wing span direction.

$$I_3^{(2)} \equiv \int_{-\infty}^{\infty} \int_{x_t'}^{\infty} \frac{\Gamma(y')}{V(y')} \frac{e^{-i\frac{\omega \xi'}{V(y')}}[x'-\xi']}{[(x'-\xi')+(y'-\eta')^2]^{3/2}} d\xi' d\eta' = \frac{2\Gamma(y')}{V(y')} \int_{x_t'}^{\infty} \frac{e^{-i\frac{\omega \xi'}{V(y')}}}{x'-\xi'} d\xi' \tag{3.14}$$

ΔI_3 is sought by $I_3 - I_3^{(2)}$, but let us rewrite slightly $I_3^{(2)}$ and I_3. Since $\Gamma(R_1')$ and $\Gamma(R_2')$ are 0

$$\frac{2\Gamma(y')}{V(y')} = \int_{R_1'}^{R_2'} \frac{d}{d\eta'}\left[\frac{\Gamma(\eta')}{V(\eta')}\right] \frac{|y'-\eta'|}{|y'-\eta'|} d\eta' \tag{3.15}$$

Eq. (3.14) can be rewritten as follows.

$$I_3^{(2)} = \int_{R_1'}^{R_2'} \int_{x_t'}^{\infty} \frac{d}{d\eta'}\left[\frac{\Gamma(\eta')}{V(\eta')}\right] \frac{e^{-i\frac{\omega \xi'}{V(y')}}|y'-\eta'|}{(x'-\xi')(y'-\eta')} d\xi' d\eta' \tag{3.16}$$

In I_3, if we perform partial integration for η', and utilize the fact that both $\Gamma(R_1')$ and $\Gamma(R_2')$ are 0, we obtain:

$$I_3=\int_{x_t'}^{\infty}\int_{R_1'}^{R_2'}\frac{\frac{\partial}{\partial\eta'}\left[e^{-i\frac{\omega\xi'}{V(\eta')}}\frac{\Gamma(\eta')}{V(\eta')}\right][y'-\eta']}{[x'-\xi']\sqrt{[x'-\xi']^2+[y'-\eta']^2}}d\xi'\eta d' \tag{3.17}$$

Subtracting Eq. (3.16) from Eq. (3.17) we seek ΔI_3. At this time, the range of integration is set at $x' \to \infty$, and the wave length factor of Eq. (3.16) is changed from $e^{-i\frac{\omega\xi'}{V(\eta')}}$ to $e^{-i\frac{\omega\xi'}{V(y')}}$.

$$\begin{aligned}\Delta I_3 \cong &\int_{R_1'}^{R_2'}\int_{x'}^{\infty}\frac{1}{x'-\xi'}\left\{\frac{\frac{\partial}{\partial\eta'}\left[e^{-i\frac{\omega\xi'}{V(\eta')}}\frac{d\Gamma(\eta')}{d\eta'}\right][y'-\eta']}{\sqrt{[x'-\xi']^2+[y'-\eta']^2}}-\frac{e^{-i\frac{\omega\xi'}{V(y')}}\frac{d}{d\eta'}\left[\frac{\Gamma(\eta')}{V(\eta')}\right]|y'-\eta'|}{[y'-\eta']}\right\}d\xi'd\eta'\\ =&\int_{R_1'}^{R_2'}e^{-i\frac{\omega x'}{V(y')}}\frac{d}{d\eta'}\left[\frac{\Gamma(\eta')}{V(\eta')}\right]\left\{-\int_0^{\infty}\frac{1}{\lambda'}\left[\frac{y'-\eta'}{\sqrt{\lambda'^2+(y'-\eta')^2}}-\frac{|y'-\eta'|}{y-\eta'}\right]e^{-i\frac{\omega\lambda'}{V(y')}}d\lambda'\right\}d\eta'\end{aligned} \tag{3.18}$$

Eq. (3.11) is rewritten as follows.

$$-\frac{1}{2\pi}\int_{x_t'}^{x_t'}\frac{\bar{\gamma}_\alpha(\xi',y')}{x'-\xi'}d\xi'=v_\alpha(x',y')+\frac{b_0'}{4\pi}[I_2-i\omega I_3^{(2)}-i\omega\Delta I_3] \tag{3.19}$$

It is clear from Eqs. (3.13), (3.14), and (3.18) that the second term on the right side does not contain ξ'.

Let us carry out the integrations contained in I_2, $I_3^{(2)}$, and ΔI_3. Variables q, τ, λ_1, and λ_2 are introduced.

/43

$$\left.\begin{aligned} q&\equiv\frac{\omega(y'-\eta')}{V(\eta')} & \tau&\equiv\frac{\omega(y'-\eta')}{V(y')}\\ \lambda_1&\equiv\frac{\omega\lambda'}{V(\eta')} & \lambda_2&\equiv\frac{\omega\lambda'}{V(y')}\end{aligned}\right\} \tag{3.20}$$

We rewrite I_2 using q, τ, λ_2, and λ_3.

$$\begin{aligned}I_2=&\int_{R_1'}^{R_2'}\frac{d\Gamma(\eta')}{d\eta'}\frac{\omega}{V(\eta')}e^{-i\frac{\omega x'}{V(\eta')}}\int_0^{\infty}\frac{e^{-i\lambda_1 q}}{[\lambda_1^2+q^2]^{3/2}}d\lambda_1 d\eta'\\ &-i\omega\int_{R_1'}^{R_2'}\Gamma(\eta')\frac{d}{d\eta'}\left[\frac{1}{V(\eta')}\right]e^{-i\frac{\omega x'}{V(\eta')}}\int_0^{\infty}\frac{\left[\lambda_1+\frac{\omega x'}{V(\eta')}\right]qe^{-i\lambda_1}}{[\lambda_1^2+q^2]^{3/2}}d\lambda_1 d\eta'\end{aligned} \tag{3.21}$$

We rewrite ΔI_3 using q, τ, λ_2, and λ_3.

$$\begin{aligned}\Delta I_3=&-\int_{R_1'}^{R_2'}\frac{d\Gamma(\eta')}{d\eta'}\frac{1}{V(\eta)}e^{-i\frac{\omega x'}{V(y')}}\int_0^{\infty}\frac{1}{\lambda_2}\left[\frac{\tau}{\sqrt{\lambda_2^2+\tau^2}}=\frac{|\tau|}{\tau}\right]e^{-i\lambda_2}d\lambda_2 d\eta'\\ &-\int_{R_1'}^{R_2'}\Gamma(\eta')\frac{d}{d\eta'}\left[\frac{1}{V(\eta')}\right]e^{-i\frac{\omega x'}{V(y')}}\int_0^{\infty}\frac{1}{\lambda_2}\left[\frac{\tau}{\sqrt{\lambda_2^2+\tau^2}}-\frac{|\tau|}{\tau}\right]e^{-i\lambda_2}d\lambda_2 d\eta'\end{aligned} \tag{3.22}$$

The functions appearing in I_2 and ΔI_3 are defined as follows:

$$\left.\begin{aligned} N_A(q) &\equiv q\int_0^\infty \frac{\lambda_1 e^{-t\lambda_1}}{[\lambda_1^2+q^2]^{3/2}}\,d\lambda_1 \\ N_B(q) &\equiv q\int_0^\infty \frac{e^{-t\lambda_1}}{[\lambda_1^2+q^2]^{3/2}}\,d\lambda_1 \\ N_C(\tau) &\equiv \int_0^\infty \left[\frac{\tau}{\sqrt{\tau^2+\lambda_2^2}}-\frac{|\tau|}{\tau}\right]\frac{e^{-t\lambda_2}}{\lambda_2}\,d\lambda_2 \end{aligned}\right\} \tag{3.23}$$

The methods of calculating $N_A(q)$, $N_B(q)$, and $N_C(\tau)$ are described separately in Appendix B.

The nondimensionalized variables are introduced as follows.

$$\left.\begin{aligned} y &= \frac{y'}{b_0'} & \eta &= \frac{\eta'}{b_0'} \\ x &= \frac{x'-(x_t'+x_l')/2}{b'} & \xi &= \frac{\xi'-(x_t'+x_l')/2}{b'} \\ x_m &= \frac{x_t'+x_l'}{2b'} \end{aligned}\right\} \tag{3.24}$$

Four types of reduced frequency are introduced.

$$\left.\begin{aligned} k(y) &\equiv \frac{\omega b'(y)}{V(y)} & k(\eta) &\equiv \frac{\omega b'(\eta)}{V(\eta)} \\ k_0(y) &= \frac{\omega b_0'}{V(y)} & k_0(\eta) &= \frac{\omega b_0'}{V(\eta')} \end{aligned}\right\} \tag{3.25}$$

I_2 can be written in the following manner.

$$\begin{aligned} I_2 = &\int_{R_1}^{R_2} \frac{d\Gamma}{d\eta}\,\frac{\omega}{V(\eta)}\,e^{-i[k(\eta)x+k_0(\eta)x_m]}N_B(k_0(\eta)[y-\eta])\,d\eta \\ &-i\omega\int_{R_1}^{R_2}\Gamma(\eta)\,\frac{d}{d\eta}\left[\frac{1}{V(\eta)}\right]e^{-i[k(\eta)x+k_0(\eta)x_m]}\{N_A(k_0(\eta)[y-\eta]+[k(\eta)x+k_0(\eta)x_m]N_B(k_0(\eta)[y-\eta]\}\,d\eta \end{aligned} \tag{3.26}$$

ΔI_3 can be written in the following manner.

$$\begin{aligned} \Delta I_3 = &-\int_{R_1}^{R_2}\frac{d\Gamma(\eta)}{d\eta}\,\frac{1}{V(\eta)}\,e^{-i[k(y)x+k_0(y)x_m]}N_C(k_0(y)[y-\eta])\,d\eta \\ &-\int_{R_1}^{R_2}\Gamma(\eta)\,\frac{d}{d\eta}\left[\frac{1}{V(\eta)}\right]e^{-i[k(y)x+k_0(y)x_m]}N_C(k_0(y)[y-\eta])\,d\eta \end{aligned} \tag{3.27}$$

The right side of Eq. (3.19) is:

$$-\frac{1}{2\pi}\int_{x_l'}^{x_t'}\frac{\gamma_a(\xi',y')}{x'-\xi'}\,d\xi' = -=-\frac{1}{2\pi}\int_{-1}^{1}\frac{\gamma_a(\xi,y)}{x-\xi}\,d\xi \tag{3.28}$$

In view of Eq. (3.14), $I_3^{(2)}$ is:

$$I_3^{(2)}=\frac{2\Gamma(y)}{V(y)}\int_1^\infty \frac{e^{-i[k(y)\xi+k_0(y)x_m]}}{x-\xi}d\xi \tag{3.29}$$

If we substitute Eqs. (3.28), (3.26), (3.29), and (3.27) into Eq. (3.19), we obtain:

$$\begin{aligned}
&\frac{1}{2\pi}\int_{-1}^{1}\frac{\bar\gamma_a(\xi,y)}{x-\xi}d\xi=-v_a(x,y)+\frac{ik_0(y)}{2\pi}\Gamma(y)e^{-ik_0(y)x_m}\int_1^\infty\frac{e^{-ik(y)\xi}}{x-\xi}d\xi\\
&-\frac{1}{4\pi}\int_{R_1}^{R_2}\frac{d\Gamma}{d\eta}k_0(\eta)\Big\{e^{-i[k_0(y)x_m+k(y)x]\frac{V(y)}{V(\eta)}}N_B(k_0(\eta)[y-\eta])\\
&+ie^{-i[k_0(y)x_m+k(y)x]}N_C(k_0(y)[y-\eta])\Big\}d\eta\\
&+\frac{ik_0(y)}{4\pi}\int_{R_1}^{R_2}\Gamma(\eta)\frac{d}{d\eta}\Big[\frac{V(y)}{V(\eta)}\Big]\Big\{e^{-i[k_0(y)x_m+k(y)x]\frac{V(y)}{V(\eta)}}\Big\langle N_A(k_0(\eta)[y-\eta])\\
&+[k_0(y)x_m+k(y)x]\frac{V(y)}{V(\eta)}N_B(k_0(\eta)[y-\eta])\Big\rangle-e^{i[k_0(y)x_m+k(y)x]}N_C(k_0(y)[y-\eta])\Big\}d\eta
\end{aligned} \tag{3.30}$$

/44

Since $\bar\gamma_a(1,y)=0$ according to Kutta's conditions, it is possible to apply Söngen's inversion formula. Before this, let us introduce the following operators.

$$\begin{aligned}
D_1\{\cdots\}&=\frac{1}{4\pi}\int_{R_1}^{R_2}\frac{d\Gamma}{d\eta}k_0(\eta)e^{-ik_0(y)x_m\frac{V(y)}{V(\eta)}}N_B(k_0(\eta)[y-\eta])\{\cdots\}d\eta\\
D_2\{\cdots\}&=\frac{i}{4\pi}\int_{R_1}^{R_2}\frac{d\Gamma}{d\eta}k_0(\eta)e^{-ik_0(y)x_m}N_C(k_0(y)[y-\eta])\{\cdots\}d\eta\\
D_3\{\cdots\}&=\frac{ik_0(y)}{4\pi}\int_{R_1}^{R_2}\Gamma(\eta)\frac{d}{d\eta}\Big[\frac{V(y)}{V(\eta)}\Big]e^{-ik_0(y)x_m\frac{V(y)}{V(\eta)}}N_A(k_0(\eta)[y-\eta])\{\cdots\}d\eta\\
D_4\{\cdots\}&=\frac{ik_0(y)}{4\pi}\int_{R_1}^{R_2}\Gamma(\eta)\frac{d}{d\eta}\Big[\frac{V(y)}{V(\eta)}\Big]e^{-ik_0(y)x_m\frac{V(y)}{V(\eta)}}\frac{V(y)}{V(\eta)}N_B(k_0(\eta)[y-\eta])\{\cdots\}d\eta\\
D_5\{\cdots\}&=\frac{ik_0(y)}{4\pi}\int_{R_1}^{R_2}\Gamma(\eta)\frac{d}{d\eta}\Big[\frac{V(y)}{V(\eta)}\Big]e^{-ik_0(y)x_m}N_C(k_0(y)[y-\eta])\{\cdots\}d\eta
\end{aligned} \tag{3.31}$$

If we write Eq. (3.30) using operators D_1, D_2, D_3, D_4, and D_5, we obtain:

$$-\{D_2+D_5\}\{e^{-ik(y)x}\}+D_4\Big\{[k_0(y)x_m+k(y)x]e^{-ik(y)x\frac{V(y)}{V(\eta)}}\Big\} \tag{3.32}$$

If we use Söngen's inversion formula, we obtain:

$$\bar{\gamma}_a(x,y)=-\frac{2}{\pi}\sqrt{\frac{1-x}{1+x}}\left\langle\int_{-1}^{1}-\sqrt{\frac{1+\xi}{1-\xi}}\,\frac{v_a(\xi,y)}{x-\xi}d\xi\right.$$
$$+\frac{ik_0(y)}{2\pi}\Gamma(y)e^{-ik_0(y)x_m}\int_{-1}^{1}\sqrt{\frac{1+\xi}{1-\xi}}\,\frac{1}{x-\xi}\int_{1}^{\infty}\frac{e^{-ik(y)\lambda}}{\xi-\lambda}d\lambda d\xi$$
$$-\{D_1-D_3\}\left\{\int_{-1}^{1}\sqrt{\frac{1+\xi}{1-\xi}}\,\frac{1}{x-\xi}e^{-ik(y)\xi}\frac{V(y)}{V(\eta)}d\xi\right\}-\{D_2+D_3\}\left\{\int_{-1}^{1}\sqrt{\frac{1+\xi}{1-\xi}}\,\frac{1}{x-\xi}e^{-ik(y)\xi}d\xi\right\}$$
$$\left.+\{D_4\}\left\{\int_{-1}^{1}\sqrt{\frac{1+\xi}{1-\xi}}\,\frac{1}{x-\xi}[k_0(y)x_m+k(y)\xi]e^{-ik(y)\xi}\frac{V(y)}{V(\eta)}d\xi\right\}\right. \tag{3.33}$$

However, when we use Eq. (3.2), we obtain:

$$\int_{x_{l'}}^{x_{l'}}\bar{\gamma}_a(x',y')dx'=b'\int_{-1}^{1}\bar{\gamma}_a(x,y)dx=\Gamma_a'(y')=b_0'e^{-i[k(y)x+k_0(y)x_m]}\Gamma(y) \tag{3.34}$$

Let us rewrite the second term on the right side of Eq. (3.33) for the purpose of integrating $\bar{\gamma}_a(x,y)$ from x = -1 to 1.

$$\int_{-1}^{1}\sqrt{\frac{1+\xi}{1-\xi}}\,\frac{1}{x-\xi}\int_{1}^{\infty}\frac{e^{-ik\lambda}}{\xi-\lambda}d\lambda d\xi=\int_{1}^{\infty}e^{-ik\lambda}\int_{-1}^{1}\sqrt{\frac{1+\xi}{1-\xi}}\,\frac{1}{x-\xi}\,\frac{1}{\xi-\lambda}d\xi d\lambda$$

Thereupon,

$$\sqrt{\frac{1+\xi}{1-\xi}}\,\frac{1}{x-\xi}\,\frac{1}{\xi-\lambda}=\frac{1}{x-\lambda}\sqrt{\frac{1+\xi}{1-\xi}}\,\frac{1}{x-\xi}+\frac{1}{\lambda-x}\sqrt{\frac{1+\xi}{1-\xi}}\,\frac{1}{\lambda-\xi}$$

$$\int_{-1}^{1}\sqrt{\frac{1+\xi}{1-\xi}}\,\frac{1}{x-\xi}d\xi=-\pi \qquad \text{for } -1\leq x\leq 1$$

$$\int_{-1}^{1}\sqrt{\frac{1+\xi}{1-\xi}}\,\frac{1}{\lambda-\xi}d\xi=\pi\left(\sqrt{\frac{\lambda+1}{\lambda-1}}-1\right) \qquad \text{for } \lambda\geq 1$$

$$\int_{-1}^{1}\sqrt{\frac{1+\xi}{1-\xi}}\,\frac{1}{x-\xi}\int_{1}^{\infty}\frac{e^{-ik\lambda}}{\xi-\lambda}d\lambda d\xi=\int_{1}^{\infty}\pi\,\frac{1}{\lambda-x}\sqrt{\frac{\lambda+1}{\lambda-1}}e^{-ik\lambda}d\lambda$$

/45

Therefore,

$$\frac{ik_0(y)}{2\pi}\Gamma(y)e^{-ik_0(y)x_m}\int_{-1}^{1}\sqrt{\frac{1+\xi}{1-\xi}}\,\frac{1}{x-\xi}\int_{1}^{\infty}\frac{e^{-ik(y)\lambda}}{\xi-\lambda}d\lambda$$
$$=\frac{ik_0(y)}{2}\Gamma(y)e^{-ik_0(y)x_m}\int_{1}^{\infty}\frac{1}{\lambda-x}\sqrt{\frac{\lambda+1}{\lambda-1}}e^{-ik(y)\lambda}d\lambda$$

If we use this, we can write Eq. (3.34) in the following manner:

$$\bar{\gamma}_a(x,y)=-\frac{2}{\pi}\sqrt{\frac{1-x}{1+x}}\left\langle\int_{-1}^{1}-\sqrt{\frac{1+\xi}{1-\xi}}\,\frac{v_a(\xi,y)}{x-\xi}d\xi+\frac{ik_0(y)}{2}\Gamma(y)e^{-ik_0(y)x_m}\int_{1}^{\infty}\frac{1}{\lambda-x}\sqrt{\frac{\lambda+1}{\lambda-1}}e^{-ik(y)\lambda}d\lambda\right.$$
$$-\{D_1-D_3\}\left\{\int_{-1}^{1}\sqrt{\frac{1+\xi}{1-\xi}}\,\frac{1}{x-\xi}e^{-ik(y)\xi}\frac{V(y)}{V(\eta)}d\xi\right\}-\{D_2+D_3\}\left\{\int_{-1}^{1}\sqrt{\frac{1+\xi}{1-\xi}}\,\frac{1}{x-\xi}e^{-ik(y)\xi}d\xi\right.$$
$$\left.\left.+D_4\left\{\int_{-1}^{1}\sqrt{\frac{1+\xi}{1+\xi}}\,\frac{1}{x-\xi}[k_0(y)x_m+k(y)\xi]e^{-ik(y)\xi}\frac{V(y)}{V(\eta)}d\xi\right\}\right\rangle\right. \tag{3.35}$$

Eq. (3.35) is substituted into Eq. (3.34) in order to eliminate $\overline{\gamma}_a$. At this time, the following integration is utilized in order to integrate $\overline{\gamma}_a(x, y)$ from x = -1 to x = 1.

$$\int_{-1}^{1}\sqrt{\frac{1-x}{1+x}}\,\frac{1}{x-\xi}\,dx=-\pi \qquad \text{for } -1\leqq\xi\leqq 1$$

$$\int_{-1}^{1}\sqrt{\frac{1-x}{1+x}}\,\frac{1}{\lambda-x}\,dx=-\pi\left(\sqrt{\frac{\lambda-1}{\lambda+1}}-1\right) \qquad \text{for } \lambda\geq 1$$

Therefore,

$$\begin{aligned}\frac{b_0'}{b'}e^{-i[k(y)x+k_0(y)x_m]}\Gamma(y)=2\int_{-1}^{1}-\sqrt{\frac{1+\xi}{1-\xi}}\,\overline{v}_a(\xi,y)\,d\xi+ik_0(y)\Gamma(y)e^{-ik_0(y)x_m}\int_{1}^{\infty}\left(1-\sqrt{\frac{\lambda+1}{\lambda-1}}\right)e^{-ik(y)\lambda}\,d\lambda\\ -2\{D_1-D_3\}\left\{\int_{-1}^{1}\sqrt{\frac{1+\xi}{1-\xi}}\,e^{-ik(y)\xi}\frac{V(y)}{V(\eta)}\,d\xi\right\}-2\{D_2+D_3\}\left\{\int_{-1}^{1}\sqrt{\frac{1+\xi}{1-\xi}}\,e^{-ik(y)\xi}\,d\xi\right\}\\ +2D_4\left\{\int_{-1}^{1}\sqrt{\frac{1+\xi}{1-\xi}}\,[k_0(y)x_m+k(y)\xi]e^{-ik(y)\xi}\frac{V(y)}{V(\eta)}\,d\xi\right\}\end{aligned} \tag{3.36}$$

Since parts of the second term on the left side and right side of Eq. (3.36) are identical,

$$\begin{aligned}2\int_{-1}^{1}\sqrt{\frac{1+\xi}{1-\xi}}\,v(\xi,y)\,d\xi=-ik_0(y)\Gamma(y)e^{-ik_0(y)x_m}\int_{1}^{\infty}\sqrt{\frac{\lambda+1}{\lambda-1}}\,e^{-ik(y)\lambda}\,d\lambda\\ -2\{D_1-D_3\}\left\{\int_{-1}^{1}\sqrt{\frac{1+\xi}{1-\xi}}\,e^{-ik(y)\xi}\frac{V(y)}{V(\eta)}\,d\xi\right\}-2\{D_2+D_3\}\left\{\int_{-1}^{1}\sqrt{\frac{1+\xi}{1-\xi}}\,e^{-ik(y)\xi}\,d\xi\right.\\ \left.+2D_4\left\{\int_{-1}^{1}\sqrt{\frac{1+\xi}{1-\xi}}\,[k_0(y)x_m+k(y)\xi]e^{-ik(y)\xi}\frac{V(y)}{V(\eta)}\,d\xi\right\}\right.\end{aligned} \tag{3.37}$$

The integration appearing on the right side of Eq. (3.37) can be expressed using Bessel functions.

$$\int_{1}^{\infty}\sqrt{\frac{\lambda+1}{\lambda-1}}\,e^{-ik\lambda}\,d\lambda=\left(\frac{\pi}{2i}H_0^{(2)}(k)-\frac{\pi}{2}H_1^{(2)}(k)\right)$$

$$\int_{-1}^{1}\sqrt{\frac{1+\xi}{1-\xi}}\,e^{-ik\xi}\,d\lambda=(\pi J_0(k)-\pi iJ_1(k))$$

$$\int_{-1}^{1}\sqrt{\frac{1+\xi}{1-\xi}}\,\xi e^{-ik\xi}\,d\xi=\pi\left(J_0(k)-\frac{1+ik}{k}J_1(k)\right)$$

The right side of Eq. (3.37) is expressed by means of Bessel functions, and both sides are divided by $\frac{\pi ik_0(y)}{2}e^{-ik_0(y)x_m}(H_1^{(2)}(k(y))+iH_0^{(2)}(k(y)))$

Further, we return the operators such as D_1 and D_2 to their original forms.

$$\Gamma^{(3)}(y)=\Gamma(y)-\frac{e^{-ik_0(y)x_m}}{\pi i[H_1^{(2)}(k(y))+iH_0^{(2)}(k(y))]}\int_{R_1}^{R_2}\frac{d\Gamma}{d\eta}\frac{V(y)}{V(\eta)}e^{-ik_0(y)x_m\frac{V(y)}{V(\eta)}}$$
$$\times N_B(k_0(\eta)[y-\eta])\left\{J_0\left(k(y)\frac{V(y)}{V(\eta)}\right)-iJ_1\left(k(y)\frac{V(y)}{V(\eta)}\right)\right\}d\eta$$
$$+\frac{e^{-ik_0(y)x_m}}{\pi i[H_1^{(2)}(k(y))+iH_0^{(2)}(k(y))]}\int_{R1}^{R_2}i\Gamma(\eta)\frac{d}{d\eta}\left[\frac{V(y)}{V(\eta)}\right]e^{-ik_0(y)x_m\frac{V(y)}{V(\eta)}}$$
$$\times N_A(k_0(\eta)[y-\eta])\left\{J_0\left(k(y)\frac{V(y)}{V(\eta)}\right)-iJ_1\left(k(y)\frac{V(y)}{V(\eta)}\right)\right\}d\eta$$
$$+\frac{e^{-ik_0(y)x_m}}{\pi i[H_1^{(2)}(k(y))+iH_0^{(2)}(k(y))]}\int_{R_1}^{R_2}i\Gamma(\eta)\frac{d}{d\eta}\left[\frac{V(y)}{V(\eta)}\right]\cdot\left[\frac{V(y)}{V(\eta)}\right]e^{-ik_0(y)x_m\frac{V(y)}{V(\eta)}}$$
$$\times N_B(k_0(\eta)[y-\eta])\left\{k_0(y)x_m\left(J_0\left(k(y)\frac{V(y)}{V(\eta)}\right)-iJ_1\left(k(y)\frac{V(y)}{V(\eta)}\right)\right)\right.$$
$$\left.+k(y)\left(J_0\left(k(y)\frac{V(y)}{V(\eta)}\right)-\frac{1+ik(y)\frac{V(y)}{V(\eta)}}{k(y)\frac{V(y)}{V(\eta)}}J_1\left(k(y)\frac{V(y)}{V(\eta)}\right)\right)\right\}d\eta$$
$$-\frac{e^{-ik_0(y)x_m}}{\pi i[H_1^{(2)}(k(y))+iH_0^{(2)}(k(y))]}\int_{R_1}^{R_2}i\frac{d\Gamma}{d\eta}\left[\frac{V(y)}{V(\eta)}\right]e^{-ik_0(y)x_m}$$
$$\times N_C(k_0(y)[y-\eta])\{J_0(k(y))-iJ_1(k(y))\}d\eta$$
$$-\frac{e^{-ik_0(y)x_m}}{\pi i[H_1^{(2)}(k(y))+iH_0^{(2)}(k(y))]}\int_{R_1}^{R_2}i\Gamma(\eta)\frac{d}{d\eta}\left[\frac{V(y)}{V(\eta)}\right]e^{-ik_0(y)x_m}$$
$$\times N_C(k_0(y)[y-\eta])\{J_0(k(y))-iJ_1(k(y))\}d\eta \qquad (3.38)$$

/46

If we solve Eq. (3.38) while considering that $\overline{\Gamma}(y)$ becomes 0 when $y = R_1$ and $y = R_2$, it will be possible to seek the distribution of the circulation along the radial direction of the blade. Here,

$$\Gamma^{(3)}(y)\equiv 4\frac{b'}{b_0'}e^{-ik_0(y)x_m}\frac{\int_{-1}^{1}\sqrt{\frac{1+\xi}{1-\xi}}v_a(\xi,y)d\xi}{\pi ik(y)[H_1^{(2)}(k(y))+iH_0^{(2)}(k(y))]} \qquad (3.39)$$

As is clear from the process described thus far, this is the equation expressing the circulation which appears in two-dimensional vibrating wing theory.

Next, let us seek the unsteady air forces operating on the wing. The following relationship applies, in accordance with exactly the same thinking as that when Eq. (2.22) was derived, between the pressure difference between the upper and lower wing surfaces and the distributed vortex with the replaced wing surfaces.

$$\frac{\Delta\bar{p}(x^*,y)}{\rho V(y)}=-\bar{\gamma}_a(x^*,y)-ik(y)\int_{-1}^{x^*}\bar{\gamma}_a(\xi,y)d\xi \qquad (3.40)$$

Let us carry out the integration of the second term on the right side. We will use Eq. (3.35) for γ_a.

$$\begin{aligned}\int_{-1}^{x^*}\gamma_a(\xi^*,y)\,d\xi^* = &-\frac{2}{\pi}\int_{-1}^{1}-\sqrt{\frac{1+\xi}{1-\xi}}\,v_a(\xi,y)\int_{-1}^{x^*}\sqrt{\frac{1-\xi^*}{1+\xi^*}}\,\frac{1}{\xi^*-\xi}\,d\xi^*d\xi\\ &-\frac{ik_0(y)\Gamma(y)}{\pi}e^{-ik_0(y)x_m}\int_1^\infty e^{-ik(y)\lambda}\sqrt{\frac{\lambda+1}{\lambda-1}}\int_{-1}^{x^*}\sqrt{\frac{1-\xi^*}{1+\xi^*}}\,\frac{1}{\lambda-\xi^*}\,d\xi^*d\lambda\\ &+\frac{2}{\pi}\{D_1-D_3\}\left\{\int_{-1}^{1}\sqrt{\frac{1+\xi}{1-\xi}}\,e^{-ik(y)\xi}\frac{V(y)}{V(\eta)}\int_{-1}^{x^*}\sqrt{\frac{1-\xi^*}{1+\xi^*}}\,\frac{1}{\xi^*-\xi}\,d\xi^*d\xi\right\}\\ &+\frac{2}{\pi}\{D_2+D_3\}\left\{\int_{-1}^{1}\sqrt{\frac{1+\xi}{1-\xi}}\,e^{-ik(y)\xi}\int_{-1}^{x^*}\sqrt{\frac{1-\xi^*}{1+\xi^*}}\,\frac{1}{\xi^*-\xi}\,d\xi^*d\xi\right\}\\ &-\frac{2}{\pi}D_4\left\{\int_{-1}^{1}\sqrt{\frac{1+\xi}{1-\xi}}\,[k_0(y)x_m+k(y)\xi]\,e^{-ik(y)\xi}\frac{V(y)}{V(\eta)}\int_{-1}^{x^*}\sqrt{\frac{1-\xi^*}{1+\xi^*}}\,\frac{1}{\xi^*-\xi}\,d\xi^*d\xi\right\}\end{aligned} \tag{3.41}$$

Whereupon,

$$\int_{-1}^{x^*}\sqrt{\frac{1-\xi^*}{1+\xi^*}}\,\frac{1}{\xi^*-\xi}\,d\xi^* = -\left(\frac{\pi}{2}+\sin^{-1}x^*\right)-\sqrt{\frac{1-\xi}{1+\xi}}\,A_1(x^*,\xi) \qquad \text{for } -1\leqq\xi\leqq1$$

Here,

$$A_1(x^*,\xi)=\frac{1}{2}\log\left|\frac{1-x^*\xi+\sqrt{1-\xi^2}\sqrt{1-x^{*2}}}{1-x^*\xi-\sqrt{1-\xi^2}\sqrt{1-x^{*2}}}\right|$$

$$\int_{-1}^{x^*}\sqrt{\frac{1-\xi^*}{1+\xi^*}}\,\frac{1}{\lambda-\xi^*}\,d\xi^* = \frac{\pi}{2}+\sin^{-1}x^*+\sqrt{\frac{\lambda-1}{\lambda+1}}\,A_2(x^*,\lambda) \qquad \text{for } \lambda\geq1$$

/47

Here,

$$A_2(x^*,\lambda)=2\tan^{-1}\sqrt{\frac{(1-x^*)(\lambda+1)}{(1+x^*)(\lambda-1)}}-\pi$$

$$\begin{aligned}\therefore\ \int_{-1}^{x^*}\gamma_a(\xi^*,y)\,d\xi^* = &\frac{2}{\pi}\int_{-1}^{1}\sqrt{\frac{1+\xi}{1-\xi}}\,v_a(\xi,y)\left[-\left(\frac{\pi}{2}+\sin^{-1}x^*\right)-\sqrt{\frac{1-\xi}{1+\xi}}\,A_1(x^*,\xi)\right]d\xi\\ &-\frac{ik_0(y)\Gamma(y)}{\pi}e^{-ik_0(y)x_m}\int_1^\infty\left[\frac{\pi}{2}+\sin^{-1}x^*+\sqrt{\frac{\lambda-1}{\lambda+1}}\,A_2(x^*,\lambda)\right]\sqrt{\frac{\lambda+1}{\lambda-1}}\,e^{-ik(y)\lambda}d\lambda\\ &+\frac{2}{\pi}\{D_1-D_3\}\left\{\int_{-1}^{1}\left[-\left(\frac{\pi}{2}+\sin^{-1}x^*\right)-\sqrt{\frac{1-\xi}{1+\xi}}\,A_1(x^*,\xi)\right]\sqrt{\frac{1+\xi}{1-\xi}}\,e^{-ik(y)\xi}\frac{V(y)}{V(\eta)}\,d\xi\right\}\\ &+\frac{2}{\pi}\{D_2+D_3\}\left\{\int_{-1}^{1}\left[-\left(\frac{\pi}{2}+\sin^{-1}x^*\right)-\sqrt{\frac{1-\xi}{1+\xi}}\,A_1(x^*,\xi)\right]\sqrt{\frac{1+\xi}{1-\xi}}\,e^{-ik(y)\xi}d\xi\right\}\\ &-\frac{2}{\pi}D_4\left\{\int_{-1}^{1}\left[-\left(\frac{\pi}{2}+\sin^{-1}x^*\right)-\sqrt{\frac{1-\xi}{1+\xi}}\,A_1(x^*,\xi)\right]\sqrt{\frac{1+\xi}{1-\xi}}\,[k_0(y)x_m+k(y)\xi]\,e^{-ik(y)\xi}\frac{V(y)}{V(\eta)}\,d\xi\right\}\end{aligned} \tag{3.42}$$

It is clear from Eq. (3.37) that those terms in Eq. (3.42) to which $\left(\frac{\pi}{2}+\sin^{-1}x^*\right)$ is applied will be 0. Therefore,

$$\int_{-1}^{x^*} p_a(\xi^*, y)\,d\xi^* = -\frac{2}{\pi}\int_{-1}^{1} A_1(x^*,\xi)\,v_a(\xi,y)\,d\xi - \frac{ik_0(y)\Gamma(y)}{\pi}e^{-ik_0(y)x_m}\int_1^\infty A_2(x^*,\lambda)e^{-ik(y)\lambda}\,d\lambda$$
$$-\frac{2}{\pi}\{D_1-D_3\}\left\{\int_{-1}^{1} A_1(x^*,\xi)e^{-ik(y)\xi}\frac{V(y)}{V(\eta)}\,d\xi\right\}-\frac{2}{\pi}\{D_2+D_3\}\left\{\int_{-1}^{1} A_1(x_\phi,\xi)e^{-ik(y)\xi}\,d\xi\right\}$$
$$+\frac{2}{\pi}D_4\left\{\int_{-1}^{1} A_1(x^*,\xi)[k_0(y)x_m+k(y)\xi]e^{-ik(y)\xi}\frac{V(y)}{V(\eta)}\,d\xi\right\} \tag{3.43}$$

However,

$$\int_1^\infty A_2(x^*,\lambda)e^{-ik(y)\lambda}\,d\lambda = -\frac{1}{ik(y)}e^{-ik(y)\lambda}A_2(x^*,\lambda)\Big|_1^\infty + \frac{1}{ik(y)}\sqrt{\frac{1-x^*}{1+x^*}}\int_1^\infty \frac{1}{\sqrt{\lambda^2-1}}e^{-ik(y)\lambda}\,d\lambda$$
$$+\frac{1}{ik(y)}\sqrt{\frac{1-x^*}{1+x^*}}\int_1^\infty\sqrt{\frac{\lambda+1}{\lambda-1}}\frac{1}{x^*-\lambda}e^{-ik(y)\lambda}\,d\lambda \tag{3.44}$$

Since it is believed that the first term on the right side will be 0,

$$-ik(y)\int_{-1}^{x^*} p_a(\xi^*,y)\,d\xi^* = \frac{2}{\pi}ik(y)\int_{-1}^{1} A_1(x^*,\xi)\,v_a(\xi,y)\,d\xi$$
$$+\frac{ik_0(y)\Gamma(y)}{\pi}e^{-ik_0(y)x_m}\sqrt{\frac{1-x^*}{1+x^*}}\int_1^\infty\frac{1}{\sqrt{\lambda^2-1}}e^{-ik(y)\lambda}\,d\lambda$$
$$+\frac{ik_0(y)\Gamma(y)}{\pi}e^{-ik_0(y)x_m}\sqrt{\frac{1-x^*}{1+x^*}}\int_1^\infty\sqrt{\frac{\lambda+1}{1+1}}\frac{1}{x^*-\lambda}e^{-ik(y)\lambda}\,d\lambda$$
$$-\frac{2}{\pi}\{D_1-D_3\}\left\{\int_{-1}^{1}-ik(y)A_1(x^*,\xi)e^{-ik(y)\xi}\frac{V(y)}{V(\eta)}\,d\xi\right\}$$
$$-\frac{2}{\pi}\{D_2+D_3\}\left\{\int_{-1}^{1}-ik(y)A_1(x^*,\xi)e^{-ik(y)\xi}\,d\xi\right\}$$
$$+\frac{2}{\pi}D_4\left\{\int_{-1}^{1}-ik(y)A_1(x^*,\xi)[k_0(y)x_m+k(y)\xi]e^{-ik(y)\xi}\frac{V(y)}{V(\eta)}\,d\xi\right\} \tag{2.45}$$
[sic]

If we substitute Eqs. (3.35) and (3.45) into Eq. (3.40), we obtain:

/48

$$\frac{\Delta\bar{p}(x^*,y)}{\rho V(y)} = -\frac{2}{\pi}\int_{-1}^{1}\left[\sqrt{\frac{1+\xi}{1-\xi}}\sqrt{\frac{1-x^*}{1+x^*}}\frac{1}{x^*-\xi}-ik(y)A_1(x^*,\xi)\right]v_a(\xi,y)\,d\xi$$
$$+\frac{ik_0(y)\Gamma(y)}{\pi}e^{-ik_0(y)x_m}\sqrt{\frac{1-x^*}{1+x^*}}\int_1^\infty\frac{1}{\sqrt{\lambda^2-1}}e^{-ik(y)\lambda}\,d\lambda$$
$$-\frac{2}{\pi}\{D_1-D_3\}\left\{\int_{-1}^{1}\left[\sqrt{\frac{1+\xi}{1-\xi}}\sqrt{\frac{1-x^*}{1+x^*}}\frac{1}{x^*-\xi}-ik(y)A_1(x^*,\xi)\right]e^{-ik(y)\xi}\frac{V(y)}{V(\eta)}\,d\xi\right\}$$
$$-\frac{2}{\pi}\{D_2+D_3\}\left\{\int_{-1}^{1}\left[\sqrt{\frac{1+\xi}{1-\xi}}\sqrt{\frac{1-x^*}{1+x^*}}\frac{1}{x^*-\xi}-ik(y)A_1(x^*,\xi)\right]e^{-ik(y)\xi}\,d\xi\right\}$$
$$+\frac{2}{\pi}D_4\left\{\int_{-1}^{1}[k_0(y)x_m+k(y)\xi]\left[\sqrt{\frac{1+\xi}{1-\xi}}\sqrt{\frac{1-x^*}{1+x^*}}\frac{1}{x^*-\xi}-ik(y)A_1(x^*,\xi)e^{-ik(y)\xi}\frac{V(y)}{V(\eta)}\,d\xi\right\}\right. \tag{3.46}$$

3.2. Analysis by Unsteady Theory

In cases then the rotor surface is performing sinusoidal movement as expressed by $\theta = \overline{\theta} \sin pt$, as was mentioned in Chapter 2, Section 2, the blades perform movement synthesizing two types of sinusoidal vibrations in which the frequencies are $\Omega + p$ and $\Omega - p$. Since Eq. (3.11) for seeking the induction velocity is linear, we can obtain one set of equations for each of these two frequency components. In blades in which the mid-chord line is a straight line and the wing chord is uniform, if we refer to Eq. (3.38), the integral equation for seeking the bound vortices with respect to the two frequency components can be written in the following manner:

$$
\begin{aligned}
\Gamma_{\pm}^{(3)}(y) = \Gamma_{\pm}(y) &- \frac{1}{\pi i[H_1^{(2)}(k_{\pm}(y)) + iH_0^{(2)}(k_{\pm}(y))]} \int_{R_1}^{R_2} \frac{d\Gamma_{\pm}(\eta)}{d\eta} \frac{V(y)}{V(\eta)} \\
&\times N_B(k_{\pm}(\eta)[y-\eta]) \{J_0(k_{\pm}(\eta)) - iJ_1(k_{\pm}(\eta))\} d\eta \\
&+ \frac{1}{\pi i[H_1^{(2)}(k_{\pm}(y)) + iH_0^{(2)}(k_{\pm}(y))]} \int_{R_1}^{R_2} i\Gamma_{\pm}(\eta) \frac{d}{d\eta}\left[\frac{V(y)}{V(\eta)}\right] \\
&\times N_A(k_{\pm}(\eta)[y-\eta]) \{J_0(k_{\pm}(\eta)) - iJ_1(k_{\pm}(\eta))\} d\eta \\
&- \frac{1}{\pi i[H_1^{(2)}(k_{\pm}(y) + iH_0^{(2)}(k_{\pm}(y))]} \int_{R_1}^{R_2} i \frac{d\Gamma_{\pm}(\eta)}{d\eta}\left[\frac{V(y)}{V(\eta)}\right] \\
&\times N_C(k_{\pm}(y)[y-\eta]) \{J_0(k_{\pm}(y)) - iJ_1(k_{\pm}(y))\} d\eta \\
&- \frac{1}{\pi i[H_1^{(2)}(k_{\pm}(y)) + iH_0^{(2)}(k_{\pm}(y))]} \int_{R_1}^{R_2} i\Gamma_{\pm}(\eta) \frac{d}{d\eta}\left[\frac{V(y)}{V(\eta)}\right] \\
&\times N_C(k_{\pm}(y)[y-\eta]) \{J_0(k_{\pm}(y)) - iJ_1(k_{\pm}(y))\} d\eta \\
&+ \frac{1}{\pi i[H_1^{(2)}(k_{\pm}(y)) + iH_0^{(2)}(k_{\pm}(y))]} \int_{R_1}^{R_2} i\Gamma_{\pm}(\eta) \frac{d}{d\eta}\left[\frac{V(y)}{V(\eta)}\right] \cdot \left[\frac{V(y)}{V(\eta)}\right] \\
&\times N_B(k_{\pm}(\eta)[y-\eta]) \cdot k_{\pm}(y) \cdot \left\{J_0(k_{\pm}(\eta)) - \frac{1+ik_{\pm}(\eta)}{k_{\pm}(\eta)} J_1(k_{\pm}(\eta))\right\} d\eta
\end{aligned}
\tag{3.47}
$$

Here,

$$
\Gamma_{\pm}^{(3)}(y) = \frac{4\int_{-1}^{1} \sqrt{\frac{1+\xi}{1-\xi}}\, d\xi \left(-\frac{1}{2} y b' \bar{\theta} p\right)}{\pi i k_{\pm}(y)\,[H_1^{(2)}(k_{\pm}(y)) + iH_0^{(2)}(k_{\pm}(y))]} \tag{3.48}
$$

Eq. (3.47) can be solved if it is rewritten in the form of a system of simultaneous equations, and the bound vortices along the radial direction of the blade can be sought. Since the method of solution is slightly different from the method of Ashley et al., it is described below.

Method of Solving the Circulation Equation

N_A, N_B, and N_C have singularity at $y = \eta$. This is described in Appendix B, but let us repeat it here.

$$\lim_{q\to 0} N_A(q) = \frac{q}{|q|}$$

$$\lim_{q\to 0} N_B(q) = \lim_{q\to 0} \frac{1}{q} - i\frac{q}{|q|}$$

$$\lim_{\tau\to 0} N_C(\tau) = \frac{\tau}{|\tau|}\lim_{\tau\to 0}\log|\tau| + \frac{\tau}{|\tau|}\left(\gamma + \log 2 + \frac{2}{\pi}i\right)$$

Next, let us introduce ΔN_A, ΔN_B, and ΔN_C.

$$N_A(q) = \Delta N_A(q) + \frac{q}{|q|} \tag{3.49}$$

$$N_B(q) = \Delta N_B(q) + \frac{1}{q} - i\frac{q}{|q|} \tag{3.50}$$

$$N_C(\tau) = \Delta N_C(\tau) + \frac{\tau}{|\tau|}\log|\tau| + \frac{\tau}{|\tau|}\left(\gamma + \log 2 + \frac{\pi}{2}i\right) \tag{3.51}$$

Changes of variables are performed as in the following equations: /49

$$y = \frac{R_2+R_1}{2} - \frac{R_2-R_1}{2}\cos\phi \qquad \eta = \frac{R_2+R_1}{2} - \frac{R_2-R_1}{2}\cos\theta \tag{3.52}$$

When the variables are changed, N_A, N_B, and N_C will be as follows:

$$N_A(k_\pm(\eta)[y-\eta]) = \Delta N_A(k_\pm(\eta)[y-\eta]) + \frac{\cos\theta-\cos\phi}{|\cos\theta-\cos\phi|} \tag{3.53}$$

(3.54)

$$N_B(k_\pm(\eta)[y-\eta]) = \Delta N_B(k_\pm(\eta)[y-\eta]) + \frac{2}{k_\pm(\eta)[R_2-R_1][\cos\theta-\cos\phi]} - i\frac{\cos\theta-\cos\phi}{|\cos\theta-\cos\phi|}$$

$$N_C(k_\pm(y)[y-\eta]) = \Delta N_C(k_\pm(y)[y-\eta]) + \frac{\cos\theta-\cos\phi}{|\cos\theta-\cos\phi|}\log|\cos\theta-\cos\phi| + \frac{\cos\theta-\cos\phi}{|\cos\theta-\cos\phi|}\left\{\log\left(k_\pm(y)\frac{R_2-R_1}{2}\right) + \gamma + \log 2 + \frac{\pi}{2}i\right\} \tag{3.55}$$

Since $\overline{\Gamma}_{\pm}(y)$ is 0 when $y = R_1$ and $y = R_2$, we apply Multhop's interpolation formula [3]. Please note that the abbreviation $F(\phi)$ is used instead of $F(\frac{R_2 + R_1}{2}\ \frac{R_2 - R_1}{2})\times \cos\phi$ in the following.

$$\Gamma_{\pm}(\phi)=\frac{2}{N+1}\sum_{n=1}^{N}\Gamma_{\pm}(\phi_i)\sum_{n=1}^{N}\sin n\phi_i \sin n\phi \tag{3.56}$$

Here,

$$\phi i = \frac{\pi i}{N+1}$$

If the interpolation formula is used, Eq. (3.47) will be written as follows.

$$\begin{aligned}
\Gamma_{\pm}(\phi)^{(3)}=&\frac{2}{N+1}\sum_{i=1}^{N}\Gamma_{\pm}(\phi_i)\sum_{n=1}^{N}\sin n\phi_i \sin n\phi \\
&+\frac{1}{\pi i[H_1^{(2)}(k_{\pm}(\phi))+iH_0^{(2)}(k_{\pm}(\phi))]}\frac{2}{N+1}\frac{R_2-R_1}{2}\sum_{i=1}^{N}\Gamma_{\pm}(\phi_i)\sin n\phi_i \\
&\times\int_0^{\pi}\sin n\theta\sin\theta\Big[i\frac{d}{d\eta}\Big[\frac{V(y)}{V(\eta)}\Big]\{J_0(k_{\pm}(\eta))-iJ_1(k_{\pm}(\eta))\}\Delta N_A(k_{\pm}(\eta)[y-\eta]) \\
&+i\frac{d}{d\eta}\Big[\frac{V(y)}{V(\eta)}\Big]\{J_0(k_{\pm}(\eta)-iJ_1(k_{\pm}(\eta))\}\frac{\cos\theta-\cos\phi}{|\cos\theta-\cos\phi|} \\
&-i\frac{d}{d\eta}\Big[\frac{V(y)}{V(\eta)}\Big]\{J_0(k_{\pm}(y))-iJ_1(k_{\pm}(y))\}\Delta N_C(k_{\pm}(y)[y-\eta]) \\
&-i\frac{d}{d\eta}\Big[\frac{V(y)}{V(\eta)}\Big]\{J_0(k_{\pm}(y))-iJ_1(k_{\pm}(y))\}\Big\{\log\Big(k_{\pm}(y)\frac{R_2-R_1}{2}\Big)+\gamma+\log 2+\frac{\pi}{2}i\Big\}\frac{\cos\theta-\cos\phi}{|\cos\theta-\cos\phi|} \\
&-i\frac{d}{d\eta}\Big[\frac{V(y)}{V(\eta)}\Big]\{J_0(k_{\pm}(y))-iJ_1(k_{\pm}(y))\}\frac{\cos\theta-\cos\phi}{|\cos\theta-\cos\phi|}\log|\cos\theta-\cos\phi| \\
&+i\frac{d}{d\eta}\Big[\frac{V(y)}{V(\eta)}\Big]\{k_{\pm}(\eta)[J_0(k_{\pm}(\eta))-iJ_1(k_{\pm}(\eta))]-J_1(k_{\pm}(\eta)\}\Delta N_B(k_{\pm}(\eta)[y-\eta]) \\
&+\frac{d}{d\eta}\Big[\frac{V(y)}{V(\eta)}\Big]\{k_{\pm}(\eta)[J_0(k_{\pm}(\eta))-iJ_1(k_{\pm}(\eta))]-J_1(k_{\pm}(\eta))\}\frac{\cos\theta-\cos\phi}{|\cos\theta-\cos\phi|} \\
&+i\frac{d}{d\eta}\Big[\frac{V(y)}{V(\eta)}\Big]\Big\{J_0(k_{\pm}(\eta))-iJ_1(k_{\pm}(\eta))]-\frac{J_1(k_{\pm}(\eta))}{k_{\pm}(\eta)}\Big\}\frac{2}{[R_2-R_1][\cos\theta-\cos\phi]}\Big]d\theta \\
&-\frac{1}{\pi i[H_1^{(2)}(k_{\pm}(\phi))+iH_0^{(2)}(k_{\pm}(\phi))]}\frac{2}{N+1}\sum_{n=1}^{N}\Gamma_{\pm}(\phi_i)\sum_{n=1}^{N}n\sin n\phi_i \\
&\times\int_0^{\pi}\cos n\theta\Big[\frac{V(y)}{V(\eta)}\{J_0(k_{\pm}(\eta))-iJ_1(k_{\pm}(\eta))\}\Delta N_B(k_{\pm}(\eta)[y-\eta]) \\
&-i\frac{V(y)}{V(\eta)}\{J_0(k_{\pm}(\eta))-iJ_1(k_{\pm}(\eta))\}\frac{\cos\theta-\cos\phi}{|\cos\theta-\cos\phi|} \\
&+\{J_0(k_{\pm}(\eta))-iJ_1(k_{\pm}(\eta))\}\frac{1}{k_{\pm}(y)}\frac{2}{R_2-R_1}\frac{1}{\cos\theta-\cos\phi} \\
&+i\frac{V(y)}{V(\eta)}\{J_0(k_{\pm}(y))-iJ_1(k_{\pm}(y))\}\Delta N_C(k_{\pm}(y)[y-\eta]) \\
&+i\frac{V(y)}{V(\eta)}\{J_0(k_{\pm}(y))-iJ_1(k_{\pm}(y))\}\Big\{\log\Big(k_{\pm}(y)\frac{R_2-R_1}{2}\Big)+\gamma+\log 2+\frac{\pi i}{2}\Big\}\frac{\cos\theta-\cos\phi}{|\cos\theta-\cos\phi|} \\
&+i\frac{V(y)}{V(\eta)}\{J_0(k_{\pm}(y))-iJ_1(k_{\pm}(y))\}\frac{\cos\theta-\cos\phi}{|\cos\theta-\cos\phi|}\log|\cos\theta-\cos\phi|\Big]d\theta
\end{aligned} \tag{3.57}$$

/50

To organize it further,

$$\Gamma_{\pm}^{(3)}(\phi)=\frac{2}{N+1}\sum_{i=1}^{N}\Gamma_{\pm}(\phi_i)\sum_{n=1}^{N}\sin n\phi_i\sin n\phi$$
$$+\frac{1}{\pi i[H_1^{(3)}(k_{\pm}(\phi))+iH_0^{(3)}(k_{\pm}(\phi))]}\frac{2}{N+1}\frac{R_2-R_1}{2}\sum_{i=1}^{N}\Gamma_{\pm}(\phi_i)\sum_{n=1}^{N}\sin n\phi_i$$
$$\times\int_0^{\pi}\sin n\theta\sin\theta\Big[K_{A1}(\phi,\theta)+K_{A2}(\phi,\theta)\frac{\cos\theta-\cos\phi}{|\cos\theta-\cos\phi|}$$
$$+K_{A3}(\phi,\theta)\frac{\cos\theta-\cos\phi}{|\cos\theta-\cos\phi|}\log|\cos\theta-\cos\phi|+K_{A4}\frac{1}{\cos\theta-\cos\phi}\Big]d\theta$$
$$-\frac{1}{\pi i[H_1^{(3)}(k_{\pm}(\phi))+iH_0^{(3)}(k_{\pm}(\phi))]}\frac{2}{N+1}\sum_{i=1}^{N}\Gamma_{\pm}(\phi_i)\sum_{n=1}^{N}n\sin n\phi_i$$
$$\times\int_0^{\pi}\cos n\theta\Big[K_{A5}(\phi,\theta)+K_{A6}(\phi,\theta)\frac{\cos\theta-\cos\phi}{|\cos\theta-\cos\phi|}$$
$$+K_{A7}(\phi,\theta)\frac{\cos\theta-\cos\phi}{|\cos\theta-\cos\phi|}\log|\cos\theta-\cos\phi|+K_{A8}\frac{1}{\cos\theta-\cos\phi}\Big]d\theta$$

(3.58)

Here,

$$K_{A1}(\phi,\theta)=i\frac{d}{d\eta}\Big[\frac{V(y)}{V(\eta)}\Big]\{J_0(k_{\pm}(\eta))-iJ_1(k_{\pm}(\eta))\}\Delta N_A(k_{\pm}(\eta)[y-\eta])$$
$$-i\frac{d}{d\eta}\Big[\frac{V(y)}{V(\eta)}\Big]\{J_0(k_{\pm}(y))-iJ_1(k_{\pm}(y))\}\Delta N_C(k_{\pm}(y)[y-\eta])$$
$$+i\frac{d}{d\eta}\Big[\frac{V(y)}{V(\eta)}\Big]\{k_{\pm}(\eta)[J_0(k_{\pm}(\eta))-iJ_1(k_{\pm}(\eta)]-J_1(k_{\pm}(\eta))\}\Delta N_B(k_{\pm}(\eta)[y-\eta])$$
$$K_{A2}(\phi,\theta)=i\frac{d}{d\eta}\Big[\frac{V(y)}{V(\eta)}\Big]\{J_0(k_{\pm}(\eta))-iJ_1(k_{\pm}(\eta))\}$$
$$-i\frac{d}{d\eta}\Big[\frac{V(y)}{V(\eta)}\Big]\{J_0(k_{\pm}(y))-iJ_1(k_{\pm}(y))\}\Big\{\log\Big(k_{\pm}(y)\frac{R_2-R_1}{2}\Big)+\gamma+\log 2+\frac{\pi}{2}i\Big\}$$
$$+\frac{d}{d\eta}\Big[\frac{V(y)}{V(\eta)}\Big]\{k_{\pm}(\eta)[J_0(k_{\pm}(\eta))-iJ_1(k_{\pm}(\eta))]-J_1(k_{\pm}(\eta))\}$$
$$K_{A3}(\phi,\theta)=-i\frac{d}{d\eta}\Big[\frac{V(y)}{V(\eta)}\Big]\{J_0(k_{\pm}(y))-iJ_1(k_{\pm}(y))\}$$
$$K_{A4}(\phi,\theta)=i\frac{2}{R_2-R_1}\frac{d}{d\eta}\Big[\frac{V(y)}{V(\eta)}\Big]\Big\{J_0(k_{\pm}(\eta))-iJ_1(k_{\pm}(\eta))-\frac{J_1(k_{\pm}(\eta))}{k_{\pm}(\eta)}\Big\}$$
$$K_{A5}(\phi,\theta)=\frac{V(y)}{V(\eta)}\{J_0(k_{\pm}(\eta))-iJ_1(k_{\pm}(\eta))\}\Delta N_B(k_{\pm}(\eta)[y-\eta])$$
$$+i\frac{V(y)}{V(\eta)}\{J_0(k_{\pm}(y))-iJ_1(k_{\pm}(y))\}\Delta N_C(k_{\pm}(y)[y-\eta])$$
$$K_{A6}(\phi,\theta)=-i\frac{V(y)}{V(\eta)}\{J_0(k_{\pm}(\eta))-iJ_1(k_{\pm}(\eta))\}$$
$$+i\frac{V(y)}{V(\eta)}\{J_0(k_{\pm}(y))-iJ_1(k_{\pm}(y))\}\Big\{\log\Big(k_{\pm}(y)\frac{R_2-R_1}{2}\Big)+\gamma+\log 2+\frac{\pi i}{2}\Big\}$$
$$K_{A7}(\phi,\theta)=i\frac{V(y)}{V(\eta)}\{J_0(k_{\pm}(y))-iJ_1(k_{\pm}(y))\}$$
$$K_{A8}(\phi,\theta)=\{J_0(k_{\pm}(\eta))-iJ_1(k_{\pm}(\eta))\}\frac{1}{k_{\pm}(y)}\frac{2}{R_2-R_1}$$

If the so-called Chebyshev interpolation formula [3,19] is used, $K_{A1}(\phi,\theta)$, $K_{A2}(\phi,\theta)$,...$K_{A8}(\phi,\theta)$ can each be written in the following manner. /51

$$K_A(\phi,\theta)=\frac{2}{J+1}\sum_{j=1}^{J+1}K_A(\phi,\theta_j)\left(\frac{1}{2}+\sum_{l+1}^{J}\cos l\theta_j\cos l\theta\right)$$
$$=\frac{2}{J+1}\sum_{j=1}^{J+1}K_A(\phi,\theta_j)\sum_{l=0}^{J}(C_{lj}\cos l\theta) \tag{3.59}$$

Here,

$$\left.\begin{aligned}C_{0j}&=1/2\\C_{lj}&=\cos l\theta_j \qquad (l=1,\ 2,\cdots J)\end{aligned}\right\} \tag{3.60}$$

Consequently, Eq. (3,58) can be written in the following manner:

$$\begin{aligned}\Gamma_{\pm}^{(3)}(\phi)=\sum_{i=1}^{N}\Gamma_{\pm}(\phi_i)\frac{2}{N+1}\sum_{n=1}^{N}\sin n\phi_i\Big\langle\sin n\phi+\frac{1}{\pi i[H_1^{(2)}(k_{\pm}(\phi))+iH_0^{(2)}(k_{\pm}(\phi))]}\\
\times\frac{2}{J+1}\Big\{\frac{R_2-R_1}{4}\sum_{j=1}^{J+1}K_{A1}(\phi,\theta_j)\sum_{l=0}^{J}C_{lj}\int_0^{\pi}\cos l\theta[\cos(n-1)\theta-\cos(n+1)\theta]d\theta\\
+\frac{R_2-R_1}{4}\sum_{j=1}^{J+1}K_{A2}(\phi,\theta_j)\sum_{l=0}^{J}C_{lj}\int_0^{\pi}\cos l\theta[\cos(n-1)\theta-\cos(n+1)\theta]\frac{\cos\theta-\cos\phi}{|\cos\theta-\cos\phi|}d\theta\\
+\frac{R_2-R_1}{4}\sum_{j=1}^{J+1}K_{A3}(\phi,\theta_j)\sum_{l=0}^{J}C_{lj}\int_0^{\pi}\cos l\theta[\cos(n-1)\theta-\cos(n+1)\theta]\frac{\cos\theta-\cos\phi}{|\cos\theta-\cos\phi|}\log|\cos\theta-\cos\phi|d\theta\\
+\frac{R_2-R_1}{4}\sum_{j=1}^{J+1}K_{A4}(\phi,\theta_j)\sum_{l=0}^{J}C_{lj}\int_0^{\pi}\cos l\theta[\cos(n-1)\theta-\cos(n+1)\theta]\frac{1}{\cos\theta-\cos\phi}d\theta\\
-n\sum_{j=1}^{J+1}K_{A5}(\phi,\theta_j)\sum_{l=1}^{J}C_{lj}\int_0^{\pi}\cos l\theta\cos n\theta d\theta\\
-n\sum_{j=1}^{J+1}K_{A6}(\phi,\theta_j)\sum_{l=1}^{J}C_{lj}\int_0^{\pi}\cos l\theta\cos n\theta\frac{\cos\theta-\cos\phi}{|\cos\theta-\cos\phi|}d\theta\\
-n\sum_{j=1}^{J+1}K_{A7}(\phi,\theta_j)\sum_{l=0}^{J}C_{lj}\int_0^{\pi}\cos l\theta\cos n\theta\frac{\cos\theta-\cos\phi}{|\cos\theta-\cos\phi|}\log|\cos\theta-\cos\phi|d\theta\\
-n\sum_{j=1}^{J+1}K_{A8}(\phi,\theta_j)\sum_{l=0}^{J}C_{lj}\int_0^{\pi}\cos l\theta\cos n\theta\frac{1}{\cos\theta-\cos\phi}d\theta\Big\}\Big\rangle\end{aligned} \tag{3.61}$$

Let us solve the four types of integrations which appear on the right side of the above equation.

$$\text{(a)}\quad FW_{pq}=\int_1^{\pi}\cos p\theta\cos q\theta\,d\theta=\begin{cases}\pi & \text{for}\quad p=q=0\\ \pi/2 & \text{for}\quad p=q\neq 0\\ 0 & \text{for}\quad p\neq q\end{cases}$$

$$\text{(b)}\quad FX_{pq}(\phi)=\int_0^{\pi}\cos p\theta\cos q\theta\frac{\cos\phi-\cos\theta}{|\cos\phi-\cos\theta|}d\theta=\begin{cases}\pi-2\phi & \text{for}\quad p=q=0\\ \dfrac{\pi-2\phi}{2}-\dfrac{\sin(p+q)\phi}{p+q} & \text{for}\quad p=q\neq 0\\ -\dfrac{\sin|p-q|\phi}{|p-q|}-\dfrac{\sin(p+q)\phi}{p+q} & \text{for}\quad p\neq q\end{cases}$$

$$(c)\quad FY_{pq}(\phi)=\int_0^{\pi}\cos p\theta\cos q\theta\,\frac{\cos\phi-\cos\theta}{|\cos\phi-\cos\theta|}\ln|\cos\phi-\cos\theta|\,d\theta=\begin{cases}-f_0(\phi) & \text{for } p=q=0\\ -\dfrac{f_0(\phi)+f_{p+q}(\phi)}{2} & \text{for } p=q\neq 0\\ -\dfrac{f_{p-q}(\phi)+f_{p+q}(\phi)}{2} & \text{for } p\neq q\end{cases}$$

Here,

$$f_k(\phi)=\int_0^{\pi}\frac{\cos\theta-\cos\phi}{|\cos\theta-\cos\phi|}(\log|\cos\theta-\cos\phi|)\cos k\theta\,d\theta$$

Reissner [21] has sought $f_k(\phi)$ for cases when $k \neq 0$. Ichikawa [3] transformed Reissner's equation and made it into an easy-to-handle equation. Ichikawa's equation is as follows.

/52

$$f_k(\phi)=\frac{2}{k}\left\{[2\log|\sin\phi|+\log 2-1]\sin k\phi-\left(\phi-\frac{\pi}{2}\right)\cos k\phi\right\}+g_k(\phi)$$

Here, $g_k(\phi)$ is sought by means of the initial conditions

$$g_1(\phi)=0$$
$$g_2(\phi)=-\frac{\sin 2\phi}{2}$$

and the recurrence formula

$$(k-1)g_{k-1}(\phi)-2k\cos\phi g_k(\phi)+(k+1)g_{k+1}(\phi)=2\left[\frac{\sin(k-1)\phi}{k-1}-\frac{\sin(k+1)\phi}{k+1}\right],\quad (k=2,\ 3,\ \cdots)$$

It is clear that the following will apply, in particular in cases when $k = 0$.

$$f_0(\phi)=\begin{cases}(\pi-2\phi)\log 2+4\displaystyle\int_{\phi}^{\pi/2}\log\sin x\,dx & \text{for } \dfrac{\pi}{2}\geq\phi\\ (\pi-2\phi)\log 2-4\displaystyle\int_{\pi-\phi}^{\pi/2}\log\sin x\,dx & \text{for } \dfrac{\pi}{2}<\phi\end{cases}$$

Here,

$$\int_{\phi}^{\pi/2}\log\sin x\,dx=-\frac{\pi}{2}\log 2-\phi\log\phi+\phi+\frac{\phi^3}{18}+\frac{\phi^5}{900}+\frac{\phi^7}{19845}+\cdots\cdots$$

$$FZ_{pq}(\phi)=\int_0^{\pi}\cos p\theta\cos q\theta\frac{1}{\cos\phi-\cos\theta}d\theta^{23)}=\begin{cases}0\\ -\dfrac{\pi}{2}\dfrac{\sin(p+q)\phi}{p+q}\\ -\dfrac{\pi}{2}\dfrac{\sin|p-q|\phi}{|p-q|}-\dfrac{\pi}{2}\dfrac{\sin(p+q)\phi}{(p+q)}\end{cases}$$

If we write Eq. (3.61 using FW, FX, FY, and FZ, we obtain:

$$\begin{aligned}\Gamma_{\pm}^{(3)}(\phi)=&\sum_{i=1}^{N}\Gamma_{\pm}(\phi_i)\frac{2}{N+1}\sum_{n=1}^{N}\sin n\phi_i\Big\langle\sin n\phi+\frac{1}{\pi i[H_1^{(2)}(k_{\pm}(\phi))+iH_0^{(2)}(k_{\pm}(\phi))]}\\ &\times\frac{2}{J+1}\Big\{\frac{R_2-R_1}{4}\sum_{j=1}^{J+1}K_{A1}(\phi,\theta_j)\sum_{i=0}^{J}C_{ij}(FW_{i,n-1}-FW_{i,n+1})-n\sum_{j=1}^{J+1}K_{A5}(\phi,\theta_j)\sum_{i=0}^{J}C_{ij}FW_{i,n}\\ &-\frac{R_2-R_1}{4}\sum_{j=1}^{J+1}K_{A2}(\phi,\theta_j)\sum_{i=0}^{J}C_{ij}(FX_{i,n-1}-FX_{i,n+1})+n\sum_{j=1}^{J+1}K_{A6}(\phi,\theta_j)\sum_{i=0}^{J}C_{ij}FX_{i,n}\\ &-\frac{R_2-R_1}{4}\sum_{j=1}^{J+1}K_{A3}(\phi,\theta_j)\sum_{i=0}^{J}C_{ij}(FY_{i,n-1}-FY_{i,n+1})+n\sum_{j=1}^{J+1}K_{A7}(\phi,\theta_j)\sum_{i=0}^{J}C_{ij}FY_{i,n}\\ &-\frac{R_2-R_1}{4}\sum_{j=1}^{J+1}K_{A4}(\phi,\theta_j)\sum_{i=0}^{J}C_{ij}(FZ_{i,n-1}-FZ_{i,n+1})+n\sum_{j=1}^{J+1}K_{A8}(\phi,\theta_j)\sum_{i=0}^{J}C_{ij}FZ_{i,n}\Big\}\Big\rangle\end{aligned}\qquad(3.62)$$

If we select N values of ϕ, Eq. (3.62) can be solved as a system of simultaneous equations, and $\Gamma\pm(\phi_i)$ can be sought.

Lift Distribution Along Radial Direction of the Blade

If we refer to Eq. (3.46), we can write as follows the equation for seeking the pressure difference between the upper and lower blade surfaces with respect to the two frequency components.

$$\begin{aligned}\frac{\Delta\bar{p}_{\pm}(x^*,y)}{\rho\bar{V}(y)}=&-\frac{2}{\pi}\int_{-1}^{1}\Big[\sqrt{\frac{1+\xi}{1-\xi}}\sqrt{\frac{1-x^*}{1+x^*}}\frac{1}{x^*-\xi}-ik_{\pm}(y)A_1(x^*,\xi)\Big]\Big(-\frac{1}{2}yb'\bar{\theta}p\Big)d\xi\\ &+\frac{ik_{\pm}(y)\Gamma_{\pm}(y)}{\pi}\sqrt{\frac{1-x^*}{1+x^*}}\int_{-1}^{\infty}\frac{1}{\sqrt{\lambda^2-1}}e^{-ik_{\pm}(y)\lambda}d\lambda\\ &-\frac{2}{\pi}\{D_1-D_3\}\Big\{\int_{-1}^{1}\Big[\sqrt{\frac{1+\xi}{1-\xi}}\sqrt{\frac{1-x^*}{1+x^*}}\frac{1}{x^*-\xi}-ik_{\pm}(y)A_1(x^*,\xi)\Big]e^{-ik_{\pm}(y)\xi}d\xi\\ &-\frac{2}{\pi}\{D_2+D_3\}\Big\{\int_{-1}^{1}\Big[\sqrt{\frac{1+\xi}{1-\xi}}\sqrt{\frac{1-x^*}{1+x^*}}\frac{1}{x^*-\xi}-ik_{\pm}(y)A_1(x^*,\xi)\Big]e^{-ik_{\pm}(y)\xi}d\xi\\ &+\frac{2}{\pi}\{D_4\}\Big\{\int_{-1}^{1}k_{\pm}(y)\xi\Big[\sqrt{\frac{1+\xi}{1-\xi}}\sqrt{\frac{1-x^*}{1+x^*}}\frac{1}{x^*-\xi}-ik_{\pm}(y)A_1(x^*,\xi)\Big]e^{-ik_{\pm}(y)\xi}d\xi\end{aligned}\qquad(3.63)$$

If we integrate $\Delta p\pm(x^*,y)$ from the front edge to the rear edge, we can obtain the lift per unit wing span. The following integrations are used at this time. /53

$$\int_{-1}^{1}\sqrt{\frac{1-x^*}{1+x^*}}\frac{1}{x^*-\xi}dx^*=-\pi$$

$$\int_{-1}^{1}A_1(x^*,\xi)dx^*=\pi\sqrt{1-\xi^2}$$

$$\int_{-1}^{1}\sqrt{\frac{1-x^*}{1+x^*}}dx^*=\pi$$

$$\begin{aligned}\int_{-1}^{1}\frac{\Delta\bar{p}_{\pm}(x^*,y)}{\rho V(y)}dx^*=2\int_{-1}^{1}\left[\sqrt{\frac{1+\xi}{1-\xi}}+ik_{\pm}(y)\sqrt{1-\xi^2}\right]\left(-\frac{1}{2}yb'\bar{\theta}p\right)d\xi\\ +ik_{\pm}(y)\Gamma_{\pm}(y)\int_{1}^{\infty}\frac{1}{\sqrt{\lambda^2-1}}e^{-ik_{\pm}(y)\lambda}d\lambda\\ +2\{D_1-D_3\}\left\{\int_{-1}^{1}\left[\sqrt{\frac{1+\xi}{1-\xi}}+ik_{\pm}(y)\sqrt{1-\xi^2}\right]e^{-ik_{\pm}(\eta)\xi}d\xi\right\}\\ +2\{D_2+D_5\}\left\{\int_{-1}^{1}\left[\sqrt{\frac{1+\xi}{1-\xi}}+ik_{\pm}(y)\sqrt{1-\xi^2}\right]e^{-ik_{\pm}(y)\xi}d\xi\right\}\\ -2\{D_4\}\left\{\int_{-1}^{1}k_{\pm}(y)\xi\left[\sqrt{\frac{1+\xi}{1-\xi}}+ik_{\pm}(y)\sqrt{1-\xi^2}\right]e^{-ik_{\pm}(\eta)\xi}d\xi\right\}\end{aligned} \tag{3.64}$$

The integration can also be indicated in the following manner using Bessel functions.

$$\int_{1}^{\infty}\frac{1}{\sqrt{\lambda^2-1}}e^{-ik_{\pm}(y)\lambda}d\lambda=\frac{\pi}{2i}H_0^{(2)}(k_{\pm}(y))$$

$$\int_{-1}^{1}\sqrt{\frac{1+\xi}{1-\xi}}e^{-ik_{\pm}(\eta)\xi}d\xi=-\pi i[J_1(k_{\pm}(\eta))+iJ_0(k_{\pm}(\eta))]$$

$$\int_{-1}^{1}ik_{\pm}(y)\sqrt{1-\xi^2}e^{-ik_{\pm}(\eta)\xi}d\xi=\frac{i\pi V(\eta)}{V(y)}J_1(k_{\pm}(\eta))$$

$$\int_{-1}^{1}\sqrt{\frac{1+\xi}{1-\xi}}e^{-ik_{\pm}(y)\xi}d\xi=-\pi i[J_1(k_{\pm}(y))+iJ_0(k_{\pm}(y))]$$

$$\int_{-1}^{1}ik_{\pm}(y)\sqrt{1-\xi^2}e^{-ik_{\pm}(y)\xi}d\xi=i\pi J_1(k_{\pm}(y))$$

$$\int_{-1}^{1}k_{\pm}(y)\xi\sqrt{\frac{1+\xi}{1-\xi}}e^{-ik_{\pm}(\eta)\xi}d\xi=\pi\left[k_{\pm}(y)J_0(k_{\pm}(\eta))-\frac{V(\eta)}{V(y)}J_1(k_{\pm}(\eta))-ik_{\pm}(y)J_1(k_{\pm}(\eta))\right]$$

$$i\int k_{\pm}^2(y)\xi\sqrt{1-\xi^2}e^{-ik_{\pm}(\eta)\xi}d\xi=\frac{2\pi V^2(\eta)}{V^2(y)}J_1(k_{\pm}(\eta))-\frac{\pi k_{\pm}(y)V(\eta)}{V(y)}J_0(k_{\pm}(\eta))$$

$$\int_{-1}^{1}\sqrt{\frac{1+\xi}{1-\xi}}d\xi=\pi$$

$$\int_{-1}^{1}\sqrt{1-\xi^2}d\xi=\frac{\pi}{2}$$

Returning the operating symbols to their previous state, the lift per unit wing span can be expressed as follows:

$$
\begin{aligned}
\bar{L}_{\pm}(y) &= -b'\int_{-1}^{1} \Delta\bar{p}(x^*, y)\,dx^* \\
&= \rho b' V(y)\left\langle 2\pi\left(1+\frac{ik_{\pm}(y)}{2}\right)\left(-\frac{1}{2}b'y\bar{\theta}p\right)+\frac{\pi k_{\pm}(y)\bar{\Gamma}_{\pm}(y)}{2}H_0^{(2)}(k_{\pm}(y))\right. \\
&\quad +\int_{R_1}^{R_2}\Gamma_{\pm}(\eta)\left\{\frac{k_{\pm}(y)}{2}\frac{d}{d\eta}\left[\frac{V(y)}{V(\eta)}\right]N_A(k_{\pm}(\eta)\,[\eta-\eta])\left[\left(\frac{V(\eta)}{V(y)}-1\right)J_0(k_{\pm}(\eta))-iJ_1(k_{\pm}(\eta))\right]\right. \\
&\quad +i\frac{k_{\pm}(y)}{2}\frac{d}{d\eta}\left[\frac{V(y)}{V(\eta)}\right]N_C(k_{\pm}(y)\,[y-\eta])J_0(k_{\pm}(y)) \\
&\quad -i\frac{k_{\pm}(y)}{2}\frac{d}{d\eta}\left[\frac{V(y)}{V(\eta)}\right]N_B(k_{\pm}(\eta)\,[y-\eta])\left[\left(2\frac{V(\eta)}{V(y)}-1-ik_{\pm}(\eta)\right)J_1(k_{\pm}(\eta))\right. \\
&\quad \left.\left.-k_{\pm}(\eta)\left(\frac{V(\eta)}{V(y)}-1\right)J_0(k_{\pm}(\eta))\right]\right\}d\eta \\
&\quad +\int_{R_1}^{R_2}\frac{d\Gamma_{\pm}(\eta)}{d\eta}\left\{\frac{ik_{\pm}(\eta)}{2}N_B(k_{\pm}(\eta)\,[y-\eta])\left[\left(\frac{V(\eta)}{V(y)}-1\right)J_1(k_{\pm}(\eta))-iJ_0(k_{\pm}(\eta))\right]\right. \\
&\quad \left.\left.+\frac{ik_{\pm}(\eta)}{2}N_C(k_{\pm}(y)\,[y-\eta])J_C(k_{\pm}(y))\right\}d\eta\right\rangle
\end{aligned}
\tag{3.65}
$$

Taking into consideration the singularity contained in N_A, N_B, and N_C, if we use Multhop's interpolation formula [3] to express $\bar{\Gamma}_{\pm}$, we can write $\bar{L}_{\pm}(\phi)$ in the following manner by exactly the same procedure as that used to derive Eq. (3.58)

$$
\begin{aligned}
\bar{L}_{\pm}(y) &= \rho b' V(\phi)\left\langle 2\pi\left(1+\frac{ik_{\pm}(\phi)}{2}\right)\left(-\frac{1}{2}b'y\bar{\theta}p\right)+\sum_{i=1}^{N}\Gamma_{\pm}(\phi_i)\frac{2}{N+1}\sum_{n=1}^{N}\sin n\phi_i\sin n\phi\,\frac{\pi k_{\pm}(\phi)}{2}H_0^{(2)}(k_{\pm}(\phi))\right. \\
&\quad +\frac{2}{N+1}\frac{R_2-R_1}{2}\sum_{i=1}^{N}\Gamma_{\pm}(\phi_i)\sum_{n=1}^{N}\sin n\phi_i\int_0^{\pi}\sin n\theta\sin\theta\left[K_{A9}(\phi,\theta)+K_{A10}(\phi,\theta)\frac{\cos\theta-\cos\phi}{|\cos\theta-\cos\phi|}\right. \\
&\quad \left.+K_{A11}(\phi,\theta)\frac{\cos\theta-\cos\phi}{|\cos\theta-\cos\phi|}\log|\cos\theta-\cos\phi|+K_{A12}(\phi,\theta)\frac{1}{\cos\phi-\cos\phi}\right]d\theta \\
&\quad +\frac{2}{N+1}\sum_{i=1}^{N}\Gamma_{\pm}(\phi_i)\sum_{n=1}^{N}n\sin n\phi_i\int_0^{\pi}\cos n\theta\left[K_{A13}(\phi,\theta)+K_{A14}(\phi,\theta)\frac{\cos\theta-\cos\phi}{|\cos\theta-\cos\phi|}\right. \\
&\quad \left.\left.+K_{A15}(\phi,\theta)\frac{\cos\theta-\cos\phi}{|\cos\theta-\cos\phi|}\log|\cos\theta-\cos\phi|+K_{A12}(\phi,\theta)\frac{1}{\cos\theta-\cos\phi}\right]d\theta\right\rangle
\end{aligned}
\tag{3.66}
$$

Here,

$$
\begin{aligned}
K_{A9}(\phi,\theta) &= \frac{k_{\pm}(y)}{2}\frac{d}{d\eta}\left[\frac{V(y)}{V(\eta)}\right]\left[\left(\frac{V(y)}{V(\eta)}-1\right)J_1(k_{\pm}(\eta))-iJ_0(k_{\pm}(\eta))\right]\Delta N_A(k_{\pm}(\eta)\,[y-\eta]) \\
&\quad +i\frac{k_{\pm}(y)}{2}\frac{d}{d\eta}\left[\frac{V(y)}{V(\eta)}\right]J_0(k_{\pm}(y))\,\Delta N_C(k_{\pm}(y)\,[y-\eta]) \\
&\quad -i\frac{k_{\pm}(y)}{2}\frac{d}{d\eta}\left[\frac{V(y)}{V(\eta)}\right]\left[\left(2\frac{V(\eta)}{V(y)}-1-ik_{\pm}(\eta)\right)J_1(k_{\pm}(\eta))\right. \\
&\quad \left.-k_{\pm}(\eta)\left(\frac{V(\eta)}{V(y)}-1\right)J_0(k_{\pm}(\eta))\right]\Delta N_B(k_{\pm}(\eta)\,[y-\eta]) \\
K_{A10}(\phi,\theta) &= \frac{k_{\pm}(y)}{2}\frac{d}{d\eta}\left[\frac{V(y)}{V(\eta)}\right]\left[\left(\frac{V(\eta)}{V(y)}-1\right)J_1(k_{\pm}(\eta))-iJ_0(k_{\pm}(\eta))\right] \\
&\quad +i\frac{k_{\pm}(y)}{2}\frac{d}{d\eta}\left[\frac{V(y)}{V(\eta)}\right]J_0(k_{\pm}(y))\left[\log\left(k_{\pm}(y)\frac{R_2-R_1}{2}\right)+\gamma+\log 2+\frac{\pi}{2}i\right] \\
&\quad +\frac{k_{\pm}(y)}{2}\frac{d}{d\eta}\left[\frac{V(y)}{V(\eta)}\right]\left[\left(2\frac{V(\eta)}{V(y)}-1-ik_{\pm}(\eta)\right)J_1(k_{\pm}(\eta))-k_{\pm}(\eta)\left(\frac{V(\eta)}{V(y)}-1\right)J_0(k_{\pm}(\eta))\right] \\
K_{A11}(\phi,\theta) &= i\frac{k_{\pm}(y)}{2}\frac{d}{d\eta}\left[\frac{V(y)}{V(\eta)}\right]J_0(k_{\pm}(y))
\end{aligned}
$$

$$K_{A12}(\phi,\theta)=-i\frac{1}{2}\frac{V(\eta)}{V(y)}\frac{d}{d\eta}\left[\frac{V(y)}{V(\eta)}\right]\left[\left(2\frac{V(\eta)}{V(y)}-1-ik_{\pm}(\eta)\right)J_1(k_{\pm}(\eta))-k_{\pm}(\eta)\left(\frac{V(\eta)}{V(y)}-1\right)J_0(k_{\pm}(\eta))\right]$$

$$K_{A13}(\phi,\theta)=\frac{ik_{\pm}(\eta)}{2}\left[\left(\frac{V(\eta)}{V(y)}-1\right)J_1(k_{\pm}(\eta))-iJ_0(k_{\pm}(\eta))\right]\Delta N_B(k_{\pm}(\eta)[y-\eta])$$
$$+i\frac{k_{\pm}(\eta)}{2}J_0(k_{\pm}(y))\Delta N_C(k_{\pm}(y)[y-\eta])$$

$$K_{A14}(\phi,\theta)=\frac{k_{\pm}(\eta)}{2}\left[\left(\frac{V(\eta)}{V(y)}-1\right)J_1(k_{\pm}(\eta))-iJ_0(k_{\pm}(\eta))\right]$$
$$+\frac{ik_{\pm}(\eta)}{2}J_0(k_{\pm}(y))\left[\log\left(k_{\pm}(y)\frac{R_2-R_1}{2}\right)+\gamma+\log 2+\frac{\pi}{2}i\right]$$

$$K_{A15}(\phi,\theta)=\frac{ik_{\pm}(\eta)}{2}J_0(k_{\pm}(y))$$

$$K_{A16}(\phi,\theta)=\frac{i}{2}\left[\left(\frac{V(\eta)}{V(y)}-1\right)J_1(k_{\pm}(\eta))-iJ_0(k_{\pm}(\eta))\right]$$

If we use the so-called Chebyshev interpolation formula [3, 19] to express $K_{A9}(\phi,\theta)$, and if we use FW to express the integration, we obtain:

/55

$$L_{\pm}(\phi)=\rho b'V(\phi)\left[2\pi\left(1+\frac{ik_{\pm}(\phi)}{2}\right)\left(-\frac{1}{2}b'y\bar{\theta}p\right)\right.$$
$$+\sum_{i=1}^{N}\Gamma_{\pm}(\phi_i)\frac{2}{N+1}\sum_{n=1}^{N}\sin n\phi_i\left\langle\sin n\phi\frac{\pi k_{\pm}(\phi)}{2}H_0^{(2)}(k_{\pm}(\phi))+\frac{2}{J+1}\right.$$
$$\times\left\{\frac{R_2-R_1}{4}\sum_{j=1}^{J+1}K_{A9}(\phi,\theta_j)\sum_{l=0}^{J}C_{lj}(FW_{l,n-1}-FW_{l,n+1})-n\sum_{j=1}^{J+1}K_{A13}(\phi,\theta_j)\sum_{l=0}^{J}C_{lj}FW_{l,n}\right.$$
$$-\frac{R_2-R_1}{4}\sum_{j=1}^{J+1}K_{A10}(\phi,\theta_j)\sum_{l=0}^{J}C_{lj}(FX_{l,n-1}-FX_{l,n+1})+n\sum_{j=1}^{J+1}K_{A14}(\phi,\theta_j)\sum_{l=0}^{J}C_{lj}FX_{l,n}$$
$$-\frac{R_2-R_1}{4}\sum_{j=1}^{J+1}K_{A11}(\phi,\theta_j)\sum_{l=0}^{J}C_{lj}(FY_{l,n-1}+FY_{l,n+1})+n\sum_{j=1}^{J+1}K_{A15}(\phi,\theta_j)\sum_{l=0}^{J}C_{lj}FY_{l,n}$$
$$\left.\left.-\frac{R_2-R_1}{4}\sum_{j=1}^{J+1}K_{A12}(\phi,\theta_j)\sum_{l=0}^{J}C_{lj}(FZ_{l,n-1}+FZ_{l,n+1})+n\sum_{j=1}^{J+1}K_{A16}(\phi,\theta_j)\sum_{l=0}^{J}C_{lj}FZ_{l,n}\right\rangle\right] \quad (3.67)$$

The amplitude of the unsteady components of the lift operating on the portion with a width dy' at a point y' from the rotor hub is:

$$\bar{L}_{\pm}dy'=\bar{L}_{\pm}(\phi)b'\frac{R_2-R_1}{2}\sin\phi d\phi$$

Since the unsteady components of the lift operating on the q-th blade have a phase advanced $2\pi q/Q$ from the standard blade,

$$\bar{L}_{\pm q}dy'=\bar{L}_{\pm}dy'e^{i2\pi p/Q}$$

On account of the unsteady components of the lift operating on the Q blades, the moment occurring around the Y axis will be:

$$M_Y=-\sum_{q=0}^{Q-1}\int_{R_1'}^{R_2'} b'^2\bar{L}_{+q}y dy\cos\left(\Omega t+\frac{2\pi q}{Q}\right)e^{i(\Omega+p)t}-\sum_{q=0}^{Q-1}\int_{R_1'}^{R_2'} b'^2\bar{L}_{-q}y dy\cos\left(\Omega t+\frac{2\pi q}{Q}\right)e^{i(\Omega-p)t}$$

In a rotor performing pitching so that the rotor surface may be expressed as $\theta = \bar{\theta}\sin pt$, the pitch damping can be calculated by the method in Appendix A if the time changes in the moment around the pitching axis are known.

$$\frac{\partial M}{\partial\theta}=\frac{1}{\pi\bar{\theta}}\int_0^{2\pi/p} M_T\cos pt\,dt \tag{3.68}$$

If we carry out the calculations, we find

$$\frac{\partial M}{\partial\theta}=\frac{-\theta b'^2}{2p\bar{\theta}}\left\{\int_{R_1}^{R_2}\bar{L}_{R+}y dy+\int_{R_1}^{R_2}\bar{L}_{R-}y dy\right\}$$

Naturally, the $\bar{\Gamma}(\phi_1)$ obtained by solving Eq. (3.62) is an approximate value. When this $\bar{\Gamma}(\phi_1)$ is used to calculate $\bar{\Gamma}(\phi)$, it does not necessarily follow that $\bar{\Gamma}(\phi)$ will be 0 at the wing tip, that is, when $\phi = 0$ and $\phi = \pi$. However, assuming that the lift will be 0 at the wing tip, let us use Multhop's interpolation formula [3,19] to express $\bar{L}_R \pm (\phi)y$

$$L_{R\pm}(\phi)\left(\frac{R_2+R_1}{2}-\frac{R_2-R_1}{2}\cos\phi\right)=\frac{2}{N+1}\sum_{m=1}^{N}\bar{L}_{R\pm}(\phi_m)\left(\frac{R_2+R_1}{2}-\frac{R_2-R_1}{2}\cos\phi_m\right)\sum_{n=1}^{N}\sin n\phi_t\sin n\phi$$

$$\therefore\ \int_{R1}^{R_2}L_{R\pm}y dy=\frac{2}{N+1}\frac{R_2-R_1}{2}\sum_{m=1}^{N}\bar{L}_{\pm R}(\phi_m)\left(\frac{R_1+R_1}{2}-\frac{R_2-R_1}{2}\cos\phi_m\right)\sin\phi_m\cdot\frac{\pi}{2}$$

The circulation distribution in the radial direction of the blade, as well as the lift distribution, at a rotor revolution speed of 300 rpm and a pitching frequency of 0.756 c/s are shown in Figs. 60 and 61. /56

In Figs. 32 to 43 are given comparisons of the values estimated from the experimental values for cases when elastic deformation of the blades would not occur, as against the pitch damping values calculated using the theory of Ashley et al. [19].

The calculated values are much larger than the measured values, but are smaller than the values based on Townsent's theory [7] and Theodorsen's theory [18]. That is, since the wing span is finite, there is a sudden decrease of the air forces in the vicinity of the wing tip, and the pitch damping is smaller than in the two-dimensional theory.

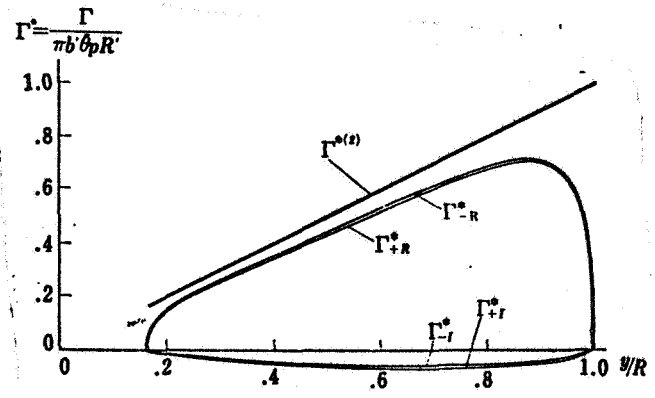

Fig. 60. Lift distribution along wing span sought by Ashley's unsteady theory. b' = 0.024 m, R_2 = 0.800 m, p = 0.756 c/s, Ω = 300 rpm. $\Gamma^{*(2)}$ is from the two-dimensional quasi-steady theory.

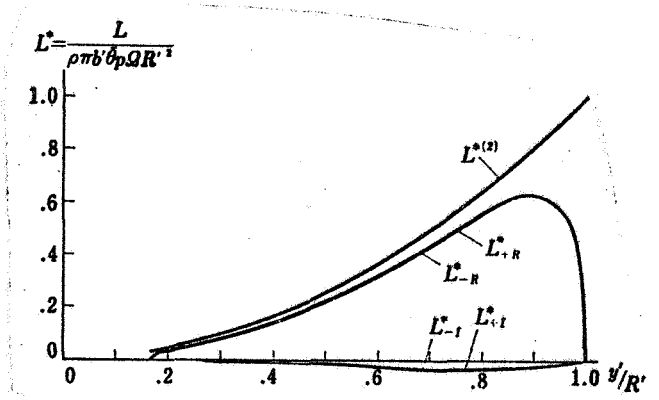

Fig. 61. Lift distribution along wing span, as sought by means of Ashley's unsteady theory. b' = 0.024 m, R_2' = 0.800 m, p = 0.756 c/s, Ω = 300 rpm. $L^{*(2)}$ is based on two-dimensional quasi-steady theory.

There is almost no change in the calculated values even when there are changes of the revolution speeds of the rotor, and the calculated values display a tendency similar to the measured values.

The relationship between the accuracy of the solution and the number of terms N in Eq. (3.56) is shown in Fig. 62. The similar relationship with respect to the number of terms J in Eq. (3.59) is shown in Fig. 63. An adequate accuracy was obtained at values of N = 9 and J = 5. /57

3.3. Introduction and Application of Theory of Ashley, et al. [19] for Cases when the Blade has Steady Motion

In a prologue to their monograph, Ashley et al. described a method of calculating the air forces operating on a blade in cases when the blade is in steady motion, taking into consideration the fact that the wing span is finite. This is introduced here.

Since the bound vortex does not undergo changes in time, there is no shed vortex in the wake; all that is present is merely a steady trailing vortex. Thus, equation (3.3) can be written as follows.

$$v_{as}(x', y') = -\frac{1}{4\pi}\iint_{R_a}\frac{\gamma_a(\xi', \eta')[x'-\xi'] + \delta_a(\xi', \eta')[y'-\eta']}{[(x'-\xi')^2+(y'-\eta')^2]^{3/2}}\,d\xi' d\eta' - \frac{1}{4\pi}\iint_{R_W}\frac{\delta_W(\xi', \eta')[y'-\eta']}{[(x'-\xi')^2+(y'-\eta')^2]^{3/2}} \quad (3.69)$$

$$\delta_W(\xi',\eta')=\frac{\partial}{\partial\eta'}\int_{x_t'}^{x_t'}\gamma_a(\lambda',\eta')d\lambda'=\frac{\partial}{\partial\eta'}\Gamma_a'(\eta')$$

$\eta'=R_1'$, $\eta'=R_2'$ で γ_a, Γ_a' が0になることを考慮しつつ変形を行なうと[25]

$$v_{as}(x',y')=-\frac{1}{4\pi}\int_{R_1'}^{R_2'}\int_{x_t'}^{x_t'}\frac{\partial\gamma_a(\xi',\eta)}{\partial\eta'}\frac{\sqrt{(x'-\xi')^2+(y'-\eta')^2}}{(x'-\xi')(y'-\eta')}d\xi'd\eta'-\frac{1}{4\pi}\int_{R_1}^{R_2}\frac{d\Gamma_a'}{d\eta'}\frac{d\eta'}{y'-\eta'} \tag{3.70}$$

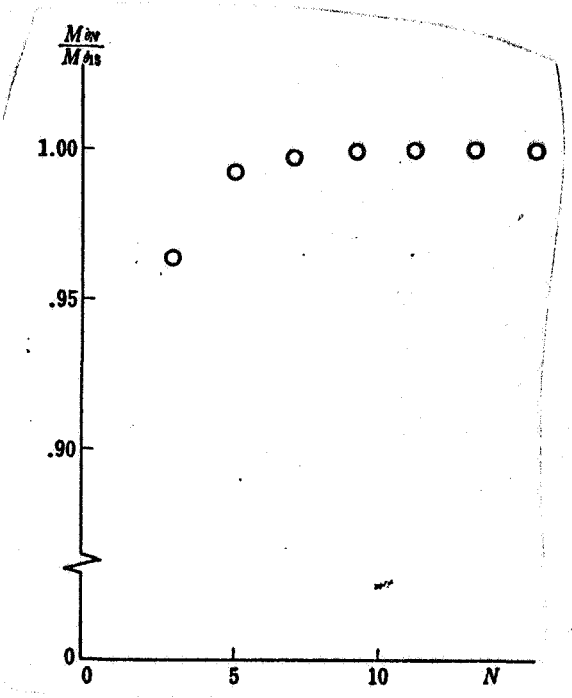

Fig. 62. Convergence of M_θ in cases when number of terms N in the interpolation formula (356) was increased

In rotor blades of helicopters, the wing span is quite large in comparison with the wing chord. Therefore, in most of the range of the wing surface, the length $|y' - \eta'|$ is large enough in comparison with the length $|x' - \xi'|$. Although this does not apply in cases when $\xi' = x'$ and $\eta' = y'$ at point (ξ',η'), $\sqrt{(x' - \xi')^2 + (y' - \eta')^2}/(x'-\xi')(y'-\eta')$ is the odd function of $(x' - \xi')$ and $(y' - \eta')$ in the rectangular region centering around point (x',y'). Thus, the influence exerted by the rectangular region on the induction velocity $v_a(x',y')$ is small as long as $\partial\gamma_a/\partial\eta'$ is not a function which changes rapidly. From the above considerations, it is supposed that $\sqrt{(x'-\xi')^2 + (y'-\eta')^2}/(x'-\xi')(y'-\eta')$ is $|y'-\eta'|/(y'-\eta')(x'-\xi')$. This approximation is exactly the approximation made by Prandtl [24] for wings advancing straight forward. The above equation can be integrated by using the approximation described above.

$$v_{as}(x',y')=-\frac{1}{2\pi}\int_{x_t'}^{x_t'}\frac{\gamma_a(\xi',y')}{x'-\xi'}d\xi'-\frac{1}{4\pi}\int_{R_1'}^{R_2'}\frac{d\Gamma_a'}{d\eta'}\frac{d\eta'}{y'-\eta'} \tag{3.71}$$

$y=y'/b_0'$
$\eta=\eta'/b_0'$
$x=\{x'-(x_t'+x_t')/2\}/b'$
$\xi=\{\xi'-(x_t'+x_t')/2\}/2\}/b'$
$\Gamma=\Gamma_a'/b_0'$

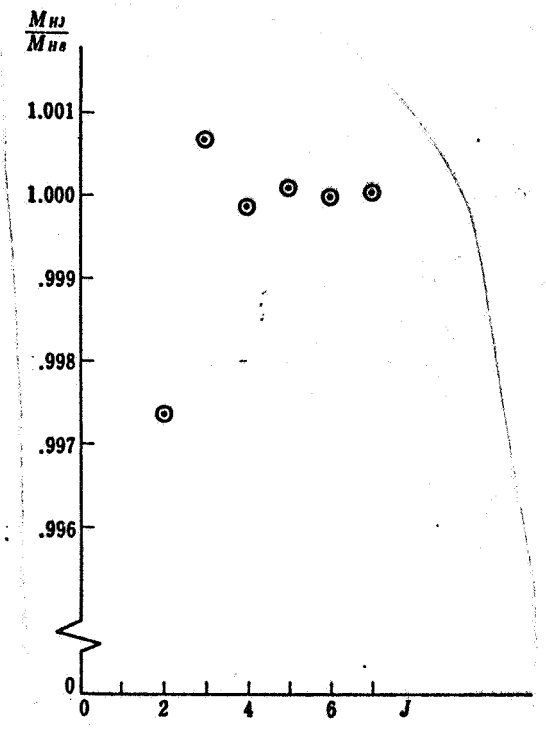

Fig. 63. Convergence of M_θ in cases when number of terms J in the interpolation formula (359) was increased

Assuming the above, let us make changes of variables.

$$v_{as}(x,y)=-\frac{1}{2\pi}\int\frac{\gamma_a(\xi,y)}{x-\xi}d\xi$$
$$-\frac{1}{4\pi}\int_{R_1}^{R_2}\frac{d\Gamma}{d\eta}\frac{d\eta}{y-\eta} \tag{3.72}$$

Multiplying both sides by $\sqrt{(1+x)/(1-x)}$, let us integrate x from -1 to 1.

$$\int_{-1}^{1}v_{as}(x,y)\sqrt{\frac{1+x}{1-x}}dx$$
$$=-\frac{1}{2}\Gamma(y)-\frac{1}{4}\int_{R_1}^{R_2}\frac{d\Gamma}{d\eta}\frac{d\eta}{y-\eta} \tag{3.73}$$

When v_{as} is determined from the boundary conditions, the above equation will become an equation using Γ as the unknown function, and it will be possible to solve it numerically. The lift operating on the wing surface can be calculated by the following equation.

$$L(y)=\rho b_0' V(y)\Gamma(y) \tag{3.74}$$

Applying Eqs. (3.73) and (3.74), we handle pitch damping problems from the quasi-steady standpoint. If we compare the results with the results obtained in Section 2 by using unsteady theory, extremely interesting results can be obtained in the sense that the unsteady effect can be evaluated in pitch damping problems.

When Eq. (3.73) was derived, it was assumed that v_{as} would be steady in time. However, in pitch damping problems, the blades have velocity components which are vertical to the rotating surface and which fluctuate in time. However, if we assume that the velocities vertical to the rotating surface at each instant are unchanging and if we equate them with $v_{as}(x,y)$, the following relationship will be valid at time t for the standard blade.

$$v_{as}(x, y) = -yb_0'\bar{\theta}p \cos pt \cos \Omega t$$

$$\therefore \quad -yb'\bar{\theta}p \cos pt \cos \Omega t = -\frac{1}{2}\Gamma(y) - \frac{1}{4}\int_{R_1}^{R_2} \frac{d\Gamma}{d\eta} \frac{d\eta}{y-\eta}$$

In the same way as in Section 2, $\Gamma(y)$ is expressed by means of Multhop's interpolation formula [3], and the second term on the right side is calculated using Glauert's integration [23].

In the case of the q-th blade,

$$v_{as}(x,y) = -yb_0'\bar{\theta}/\cos pt \cos(\Omega t + (2\pi q/Q))$$

The lift distribution is solved by utilizing Eq. (3.74). If the lift per unit wing span of the q-th blade is $L_q(y')$, then the moment generated around the pitching axis will be: /58

$$M_Y = \sum_{q=0}^{Q-1} \int_{R_1'}^{R_2'} L_q(y') y' \cos\left(\Omega t + \frac{2\pi q}{Q}\right) dy'$$

The pitch damping is calculated by the method in Appendix A.

$$M_\theta = \frac{1}{\pi\bar{\theta}} \int_0^{2\pi/p} M_Y \cos pt \, dt$$

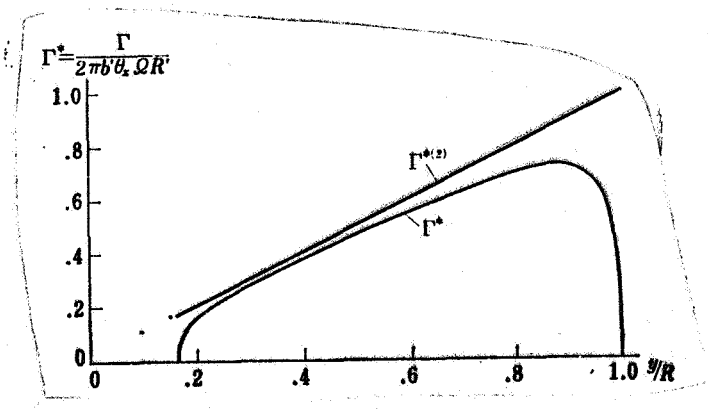

Fig. 64. Circulation distribution along wing span sought by means of Ashley's quasi-steady theory, b' = 0.024 m, R_2 = 0.800 m, p = 0.756 c/s, Ω = 300 rpm. $\Gamma^{(2)}$ is based on two-dimensional quasi-steady theory.

In Figs. 64 and 65 are shown the circulation distribution in the radial direction on the blade and the lift distribution in cases when the rotor revolution speed was 300 rpm and the pitching frequency was 0.756 c/s.

In Figs. 32 to 43, comparisons are made of the values estimated from the experimental values for cases when elastic deformation of the blades would not occur, as against the calculated values for this case (using Ashley's steady theory). In all the figures, the results obtained were almost exactly the same as the results of calculations using the unsteady theory of Ashley et al. This may be reduced to the fact that the non-dimensional

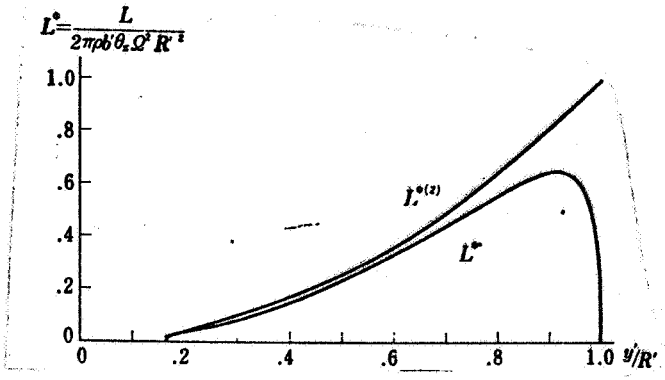

Fig. 65. Circulation distribution along wing span sought by means of Ashley's quasi-steady theory, b' = 0.024 m, R_2' = 0.800 m, p = 0.756 c/s, Ω = 300 rpm. $L^{(2)}$ is based on two-dimensional quasi-steady theory.

frequency is small. The unsteady effect seen in three-dimensional theory is smaller than the unsteady effect seen in two-dimensional theory (the difference between Townsent's theory and Theodorsen's theory).

CHAPTER 4. ANALYSIS OF PITCH DAMPING TAKING INTO CONSIDERATION FLUCTUATIONS IN DISTANCE BETWEEN VORTEX AND BLADE

4.1. Concerning the Properties which an Aerodynamic Calculating Method Ought to Have in Order to Analyze Pitch Damping

Two unsteady theories were applied for the purpose of analyzing the pitch damping of rigid rotors, but satisfactory results could not be obtained. However, the following was learned as a result of a comparison of the analyses performed thus far and the values of the pitch damping for rotors having perfectly rigid blades, as estimated from the experiments.

(1) In Loewy's theory [14], only the effect of the shed vortex in the wake was considered. As a result, it was learned, there is a considerable reduction in the pitch damping in certain cases. /59

(2) Therefore, if we were to include also the effect of the trailing vortex in the wake, it would be expected that the pitch damping would be reduced considerably.

(3) If we consider the fact that the wing span is finite, the lift in the vicinity of the wing tip is reduced considerably in comparison with two-dimensional theory, and the pitch damping also is reduced.

(4) The unsteady effect contributes very little in problems of pitch damping.

In view of the preceding, a theory for analyzing the pitch damping will have to be provided with the following properties.

(1) It must take into consideration the effect of the reduction of the air forces on account of the induction velocity caused by the vortex in the wake.

(2) It must take into consideration the fact that there is a sudden reduction of the air forces in the vicinity of the wing tip.

However, the theory does not necessarily have to be an unsteady theory.

If the moment of the air forces operating on the rotor blade root in a state of hovering were to be calculated by such a theory, it would be possible to obtain quite good results. Furthermore, the experimentally obtained air force moments operating on the rotor blade root in a state of hovering [25,26,27] are 50 - 60% of the values calculated by means of two-dimensional strip theory. Therefore, if one were to perform the calculations by the model mentioned above, similar values ought to be obtained. Consequently, the pitch damping also ought to be approximately 60% of the Townsent analysis [7] using two-dimensional strip theory. Nevertheless, the pitch damping of an entirely rigid rotor blade estimated from the experimental values is much smaller than this. Therefore, it is necessary to introduce elements which have not been taken into consideration thus far.

During rotor pitching, the position of the blade is constantly being displaced in the Z_I direction. As a result, the relative position between the vortex in the wake and the blade is not constant. When there are fluctuations in the relative position, the vortex in the wake causes fluctuations in the induction velocity which is induced on the blade, and there will also be changes in the pitch damping values. Consequently, it is desirable to include fluctuations of the relative position of the vortex in the wake and the blade when one is calculating the air forces.

Thus, taking into consideration the fact that the wing span is finite, let us derive a steady wing theory concerning rotors by which the vortex can be located at any desired position in the wake. Since this theory will be applied in performing quasi-steady analysis of the pitch damping, it is required that the wing theory itself should be as simple as possible.

4.2. Steady Theory Concerning Rotors

Steady wing theory is valid also for rotors during steady vertical flight. Taking our departure from the equation of Ichikawa in his linear theory of rotor blades [1], let us derive a simple lift line equation suitable for analyzing the pitch damping. At this time, we assume that there is a small inflow on the rotor rotating surface and that vortices located at a distance away from the standard blade which is being considered have little effect.

In the following let us show the relationship between the x'y'z' coordinates used thus far in this monograph and the τrσ coordinates used in Ichikawa's monograph.

$$\left.\begin{aligned} x' &= r\sin\frac{\tau+\sigma}{2} \\ y' &= r\cos\frac{\tau+\sigma}{2} \\ z' &= -h\frac{\tau-\sigma}{2} \end{aligned}\right\} \tag{4.1}$$

The relationship between the xyz coordinates used in Ichikawa's monograph and the x'y'z' coordinates used in this monograph is shown in Fig. 66. The following shows the relationships with the unit vectors in the coordinate axial direction.

$$\left.\begin{aligned} i_I &= \sin\phi i^* + \cos\phi j^* \\ j_I &= \cos\phi i^* - \sin\phi j^* \\ k_I &= -k \end{aligned}\right\} \tag{4.2}$$

If we use i_I, j_I, and k_I to represent the vectors r_τ and r_r in the tangential direction of the coordinate curves of the τrσ coordinates,

$$\begin{aligned} r_\tau &= \frac{1}{2}r\sin\left(\phi-\frac{\tau+\sigma}{2}\right)i_I \\ &\quad + \frac{1}{2}r\cos\left(\phi-\frac{\tau+\sigma}{2}\right)j_I + \frac{1}{2}hk_I \\ r_r &= \cos\left(\phi-\frac{\tau+\sigma}{2}\right)i_I - \sin\left(\phi-\frac{\tau+\sigma}{2}\right)j_I \end{aligned} \tag{4.3}$$

$$\left.\begin{aligned} r_\tau &= \frac{1}{2}r\cos\frac{\tau+\sigma}{2}i^* - \frac{1}{2}r\sin\frac{\tau+\sigma}{2}j^* - \frac{h}{2}k^* \\ r_r &= \sin\frac{\tau+\sigma}{2}i^* + \cos\frac{\tau+\sigma}{2}j^* \end{aligned}\right\} \tag{4.04 [sic]}$$

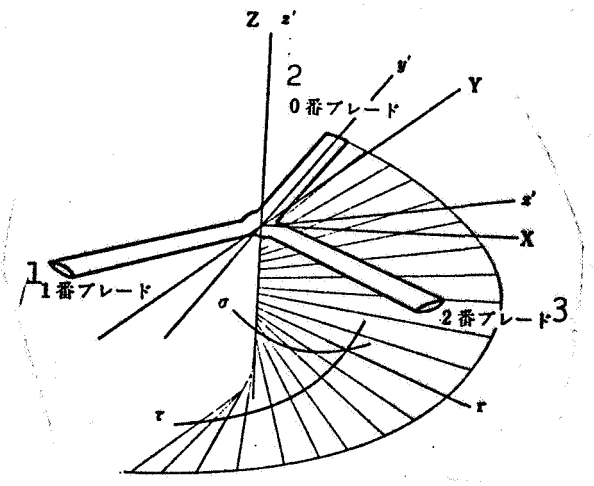

Fig. 66. Coordinate system

Key: 1. Blade 1
2. Blade 0
3. Blade 2

In Ichikawa's monograph, the surface vorticity vector γ of the vortex sheet is written in the following manner. /69

$$\gamma=\frac{1}{H(p')}(\gamma r_r-\delta r_\tau) \tag{4.5}$$

Here,

$$H(p')=\frac{1}{2}\sqrt{h^2+r'^2}$$

If γ is expressed by means of i^*, j^*, and k^*,

$$\begin{aligned}\gamma=&\frac{2}{\sqrt{h^2+r'^2}}\left[\gamma\sin\frac{\tau'+\sigma'}{2}-\delta\frac{1}{2}r'\cos\frac{\tau'+\sigma'}{2}\right]i^*\\&+\frac{2}{\sqrt{h^2+r'^2}}\left[\gamma\cos\frac{\tau'+\sigma'}{2}+\delta\frac{1}{2}r'\sin\frac{\tau'+\sigma'}{2}\right]j^*\\&+\frac{\delta h}{\sqrt{h^2+r'^2}}k^*\end{aligned} \tag{4.7}$$

[sic]

When the inflow is small, we can regard $h/\sqrt{h^2+r'^2}$ as being small, and the following can be written concerning γ, which expresses the wing surface:

$$\gamma = -\delta^N i^* + \gamma^N j^*$$

$$\begin{aligned}\delta^N=&-\frac{2}{\sqrt{h^2+r'^2}}\sin\frac{\tau'+\sigma'}{2}\cdot\gamma\\&+\frac{r'}{\sqrt{h^2+r'^2}}\cos\frac{\tau'+\sigma'}{2}\cdot\delta\\\gamma^N=&\frac{2}{\sqrt{h^2+r'^2}}\cos\frac{\tau'+\sigma'}{2}\cdot\gamma\\&+\frac{r'}{\sqrt{h^2+r'^2}}\sin\frac{\tau'+\sigma'}{2}\cdot\delta\end{aligned} \tag{4.8}$$

If this is solved with respect to γ and δ,

$$\left.\begin{aligned}\gamma=&\frac{\sqrt{h^2+r'^2}}{2}\left(\gamma^N\cos\frac{\tau'+\sigma'}{2}-\delta^N\sin\frac{\tau'+\sigma'}{2}\right)\\\delta=&\frac{\sqrt{h^2+r'^2}}{2}\left(\gamma^N\sin\frac{\tau'+\sigma'}{2}+\delta^N\cos\frac{\tau'+\sigma'}{2}\right)\end{aligned}\right\} \tag{4.9}$$

Concerning γ, which expresses the vortex surface in the wake,

$$\gamma=0 \tag{4.10}$$

$$\delta=\frac{d\Gamma'}{dr} \tag{4.11}$$

The equation for the lift surface may be written as follows, according to Ichikawa.

$$w_n(P_0)=\frac{1}{4\pi H(P_0)}\sum_{q=0}^{Q-1}\left\{\int_{r_1}^{r_2}\int_{\tau_{1q}}^{\tau_{2q}}G(P_0,P_q')\gamma_{Bq}d\tau'dr'+\int_{r_1}^{r_2}\int_{\tau_{1q}}^{\tau_{2q}}D(P_0,P_q')\delta_{Bq}d\tau'dr'+\int_{r_1}^{r_2}\int_{\tau_{2q}}^{\infty}D(P_0,P_q')\frac{d\Gamma}{dr}d\tau'dr'\right\} \tag{4.12}$$

The contribution of the vortices at a distance away from the standard blade is omitted as being small. The τ' coordinates expressing a point on the locus generated from the q-th blade, which has passed under the standard blade, and which has further moved around the Z axis n times, can be expressed as follows, using a small τ^*.

$$\frac{\tau'+\sigma'}{2}=\theta=2n\pi+\frac{\tau^*}{2} \tag{4.13}$$

At this time, the equation for the lift surface is rewritten as follows.

$$w_n(P_0)=\frac{1}{4\pi H(P_0)}\left\{\int_{r_1}^{r_2}\int_{\tau_{10}}^{\tau_{20}}G(P_0,P_0')\gamma_{B0}d\tau^*dr'+\int_{r_1}^{r_2}\int_{\tau_{10}}^{\tau_{20}}D(P_0,P_0')\delta_{B0}d\tau^*dr'+\sum_{q=0}^{Q-1}\sum_{n=0}^{\infty}\int_{r_1}^{r_2}\int_{\tau_{1nq}}^{\tau_{2nq}}D(P_0,P_q')\delta_{Wq}d\tau^*dr'\right. \tag{4.14}$$

The distance between point P and point P' is expressed by means of R(P,P'). If we write R(P,P'), G(P,P'), and D(P,P') concretely, they will be as follows when point P is on the locus surface of the standard blade:

$$R(P,P')=\left\{\frac{h^2}{4}\left(\tau-\tau^*-4\pi n-\frac{4\pi q}{Q}\right)^2+r^2+r'^2-2rr'\cos\frac{\tau-\tau^*}{2}\right\}^{1/2}$$

$$G(P,P')=-\frac{r}{2}\sin\frac{\tau-\tau^*}{2}\frac{\partial}{\partial r}\left(\frac{1}{R}\right)-\cos\frac{\tau-\tau^*}{2}\frac{\partial}{\partial\tau}\left(\frac{1}{R}\right)$$

$$D(P,P')=\frac{r'}{2}\sin\frac{\tau-\tau^*}{2}\frac{\partial}{\partial\tau}\left(\frac{1}{R}\right)-\frac{1}{4}\left\{h^2+rr'\cos\frac{\tau-\tau^*}{2}\right\}\frac{\partial}{\partial r}\left(\frac{1}{R}\right)$$

If we continue to make further calculations concerning G and D,

$$\frac{\partial}{\partial\tau}\left(\frac{1}{R}\right)=\frac{1}{R^3}\left\{-\frac{h^2}{4}\left(\tau-\tau^*-4\pi n-\frac{4\pi q}{Q}\right)-\frac{rr'}{2}\sin\frac{\tau-\tau^*}{2}\right\}$$

$$\frac{\partial}{\partial r}\left(\frac{1}{R}\right)=\frac{1}{R^3}\left\{r'\cos\frac{\tau-\tau^*}{2}-r\right\}$$

$$G(P,P')=\left\{\frac{r^2}{2}\sin\frac{\tau-\tau^*}{2}+\frac{h^2}{4}\left(\tau-\tau^*-4\pi n-\frac{4\pi q}{Q}\right)\right\}\frac{1}{R^3} \qquad /61$$

$$D(P,P')=\left\{-\frac{h^2r'}{8}\left(\tau-\tau^*-4\pi n-\frac{4\pi q}{Q}\right)\sin\frac{\tau-\tau^*}{2}-\frac{rr'^2}{4}\right.$$
$$\left.-\frac{h^2r'}{4}\cos\frac{\tau-\tau^*}{4}+\frac{h^2r}{4}+\frac{r^2r'}{4}\cos\frac{\tau-\tau^*}{2}\right\}\frac{1}{R^3}$$

If we use τ^*, Eq. (4.9) will be:

$$r=\frac{\sqrt{h^2+r'^2}}{2}\left\{\gamma^N\cos\frac{\tau^*}{2}-\delta^N\sin\frac{\tau^*}{2}\right\}$$
$$\delta=\frac{\sqrt{h^2+r'^2}}{r'}\left\{\gamma^N\sin\frac{\tau^*}{2}+\delta^N\cos\frac{\tau^*}{2}\right\} \qquad (4.15)$$

$$\therefore\ G(P_0,P_0')\gamma_{B0}+D(P_0,P_0')\delta_{B0}=\frac{\sqrt{h^2+r'^2}}{R^3}\left\{\frac{r^2}{4}\sin\frac{\tau}{2}-\frac{rr'}{4}\sin\frac{\tau'}{2}\right\}\gamma^N$$
$$+\frac{\sqrt{h^2+r'^2}}{R^3}\left\{\frac{h^2}{8}(\tau-\tau^*)\cos\frac{\tau^*}{2}-\frac{h^2}{8}(\tau-\tau^*)\sin\frac{\tau-\tau^*}{2}\sin\frac{\tau^*}{2}\right.$$
$$\left.+\frac{h^2r}{4r'}\sin\frac{\tau^*}{2}-\frac{h^2}{4}\cos\frac{\tau-\tau^*}{2}\sin\frac{\tau^*}{2}\right\}\gamma_N$$
$$+\frac{\sqrt{h^2+r'^2}}{R^3}\left\{\frac{r^2}{4}\cos\frac{\tau}{2}-\frac{rr'}{4}\cos\frac{\tau^*}{2}\right\}\delta^N+\frac{\sqrt{h^2+r'^2}}{R^3}\left\{-\frac{h^2}{8}(\tau-\tau^*)\sin\frac{\tau^*}{2}\delta^N\right.$$
$$\left.-\frac{h^2}{8}(\tau-\tau^*)\sin\frac{\tau-\tau^*}{2}\cos\frac{\tau^*}{2}-\frac{h^2}{4}\cos\frac{\tau-\tau^*}{2}\cos\frac{\tau^*}{2}+\frac{h^2r}{4r'}\cos\frac{\tau^*}{2}\right\}\delta^N$$

When the inflow is small, h/r and h/r' will be smaller than 1. At this time,

$$G(P_0,P_0')\gamma_{B0}+D(P_0,P_0')\delta_{B0}=\frac{r'}{R^3}\left\{\frac{r^2}{4}\sin\frac{\tau}{2}-\frac{rr'}{4}\sin\frac{\tau^*}{2}\right\}\gamma^N+\frac{r'}{R^3}\left\{\frac{r^2}{4}\cos\frac{\tau}{2}-\frac{rr'}{4}\cos\frac{\tau^*}{2}\right\}\delta^N \qquad (4.16)$$

$$\sum_{q=0}^{Q-1}D(P_0,P_q')\delta_{Wq}=\frac{1}{R^3}\left\{-\frac{rr'^2}{4}+\frac{r^2r'}{2}\cos\frac{\tau-\tau^*}{2}\right\}\frac{d\Gamma_0'}{dr'}$$
$$+\sum_{q=1}^{Q-1}\frac{1}{R^3(P_0,P_q')}\left\{-\frac{rr'^2}{4}+\frac{r^2r'}{4}\cos\frac{\tau-\tau^*}{2}\right\}\frac{d\Gamma_q'}{dr'}$$
$$+\sum_{n=1}^{\infty}\sum_{q=0}^{Q-1}\frac{1}{R^3(P_0,P_q')}\left\{\frac{rr'^2}{4}+\frac{r^2r'}{4}\cos\frac{\tau-\tau^*}{2}\right\}\frac{d\Gamma_q'}{dr'} \qquad (4.17)$$

Therefore, Eq. (4.14) will be:

$$w_n(P_0)=\frac{1}{4\pi r/2}\left[\int_{r_2}^{r_1}\int_{\tau_{10}}^{\tau_{20}}\frac{r'}{R^3}\left\{\frac{r^2}{4}\sin\frac{\tau}{2}-\frac{rr'}{4}\sin\frac{\tau^*}{2}\right\}\gamma^N d\tau^* dr'\right.$$
$$+\int_{r_1}^{r_2}\int_{\tau_{10}}^{\tau_{20}}\frac{r'}{R^3}\left\{\frac{r^2}{4}\cos\frac{\tau}{2}-\frac{rr'}{4}\cos\frac{\tau^*}{2}\right\}\delta^N d\tau^* dr'$$
$$+\int_{r_1}^{r_2}\int_{\tau_{20}}^{\tau_{2^*}}\frac{1}{R^3}\left\{\frac{r^2r'}{4}\cos\frac{\tau-\tau^*}{2}-\frac{rr'^2}{4}\right\}\frac{d\Gamma_0'}{dr'}d\tau^* dr'$$
$$+\sum_{q=1}^{Q-1}\int_{r_1}^{r_2}\int_{\tau_{1^*}}^{\tau_{2^*}}\frac{1}{R^3}\left\{\frac{r^2r'}{4}\cos\frac{\tau-\tau^*}{2}-\frac{rr'^2}{4}\right\}\frac{d\Gamma_q'}{dr'}d\tau^* dr'$$
$$\left.+\sum_{n=1}^{\infty}\sum_{q=0}^{Q-1}\int_{r_1}^{r_2}\int_{\tau_{1^*}}^{\tau_{2^*}}\frac{1}{R^3}\left\{\frac{r^2r'}{4}\cos\frac{\tau-\tau^*}{2}-\frac{rr'^2}{4}\right\}\frac{d\Gamma_q'}{dr'}d\tau^* dr'\right] \tag{4.18}$$

If the variables are changed to x', y', and z', we obtain:

$$w_z'=\frac{-1}{4\pi}\left[\int_{R_1'}^{R_2'}\int_{x_t'}^{x_t'}\frac{[x'-\xi']\gamma^N+[y'-\eta']\delta^N}{R^3}d\xi' d\eta'+\int_{R_1'}^{R_2'}\int_{x_t'}^{x_2'}\frac{y'-\eta'}{R^3}\frac{d\Gamma'}{d\eta'}d\xi' d\eta'\right.$$
$$\left.+\sum_{q=1}^{Q-1}\int_{R_1'}^{R_2'}\int_{x_t'}^{x_2'}\frac{y'-\eta'}{R^3}\frac{d\Gamma_q'}{d\eta'}d\xi' d\eta'+\sum_{n=1}^{\infty}\sum_{q=0}^{Q-1}\int_{R_1'}^{R_2'}\int_{x_1'}^{x_2'}\frac{y'-\eta'}{R^3}\frac{d\Gamma_q'}{d\eta'}d\xi' d\eta'\right] \tag{4.19}$$

If we regard the contribution of the distant vortices in the wake as being small,

$$w_z'=\frac{-1}{4\pi}\left[\int_{R_1'}^{R_2'}\int_{x_t'}^{x_t'}\frac{[x'-\xi']\gamma^N+[y'-\eta']\delta^N}{R^3}d\xi' d\eta'+\int_{R_1'}^{R_2'}\int_{x'_t}^{\infty}\frac{y'-\eta'}{R^3}\frac{d\Gamma_c'}{d\eta'}d\xi' d\eta'\right.$$
$$\left.+\sum_{q=1}^{Q-1}\int_{R_1'}^{R_2'}\int_{-\infty}^{\infty}\frac{y'-\eta'}{R^3}\frac{d\Gamma_q'}{d\eta'}d\xi' d\eta'+\sum_{n=0}^{\infty}\sum_{q=0}^{Q-1}\int_{R_1'}^{R_2'}\int_{-\infty}^{\infty}\frac{y'-\eta'}{R^3}\frac{d\Gamma_q'}{d\eta'}d\xi' d\eta'\right] \tag{4.20}$$

/62

The first term will be exactly the same as Eq. (3.69) in Chapter 3, Section 3, and the second term and the succeeding terms can be integrated with respect to ξ'.

$$v_{as}=\frac{-1}{4\pi}\left[2\int_{x_t'}^{x_t'}\frac{\gamma^N}{x'-\xi'}d\xi'+\int_{R_1'}^{R_2'}\frac{d\Gamma'}{d\eta'}\frac{d\eta'}{y'-\eta'}+\sum_{q=1}^{Q-1}\int_{R_1'}^{R_2'}2\frac{d\Gamma_q}{d\eta'}\frac{y'-\eta'}{[y'-\eta']^2+[x'-\zeta']^2}d\eta'\right.$$
$$\left.+\sum_{n=0}^{\infty}\sum_{q=0}^{Q-1}\int_{R_1'}^{R_2'}2\frac{d\Gamma_q}{d\eta'}\frac{y'-\eta'}{[y'-\eta']^2+[z-\zeta']^2}d\eta'\right] \tag{4.21}$$

Concerning the third and fourth terms, the vortex surface in the wake is replaced by discrete vortex filaments.

$$v_{as}=\frac{-1}{4\pi}\left[2\int_{x_t'}^{x_t'}\frac{\gamma^N}{x'-\xi'}\,d\xi'+\int_{R_t'}^{R_t'}\frac{d\Gamma'}{d\eta'}\,\frac{d\eta'}{y'-\eta'}+\sum_{q=1}^{Q-1}2\sum_{j=1}^{J}\frac{\Delta'_{qj}[y'-\eta'_{qj}]}{[y'-\eta'_{qj}]+[z'-\zeta'_{qj}]^2}\right.$$
$$\left.+\sum_{n=0}^{\infty}\sum_{q=0}^{Q-1}2\sum_{j=1}^{J}\frac{\Delta'_{qj}[y'-\eta'_{n.q.j}]}{[y'-\eta'_{n.q.j}]+z'-\zeta'_{n.q.j}]}\right]$$

Here, if we posit that

$$\Delta'_{qj}=\Gamma'_{q,j+1}-\Gamma'_{q,j} \qquad \Delta_{qj}=\frac{2}{x'_{t0}-x'_{t0}}\Delta'_{qj}$$

$$\xi'\equiv\frac{x_t'+x_t'}{2}+\frac{x_t'-x_t'}{2}\xi \qquad \eta'\equiv\frac{x'_{t0}-x'_{t0}}{2}\eta$$

we obtain:

$$v_{as}(x,y)=-\frac{1}{2\pi}\int_{-1}^{1}\frac{\gamma^N(\xi,y)}{x-\xi}\,d\xi-\frac{1}{4\pi}\int_{R_1}^{R_1}\frac{d\Gamma}{d\eta}\,\frac{d\eta}{y-\eta}-\frac{1}{2\pi}\sum_{q=1}^{Q-1}\sum_{j=1}^{J}\frac{\Delta_{qj}[y-\eta_{qj}]}{[y-\eta_{qj}]^2+[z-\zeta_{qj}]^2}$$
$$-\frac{1}{2\pi}\sum_{n=1}^{\infty}\sum_{q=0}^{Q-1}\sum_{j=1}^{J}\frac{\Delta_{qj}[y-\eta_{qj}]}{[y-\eta_{qj}]^2+[z-\zeta_{qj}]^2} \qquad (4.22)$$

If we multiply both sides by $\sqrt{1+x/1-x}$ and perform integration for x from -1 to 1, we obtain:

$$\int_{-1}^{1}\sqrt{\frac{1+x}{1-x}}\,v_{as}(x,y)\,dx=-\frac{1}{2}\Gamma(y)-\frac{1}{4}\int_{R_1}^{R_1}\frac{d\Gamma}{d\eta}\,\frac{d\eta}{y-\eta}-\frac{1}{2}\sum_{q=1}^{Q-1}\sum_{j=1}^{J}\frac{\Delta_{qj}[y-\eta_{qj}]}{[y-\eta_{qj}]^2+[z-\zeta_{qj}]^2}$$
$$-\frac{1}{2}\sum_{n=1}^{\infty}\sum_{q=0}^{Q-1}\sum_{j=1}^{J}\frac{\Delta_{qj}[y-\eta_{qj}]}{[y-\eta_{qj}]^2+[z-\zeta_{qj}]^2} \qquad (4.23)$$

4.3. Analysis of Pitch Damping

Fundamentally, the pitch damping of a rotor ought to be analyzed by assuming unsteady air forces. However, it was learned as a result of the research in Chapter 3 that it is permissible to analyze it in terms of quasi-steady air forces. Taking into consideration the fluctuations of the relative positions between the vortex and the blade, as was described in Section 1, let us make an analysis of the pitch damping by applying the theory in the previous section with respect to a rigid rotor which has pitching motion in which the inclination of the rotor surface may be expressed as $\theta = \bar{\theta}$ sin pt.

Eq. (4.23) is written as follows with reference to the q-th blade.

$$\int_{-1}^{1}\sqrt{\frac{1+x}{1-x}}v_a(x,y)dx$$
$$=-\frac{1}{2}\Gamma(y)-\frac{1}{4}\int_{R_1}^{R_2}\frac{d\Gamma}{d\eta}\frac{d\eta}{y-\eta}$$
$$-\sum_{l=1}^{L}\sum_{j=1}^{J}\frac{1}{2}\frac{\Delta_{lj}(y-\eta_{lj})}{(y-\eta_{lj})^2+(z-\zeta_{lj})^2} \qquad (4.24)$$

When applying the above equation to pitch damping problems, it is necessary to determine Δ_{lj}, η_{lj}, ζ_{lj}, and v_a. As for v_a, if we refer to Eq. (1.5) and take into consideration the boundary conditions of the tangential flow, we obtain:

$$v_{a_q}=-y'\Omega\theta_c-y'\dot{\theta}\cos\psi_q \qquad (4.25)$$

If we introduce the effective angle of incidence θ_X,

$$\theta_X=\theta_c+\dot{\theta}/\Omega\cdot\cos\psi_q \qquad (4.26)$$

$\eta_{lj}(t)$ and $\zeta_{lj}(t)$ express the position of the j-th vortex filament from the inside, making up the l-th vortex layer immediately underneath the q-th blade. However, in cases when j = J, they represent the tip vortex of the l-th wing. For $\eta_{lj}(t)$ and $\zeta_{lj}(t)$, one ought to use the values measured from moment to moment while the rotor is in a state of pitching. However, we here used the results of the smoke experiments in Chapter 1, Section 4 and determined their values approximately. The following method was used in this. The j-th vortex filament from the inside of the l-th layer, expressed by lj, was generated from the q*-th blade at a time $t' = t - 2\pi l/Q\Omega$. At the point in time when the vortex was generated, the Z_i coordinates of the q*-th blade are $z'q^*(t')$. /63 The generated vortex is swept from this position into the wake. The manner in which it is swept into the wake will naturally differ depending upon whether the rotor is simply in a state of hovering or whether it is in a state of pitching movement. However, we may view both as being approximately the same. The vortex position when pitching is not being performed, ζ_{ljST}, has already been sought by smoke experiments in Chapter 1, Section 4. Therefore, it is already known to what degree the vortex will travel during the time $2\pi l/Q\Omega$. Thus, the position of the vortex at time t is $z'v_{q^*}(t') + \zeta'_{ljST}$. On the other hand, the Z_i coordinates of the blade at time t are $z'_q(t)$. Since the pitching angle is minute,

$$\zeta'_{lj}(t)=z'_{q^*}(t')+\zeta'_{ljST} \qquad (4.27)$$

Here, $z'_{q*}(t')$ and $z'_q(t)$ can be written as follows.

$$z'_q(t) = -y' \cos\phi_q(t) \sin\theta(t) \tag{4.28}$$

$$z'_{V_{q*}}(t') = -y_{V'} \cos\phi_{q*}(t') \sin\theta(t') \tag{4.29}$$

Needless to say, $\psi_q(t) = \psi_{q*}(t')$.

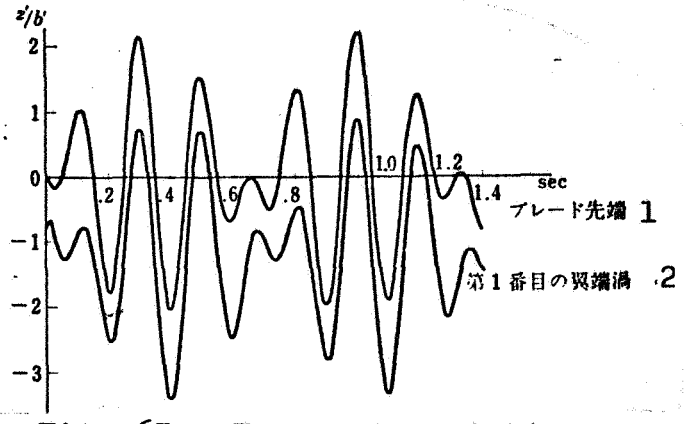

Fig. 67. Temporal variations of the position of the blade wing tip and of the position of the tip vortex of the first blade (not including bending deformation of blades)

$R_t'/b=33.33$, $\theta=0.0654$ rad, $p=0.756$ c/s, $\Omega=300$ rpm

Key: 1. Blade tip
2. Tip vortex of first blade

In Fig. 67 are plotted the Z_i coordinates $z_0'(t)$ of the wing tip with respect to the standard blade, and the Z_i coordinates $Z_{V1}'(t') + \zeta'_{1jST}$ of the vortex generated from the first blade which is immediately below the standard blade.

For $\eta'_{1j}(t)$, we use without any modifications η_{1jST}, the vortex position when there is no pitching.

Next let us consider $\Delta'_{1j}(t)$, the intensity of the vortex filament representing the wing tip vortex in the wake and the vortex layers on the inside. $\Delta'_{1j}(t)$ is the intensity of the j-th vortex filament from the inside which makes up the 1-th layer immediately underneath the q-th blade. Therefore, $\Delta'_{1j}(t)$ ought to be determined by the bound vortex at time t' of the q-th blade. However, if the pitching period is long enough in comparison with the revolution period of the rotor, it ought to be possible to determine $\Delta'_{1j}(t)$ by the bound vortex at time t of the q-th blade.

$$\Delta_{ij}(t) \fallingdotseq \Gamma_{q,j+1}(t) - \Gamma_{qj}(t) \tag{4.30}$$

The contents of this approximation are described below. That is, instead of determining the vortex in the wake by means of the bound vortex of the rotor blades operating under conditions of a pitch angle $\theta_{X(t')} = \theta_C + \frac{\theta(t')}{\Omega} \cos\psi_{q*}(t')$ and a vortex position $\zeta'_{1jq*}(t')$,

the vortex in the wake is determined by means of the bound vortex of the rotor blades operating under conditions of a pitch angle $\theta_X(t) = \theta_C + \frac{\dot{\theta}(t)}{\Omega} \cos \psi_q(t)$ and a vortex position $\zeta'_{1jq}(t)$. Consequently, errors will occur only concerning the intensity of the vortex in the wake, but their magnitude will be small. This is so because of the following reasons. Since $\psi_q^*(t')$ and $\psi_q(t)$ are the same, all of the errors occur because $\dot{\theta}(t')$ has been regarded as $\dot{\theta}(t)$, and $\theta(t')$ has been regarded as $\theta(t)$. The difference between t' and t is $2\pi l/Q\Omega$. It is short enough in comparison with the pitching period if the rotor revolution speed is great. Consequently, the error arising from the use of $\dot{\theta}(t)$ instead of $\dot{\theta}(t')$ is small. The error arising from the use of $\theta(t')$ instead of $\dot{\theta}(t')$ is p times the error arising from the use of $\theta(t)$ instead of $\theta(t')$. However, the error concerning the pitch angle itself is found by dividing this by Ω. Therefore, the error will be small enough as long as the rotor revolution period is short enough in comparison with the pitching period.

As a result of the above considerations, Eq. (4.24) will become a differential-integral equation concerning the unknown $\Gamma(y,t)$, and it will be possible to solve it numerically. If we rewrite it using the approximations described above, we obtain:

$$-\pi y b' \Omega \theta_X = -\frac{1}{2}\Gamma(y) - \frac{1}{4}\int_{R_1}^{R_2} \frac{d\Gamma}{d\eta} \frac{d\eta}{y-\eta} - \sum_{l=1}^{L}\sum_{j=1}^{J} \frac{1}{2}(\Gamma_{j+1}-\Gamma_j) \frac{y-\eta_{lj}}{(y-\eta_{lj})^2+(x-\zeta_{lj})^2} \tag{4.31}$$

In cases of sinusoidal pitching with a minute amplitude in which the inclination of the rotor surface can be expressed in terms of $\theta = \bar{\theta} \sin pt$, if Eq. (4.31) is solved successively with slight time intervals, it is possible to find the circulation on the blade at each time. The lift at each time and the moment around the pitching axis can be sought from this. When the temporal fluctuations of the moment around the pitching axis are known, it is possible to obtain the pitch damping derivative by the method in Appendix A. /64

Concrete Methods of Solving

The vortex filaments are established in the following manner.

It is anticipated that the distribution of the bound vortices along the blade in the radial direction will be as shown in Fig. 68. The trailing vortex generated in the portion between the blade tip and the point where the bound vortex reaches its maximum y_Λ is believed to be swept up and to form the tip vortex

core. There are no experimental grounds clearly guaranteeing this assumption. However, in view of the manner of flow in the vicinity of the blade tip, learned from the smoke experiments, it is believed that there is not mixing of the vortices generated from both sides of y_Λ. It is believed that strong trailing vortices, each with opposite signs, are generated from both sides of y_Λ. However, one would be justified in assuming that vortex mixture will not occur rapidly from the fact that the movements of the two vortex filaments with different intensities [28] are circular movements around their centers of gravity.

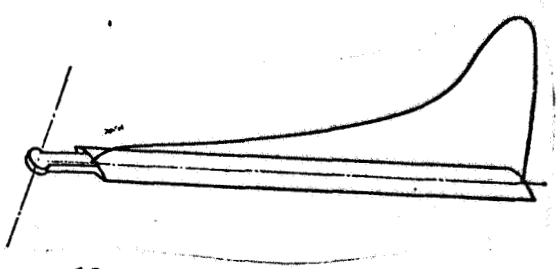

Fig. 68. Sketch of the circulation distribution in the blade wing span direction

It is clear from the smoke experiments that the vortices emerging from inside the blade will not be swept up rapidly, but can be regarded as vortex sheets over a considerable period of time. These vortex sheets, as mentioned above, are replaced by discrete vortex filaments.

θ_Λ is defined as follows.

$$y_A \equiv \frac{R_2+R_1}{2} - \frac{R_2-R_1}{2}\cos\theta_A \tag{4.32}$$

θ_j is defined as follows.

$$\theta_j \equiv \frac{\theta_A(j-1)}{J-1} \quad (j=1, 2, \cdots J) \tag{4.33}$$

η_{0j} is defined as follows.

$$\eta_{0j} \equiv \frac{R_2+R_1}{2} - \frac{R_2-R_1}{2}\cos\theta_j \tag{4.34}$$

Therefore, $\eta_{0J} = y_\Lambda$.

It is assumed that $\theta_{J+1} \equiv \pi$.

The j-th vortex filament from the inside is considered to be generated from the midpoint between η_{0j} and η_{0j+1}. It assumes positions η_{1j} and ζ_{1jST} in accordance with the vena contracta ratio shown in Table 4.

$$\left.\begin{aligned}\eta_{lj}&=CTR(l)\cdot(\eta_{0j}+\eta_{0j+1})/2\\ \zeta_{ljST}&=VPR(l)\cdot(\eta_{0j}+\eta_{0j+1})/2\end{aligned}\right\}\quad (j=1, 2, \cdots\cdots J-1) \tag{4.35}$$

η_{1J} and ζ_{1JST} are the positions of the tip vortex cores. They can be sought directly from the photographs and are shown in Table 5.

The intensity of the j-th vortex filament from the inside is determined as the difference between Γ_{j+1}, the intensity of the bound vortex at η_{0j+1}, and Γ_j, the intensity of the bound vortex at η_{0j}. This is as was described in Eq. (4.30)

Multhop's equation [3] is used as the interpolation formula for expressing the intensity of the bound vortex.

Exactly the same technique is used as that which was used in Chapter 3 to solve the circulation equation.

$$\Gamma(\phi)=\frac{2}{N+1}\sum_{i=1}^{N}\Gamma(\phi_i)\sum_{n=1}^{N}\sin n\phi_i\sin n\phi \tag{4.36}$$

The integration of (4.31) is calculated using Glauert's formula [23].

Eq. (4.31) is a simultaneous equation of the following type. It is possible to obtain $\Gamma(\phi_i)$.

$$\begin{aligned}&-\pi b'\left(\frac{R_2+R_1}{2}-\frac{R_2+R_1}{2}\cos\theta\right)\\&\quad\times(\Omega\theta_c+\bar{\theta}p\cos\phi_q\cos pt)\\&=\frac{2}{N+1}\sum_{i=1}^{N}\Gamma(\phi_i)\sum_{n=1}^{N}\sin n\phi_i\left[-\sin n\phi\left(\frac{1}{2}\right.\right.\\&\quad+\frac{n\pi}{2(R_2-R_1)\sin\phi}-\frac{1}{2}\sum_{j=1}^{J}(\sin n\theta_{j+1}\\&\quad\left.\left.-\sin n\theta_j)\sum_{l=1}^{L}\frac{y-\eta_{lj}}{(y-\eta_{lj})^2+(z-\zeta_{lj})^2}\right]\right.\end{aligned} \tag{4.37}$$

The lift distribution is sought by means of $L' = \rho b' y \Omega \Gamma'$.

If θ_Λ is assumed in a suitable manner, η_{0j} and θ_j are sought, and the circulation equation is solved, one can obtain y_Λ. From this one obtains the primary approximation of θ_Λ, and the same process is repeated. Convergence for θ_Λ was obtained after two /65 or three repetitions.

The moment around the Y axis is

$$M_Y' = -\sum_{q=0}^{Q-1} \int_{R_1'}^{R_2'} L_q' y' dy' \cos \phi_q \tag{4.38}$$

Since L_q' ought to be 0 when $y' = R_1'$ and $y' = R_2'$, the above equation is integrated by using Multhop's interpolation formula [3].

$$M_Y' = -\sum_{q=0}^{Q-1} \frac{2}{N+1} \frac{R_2' - R_1'}{2} \frac{\pi}{2} \times \sum_{i=1}^{N} L_q'(\phi_i) y_i' \sin \phi_i \cos \phi_q. \tag{4.39}$$

Here,

$$\phi_i = \frac{\pi i}{N + 1}$$

The pitch damping is sought by the teφhnique in Appendix A.

$$M_\theta = \frac{1}{\pi \dot{\theta}} \int_0^{2\pi/p} M_Y \cos pt \, dt \tag{4.40}$$

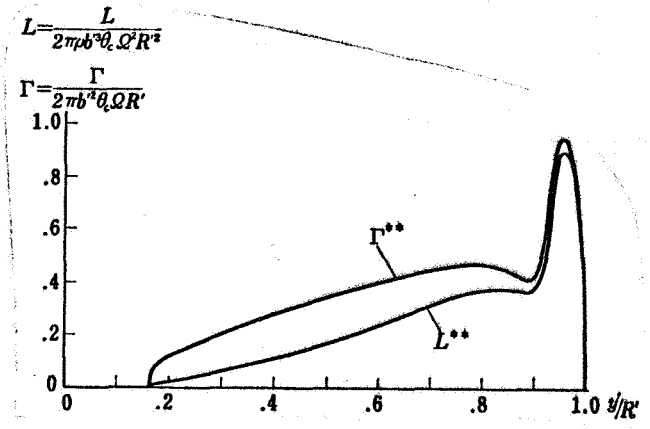

Fig. 69. Circulation and lift distribution sought by means of theory taking into consideration the fluctuations in the distance between the vortex and the blade

Time t = 0, ψ = 0°, θ_c = 4°

Typical Examples of Calculations

In Fig. 69 are given examples of calculations of the circulation and pressure distributions in the radial direction of the standard blade at time t = 0. This is an example where there was extremely close approximation between the blade and the strong returning wing tip vortex in the wake. The distance between the blade and the vortex center is 0.8 b' or 0.024 R'. For this reason, there is a sudden change in the direction of the induction velocity in the vicinity of the y'/R' value of 0.9,

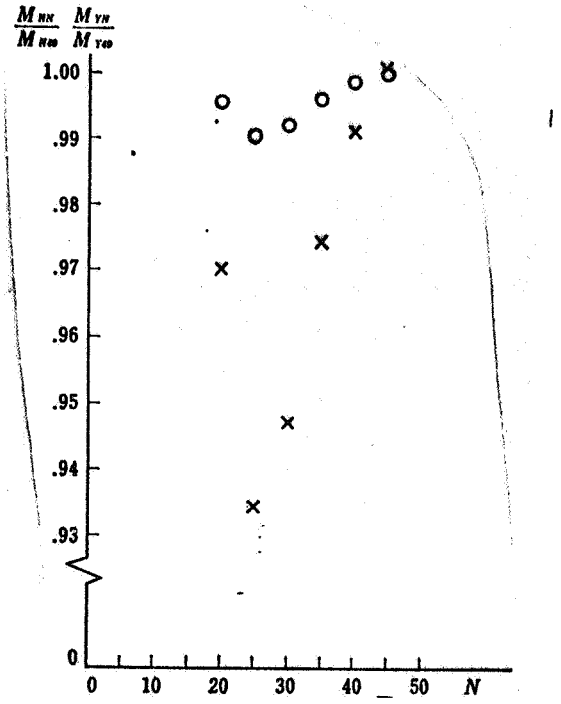

Fig. 70. Convergence between M_H, the moment around the blade root, and M_Y, the moment around the pitching axis, in cases when the number of terms N in the interpolation formula ( ) [sic] has been increased.

and it is quite difficult to converge the circulation and lift distributions. The data in this figure were calculated by assigning a value of 35 to N in Eq. (4.36). However, there is still a "valley" in the circulation and lift distributions. However, as soon as the vortex goes away from the blade, the solution convergence becomes good enough, and the "valley" in the circulation distribution disappears.

Thus, although the distribution does not have a good convergence, the convergence of the moments which are necessary for calculating the pitch damping is relatively good. In Fig. 70 is recorded the convergence between M_H, the moment around the blade root (indicated by the o mark) and M_Y, the moment around the pitching axis formed by the air forces operating on the three blades (indicated by the × mark). It is clear that when a value of 35 is adopted for N, the error of M_Y becomes about 3%. /66

Next, in Fig. 71 are plotted the calculated values of M_Y obtained every time the blade rotated 15°. The values are plotted for one pitching period. Since $z - \zeta_{1j}$ in Eq. (4.37) is time dependent, M_Y becomes a time history including high frequencies. In Fig. 72 is given another example in which M_Y cos pt is plotted similarly. In both figures, 56/144 mm on the abscissa corresponds to an azimuth angle of 15°. It is clear from these figures that a satisfactory accuracy will be obtained if the M_Y is calculated for every 15° of the azimuth angle. M_Y cos pt was calculated for every 45° of the azimuth angle, and Eq. (4.40) was integrated numerically to seek $M_{\dot{\theta}}$. The calculation results are shown in Figs. 32 to 43, where they are marked by the o mark and the letter G. In all the figures, the results obtained by this method display better results than those obtained by other theories.

In the results marked with G, it was assumed that $z - \zeta_{1j}$ in Eq. (4.37) undergoes time changes. When this was replaced by a constant value $-\zeta_{1iST}$, the results obtained are those indicated by the mark F □. F undergoes almost no changes depending on the rotor revolution speed.

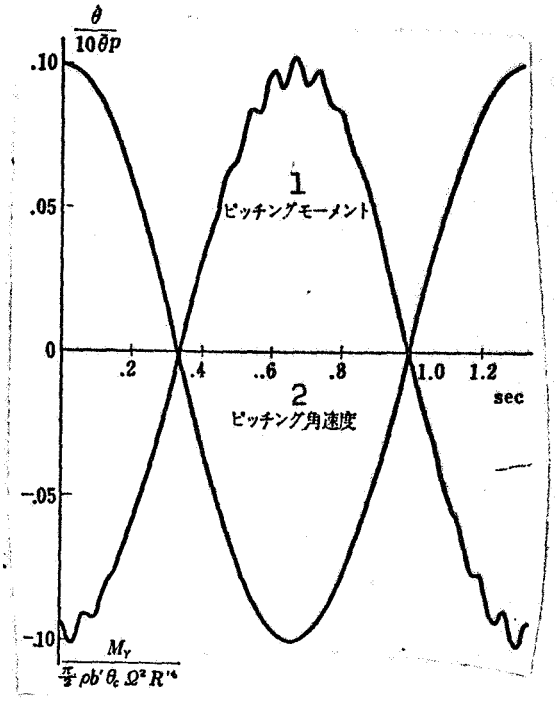

Fig. 71. Time changes of the pitching angular velocity $\dot{\theta}$ and the moment around the pitching axis M_Y

$R_3'/b'=33.33$, $\bar{\theta}=0.0654$ rad, $\Omega=300$ rpm
$p=0.756$ c/s, $\theta_c=4°$

Key: 1. Pitching moment
2. Pitching angular velocity

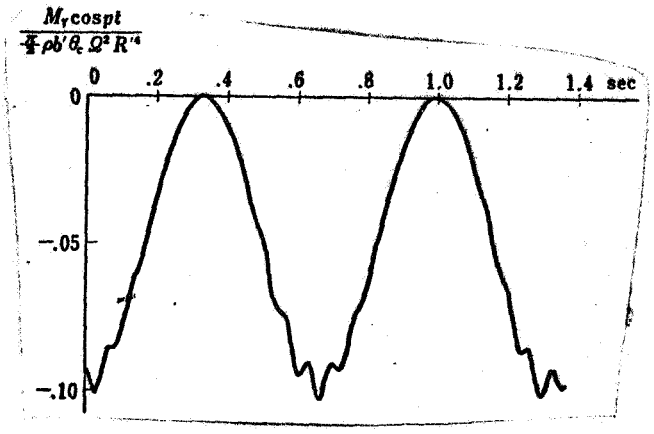

Fig. 72. Time changes of M_Y cos pt

The differences between F and G indicate the amount of decrease in the pitch damping resulting from the fact that the distance between the blade and the vortex fluctuates.

4.4. An Approximate Calculating Method for the Pitch Damping

With reference to the method of calculating the air forces to be used when seeking the pitch damping derivative of rigid helicopter rotors during hovering, it has now been clearly established by comparing the analytica and experimental data with each other that three-dimensional wing theory which merely takes into consideration the contribution of the returning vortex in the rotor wake is inadequate. It is clear that the method must take into consideration also the fluctuations of the relative positions of the blade and the vortex in the wake.

Next, let us consider the question of how to make approximate estimates of the pitch damping derivative in designing. Remarkable developments have been made recently in the aerodynamics of helicopter rotors, and attempts have been made to use electronic computers directly in solving the aerodynamic load distributions on the rotors during both hovering and forward flight in states including blade bending and twisting and deformation of the vortex surface in the wake. The calculation of pitch damping also ought to be incorporated in the near future as one link in this comprehensive calculating program. This study points out the problems /67 which ought to receive attention in one aspect of such a comprehensive method of analysis. However, in order to carry out such comprehensive calculations, it is

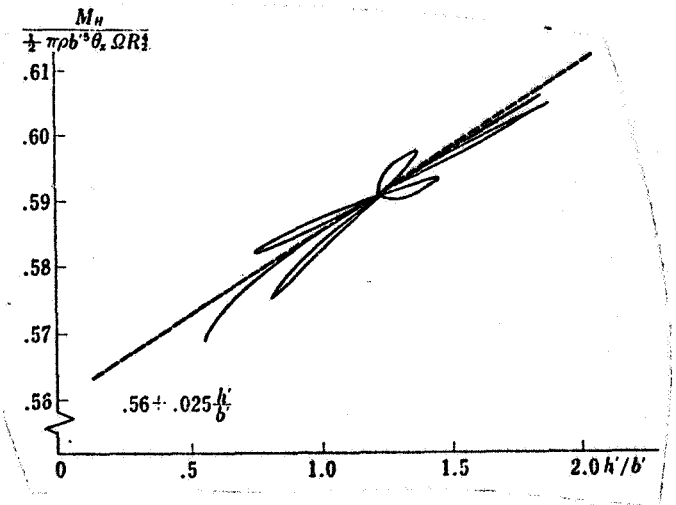

Fig. 73. Fluctuation of hub moment

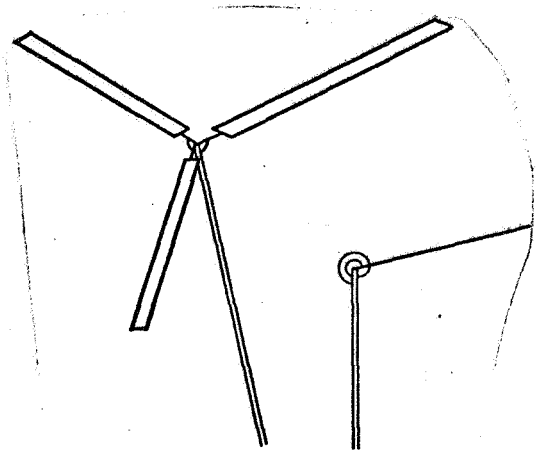

Fig. 74. Rotor with spring constrained flapping hinges

necessary to use extremely complex programs and large-size, high-speed electronic computers, and the calculations require quite a long time to carry out. On the other hand, in the initial designing stage, it is required to find a rough value of the stability derivative by a simple procedure.

In bibliography [6], Beppu introduced empirical factors ε and μ into the equation for calculating the pitch damping on the basis of the brilliant idea that there are differences in the magnitude between those portions of the air forces operating on the blade which fluctuate in direct proportion to $\sin\psi$ and those portions which are directly proportional to $\cos\psi$. Referring to Beppu's method, let us here use the results obtained in this research to propose a method of calculating the pitch damping of rigid rotors relatively simply, and compare the results with Beppu's experimental results.

It was learned as a result of this research that the pitch damping of rigid rotors is much smaller than one would expect from two-dimensional quasi-steady theory. This is true, not only because of the so-called three-dimensional effect, embracing both the vortex surface generated from the blade as well as the returning vortex, but also on account of fluctuations of the relative positions between the vortex in the wake and the blade. Thus, as the quantities representing the relative positions, we will plot on the abscissa the distance h' between the returning wing tip vortex which is closest to the blade, that is the tip vortex generated from the preceding blade, and the blade. On the ordinate we will plot the moment generated at the blade root divided by $\frac{1}{2}\pi\rho b'^5\theta_x\Omega^2R_2^4$.

If we plot the results in Chapter 4, Section 3 on this graph, we obtain the results shown in Fig. 73. From this, we obtain approximately:

$$M'_H=\frac{1}{2}\pi\rho b'^5\Omega^2R_2^4\theta_X\left\{0.56+0.025\frac{h'}{b'}\right. \tag{4.41}$$

As our approximate engineering model of a rigid helicopter rotor, we will consider a model such as that shown in Fig. 74. This model has spring constrained flapping hinges. When this model performs pitching motion around the Y axis at a constant angular velocity $\dot{\theta}$, if we assume the blade wing chord to be x, we will obtain:

$$\theta_X=\theta_0-\frac{\dot{\beta}}{\Omega}+\frac{\dot{\theta}}{\Omega}\cos\phi \tag{4.42}$$

$$\frac{h'}{c/2}=\frac{h'_H}{c/2}+\frac{R}{c/2}(-\theta\cos\phi)\frac{2\pi}{Q\Omega} \tag{4.43}$$

h'_H is the distance between the blade and the nearest returning tip vortex during hovering. It is desirable to find it from smoke experiments. In cases when it is impossible to obtain /68
h'_H experimentally, we use the mean downwash of the hovering rotor $u = \sqrt{C_T/2}R\Omega$ multiplied by the time required for the rotor blade to rotate $2\pi/Q$; this is then multiplied by a modifying coefficient of 1/2. This modifying coefficient is based on the experimental fact that the descending speed of the tip vortex is smaller than the mean downwash on the rotor surface for awhile after the generation of the vortex. This fact is reported, not only in this research, but also in bibliography [10,11]. That is,

$$h'_H=\pi\sqrt{\frac{C_T}{2}}\frac{R}{Q} \tag{4.44}$$

When we find out M'_H, the moment generated on the blade root by the air forces operating on the blade, we can seek the pitch damping in approximately the same manner as the procedures in Appendices C and D.

Eq. (C.9) is revised as follows:

$$\delta W=\sum_{q=0}^{Q-1}M_{Hq}'\cdot(\delta\beta_q-\delta\theta\cos\phi_q)+[M_Yj+M_Zk]\cdot[\delta\theta j+\delta\phi k] \tag{4.45}$$

Eq. (C.10) becomes:

$$Q_{\beta_q}=\frac{1}{4}\pi\rho cR^4\Omega^2\left(\theta_0-\frac{\dot{\beta}_q}{\Omega}+\theta/\Omega\cdot\cos\psi_q\right)\left[0.56+0.025\left\{\frac{h'_H}{c/2}+\frac{R}{c/2}(-\theta\cos\phi)\frac{2\pi}{Q\Omega}\right\}\right] \tag{4.46}$$

Eq. (C.11) becomes:

$$Q_\theta=\sum_{q=0}^{Q-1}\frac{1}{4}\rho\pi cR^4\Omega^2\left(\theta_0-\frac{\dot{\beta}_q}{\Omega}+\frac{\theta}{\Omega}\cos\psi_q\right)\left[0.56+0.025\left\{\frac{h'_H}{2/c}+\frac{R}{c/2}(-\theta\cos\phi)\frac{2\pi}{Q\Omega}\right\}\cos\psi_q+M_T\right. \tag{4.47}$$

In correspondence to Eq. (D.2), we obtain:

$$\ddot{\beta}_q+\frac{\gamma}{8}\alpha_2\dot{\beta}_q\Omega+\left(\Omega^2+\frac{K}{I_B}\right)\beta_q=-2\sin\psi_q\Omega\dot{\theta}+\frac{\gamma}{8}\alpha_2\theta\Omega\cos\psi_q+\frac{\gamma}{8}\alpha_1\theta_0\Omega^2 \tag{4.48}$$

In correspondence to Eq. (C.18), we obtain:

$$\left.\begin{aligned}&I_p\ddot{\theta}+Wl\theta-I_B(\sum\ddot{\beta}_q\cos\psi_q-\ddot{\theta}\sum\cos^2\psi_q\\&+2\Omega\dot{\theta}\sum\sin\psi_q\cos\psi_q+\Omega^2\sum\beta_q\cos\psi_q)\\&+\frac{1}{8}\rho acR^4(\alpha_1\theta_0\Omega^2\sum\cos\psi_q+\alpha_2\Omega\dot{\theta}\sum\cos^2\psi_q\\&-\alpha_2\Omega\sum\dot{\beta}_q\cos\psi_q)=M_T\end{aligned}\right. \tag{4.49}$$

Here,

$$\alpha_1\equiv 0.56+0.025\frac{h'_H}{c/2} \tag{4.50}$$

$$\alpha_2\equiv 0.56+0.025\left[\frac{h'_H}{c/2}-\theta_0\frac{R}{c/2}\frac{2\pi}{Q}\right] \tag{4.51}$$

Solving Eq. (4.48), we find:

$$\beta_q=\frac{\gamma}{8}\cdot\frac{\alpha_1\theta_0\Omega^2}{\Omega^2+K/I_B}+\frac{\sqrt{\left(\frac{\gamma}{8}\alpha_2\right)^2+4\cdot\Omega\dot{\theta}}}{\sqrt{(K/I)^2+\left(\frac{\gamma}{8}\alpha_2\Omega^2\right)^2}}\times\sin(\psi_q-\phi-\lambda) \tag{4.52}$$

Here,

$$\cos\phi=\frac{-2}{\sqrt{\left(\frac{\gamma}{8}\alpha_2\right)^2+4}}$$

$$\sin\phi=\frac{-\frac{\beta}{8}\alpha_2}{\sqrt{\left(\frac{\gamma}{8}\alpha_2\right)^2+4}}$$

$$\cos\lambda=\frac{K/I}{\sqrt{(K/I)^2+\left(\frac{\gamma}{8}\alpha_2\Omega^2\right)^2}}$$

$$\sin\lambda=\frac{\frac{\gamma}{8}\alpha_2\Omega^2}{\sqrt{(K/I)^2+\left(\frac{\gamma}{8}\alpha_2\Omega^2\right)^2}}$$

Inserting β_q, $\dot{\beta}_q$, and $\ddot{\beta}_q$ into Eq. (4.49), we calculate,

$$M_\theta\equiv\frac{-1}{\pi\theta^2 p}\int_0^{2\pi/p}M_Y\theta\,dt \tag{4.53}$$

and obtain

$$M_\theta=\frac{\gamma}{16}QI_B\alpha_2\Omega\left[\frac{\nu^2+\frac{16}{\gamma}\nu}{\nu^2+\alpha_1^2}\right] \tag{4.54}$$

Here,

$$\nu=\frac{8K}{\gamma I\Omega^2} \tag{4.55}$$

Finally, let us check the validity of the equation proposed in this section for calculating the pitch damping derivative (Eq. (4.54)) by comparison with Beppu's experiments. β_q is written as follows:

$$\beta_q=a_0-a_1\cos\phi_q-b_1\sin\phi_q \tag{4.56}$$

If we use Eq. (4.52), we find

$$a_1=\frac{\alpha_1+\frac{\gamma}{16}\nu\alpha_2}{\nu^2+\alpha_2^2}\left(-\frac{16}{\gamma\Omega}\right)\theta \tag{4.57}$$

$$b_1=\frac{\frac{1}{\Omega}\frac{16}{\gamma}\nu-\alpha_2^2\frac{1}{\Omega}}{\nu^2+\alpha_2^2}\theta \qquad (4.58)$$

If we carry out the calculations, using these in place of Eqs. (5.3.1) and (5.3.2) in Beppu's monograph, we obtain Fig. 75.

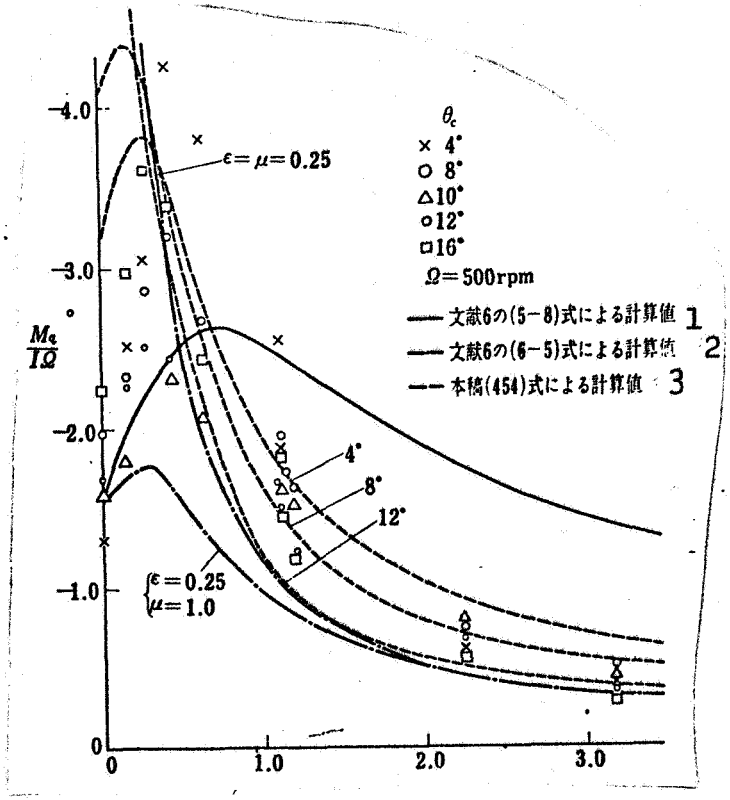

Fig. 75. Pitch damping derivative. Comparison of experimental values [6] and calculated values

Key: 1. Values calculated by Eq. (5-8) in bibliography [6]

2. Values calculated by Eq. (6-5) in bibliography [6]

3. Values calculated by Eq. (4.54) in this paper

Conclusion /69

The pitch damping was measured for two types of rotors and for altogether four types of blades, and calculations were made to discover the pitch damping at which elastic deformation of the blades would not occur from the values measured by means of the aeroelastic method. When the results were non-dimensionalized by means of Townsent's calculated values, it was discovered that they were more or less constant with respect to the revolution speed. On the other hand, it is believed that these values are different for each blade, not only because of the experimental precision, but also because of the accuracy of analysis by the aeroelastic technique.

It was supposed that the non-dimensionalized measurement values are much smaller than 1 and that the air forces which operate in pitch damping are unique. The pitch damping was calculated using a total of seven types of models for hypothetical rotor blades in which no elastic deformation occurs at all. The first five types are existing types, and the remaining two were specially designed so that it would be possible to obtain an idea of the pitch damping.

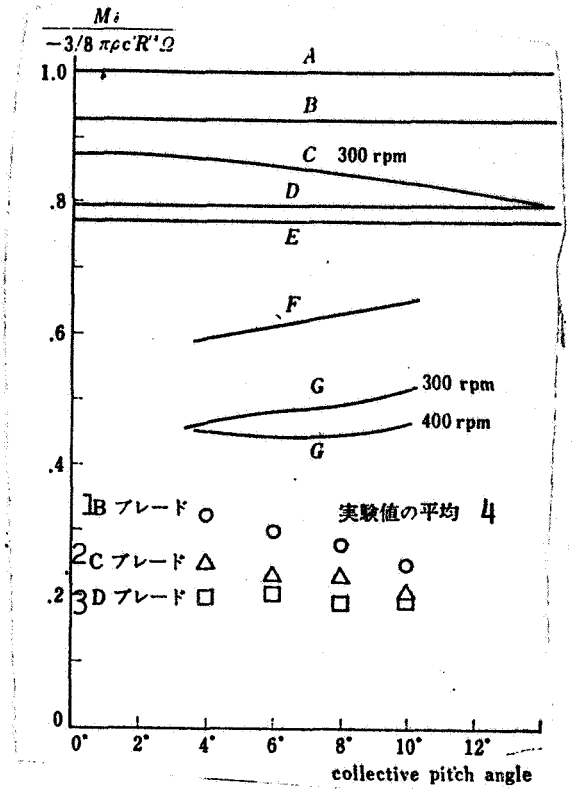

Fig. 76. Comparison of the measured values and various theoretical values of the non-dimensionalized pitch damping from which the effects of bending deformation of the blade have been removed.
A. Two-dimensional quasi-steady theory
B. Two-dimensional unsteady theory
C. Two-dimensional unsteady theory including vortex in wake
D. Three-dimensional quasi-steady theory
E. Three-dimensional unsteady theory
F. Three-dimensional quasi-steady theory including the effects of the vortex in the wake
G. Three-dimensional quasi-steady theory including even fluctuations in the distance

[cont. on next page]

In Fig. 76, the values obtained by averaging out the pitch angle data for certain blades are shown by the marks o, Δ, and □. The calculated values for the seven types of models are also shown in the same figure. A represents Townsent's theory, B represents Theodorsen's theory, C represents Loewy's theory, D represents Ashley's quasi-steady theory, and E represents Ashley's steady theory. F and G were derived from Ichikawa's linear theory and were derived under the assumption that the contribution of the distant vortices is small and that there is a small inflow.

The difference between A and B comes from the unsteady effect with respect to two-dimensional wings. The differences between A and D or between B and E are attributable to the three-dimensional effect. The difference between B and C is attributable to the contribution of the shed vortex in the returning vortex. The difference between D and F is attributable to the contribution of the trailing vortex in the wake. The difference between D and E is attributable to the unsteady effect in the three-dimensional theory, but the contribution of the shed vortex in the returning vortex is not included. The difference between F and G represents the amount of decrease in the pitch damping caused by fluctuations in the distance between the blade and the vortex.

There are still divergences between G and the experimental values. However, it is believed that these may be overcome by the following means. (1) Improvements in the aeroelastic methods of analysis, expecially in the method of determining the bending mode. (2) Improvements of the experimental precision. (3) Taking actual measurements of

between the vortex in the wake and the blade

Key: 1. B blade
2. C blade
3. D blade
4. Average of measured values

the vortex distribution during pitching and using them in calculations.

We proposed an equation for calculating simply $M_{\dot{\theta}}$, the derivative of pitch damping occurring when the rigid rotor is pitching at a definite angular velocity. By comparison with the experimental values in bibliography [6], it was proved that the results obtained by using this equation are quite good. /70

Postscript

The writer is deeply grateful to Professor Washizu, who kindly guided this research for a period of five years. Although the results, viewed today, do not seem to be entirely sufficient, the writer is profoundly aware of his deep indebtedness for the assistance of many persons. Technical officials Ichikawa and Beppu of the National Aerospace Laboratory and Assistant Professor Azuma of the Space Laboratory provided various pieces of advice and encouragement, and assistance in experimentation was provided by Mr. Naito of the Kubota Iron & Machinery Works, Ltd. and by the personnel of the Central Research Laboratory, the Washizu Research Laboratory, and the Flight Experimentation Section of the National Aerospace Laboratory. In producing the rotor blades, Mr. Toma of the Workshop and the Yamaguchi Kiki Seisakusho were so good as to produce the extremely complicated items. The large amounts of calculations were performed at the Large-Scale Computing Center of Tokyo University and at the Computing Center of the National Aerospace Laboratory. Profound thanks are expressed to all of these.

REFERENCES

1. Ichikawa, Teruo, "Linear theory of rotors (I), Lift surface theory," Kōkū Uchū Gijutsu Kinkyūsho Hōkoku [Technical reports of the National Aerospace Laboratory], TR-68 (1964).

2. Ichikawa, Teruo, "Linear theory of rotors (II), Lift line theory," Kōkū Uchū Gijutsu Kenkyūsho Hōkoku [Technical reports of the National Aerospace Laboratory], TR-85 (1965).

3. Ichikawa, Teruo, "Linear theory of rotors (III), Methods of solving lift line equations," Kōkū Uchū Gijutsu Kenkyūsho Hōkoku [Technical reports of the National Aerospace Laboratory], TR-100 (1966).

4. Reichert, G. and Oelker, P, "Handling Qualities with the Bolkow Rigid Rotor System," paper presented at the 24th Annual National Forum of American Helicopter Society, May 1968.

5. Payne, P.R., Helicopter Dynamics and Aerodynamics, Pitman & Sons Ltd., 1959.

6. Beppu, Gorō and Oka, En'ichi, "Concerning pitch damping of rotors with spring constrained blade flapping motion," Kōkū Uchū Gijutsu Kenkyūsho Shiryō [Materials of the National Aerospace Laboratory], TM-164 (1969).

7. Townsent, M.W., "Stability and Control of Unducted Stand-On Helicopter Preliminary Theoretical and Flight Test Results," Princeton University Dept. of Aeronautical Engineering Report No. 404, Nov. 1957.

8. Olossen, C.O. and Orlik-Rückemann, K., "An Electronic Apparatus for Automatic Recording of Logarithmic Decrement and Frequency of Oscillations in the Audio Frequency Range," FFA (The Aeronautical Research Institute of Sweden) Report No. 52 (1954).

9. Yanagisawa, Nitsunori, "Trial manufacture of prototype damping meter," Kōkū Uchū Gijutsu Kenkyūsho Shiryō [Materials of the National Aerospace Laboratory], TM 168.

10. Jenny, D.S., Olson, J.R. and Landgrebe, A.J., "A Reassessment of Rotor Hovering Performance Prediction Methods," Journal of A.H.S. 13(2), (April 1968).

11. Gray, R.B., "On the Motion of the Hovering Model Helicopter Rotor and its Application to the Calculation of the Spanwise Aerodynamic Loading," Princeton University Dept. of Aeronautical Engineering Report No. 313 (1955).

12. Simmons, I.A., Pacifico, R.E., and Jones, J.P., "The Movement, Structure and Breakdown of Trailing Vortices from a Rotor Blade," CAL/USAAVLABS SYMPOSIUM PROCEEDINGS 1, Propeller & Rotor Aerodynamics, (22-24), (June 1966).

13. Gessow, A. and Myers, G.C., Jr., Aerodynamics of Helicopter, Macmillan, 1952.

14. Loewy, R.G., "A Two-Dimensional Approximation to the Unsteady /71 Aerodynamics of Rotary Wings," J.A.S. 24(2), (Feb. 1957).

15. Daughaday, H., Duwaldt, F., and Gates, C., "Investigation of Helicopter Blade Flutter and Load Amplification Problem," I.A.S. Preprint no. 705, (Jan. 1957).

16. Brooks, G.W., and Silviera, M.A.,"Dynamic Model Investigation of the Damping of Flapwise Bending Modes of Two-Blade Rotor in Hovering and a Comparison with Quasi-Static and Unsteady Aerodynamic Theories," NASA TN D-175.

17. Timman, R. and van de Vooren, A.I., "Flutter of a Helicopter Rotor Rotating in its own Wake," J.A.S. 24(9), (Sept. 1957).

18. Theodorsen, T., "General Theory of Aerodynamic Instability and the Mechanism of Flutter," N.A.C.A. Report 496, 1935.

19. Ashley, H., Moser, H.H., and Dugundji, J., "Investigation of Rotor Response to Vibratory Aerodynamic Inputs," WADC TR 58-87, Oct. 1958.

20. Reissner, E., "Effect of Finite Span on the Airload Distributions for Oscillating Wings, I -- Aerodynamic Theory of Oscillating Wings of Finite Span," NACA TN-1194, 1947.

21. Reissner, E. and Stevens, J.E., "Effect of Finite Span on the Airload Distributions for Oscillating Wings II -- Method of Calculations and Examples of Application," NACA TN-1195, 1947.

22. Moriguchi, Shigekazu, Sūgaku koshiki [Mathematical formulas], I, Iwanami.

23. Rauscher, M., Introduction to Aerodynamics, John Wiley & Sons, Inc., 1953.

24. Bisplinghoff, R.L., Ashley, H., and Halfman, R.L., Aeroelasticity, Addison-Wesley 1955.

25. Rabbott, J.P. Jr., "Static-Thrust Measurements of the Aerodynamics Loading on a Helicopter Rotor Blade," NACA TN 3688 (1956).

26. Meyer, J.R. and Falabella, G. Jr., "An Investigation of the Experimental Aerodynamic Loading on a Model Helicopter Rotor Blade," NACA TN 2953 (1953).

27. Sachio, Jirō and Ika, En'ichi, "Experiments concerning rotors of helicopters hovering near the ground surface," Kōkū Uchū Gijutsu Kenkyūsho Hōkoku [Technical reports of the National Aerospace Laboratory], TR-113.

28. Lamb, H., Hydrodynamics, 6th Edition, Dover Publications, 1945.

29. Yamana, Masao and Nakaguchi, Hiroshi, Hikōki sekkei ron [Aircraft design theory], Yōkendo, 1968, pp. 486.

30. Watson, G.N., "A Treatise on the theory of Bessel functions," Cambridge.

31. Moriya, Tomijirō and Washizu, Hisaichirō, Rikigaku gairon [Outline of dynamics], Baifūkan, 1970.

32. Minorsky, N., "Introduction to Non-Linear Mechanics," Ann Arbor, 1947.

APPENDIX A [32]. CONCERNING THE PITCH DAMPING DERIVATIVE

When a rotor blade such as that shown in Fig. 6 performs pitching motion without rotating, its kinetic equation may be written as follows if we ignore the air resistance and the frictional forces:

$$I\ddot{\theta}+Wl\theta=0 \tag{A.1}$$

When the rotor is turning, the moment due to the air forces operating on the blade and to the blade deformation $\gamma(\theta,\dot{\theta},\ldots)$ will operate. This moment $\gamma(\theta,\dot{\theta},\ldots)$ is quite small in comparison with the moment of inertia $-I\ddot{\theta}$ and the restoring moment $-Wl\theta$. The kinetic equation for the system may be written as follows:

$$I\ddot{\theta}-\gamma(\theta,\dot{\theta},\cdots)+Wl\theta=0 \tag{A.2}$$

Let us consider a case when the rotor is turning and a moment M_Y is applied from outside so that the pitching movement will become $\theta^* = \bar{\theta}\sin pt$. Particularly in cases when $p^2 = Wl/I$, $I\ddot{\theta}^* - \gamma(\theta^*,\dot{\theta}^*,\ldots) + Wl\theta^* = M_{Y(t)}$. That is,

$$-\gamma(\bar{\theta},p)=M_{Y(t)} \tag{A.3}$$

Let us return once again to Eq. (A.2) Since $\gamma(\theta,\dot{\theta}\ldots)$ is present in the motion of the system, we assume that it will be damped gradually, and it is our desire to seek the derivative of damping. In cases when $\gamma = 0$, the system is described by Eq. (A.1), and the solution is $\theta = \bar{\theta}\sin(pt + \phi)$, $\theta = \bar{\theta}p\cos(pt + \phi)$. In cases when $\gamma(\theta,\dot{\theta},\ldots)$ is zero, the movement of the system will become somewhat different, and it is believed that $\bar{\theta}$ and ϕ will fluctuate together with the time.

$$\theta=\bar{\theta}_{(t)}\sin(pt+\phi_{(t)}) \tag{A.4}$$

$$\dot{\theta}=\bar{\theta}_{(t)}p\cos(pt+\phi_{(t)}) \tag{A.5}$$

If we differentiate Eq. (A.4) by the time, we obtain:

$$\dot{\theta}=\dot{\bar{\theta}}\sin(pt+\phi_{(t)})+\bar{\theta}_{(t)}p\cos(pt+\phi_{(t)})+\bar{\theta}_{(t)}\dot{\phi}\cos(pt+\phi_{(t)})$$

If we take the difference between this and (A.5), we find:

$$\dot{\bar{\theta}}\sin(pt+\phi_{(t)})+\bar{\theta}_{(t)}\dot{\phi}\cos(pt+\phi_{(t)})=0 \tag{A.6}$$

If we differentiate Eq. (A.5), we obtain:

$$\ddot{\theta}=\ddot{\bar{\theta}}p\cos(pt+\phi_{(t)})-\bar{\theta}_{(t)}p^2\sin(pt+\phi_{(t)}) -\dot{\bar{\theta}}_{(t)}p\dot{\phi}\sin(pt+\phi_{(t)}) \tag{A.7}$$

We insert θ from (A.4) and $\ddot{\theta}$ from (A.7) into Eq. (A.2).

$$\ddot{\bar{\theta}}_{(t)}p\cos(pt+\phi_{(t)})-\dot{\bar{\theta}}_{(t)}p\dot{\phi}\sin(pt+\phi_{(t)})=r/I \tag{A.8}$$

If we solve (A.6) and (A.8) with respect to $\dot{\bar{\theta}}$ and $\dot{\phi}$,

$$\dot{\bar{\theta}}=\frac{r}{Ip}\cos(pt+\phi_{(t)}) \tag{A.9}$$

$$\dot{\phi}=-\frac{r}{Ip\bar{\theta}_{(t)}}\sin(pt+\phi_{(t)}) \tag{A.10}$$

Since the coefficients on the right sides of (A.9) and (A.10) /72 are both minute, the temporal variation ratio of $\bar{\theta}(t)$ and $\phi(t)$ is small. Therefore, when we are seeking $\bar{\theta}(t_2)/\bar{\theta}(t_1)$, the amplitude ratio of the angle of pitch between time t_1 and time $t_2 = t_1 + 2\pi/p$, we may assume that there are almost no changes of $\bar{\theta}(t)$ and $\phi(t)$ between t_1 and t_2. Since in this case the motion of the system is close to a sinusoidal movement with a period of $2\pi/p$, it is also possible to seek γ by means of Eq. (A.3)

$$\begin{aligned}\bar{\theta}(t_2)-\bar{\theta}(t_1)&=\int_{t_1}^{t_2}\dot{\bar{\theta}}dt=\int_{t_1}^{t_2}\frac{r}{Ip}\cos(pt+\phi(t_1))dt\\&=\int_{t_1}^{t_2}-\frac{M_Y}{Ip}\cos(pt+\phi(t_1))dt\\\therefore\ \ln\left\{\frac{\bar{\theta}(t_2)}{\bar{\theta}(t_1)}\right\}&=\ln\left\{1+\frac{1}{\bar{\theta}(t_1)}\int_{t_1}^{t_2}\frac{r}{Ip}\cos(pt+\phi(t_1))dt\right\}\\&\doteqdot\frac{1}{\bar{\theta}(t_1)}\int_{t_1}^{t_2}\frac{r}{Ip}\cos(pt+\phi(t_1))dt\\&=\frac{-1}{\bar{\theta}(t_1)}\int_{t_1}^{t_2}\frac{M_Y}{Ip}\cos(pt+\phi(t_1))dt\end{aligned} \tag{A.11}$$

In systems expressed in terms of a differential equation with two-storied constant coefficients, $\ln\{\bar{\theta}(t_2)/\bar{\theta}(t_1)\} \times 2I/(2\pi/p)$ will be the damping coefficient. In accordance with this, let us agree to call (A.11) multiplied by $2I/(2\pi/p)$ the pitch damping coefficient, and adopt the following definition:

$$M_\theta \equiv \frac{Ip}{\pi\bar{\theta}(t_1)}\int_{t_1}^{t_2}\frac{\gamma}{Ip}\cos(pt+\phi(t_1))dt = \frac{-Ip}{\pi\bar{\theta}(t_1)}\int_{t_1}^{t_2}\frac{M_Y}{Ip}\cos(pt+\phi(t_1))dt \tag{A.12}$$

General validity will not be lost even if t_1 is set at $\phi(t_1) = 0$. The following can also be written:

$$M_\theta \equiv \frac{1}{\pi\bar{\theta}p^2}\int_{t_1}^{t_2}\gamma\theta dt = \frac{-1}{\pi\bar{\theta}p^2}\int_{t_1}^{t_2}M_Y\theta dt \tag{A.13}$$

APPENDIX B

Concerning the methods of calculating $N_A(q)$, $N_B(q)$ and $N_C(\tau)$.

(1) Method of Calculating $N_A(q)$

We rewrite Eq. (3.23).

$$N_A(q) \equiv q\int_0^\infty \frac{\lambda_1 e^{-t\lambda_1}}{[\lambda_1^2+q^2]^{3/2}}d\lambda_1 \tag{B.1}$$

If $q > 0$, we posit $\lambda_1 = ql$. Then,

$$N_A(q) = \int_0^\infty \frac{le^{-iql}}{[l^2+1]^{3/2}}dl = 1 - iq\left[\int_0^\infty \frac{\cos ql}{\sqrt{l^2+1}}dl - i\int_0^\infty \frac{\sin ql}{\sqrt{l^2+1}}dl\right] \tag{B.2}$$

According to bibliography [30], p. 172, the following equation applies when $R(\nu + \frac{1}{2}) \geq 0$, $x > 0$, and $|\arg z| < \frac{\pi}{2}$:

$$K_\nu(xz) = \frac{\Gamma\left(\nu+\frac{1}{2}\right)\cdot(2z)^\nu}{x^\nu\cdot\Gamma\left(\frac{1}{2}\right)}\int_0^\infty \frac{\cos xu}{(u^2+z^2)^{\nu+1/2}}du \tag{B.3}$$

$$\therefore \quad \int_0^\infty \frac{\cos ql}{\sqrt{l^2+1}}\,dl = K_0(q) \tag{B.4}$$

According to bibliography [30], p. 332, the following equation applies when R (ν) > $\frac{1}{2}$ and x > 0:

$$L_\nu(x) = I_{-\nu}(x) - \frac{2\left(\frac{1}{2}x\right)^\nu}{\Gamma\left(\nu+\frac{1}{2}\right)\Gamma\left(\frac{1}{2}\right)} \int_0^\infty \sin xu \times (1+u^2)^{\nu-1/2}\,du \tag{B.5}$$

Here,

$$L_\nu(x) = \sum_{m=0}^{\infty} \frac{\left(\frac{x}{2}\right)^{\nu+2m+1}}{\Gamma\left(m+\frac{3}{2}\right)\Gamma\left(\nu+m+\frac{3}{2}\right)} \tag{B.6}$$

$$\therefore \quad \int_0^\infty \frac{\sin ql}{\sqrt{l^2+1}}\,dl = \frac{\pi}{2}[I_0(q) - L_0(q)] \tag{B.7}$$

$$\therefore \quad N_A(q) = 1 - iq\left[K_0(q) - i\frac{\pi}{2}(I_0(q) - L_0(q))\right] \tag{B.8}$$

When q < 0, it is obvious from Eq. (B.1) that

$$N_A(q) = -1 - iq\left[K_0(-q) - i\frac{\pi}{2}(I_0(-q) - L_0(-q)\right] \tag{B.9}$$

At the ultimate extreme, when q has been brought close to 0,

$$\begin{aligned} &\lim_{q\to 0} I_0(q) = 0 \\ &\lim_{q\to 0} L_0(q) = 0 \\ &\lim_{q\to 0} qK_0(q) = 0 \\ &\lim_{q\to 0} N_A(q) = \frac{q}{|q|} \end{aligned} \tag{B.10}$$

(2) Method of Calculating $N_B(q)$

We rewrite Eq. (3.23)

$$N_B(q) \equiv q\int_0^\infty \frac{e^{-i\lambda_1}}{[\lambda_1^2+q^2]^{3/2}}\, d\lambda_1 \tag{B.11}$$

If $q > 0$, we posit $\lambda_1 = ql$. Then,

$$N_B(q) = \frac{1}{q}\int_0^\infty \frac{e^{-iql}}{[l^2+1]^{3/2}}\, dl = \frac{1}{q}\frac{\cos ql - i\sin ql}{[l^2+1]^{3/2}}\, dl \tag{B.12}$$

If we use Eqs. (B.3) and (B.5), we obtain:

$$\frac{1}{q}\int_0^\infty \frac{\cos ql}{[l^2+1]^{3/2}}\, dl = K_1(q) \tag{B.13}$$

$$\frac{1}{q}\int_0^\infty \frac{\sin ql}{[l^2+1]^{3/2}}\, dl = 1 - \frac{\pi}{2}[I_1(q) - L_1(q)] \tag{B.14}$$

/73

$$\therefore \quad N_B(q) = K_1(q) - i + \frac{\pi i}{2}[I_1(q) - L_1(q)] \tag{B.15}$$

When $q < 0$, it is clear from Eq. (B.11) that

$$N_B(q) = -K_1(-q) + i - \frac{\pi i}{2}[I_1(-q) - L_1(-q)] \tag{B.16}$$

At the ultimate extreme, when q has been brought close to 0, we obtain:

$$\begin{aligned} &\lim_{q\to 0} I_1(q) = 0 \\ &\lim_{q\to 0} L_1(q) = 0 \\ &\lim_{q\to 0} K_1(q) = \frac{1}{q} \\ &\lim_{q\to 0} N_B(q) = \frac{1}{q} - i\frac{q}{|q|} \end{aligned} \tag{B.17}$$

(3) Method of Calculating $N_C(\tau)$

We rewrite Eq. (3.23).

$$N_c(\tau)=\int_0^\infty\left[\frac{\tau}{\sqrt{\lambda_2^2+\tau^2}}-\frac{\tau}{|\tau|}\right]\frac{e^{-i\lambda_2}}{\lambda_2}\,d\lambda_2 \tag{B.18}$$

If $\tau > 0$, we posit $\lambda_2 = \tau x$. Then,

$$N_c(\tau)=\int_0^\infty\left[\frac{1}{\sqrt{x^2+1}}-1\right]\frac{e^{-i\tau x}}{x}\,dx=I_1+I_2+I_3 \tag{B.19}$$

$$\text{(a)}\quad I_1=\int_0^{X_1}\left[\frac{1}{\sqrt{x^2+1}}-1\right]\frac{e^{-i\tau x}}{x}\,dx \tag{B.20}$$

Let us develop the integrand in a Taylor series and integrate.

$$I_1=\sum_{n=1}^{\infty}\sum_{j=1}^{[(n+1)/2]}\frac{(-1)^j(2j-1)!!(-i\tau)^{n-2j+1}}{j!\,2^j(n-2j+1)!}\times\frac{X_1^{n+1}}{n+1} \tag{B.21}$$

$$\text{(b)}\quad I_2=\int_{X_1}^{X_2}\left[\frac{1}{\sqrt{x^2+1}}-1\right]\frac{e^{-i\tau x}}{x}\,dx \tag{B.22}$$

Let us integrate using Sympson's formula.

$$\text{(c)}\quad I_3=\int_{X_2}^{\infty}\left[\frac{1}{\sqrt{x^2+1}}-1\right]\frac{e^{-i\tau x}}{x}\,dx \tag{B.23}$$

$$\left[\frac{1}{\sqrt{x^2+1}}-1\right]\frac{1}{x}=\frac{1/x^2}{\sqrt{1+1/x^2}}-\frac{1}{x}$$
$$=-\frac{1}{x}+\frac{1}{x^2}-\frac{1}{2}\frac{1}{x^4}+\frac{3}{8}\frac{1}{x^6}-\frac{5}{16}\frac{1}{x_8}+\frac{35}{128}\frac{1}{x^{10}}-\cdots\cdots \tag{B.24}$$

$$\int_{X_2}^{\infty}-\frac{e^{-i\tau x}}{x}\,dx=\int_{\tau X_2}^{\infty}-\frac{\cos\lambda_2-i\sin\lambda_2}{\lambda_2}\,d\lambda_2$$
$$=C_i(\tau X_2)+i\left\{\frac{\pi}{2}-S_i(\tau X_2)\right\} \tag{B.25}$$

$$\int_{X_2}^{\infty} \frac{e^{-i\tau x}}{x^2}\,dx=\sum_{j=1}^{2n-1}\frac{(2n-j-1)!\,(-i\tau)^{j-1}}{(2n-1)!\,X_2^{2n-j}} \times e^{-i\tau X_2}+\frac{(-i\tau)^{2n-1}}{(2n-1)!}\left\{-C_i(\tau X_2) +i\left(S_i(\tau X_2)-\frac{\pi}{2}\right)\right\} \tag{B.26}$$

At $X_2 > 1$, when n becomes fairly large, it can be omitted because

$$\left|\int_{X_2}^{\infty}\frac{e^{-i\tau x}}{x^{2n}}\,dx\right|<\int_{X_2}^{\infty}\frac{1}{x^{2n}}\,dx=\frac{X^{-(2n+1)}}{2n+1} \tag{B.27}$$

I_3 can be calculated using (B.25) and (B.26).

When $\tau < 0$, it is obvious from Eq. (B.18) that

$$N_e(\tau)=-N_e(-\tau) \tag{B.28}$$

At the ultimate extreme, when τ has been brought close to 0, we can use Eq. (B.18) to obtain:

$$\begin{aligned}\lim_{\tau\to 0+} N_e(\tau)&=\lim_{\tau\to 0+}\left\{\int_0^{\tau}\left[\frac{\tau}{\sqrt{\lambda_2^2+\tau^2}}-1\right]\frac{e^{-i\lambda_2}}{\lambda_2}\,d\lambda_2 +\int_{\tau}^{\infty}\left[\frac{\tau}{\sqrt{\lambda_2^2+\tau^2}}-1\right]\frac{e^{-i\lambda_2}}{\lambda_2}\,d\lambda_2\right\}\\ &=\lim_{\tau\to 0+}\left\{\int_0^1\left(\frac{1}{\sqrt{x^2+1}}-1\right)\frac{e^{-i\tau x}}{x}\,dx +\int_1^{\infty}\frac{1}{\sqrt{x^2+1}}\frac{e^{-i\tau x}}{x}\,dx-\int_{\tau}^{\infty}\frac{e^{-i\lambda_2}}{\lambda_2}\,d\lambda_2\right\}\\ &=\lim_{\tau\to 0+}\left\{-\int\frac{e^{-i\lambda_2}}{\lambda_2}\,d\lambda_2\right\}+\int_0^1\left(\frac{1}{\sqrt{x^2+1}}-1\right) \times\frac{1}{x}\,dx+\int_1^{\infty}\frac{1}{\sqrt{x^2+1}}\frac{1}{x}\,dx\\ &=\lim_{\tau\to 0+}\log\tau+\gamma+\frac{\pi}{2}\,i+\log 2\end{aligned} \tag{B.29}$$

Generally speaking,

$$\lim_{\tau\to 0} N_e(\tau)=\lim_{\tau\to 0}\frac{\tau}{|\tau|}\left\{\log|\tau|+\gamma+\frac{\pi}{2}\,i+\log 2\right\} \tag{B.30}$$

APPENDIX C. KINETIC EQUATION WITH THREE DEGREES OF FREEDOM FOR SIMPLIFIED RIGID ROTOR MODELS

Let us analyze the movement of a rotor blade system with spring constrained flapping hinges such as that shown in Fig. 74. When the system is constrained so that it cannot have rolling motion during hovering, the system's movements will have three degrees of freedom: pitching, flapping, and rotation around the shaft axis. It is assumed that the system consists of the blade portion and the pendulum portion which performs pitching only. A precise kinetic equation is derived for cases when the moment M_y around the pitching axis and the torque M_z around the shaft axis are added to the system from outside. As for the air forces operating on the blade, we will consider only the left components based on two- /74
dimensional quasi-steady theory.

Next, we will derive an approximate kinetic equation for cases when $\dot{\psi}$ has a constant value Ω and the movement is also leisurely.

The position vector r at a point on the blade corresponds to Eq. (1.5)

$$r=r\cos\beta_q i_q^*+r\sin\beta_q k_q^* \tag{C.1}$$

The velocity vector v at this point corresponds to Eq. (1.6).

$$\begin{aligned} v=&(r\sin\beta_q\sin\psi_q\dot{\theta}-r\cos\beta_q\dot{\psi})i_q^*\\ &+(-r\sin\beta_q\dot{\beta}_q+r\sin\beta_q\cos\psi_q\dot{\theta})j_q^*\\ &+(r\cos\beta_q\dot{\beta}_q-r\cos\beta_q\cos\psi_q\dot{\theta})k_q^* \end{aligned} \tag{C.2}$$

The kinetic energy of the blade is

$$\begin{aligned} T_B=\sum_{q=0}^{Q-1}\frac{1}{2}\int_0^R \nu|v|^2dr=\sum_{q=0}^{Q-1}\frac{I_B}{2}&(\sin^2\beta_q\sin^2\psi_q\dot{\theta}^2\\ &-2\sin\beta_q\cos\beta_q\sin\psi_q\dot{\psi}_q\dot{\theta}+\cos^2\beta_q\dot{\psi}_q^2\\ &+\dot{\beta}_q^2-2\cos\psi_q\dot{\beta}\dot{\theta}+\cos^2\psi_q\dot{\theta}^2) \end{aligned} \tag{C.3}$$

The kinetic energy of the pendulum is

$$T_p=\frac{I_p}{2}\dot{\theta}^2 \tag{C.4}$$

The position energy of the pendulum is

$$U_p=\frac{Wl}{2}\theta^2 \tag{C.5}$$

The strain energy stored up in the spring is

$$U=\sum_{q=0}^{Q-1}\frac{k}{2}\beta_q^2 \tag{C.6}$$

In cases when virtual displacements $\delta\beta_q$, $\delta\theta$, and $\delta\psi$ have occurred in the three degrees of freedom β_q, θ, and ψ, the virtual displacement δu_q occurring at a point on the blade will be:

$$\begin{aligned}\delta u_q=&(\delta\theta\sin\psi_q-\delta\psi r\cos\beta_q)\,i_q^*+(-r\sin\beta_q\delta\beta_q\\&+\delta\theta\cos\psi_q r\sin\beta_q)\,j_q^*+(r\cos\beta_q\\&\times\delta\beta_q-\delta\theta\cos\psi_q r\cos\beta_q)\,k_q^*\end{aligned} \tag{C.7}$$

When seeking the air forces operating on the blade, if we consider only the thrust components and use two-dimensional quasi-steady theory, we obtain:

$$\begin{aligned}F_{Aq}dr=&\frac{1}{2}\rho acr^2\dot\psi^2dr\left[\theta_0+\frac{\dot\theta}{\dot\psi}\cos\psi_q-\frac{\dot\beta_q}{\dot\psi}\right]\\&\times[-\sin\beta_q i_q^*+\cos\beta_q k_q^*]\end{aligned} \tag{C.8}$$

The virtual work is:

$$\delta W=\sum_{q=0}^{Q-1}\int_0^R F_{Aq}\cdot\delta u_q dr+[M_Y i+M_Z k]\cdot[\delta\theta j+\delta\psi k] \tag{C.9}$$

If we take the variations for β_q, θ, and ψ,

$$Q_{\beta_q}=\frac{1}{8}\rho_{ac}R^4\dot\psi^2\left[\theta_0+\frac{\dot\theta}{\dot\psi}\cos\psi_q-\frac{\dot\beta_q}{\dot\psi}\right] \tag{C.10}$$

$$Q_\theta=-\frac{1}{8}\rho_{ac}R^4\dot\psi^2\left[\theta_0+\frac{\dot\theta}{\dot\psi}\cos\psi_q-\frac{\dot\beta_q}{\dot\psi}\right]\cos\psi_q+M_Y \tag{C.11}$$

$$Q_\psi=M_Z \tag{C.12}$$

The Lagrange equations are:

$$\begin{aligned}&\frac{d}{dt}\left(\frac{\partial T_B}{\partial\dot\beta_q}\right)-\frac{\partial T_B}{\partial\beta_q}+\frac{\partial U}{\partial\beta_q}=Q\beta_q\\&\frac{d}{dt}\left(\frac{\partial T_B}{\partial\dot\theta}\right)+\frac{d}{dt}\left(\frac{\partial T_B}{\partial\theta}\right)+\frac{\partial U_q}{\partial\theta}=Q_\theta\\&\frac{d}{dt}\left(\frac{\partial T_B}{\partial\dot\psi}\right)-\frac{\partial T_B}{\partial\psi}=Q_\psi\end{aligned}$$

If written concretely, they are:

$$I_B(\ddot{\beta}_q-\ddot{\theta}\cos\psi_q+2\dot{\psi}\dot{\theta}\cos^2\beta_q\sin\psi_q+\dot{\psi}^2\sin\beta_q\cos\beta_q -\theta^2\sin\beta_q\cos\beta_q\sin^2\psi_q) -\frac{1}{8}\rho acR^4(\theta_0\dot{\psi}^2+\dot{\psi}\dot{\theta}\cos\psi_q-\dot{\psi}\dot{\beta}_q)+K\beta_q=0 \tag{C.13}$$

$$I_p\ddot{\theta}+Wl\theta-I_B(\sum\ddot{\beta}_q\cos\psi_q-\ddot{\theta}\sum\cos^2\psi_q +2\dot{\psi}\dot{\theta}\sum\cos^2\beta_q\sin\psi_q\cos\psi_q+\dot{\psi}^2\sum\sin\beta_q\cos\beta_q \times\cos\psi_q-2\dot{\psi}\sum\sin^2\beta_q\sin\psi_q\dot{\beta}_q-2\dot{\theta}\sum\sin\beta_q \times\cos\beta_q\sin^2\psi_q\dot{\beta}_q-\ddot{\theta}\sum\sin^2\beta_q\sin^2\psi_q+\ddot{\psi}\sum\sin\beta_q \times\cos\beta_q\sin\psi_q)+\frac{1}{8}\rho acR^4(\theta_0\dot{\psi}^2\sum\cos\psi_q +\theta\dot{\psi}\sum\cos^2\psi_q-\dot{\psi}\sum\beta_q\cos\psi_q)=M_Y \tag{C.14}$$

$$I_B(-2\dot{\psi}\sum\sin\beta_q\cos\beta_q\dot{\beta}_q-2\dot{\theta}\sum\dot{\beta}_q\cos^2\beta_q\sin\psi_q -\ddot{\theta}\sum\sin\beta_q\cos\beta_q\sin\psi_q+\dot{\theta}^2\sum\cos^2\beta_q\sin\psi_q\cos\psi_q +\ddot{\psi}\sum\cos^2\beta_q)=M_Z \tag{C.15}$$

Next, in cases when the rotating angular velocity $\dot{\psi}$ around the rotor shaft axis has a constant value Ω, when β, $\dot{\beta}/\Omega$, $\dot{\theta}/\Omega$, and θ/Ω^2 are minute, if we omit minute quantities of the third order or above, we obtain:

$$T_B=\frac{I_B}{2}(-2\Omega\dot{\theta}\sum\beta_q\sin\psi_q+\Omega^2\sum(1-\beta_q^2) +\sum\dot{\beta}_q^2-2\dot{\theta}\sum\dot{\beta}_q\cos\psi_q+\dot{\theta}^2\sum\cos^2\psi_q) \tag{C.16}$$

If we use this, the kinetic equations become:

$$-\frac{1}{8}\rho acR^4(\theta_0\Omega^2+\Omega\dot{\theta}\cos\psi_q-\Omega\dot{\beta}_q)+K\beta_q=0 \tag{C.17}$$

$$I_p\ddot{\theta}+Wl\theta-I_B(\sum\ddot{\beta}_q\cos\psi_q-\ddot{\theta}\sum\cos^2\psi_q +2\Omega\dot{\theta}\sum\sin\psi_q\cos\psi_q+\Omega^2\sum\beta_q\cos\psi_q) +\frac{1}{8}\rho acR^4(\theta_0\Omega^2\sum\cos\psi_q+\Omega\dot{\theta}\sum\cos^2\psi_q -\Omega\sum\dot{\beta}_q\cos\psi_q)=M_Y \tag{C.18}$$

$$I_B(-2\Omega\sum\beta_q\dot{\beta}_q-2\dot{\theta}\sum\dot{\beta}_q\sin\psi_q-\ddot{\theta}\sum\beta_q\sin\psi_q +\dot{\theta}^2\sum\sin\psi_q\cos\psi_q)=M_Z \tag{C.19}$$

Naturally, these agree with the data obtained before in the strict kinetic equation, where it was assumed that $\dot{\psi}=\Omega$ and the minute quantities of the third order or above were omitted.

APPENDIX D. DAMPING COEFFICIENTS SOUGHT FOR FORCED VIBRATIONS /75

Let us consider a rotor with a number of blades Q of 3 or more and with an I_p much larger than I_B. We will consider cases in which the pitching moment M_Y and torque M_Z are administered to this rotor from outside, and the rotor is made to continue movement so that $\theta = \bar{\theta} \sin pt$. As was defined in Appendix A, the damping coefficient is determined by:

$$M_\theta \equiv \frac{-1}{\pi \bar{\theta}^2 p} \int_0^{2\pi/p} M_Y(t) \dot{\theta} dt \tag{D.1}$$

Here, $p \equiv \sqrt{WI/I_p}$.

If we rewrite Eq. (C.17) and use $\gamma = \rho acR^4/I_B$ and $C_K = K/I_B\Omega^2$,

$$\begin{aligned} &\ddot{\beta} + \gamma/8 \cdot \Omega \dot{\beta} + (1+C_k)\Omega^2 \beta = \bar{\theta} \cos\phi \\ &\quad -2\Omega\dot{\theta} \sin\phi + \gamma/8 \cdot \Omega\theta \cos\phi + \gamma/8 \cdot \Omega^2\theta_0 \end{aligned} \tag{D.2}$$

Then the forced vibration solution for flapping will be:

$$\begin{aligned} \beta = B_1 &\left\{ -\left(\frac{1}{2}\bar{\theta}p^2 + \Omega\bar{\theta}p\right)\sin(\phi + pt - \lambda_1) \right. \\ &\left. + \frac{\gamma}{16}\Omega\bar{\theta}p\cos(\phi + pt - \lambda_1) \right\} + B_2 \left\{ \left(\frac{1}{2}\bar{\theta}p^2 \right.\right. \\ &\left.\left. - \Omega\bar{\theta}p\right)\sin(\phi - pt - \lambda_2) + \frac{\gamma}{16}\Omega\bar{\theta}p\cos(\phi - pt - \lambda_2) \right\} \\ &+ \frac{(\gamma/8)\theta_0}{1+C_k} \end{aligned} \tag{D.3}$$

Here,

$$B_1 = \frac{1}{\sqrt{\{(1+C_k)\Omega^2 - (\Omega+p)^2\}^2 + (\gamma/8)^2\Omega^2(\Omega+p)^2}} \tag{D.4}$$

$$B_2 = \frac{1}{\sqrt{\{(1+C_k)\Omega^2 - (\Omega-p)^2\}^2 + (\gamma/8)^2\Omega^2(\Omega-p)^2}} \tag{D.5}$$

$$\begin{aligned} \cos\lambda_1 &= \{(1+C_k)\Omega^2 - (\Omega+p)^2\}B_1, \\ \sin\lambda_1 &= (\gamma/8)\Omega(\Omega+p)B_1 \\ \cos\lambda_2 &= \{(1-C_k)\Omega^2 - (\Omega-p)^2\}B_2, \\ \sin\lambda_2 &= (\gamma/8)\Omega(\Omega-p)B_2 \end{aligned} \tag{D.6}$$

(D.7)

If we substitute Eq. (C.18) into Eq. (D.1), we obtain:

$$M_\theta=\frac{-1}{\pi\bar{\theta}^2 p}\int_0^{2\pi/p}\Big\{\frac{1}{8}\rho acR^4(\theta_0\Omega^2\sum\cos\psi+\Omega\dot{\theta}\sum\cos^2\psi-\Omega\sum\beta\cos\psi)\theta-I_B(\sum\ddot{\beta}\cos\psi-\ddot{\theta}\sum\cos^2\psi+2\Omega\dot{\theta}\sum\sin\psi\cos\psi+\Omega^2\sum\beta\cos\psi)\theta\Big\}dt \tag{D.8}$$

The first term on the right side of Eq. (D.8) is the contribution of the moment produced around the pitching axis by the air forces operating on the blade, and the second term on the right side is the contribution of the moment produced around the pitching axis by the force of inertia operating on the blade. Eq. (D.8) corresponds exactly with Eq. (1.22) in the main text. If we substitute Eq. (D.3) into Eq. (D.8) and carry out the calculations, we obtain:

$$\begin{aligned}M_\theta=&-\frac{Q}{16}\rho acR^4\Omega-\frac{Q}{16}\rho acR^4\Big[\Big\{\frac{1}{2}(\Omega+p)p\cos\lambda_1+(\Omega+p)\Omega\cos\lambda_1-\frac{\gamma}{16}(\Omega+p)\Omega\sin\lambda_1\Big\}B_1\\&+\Big\{-\frac{1}{2}(\Omega-p)p\cos\lambda_2+(\Omega-p)\Omega\cos\lambda_2-\frac{\gamma}{16}(\Omega-p)\Omega\sin\lambda_2\Big\}B_2\Big]+\frac{Q}{2}I_B\Omega\\&\times\Big[\Big\{-\frac{1}{2}(2\Omega+p)\frac{p^2}{\Omega}\sin\lambda_1-p(2\Omega+p)\sin\lambda_1-\frac{\gamma}{16}p(2\Omega+p)\cos\lambda_1\Big\}B_1+\Big\{-\frac{1}{2}(2\Omega-p)\\&\times\frac{p^2}{\Omega}\sin\lambda_2+p(2\Omega-p)\sin\lambda_2+\frac{\gamma}{16}p(2\Omega-p)\cos\lambda_2\Big\}B_2\Big]\end{aligned} \tag{D.9}$$

The first, second, and third terms on the right side of (D.9) correspond with the first, second, and third terms on the right side of Eq. (1.23). If we continue the calculations further, using $p \equiv p/\Omega$, we obtain:

$$M_\theta=-\frac{Q}{2}C_kI_B\Omega\left\{\frac{\left(\frac{1}{2}p+1\right)(\gamma/8)(1+p)+(\gamma/16)\{(1+C_k)-(1+p)^2\}}{\{(1+C_k)-(1+p)^2\}^2+(\gamma/8)^2(1+p)^2}+\frac{(1-p/2)(\gamma/8)(1-p)+(\gamma/16)\{(1+C_k)-(1-p)^2\}}{\{(1+C_k)-(1-p)^2\}^2+(\gamma/8)^2(1-p)^2}\right\} \tag{D.10}$$

APPENDIX E. DAMPING WHEN THERE ARE FREE VIBRATIONS

Let us consider a rotor with a number of blades Q of 3 or more and with an I_p much larger than I_B. We will seek the characteristic root of pitching when this rotor performs free vibrations of pitching. It can be demonstrated that the real part of the characteristic root has the following relationship with $M_{\dot{\theta}}$ as sought in Appendix D.

$$\lambda_R=\frac{Ml_\theta}{2I_p} \tag{E.1}$$

In cases when the pitching consists of free vibration, only the torque M_Z will be applied to the rotor from the outside, and the rotating angular velocity around the rotor shaft axis will be maintained at a constant value Ω. The kinetic equations in this case will be:

/76

$$I_B(\ddot{\beta}_q-\ddot{\theta}\cos\psi_q+2\Omega\dot{\theta}\sin\psi_q+\Omega^2\beta_q) -\frac{1}{8}\rho acR^4(\theta_0\Omega^2+\Omega\dot{\theta}\cos\psi_q-\Omega\dot{\beta}_q)+K\beta_q=0 \tag{E.2}$$

$$I_p\ddot{\theta}+Wl\theta-I_B(\sum\beta_q\cos\psi_q-\ddot{\theta}\sum\cos^2\psi_q +2\Omega\dot{\theta}\sum\sin\psi\cos\psi_q+\Omega^2\sum\beta_q\cos\psi_q) +\frac{1}{8}\rho acR^4(\theta_0\Omega^2\sum\cos\psi_q+\Omega\dot{\theta}\sum\cos^2\psi_q -\Omega\sum\dot{\beta}_q\cos\psi_q)=0 \tag{E.3}$$

$$I_B(-2\Omega\sum\beta_q\dot{\beta}_q-2\dot{\theta}\sum\dot{\beta}_q\sin\psi_q-\ddot{\theta}\sum\beta_q\sin\psi_q +\dot{\theta}^2\sum\sin\psi_q\cos\psi_q)=M_z \tag{E.4}$$

Actually, (E.4) is the equation defining the torque which ought to be applied from the outside because the movement described above is continued.

(E.2) and (E.3) are linear simultaneous differential equations containing variable t in the coefficients in the form of sin ψ and cos ψ. Now let us change the variables:

$$\beta_q=a_{0(t)}-a_{1(t)}\cos\psi_q-b_{1(t)}\sin\psi_q \tag{E.5}$$

$$\dot{\beta}_q=\dot{a}_0-(\dot{a}_1+b_1\Omega)\cos\psi_q-(\dot{b}_1-a_1\Omega)\sin\psi_q$$
$$\ddot{\beta}_q=\ddot{a}_0-(\ddot{a}_1+2\dot{b}_1\Omega-a_1\Omega^2)\cos\psi_q-(\ddot{b}_1-2\dot{a}_1\Omega -b_1\Omega^2)\sin\psi_q$$

In particular in cases when Q ≥ 3,

$$\Sigma \cos\psi_q \beta_q = -\frac{Q}{2}(\ddot{a}_1 + 2\dot{b}_1\Omega - a_1\Omega^2)$$

$$\Sigma \cos\psi_q \beta_q = -\frac{Q}{2}(\dot{a}_1 + b_1\Omega)$$

$$\Sigma \cos\psi_q \beta_q = -\frac{Q}{2} a_1$$

Inserting this into Eq. (E.2), we divide the terms up into those involving sin ψ_q and cos ψ_q and those not involving them.

$$I_B\ddot{a}_0 + \frac{1}{8}\rho acR^4\Omega\dot{a}_0 + \left(I_B\Omega^2 + K\right)a_0 = \frac{1}{8}\rho acR^4\Omega^2\theta_0 \tag{E.6}$$

$$-I_B(\ddot{a}_1 + 2\dot{b}_1\Omega - a_1\Omega^2) - \frac{1}{8}\rho acR^4\Omega(\dot{a}_1 + b_1\Omega) - (I_B\Omega^2 + K)a_1 - I_B\ddot{\theta} - \frac{1}{8}\rho acR^4\Omega\theta = 0 \tag{E.7}$$

$$-I_B(\ddot{b}_1 - 2\dot{a}_1\Omega - b_1\Omega^2) - \frac{1}{8}\rho acR^4\Omega(\dot{b}_1 - a_1\Omega) - (I_B\Omega^2 + K)b_1 + 2I_B\Omega\dot{\theta} = 0 \tag{E.8}$$

If we insert this into (E.3), we obtain:

$$I_p\ddot{\theta} + W l\theta - I_B\left\{-\frac{Q}{2}\ddot{a}_1 + 2\dot{b}_1\Omega - a_1\Omega^2) - \frac{Q}{2}\ddot{\theta} - \frac{Q}{2}\Omega^2 a_1\right\} + \frac{1}{8}\rho acR^4\left\{\frac{Q}{2}\Omega\dot{\theta} + \frac{Q}{2}\Omega(\dot{a}_1 + b_1\Omega)\right\} = 0 \tag{E.9}$$

If we reorganize (E.6), (E.7), (E.8), and (E.9) using $L \equiv I_p/I_B$, we obtain:

$$\ddot{a}_0 + \gamma/8\Omega\dot{a}_0 + (1 + C_k)\Omega^2 a_0 = (\gamma/8)\Omega^2\theta_0 \tag{E.10}$$

$$\ddot{a}_1 + \gamma/8\Omega\dot{a}_1 + C_k\Omega^2 a_1 + 2\Omega\dot{b}_1 + (\gamma/8)\Omega^2 b_1 + \ddot{\theta} + (\gamma/8)\Omega\dot{\theta} = 0 \tag{E.11}$$

$$2\Omega\dot{a}_1+(\gamma/8)\Omega^2a_1-\dot{b}_1-(\gamma/8)\Omega b_1-C_k\Omega^2b_1 +2\Omega\dot{\theta}=0 \quad \text{(E.12)}$$

$$\ddot{a}_1+(\gamma/8)\Omega\dot{a}_1+2\Omega\dot{b}_1+(\gamma/8)\Omega^2b_1+(1+2L/Q)\ddot{\theta} +(\gamma/8)\Omega\dot{\theta}+2p^2L/Q\Omega^2\theta=0 \quad \text{(E.13)}$$

This signifies that (E.10) is independent and that the coning will finally settle down to $(\gamma/8)(1 + C_k)$. (E.11), (E.12), and (E.13) are linear simultaneous differential equations for the constant coefficients.

Eq. (E.3) is the simultaneous equation for pitching. Since I_p is sufficiently large in comparison with I_B, the pitching movement ought to be close to a sinusoidal movement with a period of $2\pi/p$. It ought to be possible to write two of the roots of the characteristic equations obtained from (E.11), (E.12), and (E.13) in the following manner:

$$\delta\Omega \pm (p + \varepsilon)\Omega i$$

Naturally, δ and ε will be small enough in comparison with p.

If we posit $a_1=A_1e^{\lambda\Omega t}$, $b_1=B_1e^{\lambda\Omega t}$, $\theta=\Theta e^{\lambda\Omega t}$

$$\begin{vmatrix} \lambda^2+(\gamma/8)\lambda+C_k & 2\lambda+\gamma/8 & \lambda^2+(\gamma/8)\lambda \\ 2\lambda+\gamma/8 & -(\lambda^2+(\gamma/8)\lambda+C_k) & 2\lambda \\ \lambda^2+(\lambda/8)\lambda & 2\lambda+\gamma/8 & (1+2L/Q)\lambda^2+(\gamma/8)\lambda+2p^2L/Q \end{vmatrix}=0$$

That is,

$$\begin{vmatrix} \lambda^2+(\gamma/8)\lambda+C_k & 2\lambda+\gamma/8 & \lambda^2+(\gamma/8\lambda) \\ 2\lambda+\lambda/8 & -(\lambda^2+(\gamma/8)\lambda+C_k) & 2\lambda \\ -\varepsilon & 0 & \lambda^2+p^2 \end{vmatrix}=0 \quad \text{(E.14)}$$

Two of these roots are:

$$\lambda=\delta\pm(p+\varepsilon)i \quad \text{(E.15)}$$

Here,

$$\varepsilon\equiv C_kQ/(2L) \quad \text{(E.16)}$$

is a minute quantity since L is large enough. /77

If we substitute (E.15) in (E.14), assuming that κ, δ, and ε are minute quantities, it will be possible to determine δ and ε by omitting the minute quantities of a high order.

$$\delta=\frac{\left\{\begin{array}{c}-\kappa p(C_k-p^2)+(\gamma/8)^2p+4p][4(C_k-p^2)(\gamma/8)p+8(\gamma/8p)]+\kappa[(\gamma/8)p^2-(C_k-p^2)(\gamma/8)\\-2(\gamma/8)][2\{(C_k-p^2))^2-(\gamma/8)^2p^2\}+2\{(\lambda/8)^2-4p^2\}]\end{array}\right\}}{[4(C_k-p^2)(\gamma/8)p+8(\gamma/8)p]^2+[2\{(C_k-p^2)^2-(\gamma/8)^2p^2\}+2\{(\gamma/8)^2-4p^2\}]^2} \tag{E.17}$$

$$\varepsilon=\frac{\left\{\begin{array}{c}-\kappa[p(C_k-p^2)+(\gamma/8)^2p+4p][2\{(C_k-p^2)^2-(\gamma/8)^2p^2\}+2\{(\gamma/8)^2-4p^2\}]-\kappa[(\gamma/8)p^2\\-(C_k-p^2)(\gamma/8)-2(\gamma/8)][4(C_k-p^2)(\gamma/8)\gamma+8(\gamma/8)p]\end{array}\right\}}{[4(C_k-p^2)(\gamma/8)p+8(\gamma/8)p]^2+[2\{(C_k-p^2)^2-(\gamma/8)^2p^2\}+2\{(\gamma/8)^2-4p^2\}]^2} \tag{E.18}$$

From (D.10), we find that

$$\frac{M_\theta}{2I_p\Omega}=\frac{\left\{\begin{array}{l}-\kappa[(2+p)(\gamma/8)(1+p)+(\gamma/8)\{(1+C_k)-(1+p)^2\}][\{(1+C_k)-(1-p)^2\}^2+(\gamma/8)^2(1-p)^2]\\-\kappa[(2-p)(\gamma/8)(1-p)+(\gamma/8)\{(1+C_k)-(1-p)^2\}][\{(1+C_k)-(1+p)^2\}^2+(\gamma/8)^2(1+p)^2]\end{array}\right\}}{4[\{1+C_k)-(1+p)^2\}^2+(\gamma/8)(1+p)^2][\{(1+C_k)-(1-p)^2\}^2+(\gamma/8)^2(1-p)^2]} \tag{E.19}$$

This indicates that (E.17) and (E.19) coincide.

The denominator of (E.17) is

$$\begin{aligned}&16(C_k-p^2)^2(\gamma/8)^2p^2+64(C_k-p^2)(\gamma/8)^2p^2+64(\gamma/8)^2p^2+4\{(C_k-p^2)^2-4p^2\}^2\\&+8\{(C_k-p^2)^2-4p^2\}(\gamma/8)^2(1-p^2)+4(\gamma/8)^4(1-p^2)^2\\=&4\{(C_k-p^2)^2-4p^2\}^2+4(\gamma/8)^4(1-p)^2+8(C_k-p^2)^2(\gamma/8)^2(1+p^2)+64(C_k-p^2)(\gamma/8)^2p^2\\&+64(\gamma/8)^2p^2-32p^2(\gamma/8)^2(1-p^2)\end{aligned}$$

The denominator of (E.19) is

$$\begin{aligned}&4\{(C_k-p^2)^2-4p^2\}^2+4\{(C_k-p^2)-2p\}^2(\gamma/8)^2(1-p)^2\\&4\{(C_k-p^2)+2p\}^2(\gamma/8)^2(1+p)^2+4(\gamma/8)^4(1-p^2)^2\\=&4\{(C_k-p^2)^2-4p^2\}^2+4(\gamma/8)^4(1-p^2)^2+8(C_k-p^2)^2(\gamma/8)^2(1+p^2)+64(C_k-p^2)p(\gamma/8)^2p\\&+32p^2(\gamma/8)^2(1+p^2)\end{aligned}$$

Thus, the denominators of (E.17) and (E.19) are equal.

The numerator of (E.17) is

$$
\begin{aligned}
&-\kappa[4(C_k-p^2)^2(\gamma/8)p^2+8(\gamma/8)(C_k-p^2)p^2+4(C_k-p^2)(\gamma/8)^2p^2+8(\gamma/8)^2p^2+16(C_k-p^2)(\gamma/8)p^2\\
&+32(\gamma/8)p^2-2(\gamma/8)p^2(C_k-p^2)^2+2(\gamma/8)^2p^4-2(\gamma/8)^2p^2+8(\gamma/8)p^4+2(C_k-p^2)^2(\gamma/8)\\
&-2(\gamma/8)^2p^2(C_k-p^2)+2(C_k-p^2)(\gamma/8)^2-(C_k-p^2)8p^2(\gamma/8)+4(\gamma/8)(C_k-p^2)^2\\
&-4(\gamma/8)^2p^2+4(\gamma/8)^2-16(\gamma/8)p^2]\\
=&-\kappa[2(\gamma/8)(C_k-p^2)^2+(\gamma/8)(C_k-p^2)^2(2p^2+4)+(\gamma/8)^2(C_k-p^2)(2+2p^2)\\
&+16(\gamma/8)(C_k-p^2)p^2+(\gamma/8)^2(2p^4+2p^2+4)+(\gamma/8)(8p^4+16p^2)]
\end{aligned}
$$

The numerator of (E.19) is

$$
\begin{aligned}
&-\kappa[(\gamma/8)(p^2+p+2)+(\gamma/8)(C_k-p^2)][(C_k-p^2)^2+4p(C_k-p^2)+(\gamma/8)^2(1-p)^2+4p^2]\\
&-\kappa[(\gamma/8)(p^2-p+2)+(\gamma/8)(C_k-p^2)][(C_k-p^2)^2-4p(C_k-p^2)+(\gamma/8)^2(1+p)^2+4p^2]\\
=&-\kappa[2(\gamma/8)(C_k-p^2)^2+2(\gamma/8)(C_k-p^2)^2+(\gamma/8)8p^2(C_k-p^2)+2(\gamma/8)^2(p^2+2)(1+p^2)\\
&+4(\gamma/8)^2(-p^2)+2(\gamma/8)^2(C_k-p^2)(1+p^2)+8p^2(\gamma/8)(p^2+2)+8p^2(\gamma/8)(C_k-p^2)]\\
=&-\kappa[2(\gamma/8)(C_k-p^2)^2+(\gamma/8)(C_k-p^2)^2(2p^2+4)+(\gamma/8)^2(C_k-p^2)(2+2p^2)+16(\gamma/8)(C_k-p^2)p^2\\
&+(\gamma/8)^2(2p^4+2p^2+4)+(\gamma/8)(8p^4+16p^2)]
\end{aligned}
$$

Thus, the numerators of (E.17) and (E.19) are equal.

$$
\therefore \quad \frac{M_\theta}{2I_p\Omega}=\delta \tag{E.20}
$$

In other words, the real part of the root of the characteristic equation is equal to $M_\theta/2I_p$.

APPENDIX F. ENERGY BALANCE IN CASES OF FORCED VIBRATION

Let us investigate the manner in which the work done by moments M_Y and M_Z, which are applied from the outside in cases of forced vibration (refer to Appendix D)..is consumed. If we use the flapping sought by (D.3) and calculate $\Sigma\beta_q \cos\psi_q$, $\Sigma\dot{\beta}_q \cos\psi_q$, $\Sigma\beta_q \cos\psi_q$, $\Sigma\beta_q\dot{\beta}_q$, $\Sigma\beta_q \sin\psi_q$, and $\Sigma\beta_q \sin\psi_q$, we learn that in each case they are linear combinations of sin pt and cos pt. Consequently, it is clear that the period $2\pi/p$ is present in the case of forced vibrations.

Let us calculate the work performed by the pitching moment M_Y during one period $[0, 2\pi/p]$. If we use the pitching equation (C.18), we obtain

$$\int_0^{2\pi/p} M_Y\theta dt=\int_0^{2\pi/p} I_p\ddot{\theta}\theta pt+\int_0^{2\pi/p} wl\theta\theta dt-I_B\int_0^{2\pi/p}(\sum\ddot{\beta}_q\cos\psi_q-\ddot{\theta}\sum\cos^2\psi_q+2\Omega\dot{\theta}\sum\sin\psi_q\cos\psi_q$$
$$+\Omega^2\sum\beta_q\cos\psi_q)\theta dt+\frac{1}{8}\rho acR^4\int_0^{2\pi/p}(\theta_0\Omega^2\sum\cos\psi_q+\Omega\dot{\theta}\sum\cos^2\psi_q-\Omega\sum\dot{\beta}_q\cos\psi_q)\theta dt$$
$$=-\frac{1}{8}\rho acR^4\int_0^{2\pi/p}\sum(\theta_0\Omega^2+\Omega\dot{\theta}\cos\psi_q-\Omega\dot{\beta}_q)(\dot{\beta}_q-\dot{\theta}\cos\psi_q)dt$$
$$-I_B\int_0^{2\pi/p}(\sum\ddot{\beta}_q\cos\psi_q-\ddot{\theta}\sum\cos^2\psi_q+2\Omega\dot{\theta}\sum\sin\psi_q\cos\psi_q+\Omega^2\sum\beta_q\cos\psi_q)\theta dt$$
$$+\frac{1}{8}\rho acR^4\int_0^{2\pi/p}\sum(\theta_0\Omega^2+\Omega\dot{\theta}\cos\psi_q-\Omega\dot{\beta}_q)\dot{\beta}_q dt \qquad (F.1)$$

If we rewrite the third term by means of the flapping equation (C.17), we obtain:

$$\int_0^{2\pi/p} M_Y\theta dt=-\frac{1}{8}\rho acR^4\int_0^{2\pi/p}\sum(\theta_0\Omega^2+\Omega\dot{\theta}\cos\psi_q-\Omega\dot{\beta}_q)(\dot{\beta}_q-\dot{\theta}\cos\psi_q)dt$$
$$-I_B\int_0^{2\pi/p}\sum\ddot{\beta}_q\cos\psi_q-\ddot{\theta}\sum\cos^2\psi_q+2\Omega\dot{\theta}\sum\sin\psi_q\cos\psi_q+\Omega^2\sum\beta_q\cos\psi_q)\theta dt$$
$$+I_B\int_0^{2\pi/p}\sum(\ddot{\beta}_q-\ddot{\theta}\cos\psi_q+2\Omega\dot{\theta}\sin\psi_q+\Omega^2\beta_q)\dot{\beta}_q pt+K\int_0^{2\pi/p}\sum\dot{\beta}_q\beta_q dt \qquad (F.2)$$

Let us calculate the work performed by the torque during one period $[0,2\pi/p]$. Using the torque equation (C.19), we obtain

$$\int_0^{2\pi/p} M_z\Omega dt=I_B\int_0^{2\pi/p}(-2\Omega\sum\beta_q\dot{\beta}_q-2\dot{\theta}\sum\dot{\beta}_q\sin\psi_q-\ddot{\theta}\sum\beta_q\sin\psi_q+\dot{\theta}^2M\sin\psi_q\cos\psi_q)dt \qquad (F.3)$$

However, according to (C.16),

$$-I_B\int_0^{2\pi/p}(\sum\ddot{\beta}_q\cos\psi_q-\ddot{\theta}\sum\cos^2\psi_q+2\Omega\dot{\theta}\sum\sin\psi_q\cos\psi_q+\Omega^2\sum\beta_q\cos\psi_q)\theta dt$$
$$+I_B\int_0^{2\pi/p}\sum(\ddot{\beta}_q-\ddot{\theta}\cos\psi_q+2\Omega\dot{\theta}\sin\psi_q+\Omega^2\beta_q)\dot{\beta}_q dt$$
$$+I_B\int_0^{2\pi/p}(-2\Omega\sum\beta_q\dot{\beta}_q-2\dot{\theta}\sum\dot{\beta}_q\sin\psi_q-\ddot{\theta}\sum\beta_q\sin\psi_q+\dot{\theta}^2\sum\sin\psi_q\cos\psi_q)dt$$
$$=\int_0^{2\pi/p}\frac{dT_B}{dt}dt=0 \qquad (F.4)$$

According to (C.6),

$$K\int_0^{2\pi/p}\sum\beta_q\dot{\beta}_q=\int_0^{2\pi/p}\frac{dU}{dt}dt=0 \qquad (F.5)$$

$$\therefore\quad \int_0^{2\pi/p} M_Y\theta dt+\int_0^{2\pi/p} M_z\Omega dt=-\frac{1}{8}\rho acR^4\int_0^{2\pi/p}\sum(\theta_0\Omega^2+\Omega\dot{\theta}\cos\psi_q-\Omega\dot{\beta}_q)(\dot{\beta}_q-\dot{\theta}\cos\psi_q)dt \qquad (F.6)$$

In other words, it is clear that the work performed by the external forces is equal to the work consumed by the blade moving the air. Also, in accordance with (F.1) and (F.6),

$$-I_B\int_0^{2\pi/p}(\sum\ddot{b}_q\cos\psi_q-\ddot{\theta}\sum\cos^2\psi_q+2\Omega\dot{\theta}\sum\sin\psi_q\cos\psi_q+\Omega^2\sum\beta_q\cos\psi_q)\dot{\theta}dt$$
$$=-\frac{1}{8}\rho acR^4\int_0^{2\pi/p}\sum(\theta_0\Omega^2+\Omega\dot{\theta}\cos\psi_q-\Omega\dot{\beta}_q)\dot{\beta}_q dt-\int_0^{2\pi/p}M_z\Omega dt \qquad (F.7)$$

It is clear that the term originating in the inertial forces operating on the blade which appeared in Eq. (D.8) expressing the pitch damping is the work consumed by the blade during flapping when it moves the air /79

$$-\frac{1}{8}\rho acR^4\int_0^{2\pi/p}\sum(\theta_0\Omega^2+\Omega\dot{\theta}\cos\psi_q-\Omega\dot{\beta}_q)\dot{\beta}_q dt$$

from which the work performed by the torque $\int_0^{2\pi/p}M_z\Omega dt$ has been subtracted.

APPENDIX G. ENERGY BALANCE IN CASES OF FREE VIBRATIONS

Pitching has a period defined by the root in the characteristic equation (E.14). If we calculate the work performed by the torque M_Z during one period of pitching $[0,\tau]$,

$$\int_0^\tau M_z\Omega dt=I_B\int_0^\tau(-2\Omega\sum\beta_q\dot{\beta}_q-2\dot{\theta}\sum\dot{\beta}_q\sin\psi_q-\ddot{\theta}\sum\beta_q\sin\psi_q+\ddot{\theta}\sum\sin\psi_q\cos\psi_q)dt \qquad (G.1)$$

The total energy fluctuations occurring in the pendulum during $[0,\tau]$ are

$$(T_{p(\tau)}-T_{p(0)})+(U_{p(\tau)}-U_{p(0)})=\int_0^\tau I_p\ddot{\theta}\dot{\theta}dt+\int_0^\tau Wl\theta\dot{\theta}dt$$

If we rewrite this using the pitching equation (E.3),

$$\begin{aligned}(T_{p(\tau)}-T_{p(0)})+(U_{p(\tau)}-U_{p(0)})&=I_B\int_0^\tau(\sum\ddot{\beta}_q\cos\psi_q-\ddot{\theta}\sum\cos^2\psi_q+2\Omega\dot{\theta}\sum\sin\psi_q\cos\psi_q+\Omega^2\sum\beta_q\cos\psi_q)\dot{\theta}dt\\&-\frac{1}{8}\rho acR^4\int_0^\tau(\theta_0\Omega^2\sum\cos\psi_q+\Omega\dot{\theta}\sum\cos^2\psi_q-\Omega\sum\dot{\beta}_q\cos\psi_q)\dot{\theta}dt\\&=I_B\int_0^\tau(\sum\ddot{\beta}_q\cos\psi_q-\ddot{\theta}\sum\cos^2\psi_q+2\Omega\dot{\theta}\sum\sin\psi_q\cos\psi_q+\Omega^2\sum\beta_q\cos\psi_q)\dot{\theta}dt\\&+\frac{1}{8}\rho acR^4\int_0^\tau\sum(\theta_0\Omega^2+\Omega\dot{\theta}\cos\psi_q-\Omega\dot{\beta}_q)(\dot{\beta}_q-\dot{\theta}\cos\psi_q)dt\\&-\frac{1}{8}\rho acR^4\int_0^\tau\sum(\theta_0\Omega^2+\Omega\dot{\theta}\cos\psi_q-\Omega\dot{\beta}_q)\dot{\beta}_q dt\end{aligned} \qquad (G.2)$$

If we rewrite the third term using the flapping equation (C.17),

$$(T_{p(\tau)}-T_{p(0)})+(U_{p(\tau)}-U_{p(0)})=\frac{1}{8}\rho acR^4\int_0^\tau\sum(\theta_0\Omega^2+\Omega\dot\theta\cos\psi_q-\Omega\dot\beta_q)(\dot\beta_q-\dot\theta\cos\psi_q)dt$$
$$+I_B\int_0^\tau(\sum\ddot\beta_q\cos\psi_q-\ddot\theta\sum\cos^2\psi_q+2\Omega\dot\theta\sum\sin\psi_q\cos\psi_q+\Omega^2\sum\beta_q\cos\psi_q)\dot\theta dt$$
$$-I_B\int_0^\tau\sum(\ddot\beta_q-\ddot\theta\cos\psi_q+2\Omega\dot\theta\sin\psi_q+\Omega^2\beta_q)\dot\beta_q dt-K\int_0^\tau\sum\beta_q\dot\beta_q dt$$

However, according to (C.16)

$$I_B\int_0^\tau(\sum\ddot\beta_q\cos\psi_q-\ddot\theta\sum\cos^2\psi_q+2\Omega\dot\theta\sum\sin\psi_q\cos\psi_q+\Omega^2\sum\beta_q\cos\psi_q)\dot\theta dt$$
$$-I_B\int_0^\tau\sum(\ddot\beta_q-\ddot\theta\cos\psi_q+2\Omega\dot\theta\sin\psi_q+\Omega^2\beta_q)\dot\beta_q dt$$
$$-I_B\int_0^\tau(-2\Omega\sum\beta_q\dot\beta_q-2\dot\theta\sum\dot\beta_q\sin\psi_q-\ddot\theta\sum\beta_q\sin\psi_q+\dot\theta^2\sum\sin\psi_q\cos\psi_q)dt$$
$$=-\int_0^\tau\frac{dT_B}{dt}dt-K\int_0^{2\pi}\sum\beta_q\dot\beta_q=-\int_0^\tau\frac{dU}{dt}dt$$
$$\therefore\ (T_{p(\tau)}-T_{p(0)})+(U_{p(\tau)}-U_{(0)})+(T_{B(\tau)}-T_{B(0)})+(U_{(\tau)}-U_{(0)})$$
$$=\frac{1}{8}\rho acR^4\int_0^\tau\sum(\theta_0\Omega^2+\Omega\dot\theta\cos\psi_q-\Omega\dot\beta_q)(\dot\beta_q-\dot\theta\cos\psi_q)dt+\int_0^\tau M_z\Omega dt \qquad (G.3)$$

In other words, the total energy fluctuations of the system are equal to the work performed by the external forces. According to (G.2) and (G.3),

$$-I_B\int_0^\tau(\sum\ddot\beta_q\cos\psi_q-\ddot\theta\sum\cos\psi_q+2\Omega\dot\theta\sum\sin\psi_q\cos\psi_q+\Omega^2\sum\beta_q\cos\psi_q)\dot\theta dt=(T_{B(\tau)}-T_{B(0)})+(U_{(\tau)}-U_{(0)})$$
$$-\int_0^\tau M_z\Omega dt-\frac{1}{8}\rho acR^4\int_0^\tau\sum(\theta_0\Omega^2+\Omega\dot\theta\cos\psi_q-\Omega\dot\beta_q)\dot\beta_q dt \qquad (G.4)$$ /80

In other words, $-I_B\int_0^\tau(\sum\ddot\beta_q\cos\psi_q-\ddot\theta\sum\cos\psi_q+2\Omega\dot\theta\sum\sin\psi_q\cos\psi_q+\Omega^2\sum\beta_q\cos\psi_q)\dot\theta dt$, is equal to the work consumed by the blade during flapping when it moves the air, from which the work performed by the torque and the reduction in the total energy of the blade part $(T_{B(0)}-T_{B(\tau)})+(U_{(0)}-U_{(\tau)})$ have been subtracted.

APPENDIX H. CONCERNING FLUCUTATIONS IN THE ROTOR REVOLUTION SPEED

The pitch damping sought by Eq. (1.23) was derived under the assumption that the rotor revolution speed is maintained at a constant value Ω. However, the torque M_Z must be supplied to the motor in order to maintain this movement. If the torque M_Z is not applied by the motor and if the rotating angular velocity fluctuates, what will be its magnitude? If we calculate by inserting Eq. (D.3) into Eq. (C.19), we obtain

$$M_z=QI_B\bar\theta^2p^2\Omega^4B_1B_2\{2p[(r/8)^2+1-(p/2)^2]\sin(2pt-\lambda_1+\lambda_2)+(\gamma/8)p^2\cos(2pt-\lambda_1+\lambda_2)\}$$
$$+QI_B\bar\theta^2p^2\Omega^2B_1\left\{-\frac{1}{2}\left[(1+p/2)(1+2p)\sin(2pt-\lambda_1)-\frac{\gamma}{16}(1+2p)\cos(2pt-\lambda_1)\right]\right\}$$
$$+QI_B\bar\theta^2p^2\Omega^2B_2\left\{\frac{-1}{2}\left[(1-p/2)(1-2p)\sin(2pt+\lambda_2)+\frac{\gamma}{16}(1-2p)\cos(2pt+\lambda_2)\right]\right\}$$
$$+QI_B\bar\theta^2p^2\Omega^2B_1\left\{\frac{1}{2}\left[\left(1+\frac{p}{2}\right)\sin\lambda_1+\frac{\gamma}{16}\cos\lambda_1\right]\right\}+QI_B\bar\theta^2p^2\Omega^2B_2\left\{\frac{1}{2}\left[\left(1-\frac{p}{2}\right)\sin\lambda_2+\frac{\gamma}{16}\cos\gamma_2\right]\right\} \qquad (H.1)$$

$\Omega^4 B_1 B$, $\Omega^2 B_1$, and $B_2\Omega^2$ are each approximately 1, $\gamma/8$ is smaller than 1, and p is approximately 0.2. Therefore, M_Z is about $QI_B\bar{\theta}^2p^2$. In the experiments, the voltage applied to the motor is maintained uniform. Therefore, there are some fluctuations of Ω when the rotor performs pitching. If we suppose that Ω declines to $\Omega - \Delta\Omega$, in addition to the increase in the torque generated by the motor, there will also be a reduction of the torque consumed by the aerodynamic resistance of the rotor, and the fluctuations of Ω will be suppressed. Even if we do not consider the increase in the torque generated by the motor,

$$\frac{\Delta\Omega}{\Omega}=\frac{QI_B\bar{\theta}^2p^2}{2C_Q\pi\rho R^5\Omega^2}\fallingdotseq\frac{1}{10^3} \tag{H.2}$$

Actually, the torque generated by the motor increases, and therefore the fluctuations of Ω will be even smaller.

TR-236T	Small-Strain Deformations Superposed on Finite Deformations of Highly Elastic Incompressible Materials —Part I Constitutive Equations—	June 1971	Tastuzo KOGA
TR-237	自由飛行模型 FFM-10 による縦の動安定特性の飛しょう実験 Free Flight Tests on Longitudinal Dynamics Characteristic of FFM-10 Model	1971年4月	河崎俊夫，塙　武敏 斎藤秀夫，高島一明 河本　巌
TR-238	リフトジェットエンジン JR 100H の動特性について Dynamic Characteristic of Lift Jet Engine JR 100H	1971年5月	西尾健二，杉山七契 大畑敏美，遠藤征紀 越沼　威
TR-239	昇華アブレーションの直接解法 A Direct Calculation of Sublimating Ablation	1971年6月	久保田弘敏
TR-240T	A Method for the Calculation of Lifting Potential Flow Problems —Part I Theoretical Basis—	July 1971	Masao EBIHARA
TR-241	YS-11A-500/600 型主翼疲れ試験（I セーフライフ試験荷重と試験方式） Full-Scale Fatigue Test of YS-11A-500/600 Turboprop Transport Wing (I Safe-Lie Fatigue Test Loads and Test Method)	1971年7月	竹内和之，野原利雄 朝田洋雄
TR-242	熱線による3次元平均速度ベクトルとレイノルズ応力の測定 Measurement of Three-Dimensional Mean Velocity Vector and Reynolds Stress by Single Rotatable Hot-Wire	1971年7月	林　良生，中谷輝臣
TR-243	揚力をもつ物体のまわりのポテンシャル流れの計算法 I　その理論的基礎 A Method for the Calculation of Lifting Potential Flow Problems —Part 1 Theoretical Basis—	1971年7月	海老原正夫
TR-244	超音速風洞における動安定微係数の測定 Measurements of Dynamic Stability Derivatives in Supersonic Blowdown Wind Tunnel	1971年7月	高島一明，榊原盛三 関根英夫
TR-245	ヘリコプタ高度・速度線図および臨界決定点の解析的推定法 An Analytical Method to Predict Height-Velocity Diagram Critical Decision Point of Rotorcraft	1971年8月	古茂田真幸
TR-246	梁の大変形問題の解析について On Analysis of Large Deformation Problems of Beam	1971年11月	泉　日出夫
TR-247	任意物体のまわりの自由流線理論 On the Theory of Free Streamlines Past an Arbitrary Shape	1971年9月	高橋　侔
TR-248	亜音速流中における二次元翼上の圧力分布の粘性効果を考慮に入れた計算法のプログラム A Description of the Ideas Underlying a Computer Programme for Predicting the Aerofoil Pressure Distributions in Subcritical Viscous Flows	1971年11月	海老原正夫，石田洋治 小此木時雄

TR-249	一般化 Newton-Raphson 法の計算機容量問題に対する改良最適化アルゴリズム Modified Optimization Algorithm for Computer Storage Problems in Generalized Newton-Raphson Method	1971年10月 志甫 徹
TR-250	はりの大変形解析 Large Deflection of Cantilever Beams	1971年10月 多田保夫，日下和夫
TR-251	対称スピン衛星のニューテーション運動による慣性力の場とそのニューテーションダンパへの応用 Inertial Force Field Due to Nutational Motion of Spinning Axi-Symmetric Sattellite and Its Application to Nutation Damper	1971年11月 村上 力，狼 嘉彰
TR-252T	A Study of Subsonic Two-Dimensional Wall-Interference Effects in a Perforated Wind Tunnel with Particular Reference to the NAL 2m×2m Transonic Wind Tunnel Inapplicability of the Conventional Boundary Condition	1971年12月 Masao Ebihara
TR-253	圧縮性流れにおける翼型抗力の計算 A Calculation of Profile Drag of Airfoils in Compressible Flow	1971年11月 石田洋治
TR-254	翼と不連続境界との干渉について Interference Between Wing and Surface of Velocity Discontinuity	1971年11月 犬丸矩夫
TR-255	地球の重力の作用下にある人工衛星の運動に関する研究 The Study on the Motion of an Artificial Satellite in the Earth's Gravitational Field	1971年12月 武内澄夫，松島弘一

航空宇宙技術研究所報告256号

昭和46年11月発行

発行所 航空宇宙技術研究所
東京都調布市深大寺町1880
電話武蔵野三鷹(0422)47-5911(大代表)〒182

印刷所 株式会社 東京プレス
東京都板橋区桜川 2-27-12